



GEOSCIENCE BC SUMMARY OF ACTIVITIES 2011





GEOSCIENCE BC SUMMARY OF ACTIVITIES 2011



© 2012 by Geoscience BC.

All rights reserved. Electronic edition published 2012.

This publication is also available, free of charge, as colour digital files in Adobe Acrobat® PDF format from the Geoscience BC website: <http://www.geosciencebc.com/s/DataReleases.asp>.

Every reasonable effort is made to ensure the accuracy of the information contained in this report, but Geoscience BC does not assume any liability for errors that may occur. Source references are included in the report and users should verify critical information.

When using information from this publication in other publications or presentations, due acknowledgment should be given to Geoscience BC. The recommended reference is included on the title page of each paper. The complete volume should be referenced as follows:

Geoscience BC (2012): Geoscience BC Summary of Activities 2011; Geoscience BC, Report 2012-1, 162 p.

ISSN 1916-2960 Summary of Activities (Geoscience BC)

Cover photo: Stream-sediment sampling in the QUEST-Northwest project area, northwestern British Columbia.

Photo credit: Wayne Jackaman, Noble Exploration Services Ltd., 2011.

Foreword

Geoscience BC is pleased to present results of many of our ongoing and recently completed geoscience projects and surveys in this, our fifth edition of the *Geoscience BC Summary of Activities*. The volume is divided into three sections, and contains a total of 16 papers.

The first section contains three papers from the QUEST-Northwest project, Geoscience BC's latest major mineral geoscience initiative. The QUEST-Northwest project is designed to stimulate new mineral exploration activity in the north-western part of the province, and to enhance the success of existing exploration activities in the region. Like the QUEST, QUEST-West and QUEST-South projects before it, QUEST-Northwest includes both airborne geophysical surveys and regional geochemical programs. However, the QUEST-Northwest program also includes a regional mapping component, which was undertaken in partnership with the BC Geological Survey. Simpson and Jackaman describe the airborne magnetic surveys and regional geochemical surveys respectively, while Logan et al. discuss the regional mapping program (also discussed in the BC Geological Survey's *Geological Fieldwork 2011* volume).

The second section of this volume describes ongoing Geoscience BC-supported mineral geoscience projects throughout BC, and is roughly organized by project type and area. Devine provides an update on Geoscience BC's Porphyry Integration Project, which is currently pulling together existing geological, geochemical and geophysical datasets from select BC porphyry deposits. This project is complementary to the work of Blaine and Hart, who are developing geochemical-exploration models for BC porphyry deposits. Muezelaar and Monecke provide a final report on their geochemical modelling project aimed at constraining fluid controls on ore genesis in the Eskay Creek deposit.

Two papers deal with till sampling programs in central British Columbia: Stumpf discusses the development of a till database for the Bulkley River valley region, and Ward et al. provide an update on heavy-mineral analysis of till samples in the QUEST Project area. Vasa et al. discuss chemical variations in pyroxene and Fe-Ti-oxide crystals in basalts of the Nicola Group in southern BC, and relate the results to magma alkalinity and the location of known deposits. Finally, Höy and Jackaman describe a new Geoscience BC mapping project that will focus on the Burrell Creek map area in southeastern BC. This work is a continuation of work the authors previously undertook for Geoscience BC in the Deer Park map area in 2009.

The third section of this volume discusses Geoscience BC's oil and gas projects, which are split between northeastern BC and the Nechako Basin in central BC. Chapman et al. describe a partnership project between Geoscience BC and the BC Oil and Gas Commission aimed at completing hydrological modelling in northeastern BC, which will help guide use and development of water resources in the region, including potential use in unconventional gas development. This project is complementary to the two major projects Geoscience BC has undertaken in northeastern BC over the past few years: the Horn River Basin Aquifer Project (Phases 1 and 2) and the Montney Water Project. These projects are focused on understanding surface and subsurface water sources in the Horn River Basin and Montney gas play respectively. Also in northeastern BC, Chalmers et al. examine geological controls on tight-gas in the Montney play, and Golding et al. and Henderson et al. undertake stratigraphic studies in the area. Finally, Kushnir et al. present the results of a rock-property study in the Nechako Basin (raw data released as Geoscience BC Report 2011-10; see below), and Spratt et al. discuss the use of magnetotelluric transfer functions to test the usefulness of ZTEM data in the Nechako Basin.

Readers are encouraged to visit the website for additional information on all Geoscience BC-funded projects, including project descriptions, posters and presentations, previous *Summary of Activities* or *Geological Fieldwork* papers, and final datasets and reports. All papers in this and past volumes are available for download through Geoscience BC's website (www.geosciencebc.com). Limited copies of past volumes are also available from the Geoscience BC office.

Geoscience BC Publications 2011

In addition to this *Summary of Activities* volume, Geoscience BC releases interim and final products from our projects as Geoscience BC Reports. All Geoscience BC data and reports can be accessed through our website at www.geosciencebc.com/s/DataReleases.asp. Geoscience BC datasets and reports released in 2011 include the following:

- 25 technical papers in the *Geoscience BC Summary of Activities 2010* volume
- ***Northern BC Sample Reanalysis Project***, by W. Jackaman (Geoscience BC Report 2011-2)
- ***The application of surface organic materials as sample media over deeply buried mineralization at the Kwanika Central Zone, North-Central British Columbia***, by D.R. Heberlein and C.E. Dunn (Geoscience BC Report 2011-3)

- **Regional Stream Sediment and Water Geochemical Data, Vancouver Island, British Columbia**, by W. Jackaman (Geoscience BC Report 2011-4)
- **Catchment Analysis and Interpretation of Stream Sediment Data from QUEST-South, British Columbia**, by D.C. Arne and E.B. Bluemel (Geoscience BC Report 2011-5)
- **Ground Testing of Predicted Geology Based on Stream and Lake Sediment Geochemistry in the QUEST Area, Using Previously Undocumented Bedrock Exposures**, by T. Bissig, J. Logan, D.R. Heberlein and F. Ma (Geoscience BC 2011-6)
- **Preliminary Bedrock Topography and Drift Thickness of the Montney Play**, by A.S. Hickin and M.A. Fournier (Geoscience BC Report 2011-7 / BC Ministry of Energy and Mines, Energy Open File 2011-1)
- **Compilation of Geological Survey of Canada Surficial Geology Maps for NTS 094A and 093P**, by A.S. Hickin (Geoscience BC Map 2011-8-1 / BC Ministry of Energy and Mines, Energy Open File 2011-2)
- **Till Geochemistry of the Colleymount Map Area (093L/01), West-Central British Columbia**, by T. Ferbey (Geoscience BC Report 2011-9 / BC Geological Survey Open File 2011-06)
- **Rock Physical Property Measurements to Aid Geophysical Surveys in the Nechako Basin Oil and Gas Region, Central British Columbia**, by G. Andrews, S. Quane, R.J. Enkin, K. Russell, A. Kushnir, L. Kennedy, N. Hayward and M. Heap (Geoscience BC Report 2011-10)
- **Montney Water Project: Watershed Posters**, by Foundry Spatial Ltd. (Geoscience BC Report 2011-12)
- **Preliminary Lithological and Structural Framework of Eocene Volcanic Rocks in the Nechako Region, Central British Columbia**, by E. Bordet, C.J.R. Hart, and D. Mitchinson (Geoscience BC Report 2011-13)
- **Regional 3-D Inversion Modelling of Airborne Gravity and Magnetic Data: QUEST-South, BC, Canada**, by Mira Geoscience Ltd. (Geoscience BC Report 2011-14)
- **Regional 3-D Inversion Modelling of Airborne Gravity, Magnetic, and Electromagnetic Data, Central BC, Canada**, by Mira Geoscience Ltd. (Geoscience BC Report 2011-15)
- **The Characteristics, Origin and Exploration Potential for Sediment-Hosted Cu±Ag Mineralization in the Purcell Supergroup, Canada**, by R.P. Hartlaub, W. J. Davis and C.E. Dunn (Geoscience BC Report 2011-16)
- **Porphyry Indicator Minerals (PIMS): A New Exploration Tool for Concealed Deposits in South-Central British Columbia**, by F. Bouzari, C.J.R. Hart, S. Barker and T. Bissig (Geoscience BC Report 2011-17)

All releases of Geoscience BC reports and data are announced through our website and e-mail list. If you are interested in receiving e-mail regarding these reports and other Geoscience BC news, please contact info@geosciencebc.com.

Acknowledgments

Geoscience BC would like to thank all authors of the *Summary of Activities* papers, including project proponents, graduate students, consultants and staff, for their contributions to this volume. RnD Technical is also thanked for their work in editing and assembling this volume.

Christa Sluggett, M.Sc.
Project Geologist and Communications Co-ordinator
Geoscience BC
www.geosciencebc.com

Contents

QUEST-Northwest Projects

- Simpson, K.A.:** QUEST-Northwest: Geoscience BC's new minerals project in northwestern British Columbia. 1
- Logan, J.M., Diakow, L.J., van Straaten, B.I., Moynihan, D.P. and Iverson, O.:** QUEST-Northwest mapping: BC Geological Survey Dease Lake Geoscience Project, northern British Columbia. 5
- Jackaman, W.:** QUEST Northwest Project: new regional geochemical survey and sample reanalysis data, northern British Columbia. 15

Minerals Projects

- Devine, F.:** Porphyry Integration Project: bringing together geoscience and exploration datasets for British Columbia's porphyry districts 19
- Blaine, F.A. and Hart, C.J.R.:** Geochemical-exploration models for porphyry deposits in British Columbia 29
- Meuzelaar, T. and Monecke, T.:** Fluid controls on ore genesis in the Eskay Creek deposit, northwestern British Columbia 41
- Stumpf, A.J.:** Development of a database for geoscience field observations, west-central British Columbia 53
- Ward, B.C., Leybourne, M.I. and Sacco, D.A.:** Heavy mineral analysis of till samples within the QUEST Project area, central British Columbia 59
- Vaca, S., Bissig, T., Raudsepp, M. and Hart, C.J.R.:** Chemical variations of pyroxene and Fe-Ti-oxide crystals in basalts hosting Cu-Au porphyry mineralization in the Quesnel terrane, interior British Columbia. 69

- Höy, T. and Jackaman, W.:** Geological mapping, regional data compilation and mineral evaluation in the Burrell Creek map area, southeastern British Columbia 79

Oil and Gas Projects

- Chapman, A., Kerr, B. and Wilford, D.:** Hydrological modelling and decision-support tool development for water allocation, northeastern British Columbia 81
- Chalmers, G.R.L., Bustin, R.M. and Bustin, A.A.M.:** Geological controls on matrix permeability of the Doig-Montney hybrid shale-gas-tight-gas reservoir, northeastern British Columbia. 87
- Golding, M.L., Mortensen, J.K., Zonneveld, J-P. and Orchard, M.J.:** Biostratigraphy and sedimentary provenance of Lower and Middle Triassic natural-gas-bearing rocks in northeastern British Columbia: progress report. 97
- Henderson, C.M., Zubin-Stathopoulos, K.D. and Dean, G.J.:** Chronostratigraphic and tectonostratigraphic summary of the Late Paleozoic and Early Triassic succession in east-central British Columbia 115
- Kushnir, A., Andrews, G., Russell, J.K., Enkin, R.J., Kennedy, L.A., Heap, M.J. and Quane, S.:** Rock physical-property measurements for the Nechako Basin oil and gas region, central British Columbia 125
- Spratt, J.E., Farquharson, C.G. and Craven, J.A.:** Analysis of magnetotelluric transfer functions to determine the usefulness of ZTEM data in the Nechako Basin, south-central British Columbia 151

QUEST-Northwest: Geoscience BC's New Minerals Project in Northwestern British Columbia (NTS 104G, J, Parts of NTS 104A, B, F, H, I, K, 103O, P)

K.A. Simpson, Geoscience BC, Vancouver, BC, simpson@geosciencebc.com

Simpson, K.A. (2012): QUEST-Northwest: Geoscience BC's new minerals project in northwestern British Columbia (NTS 104G, J, parts of NTS 104A, B, F, H, I, K, 103O, P); in Geoscience BC Summary of Activities 2011, Geoscience BC, Report 2012-1, p. 1-4.

Introduction

Geoscience BC launched its latest regional project, QUEST-Northwest, in April 2011. The QUEST-Northwest area is host to a number of known mineral deposits and remains a highly prospective area for the discovery of new copper, gold, silver and molybdenum resources. The project aims to compile and update existing datasets as well as provide new geoscience data to help focus exploration. The QUEST-Northwest project coincides with the approval of the Northwest Transmission Line, which will provide critical infrastructure that will make exploration and development in this part of the province more viable and attractive.

The QUEST-Northwest project's main activities include bedrock geological mapping, a regional ground geochemical program and two airborne magnetic surveys flown at a line spacing of 250 m (Figure 1). The high-resolution airborne magnetic surveys in the north will be complemented by a compilation of existing high-quality industry airborne magnetic data in the Stewart area to the south (Figure 1). Additional projects in the QUEST-Northwest area will involve adding value to the airborne magnetic surveys and regional geochemical data as well as acquisition of new data.

Regional Bedrock Mapping

The QUEST-Northwest regional bedrock mapping program is a partnership between Geoscience BC and the British Columbia Geological Survey. Field mapping was led by the BC Geological Survey and was undertaken in July and August 2011. Mapping was undertaken at a 1:50 000 scale in the Dease Lake area (Figure 1). Additional follow-up analyses include geochronology, petrography, geochemistry and fossil identification. For more detailed information on the regional bedrock mapping program, see Logan et al. (2012). Release of the new mapping is planned for the Mineral Exploration Roundup 2012 in Vancouver, BC.

Geochemical Program

The QUEST-Northwest geochemical program involved the collection of new stream sediment and water samples as well as the reanalysis of archived samples from 1987. The new infill geochemical sampling was undertaken in August 2011 and a total of 441 stream sediment and water samples were collected. Details of the geochemical program are outlined in Jackaman (2012). Results of the new sampling will be released in late spring 2012. The results of the reanalysis (997 samples) will be released at Roundup 2012.

Geophysical Program

The QUEST-Northwest geophysical program includes two airborne magnetic surveys, in the Dease Lake and Telegraph Creek areas (Block 1 and Block 2; Figure 1). Both surveys were flown at a line spacing of 250 m, in an east-west orientation with 2500 m spaced tie lines. The flights were flown at a nominal height of 80 m above ground level. The terrain in both survey areas is rugged and varied, ranging from 400 m to more than 2000 m elevation (Figure 2). Block 1 was flown by Aeroquest Airborne (Mississauga, Ontario) using a HeliMAG stinger system. The survey covered approximately 5755 km² with a total of 25 357 line km flown. Block 2 was flown by Geo Data Solutions Inc. (Laval, Quebec), also using a HeliMAG stinger system (Figure 3). The survey covered approximately 2361 km² with a total of 11 337 line km flown. Release of the geophysical data from both surveys is planned for Roundup 2012.

In addition to the new data acquisition, a data compilation project is in development in the southern portion of the QUEST-Northwest area (Figure 1). High-quality industry airborne magnetic data exist in the Stewart area and Geoscience BC is currently investigating the possibility of compiling these datasets.

Summary

The QUEST-Northwest Project is a multidisciplinary, integrated project located in a region with a high potential for new discoveries. It currently includes the acquisition of new airborne magnetic surveys, stream sediment and water samples, and 1:50 000 mapping (and associated analytical analyses). In addition, it involves the compilation of exist-

Keywords: *airborne magnetics, geochemistry, mapping, Quesnel terrane, Stikine terrane, QUEST-Northwest Project*

This publication is also available, free of charge, as colour digital files in Adobe Acrobat® PDF format from the Geoscience BC website: <http://www.geosciencebc.com/s/DataReleases.asp>.

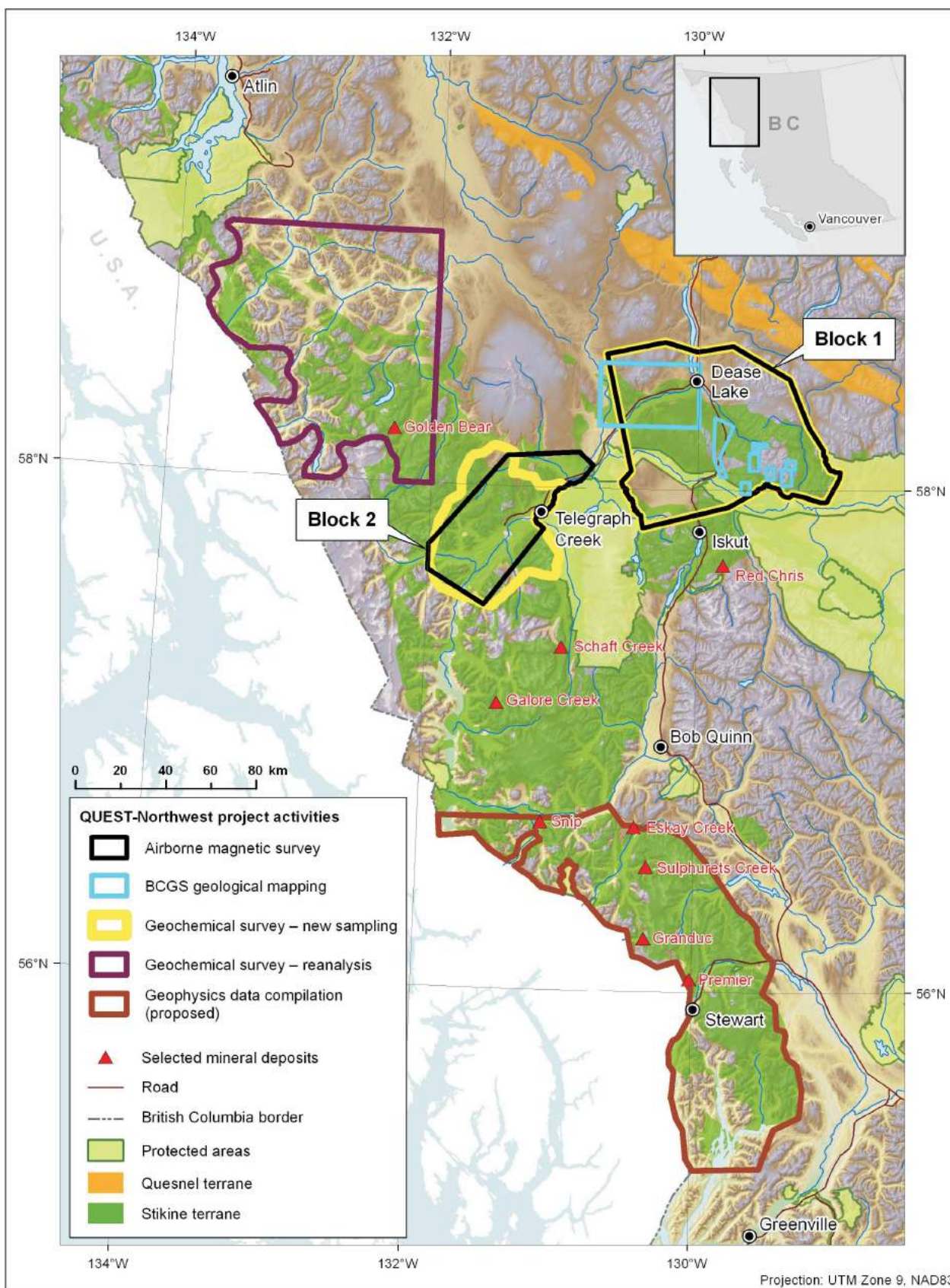


Figure 1. Geoscience BC's QUEST-Northwest Project area. The major project activities are outlined. Data from Canadian Council on Geomatics (2000), Massey et al. (2005), Natural Resources Canada (2007), Province of British Columbia (2008) and BC Geological Survey (2011).



Figure 2. Typical terrain within the Block 1 survey area, in the Dease Lake and Telegraph Creek areas. Photo courtesy of L. Luke, Aeroquest Ltd., Vancouver, British Columbia.



Figure 3. HeliMAG stinger system used by Geo Data Solutions Inc. to fly the Block 2 survey in the Dease Lake and Telegraph Creek areas. Photo courtesy of Geo Data Solutions Inc., Laval, Quebec.

ing geological and geophysical data and the reanalysis of archived geochemical samples. It is anticipated that additional studies will be undertaken to add value to, and build on, these new datasets. The results from the project will provide fundamental geoscience data to assist mineral exploration. QUEST-Northwest data will be made available on Geoscience BC's website (<http://www.geosciencebc.com/s/DataReleases.asp>) starting in early 2011.

Acknowledgments

The digital elevation model in Figure 1 was prepared by K. Shimamura and F. Ma created the final figure. Aeroquest Ltd. and Geo Data Solutions Inc. are thanked for providing images for the manuscript. The manuscript benefited from reviews by P. Kowalczyk and C. Slugett.

References

- BC Geological Survey (2011): MINFILE BC mineral deposits database; BC Ministry of Energy and Mines, URL <<http://minfile.ca/>> [May 2011].
- Canadian Council on Geomatics (2000): Canadian digital elevation data; Natural Resources Canada, GeoBase®, URL <<http://www.geobase.ca/geobase/en/data/cded/description.html>> [October 2004].
- Jackaman, W. (2012): QUEST-Northwest Project: new regional geochemical survey and sample reanalysis data, northern British Columbia (NTS 104F, G, H, I, J, K); *in* Geoscience BC Summary of Activities 2011, Geoscience BC, Report 2012-1, p. 15–18.
- Logan, J.M., Diakow, L.J., van Straaten, B.I., Moynihan, D.P. and Iverson, O. (2012): QUEST-Northwest mapping: BC Geological Survey Dease Lake Geoscience Project, northern British Columbia (NTS 104I, J); *in* Geoscience BC Summary of Activities 2011, Geoscience BC, Report 2012-1, p. 5–14.
- Massey, N.W.D, MacIntyre, D.G., Desjardins, P.J. and Cooney, R.T. (2005): Digital geology map of British Columbia: whole province; BC Ministry of Energy and Mines, GeoFile 2005-1, URL <<http://www.empr.gov.bc.ca/Mining/Geoscience/PublicationsCatalogue/GeoFiles/Pages/2005-1.aspx>> [November 2011].
- Natural Resources Canada (2007): Atlas of Canada base maps; Natural Resources Canada, Earth Sciences Sector, URL <<http://geogratis.gc.ca/geogratis/en/option/select.do?id=0BCF289A-0131-247B-FDBD-4CC70989CBCB>> [November 2011].
- Province of British Columbia (2008): TANTALIS—parks, ecological reserves, and protected areas; GeoBC (distributor), URL <<https://apps.gov.bc.ca/pub/geometadata/metadataDetail.do?recordUID=54259&recordSet=ISO19115>> [March 2011].

QUEST-Northwest Mapping: BC Geological Survey Dease Lake Geoscience Project, Northern British Columbia (NTS 104I, J)

J.M. Logan, British Columbia Ministry of Energy and Mines, Victoria, BC, Jim.Logan@gov.bc.ca

L.J. Diakow, British Columbia Ministry of Energy and Mines, Victoria, BC

B.I. van Straaten, British Columbia Ministry of Energy and Mines, Victoria, BC

D.P. Moynihan, University of Calgary, Calgary, AB

O. Iverson, University of Wisconsin–Eau Claire, WI, USA

Logan, J.M., Diakow, L.J., van Straaten, B.I., Moynihan, D.P. and Iverson, O. (2012): QUEST-Northwest mapping: BC Geological Survey Dease Lake Geoscience Project, northern British Columbia (NTS 104I, J); *in* Geoscience BC Summary of Activities 2011, Geoscience BC, Report 2012-1, p. 5–14.

Introduction

The British Columbia Geological Survey Dease Lake Geoscience Project is part of the Geoscience BC's QUEST-Northwest initiative, a program launched in 2011 to stimulate exploration in the northwestern part of the province along Highway 37 (Figure 1). Geoscience BC has committed \$3.25 million in funding to provide two high-resolution (with a line spacing of 250 m) airborne magnetic surveys, a collection and analysis of new regional stream sediment samples, a reanalysis of stream sediment samples and the new bedrock mapping described in this paper. The 2011 program of bedrock mapping and mineral deposit studies undertaken by the BC Geological Survey, with involvement from the University of Wisconsin–Eau Claire, is complementary to the geophysical and geochemical programs directly administered through Geoscience BC (see Jackaman, 2012 and Simpson, 2012). Collectively, these programs will provide detailed, high-quality geoscience data that is intended to enhance metallic mineral exploration in an area of prospective geology adjacent to Highway 37, near Dease Lake, in northern British Columbia.

The Dease Lake study area is situated within the Stikine terrane, an extensive subduction-generated island arc magmatic system responsible for recurring calcalkaline and/or alkaline plutonic events and associated Cu-Au mineralization, mainly during Late Triassic and Early Jurassic. Prospective Mesozoic volcanic rocks exposed around the margins of the Bowser Basin form an arcuate belt containing

porphyry deposits that include KSM (MINFILE 104B 103; BC Geological Survey, 2011), Galore (MINFILE 104G 090) and Schaft Creek (MINFILE 104G 015) deposits to the west and the Kemess deposits (MINFILE 094E 094) to the east. The Dease Lake study area is located at the apex of this arcuate belt, immediately north of the Red Chris Cu-Au porphyry deposit (MINFILE 104H 005) and also adjacent to the Hotailuh batholith, a large composite intrusive complex similar in age to the intrusions hosting porphyry mineralization at the Galore and Schaft Creek deposits.

Numerous small plutons project through mainly Late Triassic arc stratigraphy in the Dease Lake area. Neither the plutons nor the volcanosedimentary rocks have undergone a thorough regional geological re-evaluation for mineral potential since being mapped by the Geological Survey of Canada in the late 1970s and early 1980s (Gabrielse, 1980; Anderson, 1983, 1984). Modern detailed bedrock mapping is essential to characterize and refine time-space relationships of this arc segment around Dease Lake to assess significance for mineralization, comparison with mineralized arc segments elsewhere and integration with the airborne magnetic program. In addition, the project will provide supplementary databases including rock geochemical classification, magnetic susceptibility and geochronology. These data will integrate with Regional Geochemical Survey (RGS) data and airborne geophysics to ensure cost-effective exploration targeting porphyry-style mineralization.

In 2011, the BC Geological Survey completed four field-based geology studies located within a 70 km radius of the Dease Lake community (Figure 1b). These standalone components collectively make up the Dease Lake Geoscience Project, and they consist of

- Dease Lake regional bedrock mapping;
- Hotailuh batholith: intrusive phases, ages and related mineralization;

Keywords: *QUEST-Northwest mapping, Geoscience BC, regional bedrock mapping, integrated multidisciplinary studies, geochemistry, Cu-Au metallogeny, molybdenite, Triassic, Jurassic, Cretaceous, plutonism, Tsaybahe, Stuhini, Hotailuh, Snow Peak, target generation, GIS*

This publication is also available, free of charge, as colour digital files in Adobe Acrobat® PDF format from the Geoscience BC website: <http://www.geosciencebc.com/s/DataReleases.asp>.

- Snow Peak pluton: age, emplacement and molybdenum mineralization; and
- Tsaybahe group: lithological and geochemical characterization of Middle Triassic volcanism.

Regional Geology and Previous Work

Kerr (1925; 1948) carried out the earliest geological bedrock mapping surveys in the area around Dease Lake. Systematic regional mapping by the Geological Survey of Canada began in 1956 with Operation Stikine, a reconnaissance mapping program covering four adjoining 1:250 000 map areas in northwestern BC (Geological Survey of Canada, 1957). Mapping and thematic studies conducted between 1956 and 1991 in the NTS 104I and 104J map areas are summarized by Gabrielse (1998). Most relevant to the current study is Anderson's work on the Hotailuh and Stikine batholiths (1983; 1984) and, more recently, 1:250 000 scale geological mapping of the Iskut River area (Anderson, 1993). P. Read of Geotex Consultants Ltd. (Vancouver, British Columbia) has conducted detailed mapping for the Geological Survey of Canada in the Stikine Canyon area (Read, 1983, 1984; Read and Psutka, 1990). Regional mapping projects by the BC Geological Survey include work to the south by Ash et al. (1997) around Tatogga Lake and farther west by Brown et al. (1996) in the Stikine River area.

The Dease Lake map area straddles the early Middle Jurassic thrust-imbricated boundary between the Cache Creek and Stikine terranes (Figure 2). At this latitude, the Stikine terrane comprises three overlapping island arc successions, which span 200 m.y. from Devonian to Middle Jurassic and include Stikine, Stuhini and Hazelton volcanic and sedimentary rocks. Their genetically related plutonic suites include the Devonian-Carboniferous Forrest Kerr, the Late Triassic Stikine and Copper Mountain, the Early Jurassic Texas Creek and the Middle Jurassic Three Sisters (Anderson, 1983, 1993; Brown et al., 1996; Logan et al., 2000). These plutonic suites are the roots of cospatial arc rocks exposed along the Stikine arch, an east-trending area of uplifted Jurassic and older rocks that bound the northern margin of the Bowser Basin. Long-lived arc magmatism in the Stikine arch has produced diverse styles of magmatism (calcalkaline and alkaline) and large Cu–Au–Ag±Mo mineral deposits associated with some intrusive centres (i.e., KSM, Snip [MINFILE 104B 004], Galore Creek, Schaft Creek and Kemess).

The Cache Creek terrane, lying north of the King Salmon fault (KSF), consists of oceanic basalt, siliciclastic rocks and limestone of Carboniferous to Early Jurassic age. The terrane for the most part is overlain by Jurassic clastic sediments of the Inklin Formation comprising the southeastern extent of the Whitehorse Trough.

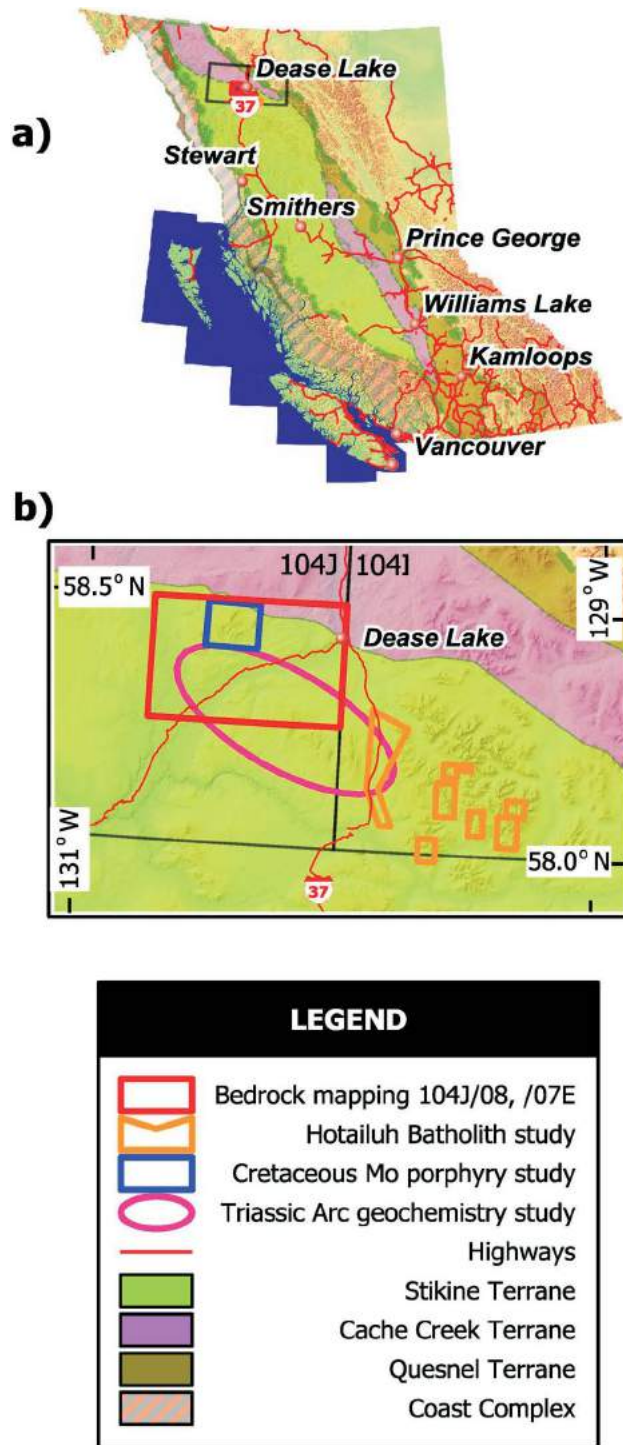


Figure 1. Location of the QUEST-Northwest mapping: British Columbia Geological Survey Dease Lake Geoscience Project on the a) BC terrane map (after Massey et al., 2005); b) detailed view straddles NTS 104J and 104I 1:250 000 map areas at Dease Lake, showing the locations of the bedrock mapping study (NTS 104J/08, /07E), the Hotailuh batholith study, the Snow Peak pluton study and the Triassic arc geochemistry study.

Project Objectives and Results to Date

The Dease Lake Geoscience Project consists of a systematic bedrock mapping study and three integrated topical studies. Together they cover regional aspects of stratigraphy, magmatic evolution and metallogeny along part of the Stikine arch and also within the broader footprint of the QUEST-Northwest airborne geophysical survey (Simpson, 2012).

Dease Lake Regional Bedrock Mapping

The main component, systematic regional bedrock mapping of the NTS 104J/08 and the east half NTS 104J/07 map areas was delivered with the following objectives:

- publishing 1:50 000 scale geological maps for 104J/08 and the east half of NTS 104J/07, a cumulative area of 1275 km², located immediately west of Dease Lake;
- determining U-Pb and Ar-Ar ages for layered and intrusive rock units as well as mineralized rocks in order to constrain magmatic and mineralizing events;
- establishing the geological controls for mineralized rocks, then comparing these regionally to metallogenic epochs between 220 and 190 Ma (i.e., Late Triassic [Cu–Mo±Au], Late Triassic to Early Jurassic [Cu–Au–Ag] and Cretaceous to Tertiary [Cu–Mo–W]), related to alkaline and calcalkaline plutonism known elsewhere in the Stikine terrane;

- determining the history of magmatism, tectonism and mineralization along the Dease Lake transect for comparison to other parts of the Stikine magmatic arc system.

Results

Regional-scale geological mapping was completed over a 1275 km² area extending southwest from the community of Dease Lake to the Tuya River during the 2011 summer field season. The map area includes NTS 104J/08 and the east half of NTS 104J/07 (Figure 3). Traverses were helicopter supported.

The map is underlain mainly by Paleozoic to Late Triassic sedimentary, volcanic and plutonic arc rocks of the Stikine terrane. In the northeastern part of the map, these are thrust imbricated with similarly aged volcanic and sedimentary oceanic rocks of the Cache Creek terrane along the north-dipping King Salmon fault. Early–Middle Jurassic sedimentary rocks of the Takwahoni and Inklin formations of the Whitehorse Trough overlie the Stikine and Cache Creek terrane rocks, respectively. An equidimensional Late Cretaceous granite intrudes the Early Jurassic Takwahoni sedimentary rocks, and columnar basalts of the Miocene–Pliocene Tuya Formation unconformably cap some of the highest peaks in the area. Preserved beneath these young basalts in the southwestern corner of the map are lower Ter-

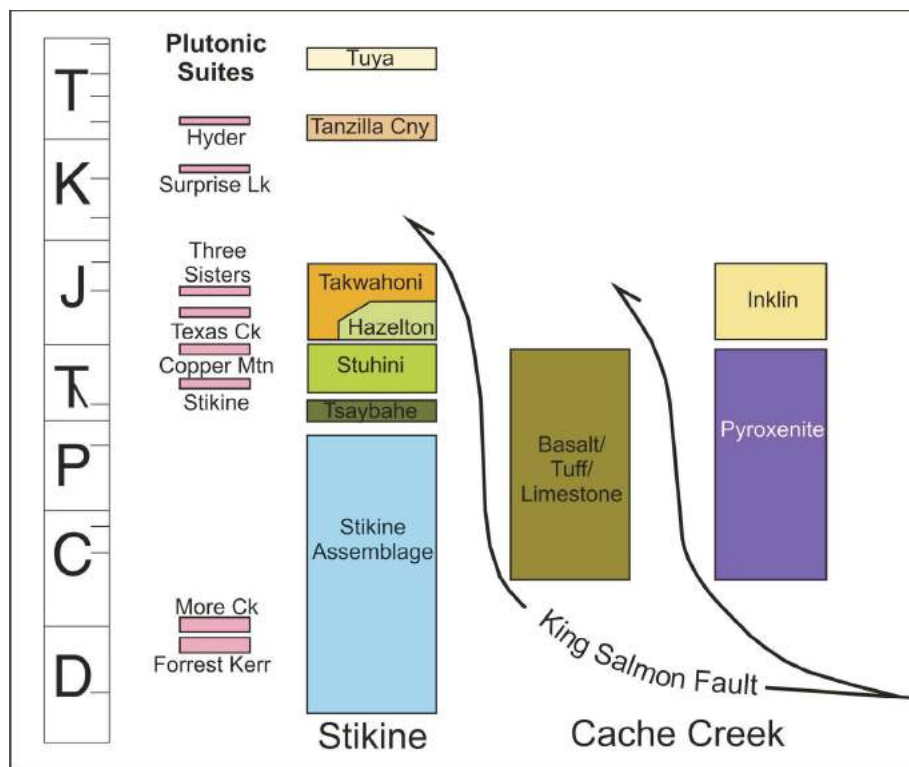


Figure 2. Schematic stratigraphic, plutonic and structural relationships for Stikine and Cache Creek terrane rocks within the map area (Abbreviations: Ck, creek; Cny, canyon; Mtn, mountain).

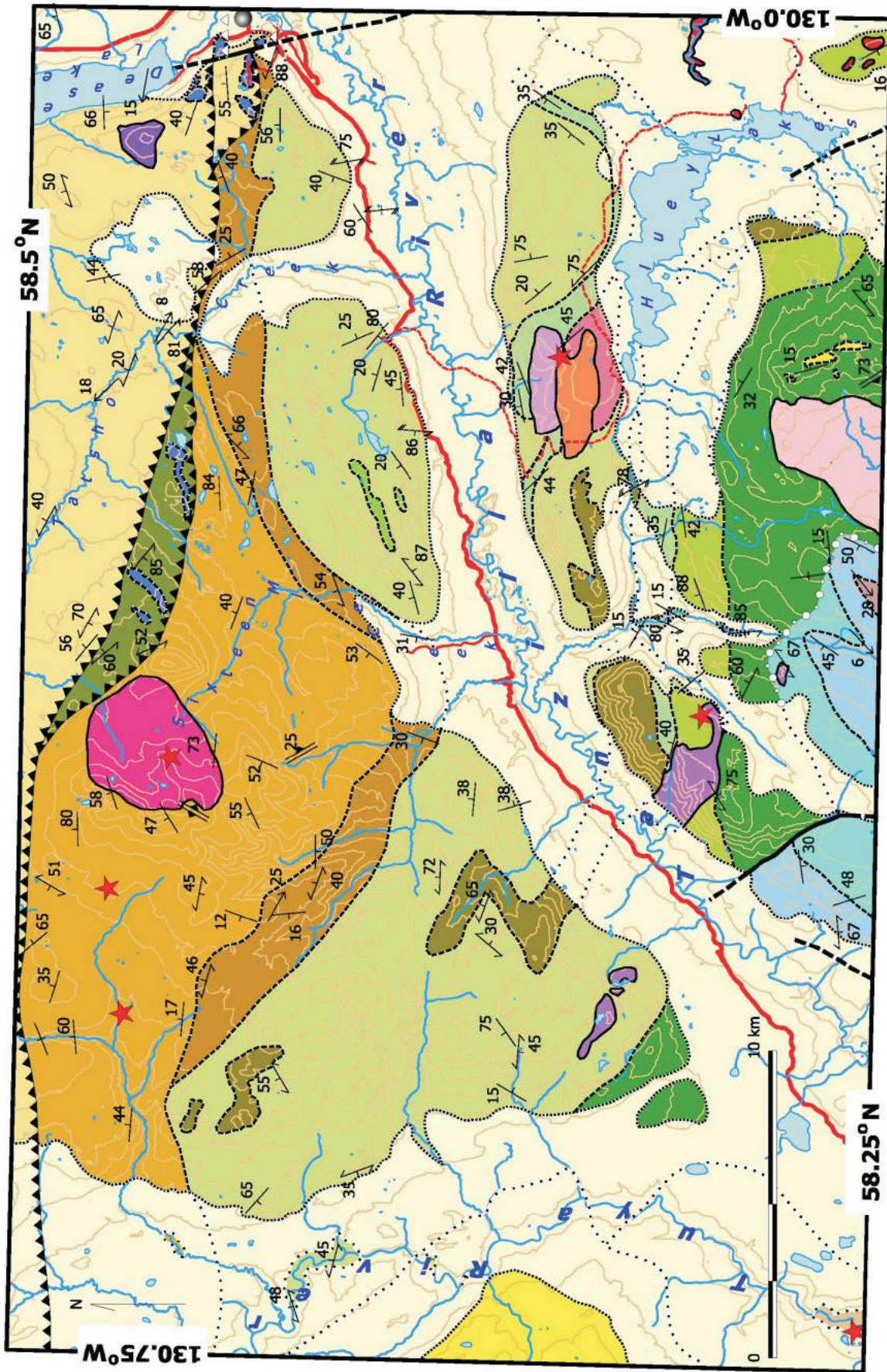


Figure 3. Generalized geology of the NTS 104J/08 and the east half of NTS 104J/07E map areas, including work by Ryan (1991) and Gabrielse (1998). Abbreviations: bio, biotite; brcc, breccia; congl, conglomerate; crse, coarse; hnb1, hornblende; monzn, monzonite; mudstn, mudstone; plag, plagioclase; px, pyroxene; qtz, quartz; sndst, sandstone; siltst, siltstone; xstf, crystal.

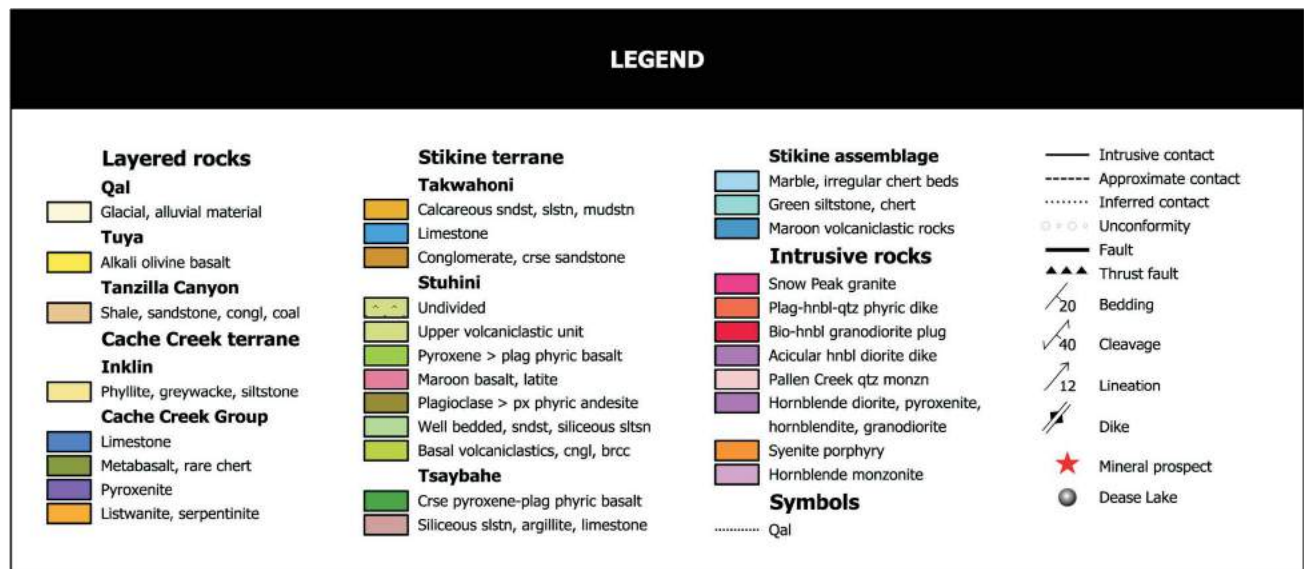
tiary coal-bearing sediments of the Tanzilla Canyon Formation.

South of the King Salmon fault, the oldest rocks in the map area are Permian limestone, phyllite, chert and metavolcanic rocks exposed in north- to northeasterly trending structural culminations (Figure 3). Despite generally poor exposures throughout the map area, a general stratigraphy can be recognized for the Triassic Stuhini Group, which in one locale (the headwaters of Itsillitu Creek) appears to unconformably overlie foliated limestone, chert and metavolcanic rocks of presumed late Paleozoic age. Here, the stratigraphic base comprises volcanoclastic beds and coarse pyroxene breccias. Early work on adjoining map areas to the south (Read, 1983, 1984) reported Early and Middle Triassic paleontological ages from cherty sedimentary rocks and coarse pyroxene breccias of the Tsaybahe group. However, no direct age constraints are known for the overlying pyroxene breccias in the current study area, which are characterized by thick accumulations of crowded augite-phyric basalt breccias and clastic volcanic rocks exposed at the tops of the ridges in the southern part of the map. These correlative Tsaybahe group basalt breccias dip north below a thick pile of mixed, bedded and reworked volcanoclastic rocks and rare basalt flows that generally fined upward into a well-bedded siliceous section of siltstone with Upper Triassic (?) bivalves. These are overlain by a thick package of coarse plagioclase-phyric andesitic basalt flows, in turn overlain by more massive plagioclase- and pyroxene-dominated volcanoclastic units (Stuhini?) identical to the thick-bedded volcanoclastic units that overlie the Tsaybahe group basalts. The uppermost Triassic volcanoclastic and flow unit is unconformably (?) overlain by quartz-bearing conglomerate and sandstone rocks of the Early Jurassic Takwahoni Formation.

North of the King Salmon fault are structurally imbricated north-dipping panels of Cache Creek rocks that comprise the King Salmon allochthon (Figures 2, 3). The structurally lowest panel consists of massive metabasite, tuff and limestone of presumed Carboniferous–Permian age and is marked along its structural hangingwall contact by serpentinized ultramafic rocks and zones of listwanite alteration. The latter is characterized by dun- to orange-weathering foliated zones containing various amounts of chrome-rich mica, quartz veining and often pyrite. Structurally overlying this panel and comprising the northeastern portion of the map area are fine-grained, well-bedded and variably foliated clastic rocks of the Inklin Formation. Within this panel and west of the south end of Dease Lake are a large pyroxenite body and three west-trending large outcrops of recrystallized massive limestone correlated with the Upper Triassic Sinwa limestone (Gabielse, 1998).

Two stages of deformation affect rocks within the map: the earlier is characterized by northwest-trending, southwest-verging folds and faults associated with the King Salmon fault. This deformation is related to the early Middle Jurassic obduction of the Cache Creek terrane onto the Stikine terrane. The later deformational event is characterized by north-trending structures that gently warp the earlier northwest-trending structures and fold rocks as young as Tertiary (Ryan, 1991).

Metallic mineral occurrences within the map area include two alkalic porphyry Cu-Au prospects located south of the Tanzilla River in massive volcanoclastic rocks of the Stuhini Group, a porphyry Mo-Cu-W prospect (Mack; MINFILE 104J 014) within the Cretaceous Snow Peak pluton that intruded Takwahoni sediments near the headwaters of Sixteen Mile Creek, and a Ag–Pb–Zn±Au quartz vein showing (Mac; MINFILE 104J 064) associated with



dikes cutting Takwahoni sedimentary rocks west of the Mack prospect. The Hu alkalic porphyry Cu-Au prospect (MINFILE 104J 013) is associated with an east-trending multiphase syenite-monzonite intrusion adjacent to the Hleuy Lake Hydroelectric Power Station and the Tan showing (MINFILE 104J 036) is related to a southeast-trending composite pyroxenite-amphibolite-monzonite body. Geochemical and assay samples (n = 15) characterizing base- and precious-metal mineralization have been collected and submitted for analyses at Acme Labs in Vancouver, British Columbia and will be reported in the BC Geological Survey's Geological Fieldwork 2011 volume (Logan et al., 2012).

Along Tuya Creek, at the southwestern margin of the map (Figure 3), between 5 to 30 m of high volatile B bituminous coal occurs within the Lower Tertiary, Paleocene sediments of the Tuya River coal basin (Ryan, 1991). This area was not visited during the current mapping program.

In addition to collecting lithological descriptions, structure data and geochemical and assay rock samples, magnetic susceptibilities were routinely collected for stratified and plutonic rocks from the map areas. This data provides rock-type-specific characterization and ground-truthing capabilities to interpret the airborne magnetic survey results.

Isotopic age dating is currently underway to provide constraints on volcanic, plutonic and mineralizing events. Eleven samples have been submitted for U-Pb, zircon crystallization age determinations by laser ablation inductively coupled plasma-mass spectrometry (ICP-MS) and eight samples for Ar-Ar step heating on hornblende and biotite separates. These data will be reported on as results are received. In addition, two detrital zircon samples will be analyzed to complement other samples of the Tsaybahe group collected in the Tsaybahe study (Iverson and Mahoney, 2012).

Detrital zircon samples were collected from medium-grained sandstone in a Stuhini volcanoclastic member, and from the basal section of the Takwahoni Formation. They will be used to evaluate the uplift and evolution of sediment source regions and complement the stratigraphy determined from field mapping. These results compared to detrital zircons recovered from the Tsaybahe study (Iverson and Mahoney, 2012) will test if the Stuhini Group is significantly younger than rocks assigned to the Tsaybahe group.

Hotailuh Batholith: Intrusive Phases, Ages and Related Mineralization

The Hotailuh batholith study, led by B. van Straaten, focuses on the magmatic evolution and mineral potential of the Triassic-Jurassic Hotailuh batholith and its surrounding volcanosedimentary rocks. The Hotailuh batholith is well exposed in a 2275 km² area southeast of Dease Lake

and mainly east of Highway 37. The batholith coincides with approximately one third of the QUEST-Northwest Block 1 airborne geophysical survey (Simpson, 2012) and contains a wide variety of intrusion-related mineral occurrences including the Gnat Pass porphyry Cu developed prospect (Figure 1). The objectives of this project include

- further developing the temporal magmatic and geochemical evolution of the Hotailuh batholith and refining the geochronology (U-Pb) of magmatic events and the geochemistry of plutons;
- establishing the formation and preservation potential for magmatic-hydrothermal mineral deposits within the batholith;
- reconstructing the pressure, temperature, time and deformation (P-T-t-D) history of plutonic suites using geothermobarometry, geochronology and thermochronology; and
- building a metallogenic framework that relates mineralizing and magmatic events.

Results

Nine weeks of fieldwork by two people covered an area of 30 × 40 km, focused on mapping within the mineralized Gnat Pass corridor and seven smaller areas (Figure 1) chosen for their association with mineral occurrences and suitability for understanding the internal geology of the batholith. The Hotailuh batholith comprises three distinct plutonic suites (Anderson, 1983; Anderson and Bevier, 1990): the Late Triassic Stikine (Cake Hill, Beggerlay Creek and Gnat Lake plutons), the Early Jurassic Texas Creek (McBride River pluton) and the Middle Jurassic Three Sisters (Three Sisters pluton; Figure 2, Table 1). Each plutonic suite generally consists of several individual plutons and/or plutonic phases. The crosscutting relationships between plutonic suites established by Anderson

Table 1. Ages of plutonic suites and composition of plutons comprising the Hotailuh batholith.

Age	Pluton	Lithology
Middle Jurassic	Three Sisters, potassic phase	Biotite quartz syenite, granite
	Three Sisters, central phase	Biotite quartz monzonite, quartz monzodiorite
	Three Sisters, mafic phase	Acicular hornblende diorite
	Three Sisters, fine-grained phase	Hornblende diorite
Early Jurassic	McBride River	Hornblende granodiorite
Late Triassic	Beggerlay Creek	Hornblende-rich diorite/gabbro
	Cake Hill	Hornblende quartz monzodiorite, quartz monzonite
	Gnat Lake	Plagioclase-bearing ultramafic

(1983) were mostly confirmed in this study; however, a notable exception is the Gnat Lake ultramafite, which is cross-cut by Cake Hill dikes at one location (van Straaten, 2012). Contact relationships between the Late Triassic (?) Beggerlay Creek and Cake Hill plutons was not observed, nor was the relationship between the apparently oldest fine-grained mafic phase of the Three Sisters pluton with any younger phases, due to the lack of exposed contacts. However, several external contact relationships were (re)defined. For example, the plutonic rocks that contact metamorphosed Toarcian sediments were previously assigned to the Late Triassic Cake Hill, but they are more likely related to the McBride River pluton. Also, the predominantly mafic Beggerlay Creek pluton was shown to comprise several ultramafic domains that resemble the Gnat Lake ultramafite. Litho-geochemistry and geochronology is underway to test this suggestive genetic link between the Beggerlay Creek and Gnat Lake bodies.

Results of the field program include 331 field stations and 134 samples collected for follow-up study and analysis. Five mineral showings were visited (Gnat Pass [MINFILE 104I 001], BCR [MINFILE 104I 068], Pat [MINFILE 104I 043], Mat [MINFILE 104I 034] and Dalvenie [MINFILE 104I 003]). Fieldwork also resulted in the discovery of seven new mineralized and altered zones within the Hotailuh batholith. Mineralized samples were collected and submitted for base- and precious-metal analyses; results are pending. Four of the new zones are hosted in Late Triassic rocks and include 1) a 10 cm wide vein of massive pyrite with trace copper in the Cake Hill pluton close to Highway 37; 2) metre-scale zones of disseminated pyrite and bornite in the Cake Hill pluton 3 km northeast of the Mat showing; 3) several percent disseminated pyrite in narrow zones within the Gnat Lakes ultramafite; and 4) pyritic fault zones cutting a large Stuhini inclusion within the Cake Hill pluton, approximately 9 km north-northwest of the McBride–Stikine river confluence. The remaining three zones are hosted in Middle Jurassic intrusive rocks and include quartz+pyrite±copper sulphide veins located 1) approximately 5 km southwest of the Pat showing, 2) on the northern edge of the Three Sisters fine-grained body, and 3) approximately 3 km north of the Three Sisters fine-grained body (van Straaten, 2012).

The presence of mineralization in both the Late Triassic (Cake Hill) and Middle Jurassic (Three Sisters) rocks is suggestive of at least two mineralizing events within the Hotailuh batholith. Based on current observation within the batholith, the ca. 171 Ma Three Sisters intrusions apparently host more mineral showings than the ca. 221 Ma Cake Hill intrusions.

The Cake Hill pluton is overlain nonconformably by Upper Triassic and younger rocks (Anderson, 1983; Gabrielse, 1998), suggesting uplift and erosion following its emplace-

ment but prior to the end of Late Triassic arc magmatism and later intrusion by Middle Jurassic Three Sisters plutonism. The determination of relative pluton emplacement depths and subsequent exhumation levels have important implications for the formation and preservation potential of porphyry and epithermal deposits. Hornblende geothermobarometry and zircon thermochronology on a select suite of plutonic rocks associated with mineral prospects will be used to assess depth of emplacement and levels of erosion.

Snow Peak Pluton: Age, Emplacement and Mineralization

Late Cretaceous Mo and Cu-Mo mineralization is a well-established Cordilleran-wide metallogenic event. At Snow Peak, sedimentary rocks of the Jurassic Takwahoni Formation are intruded by pre-, syn- and postkinematic porphyry dikes and a circular Cretaceous granitoid. Porphyry Cu-Mo mineralization is present in the Cretaceous Snow Peak pluton and evaluating the magma evolution, emplacement depth and controls on mineralization was the focus of D. Moynihan's fieldwork (Moynihan, 2012). The objectives of his research include

- establishing the age relationships between the Cretaceous Snow Peak pluton and spatially associated minor intrusions; and
- characterizing the molybdenite mineralization associated with Cretaceous magmatism at the Snow Peak (i.e., Mack) prospect.

Results

The Snow Peak pluton is a steep-sided 15 km² equidimensional body that was intruded into Early Jurassic rocks of the Takwahoni Formation in the Late Cretaceous. The intrusion is a biotite-hornblende monzogranite to quartz monzonite with equigranular and locally K-feldspar–phyric textures. Molybdenite mineralization is developed along west-northwest-trending brittle fracture planes in the central part of the pluton.

The Takwahoni Formation adjacent to the Snow Peak pluton hosts a swarm of dikes and sills, many of which are hornblende-bearing plagioclase porphyry with distinctive round quartz phenocrysts. Field relations indicate that the dike swarm is crosscut by the pluton, suggesting dikes may have a separate origin unrelated to the pluton and its Mo-Cu mineralization. The U-Pb and Re-Os geochronology is currently being undertaken to establish absolute ages of the pluton, the dike swarm and Mo mineralization.

Intrusion of the Snow Peak pluton led to the formation of a contact metamorphic aureole in surrounding rocks of the Takwahoni Formation. The aureole is manifested in a rusty zone of hornfelsed rock, often with a purple tint. Contact metamorphic biotite is developed over a broad area, and adjacent to the contact, metasiltstone and mudstone have been

converted to spotted hornfels with abundant cordierite porphyroblasts. Cordierite-bearing assemblages indicate low-pressure metamorphism, and petrological work is in progress to provide quantitative constraints on the emplacement depth.

Depositional Setting and Geochemical Evolution of Tsaybahe and Stuhini Volcanism

A final study undertaken by O. Iverson will compare lithostratigraphic features and geochemical data collected from several reference stratigraphic sections through the Middle Triassic Tsaybahe group and the Late Triassic Stuhini Group. This research aims to test the consanguinity of these superposed stratigraphic successions, potentially providing insight on earliest deposition and evolution of the Triassic arc magmatism in the Stikine arch.

In the vicinity of the Stikine Canyon, the Tsaybahe group (Read, 1984; Read and Psutka, 1990) was named informally for sedimentary and volcanic rocks characterized by abundant coarse pyroxene-phyric breccias and Early and Middle Triassic fossils. They distinguished it from the Stuhini Group, which they characterized as being primarily sedimentary and Late Triassic in age. Subsequent workers (Gabrielse, 1998; Evenchick and Thorkelson, 2005) could not distinguish the volcanic and sedimentary rocks of the Tsaybahe group from those of the Stuhini Group on a regional basis and therefore consigned all Triassic units to the Stuhini Group.

Iverson collected rock samples from both stratigraphic packages as part of a B.Sc. thesis supervised by Mahoney at the University of Wisconsin. The objectives of her research include

- comparing litho-geochemical features of Tsaybahe and Stuhini group volcanic rocks; and
- proposing a model for deposition of the Tsaybahe group and its relationship to the Stuhini Group.

Results

Litho-geochemical samples of the Tsaybahe group ($n = 22$, primarily clinopyroxene-phyric basalt), the Stuhini Group (mixed pyroxene-phyric, plagioclase-phyric, alkalic latite, $n = 17$) and the Hazelton Group (plagioclase-phyric andesite, $n = 1$) volcanic rocks were collected during the course of the mapping following the unit designations of Read and Psutka (1990), Gabrielse (1998) and this study.

Detrital zircon samples were collected from fine-grained sediments located structurally and stratigraphically below the coarse clinopyroxene-phyric breccias of the Tsaybahe group at two locations: 5 km east of Gnat Pass and 2 km east of Tsenaglode Lake. The former sample was collected from a quartz-bearing tuffaceous horizon recognized within a well-bedded, 800 m thick section of dark siltstone, sandstone and lesser conglomerate that underlies the volcanic

rocks. East of Tsenaglode Lake, similar fine-grained siltstone and sandstone underlie a 200 m thick pile of coarse pyroxene-phyric breccias but here the contact is intruded and the sediments are contact metamorphosed by Middle Jurassic (?) monzonite.

Chemical analyses of the volcanic samples and heavy mineral separation for detrital zircon studies of interlayered sedimentary horizons are currently underway at the University of Wisconsin. The results of these studies together with a stratigraphy and environment of deposition constitute Iverson's thesis study (Iverson and Mahoney, 2012).

Conclusions

The BC Geological Survey Dease Lake Geoscience Project is part of the new QUEST-Northwest project initiated by Geoscience BC. The program consists of four field-based integrated research projects designed to investigate the stratigraphy, magmatic evolution and metallogeny along the Stikine arch in the vicinity of Dease Lake. The project was initiated in the summer of 2011 and results of the mapping project will be released as a Geoscience BC Report and a BC Geological Survey open file. Preliminary accounts of the integrated research projects will also be published in BC Geological Survey's Geological Fieldwork 2011 volume.

Acknowledgments

The authors acknowledge contributions from many people regarding various aspects of this study. Discussions with M. Mihalyuk and G. Nixon of the BC Geological Survey and B. Anderson of the Geological Survey of Canada were important at the inception stage and ongoing phases of the study and are much appreciated. Capable and enthusiastic assistance throughout the 2011 field season was provided by T. McCarron, C. Young and M. Hogg. The co-operation and free discussion of geological ideas with various mineral exploration companies made this study possible from its earliest stage. Safe and courteous flying by Pacific Northwest Helicopters in Dease Lake was the norm and was much appreciated.

P. McIntosh is thanked for opening her home and ranch for the team's use during the summer mapping project and for providing two gracious hosts: cook J. Anderson and bull cook and local historian D. Callison.

Geoscience BC provided financial support for the field and analytical programs, and salary support for B.I. van Straaten, D. Moynihan, O. Iverson and the field assistants.

References

- Anderson, R.G. (1983): Geology of the Hotailuh batholith and surrounding volcanic and sedimentary rocks, north-central British Columbia; Ph.D. thesis, Carleton University, 669 p.
- Anderson, R.G. (1984): Late Triassic and Jurassic magmatism along the Stikine arch and the geology of the Stikine batholith, north-central British Columbia; *in* Current Research, Part A, Geological Survey of Canada, Paper 84-1A, p. 67–73.
- Anderson, R.G. (1993): A Mesozoic stratigraphic and plutonic framework for northwestern Stikinia (Iskut River area), northwestern British Columbia, Canada; *in* Mesozoic Paleogeography of the Western United States — Part II, G. Dunne and K. McDougall (ed.); Society of Economic Paleontologists and Mineralogists, v. 71, p. 477–494.
- Anderson, R.G. and Bevier, M.L. (1990): A note on Mesozoic and Tertiary geochronometry of plutonic suites, Iskut River area, northwestern British Columbia; *in* Current Research, Part A, Geological Survey of Canada, Paper 90-1E, p. 141–147.
- Ash, C.H., Macdonald, R.W.J., Stinson, P.K., Fraser, T.M., Nelson, K.J., Arden, K.M. and Lefebure, D.V. (1997): Geology and mineral occurrences of the Tatogga Lake area; BC Ministry of Energy and Mines, Open File 1997-3, URL <<http://www.empr.gov.bc.ca/Mining/Geoscience/PublicationsCatalogue/OpenFiles/1997/Pages/1997-3.aspx>> [November 2011].
- BC Geological Survey (2011): MINFILE BC mineral deposits database; BC Ministry of Energy and Mines, URL <<http://minfile.ca>> [November 2011].
- Brown, D.A., Gunning, M.H. and Greig, C.J. (1996): The Stikine Project: geology of Western Telegraph Creek map area, northwestern British Columbia; BC Ministry of Energy and Mines, Bulletin 95, 176 p, URL <<http://www.empr.gov.bc.ca/Mining/Geoscience/PublicationsCatalogue/BulletinInformation/BulletinsAfter1940/Pages/Bulletin95.aspx>> [November 2011].
- Evenchick, C.A. and Thorkelson, D.J. (2005): Geology of the Spatsizi River map area, north-central British Columbia; Geological Survey of Canada, Bulletin 577, 276 p.
- Gabrielse, H., Monger, J.W.H., Leaming, S.F., Anderson, R.G. and Tipper, H.W. (1980): Geology of Dease Lake (104J) map-area, northwestern British Columbia; Geological Survey of Canada, Open File 707.
- Gabrielse, H. (1998): Geology of Cry Lake and Dease Lake map areas, north-central British Columbia; Geological Survey of Canada, Bulletin 504, 147 p.
- Geological Survey of Canada (1957): Operation Stikine; Geological Survey of Canada, Map 9-1957.
- Iverson, O. and Mahoney, B. (2012): Tsaybahe Group – lithological and geochemical characterization of Middle Triassic volcanism; *in* Geological Fieldwork 2011, BC Ministry of Energy and Mines, Paper 2012-1.
- Jackaman, W. (2012): QUEST-Northwest Project: new regional geochemical survey and sample reanalysis data, northern British Columbia (NTS 104F, G, H, I, J); *in* Geoscience BC Summary of Activities 2011, Geoscience BC, Report 2012-1, p. 15–18.
- Kerr, F.A. (1926): Dease Lake area, Cassiar District British Columbia; Geological Survey of Canada, Map 2104.
- Kerr, F.A. (1948): Lower Stikine and Iskut River areas, British Columbia; Geological Survey of Canada, Memoir 246, 94 p.
- Logan, J.M., Drobe, J.R. and McClelland, W.C. (2000): Geology of the Forrest Kerr-Mess Creek area, northwestern British Columbia (NTS 104B/10, 15 & 104G/2 & 7W); BC Ministry of Energy and Mines, Bulletin 104, 163 p., URL <<http://www.empr.gov.bc.ca/Mining/Geoscience/PublicationsCatalogue/BulletinInformation/BulletinsAfter1940/Pages/Bulletin104.aspx>> [November 2011].
- Logan, J.M., Moynihan, D.P. and Diakow, L.J. (2012): Geology and mineralization of the Dease Lake (104J/8) and east-half of the Little Tuya River (104J/7E) map sheets; *in* Geological Fieldwork 2011, BC Ministry of Energy and Mines, Paper 2012-1.
- Massey, N.W.D., MacIntyre, D.G., Desjardins, P.J. and Cooney, R.T. (2005): Digital geology map of British Columbia: whole province; BC Ministry of Energy and Mines, GeoFile 2005-1, URL <<http://www.empr.gov.bc.ca/Mining/Geoscience/PublicationsCatalogue/GeoFiles/Pages/2005-1.aspx>> [November 2011].
- Moynihan, D.P. (2012): Age, emplacement and mineralization of the Cretaceous Snow Peak pluton; *in* Geological Fieldwork 2011, BC Ministry of Energy and Mines, Paper 2012-1.
- Read, P.B. (1983): Geology, Classy Creek (10J/2E) and Stikine Canyon (104J/1W), British Columbia; Geological Survey of Canada, Open File 940.
- Read, P.B. (1984): Geology Klastline River (104G/16E), Ealue Lake (104H/13W), Cake Hill (104I/4W), and Stikine Canyon (104J/1E), British Columbia; Geological Survey of Canada, Open File 1080.
- Read, P.B. and Psutka, J.F. (1990): Geology of Ealue Lake east-half (104H/13E) and Cullivan Creek (104H/14) map areas, British Columbia; Geological Survey of Canada, Open File 2241.
- Ryan, B. (1991): Geology and potential coal and coalbed methane resource of the Tuya River coal basin (104J/2, 7); *in* Geological Fieldwork 1990, BC Ministry of Energy and Mines, Paper 1991-1, p. 419–432, URL <<http://www.empr.gov.bc.ca/Mining/Geoscience/PublicationsCatalogue/Fieldwork/Documents/1990/419-430-ryan.pdf>> [November 2011].
- Simpson, K.A. (2012): QUEST-Northwest: Geoscience BC's new minerals project in northwest British Columbia (NTS 104G, 104J, parts of NTS 104A, B, F, H, I, K, 103O, P); *in* Geoscience BC Summary of Activities 2011, Geoscience BC, Report 2012-1, p. 1–4.
- van Straaten, B. (2012): Geology and mineralization of the Hotailuh batholith and surrounding rocks (104I/3, 4) map sheets; *in* Geological Fieldwork 2011, BC Ministry of Energy and Mines, Paper 2012-1.

QUEST-Northwest Project: New Regional Geochemical Survey and Sample Reanalysis Data, Northwestern British Columbia (NTS 104F, G, H, I, J, K)

W. Jackaman, Noble Exploration Services Ltd., Sooke, BC, wjackaman@shaw.ca

Jackaman, W. (2012): QUEST-Northwest Project: new regional geochemical survey and sample reanalysis data (NTS 104F, G, H, I, J, K), northwestern British Columbia (NTS 104F, G, H, I, J, K); in Geoscience BC Summary of Activities 2011, Geoscience BC, Report 2012-1, p. 15–18.

Introduction

Since 2005, Geoscience BC has supported significant enhancements to the British Columbia regional geochemical database (Jackaman, 2011a). As part of the QUEST-Northwest Project, the database is being further upgraded with new field survey results and sample reanalysis data. This information will be compiled as part of a large-scale geoscience initiative, which to date has included stream-based infill sampling and the reanalysis of sediment pulps saved from previous government-funded surveys. Results will generate a vast array of geochemical information that complements other components of the QUEST-Northwest Project, such as the airborne geophysical surveys and bedrock mapping (Simpson, 2012; Logan, 2012, respectively). This collection of high-quality geochemical information will help promote and stimulate exploration interest in the project area.

Northwestern BC has been the focus of several government-funded reconnaissance-scale regional geochemical surveys completed between 1987 and 2004 (Lett, 2005). Although results from this work produced a solid base of geochemical information that has guided numerous exploration activities, limitations associated with sample site density and the existing geochemical database identified a need to increase the number of sample sites and upgrade the ca-

Keywords: Telegraph Creek, Dease Lake, mineral exploration, geochemistry, regional geochemical survey, RGS, multi-element reanalysis, stream sediment

This publication is also available, free of charge, as colour digital files in Adobe Acrobat® PDF format from the Geoscience BC website: <http://www.geosciencebc.com/s/DataReleases.asp>.

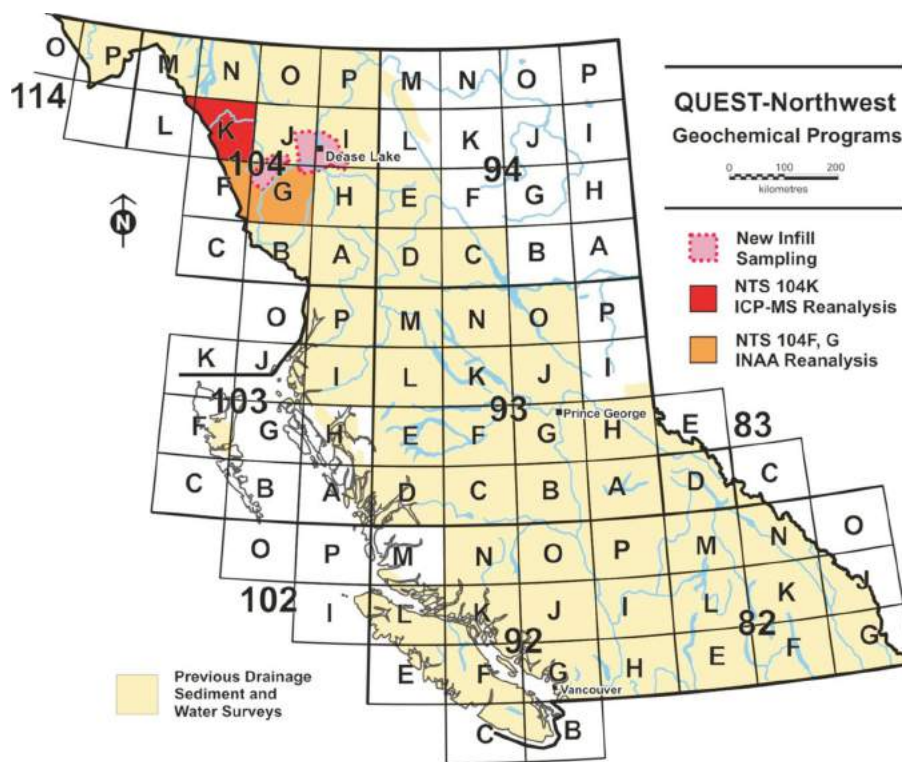


Figure 1. Location of the 2011 QUEST-Northwest geochemical infill sampling and reanalysis programs, northwestern British Columbia.

capacity of the associated analytical package. To address these deficiencies, stream-based infill sampling was conducted over parts of the study area and the reanalysis of archived sediment pulps is also being completed.

QUEST-Northwest Project Area

Sample reanalysis work covers NTS 104F, G and K 1:250 000 map areas (Figure 1). The infill sampling component included parts of NTS 104G, H, I and J 1:250 000 map areas. To co-ordinate geochemical coverage with the airborne geophysics work, the stream sampling was divided into the Telegraph Creek and Dease Lake survey areas (Figure 2).

The Telegraph Creek survey covers an area of more than 3500 km² and extends west from the community of Telegraph Creek, straddling the wide and heavily forested

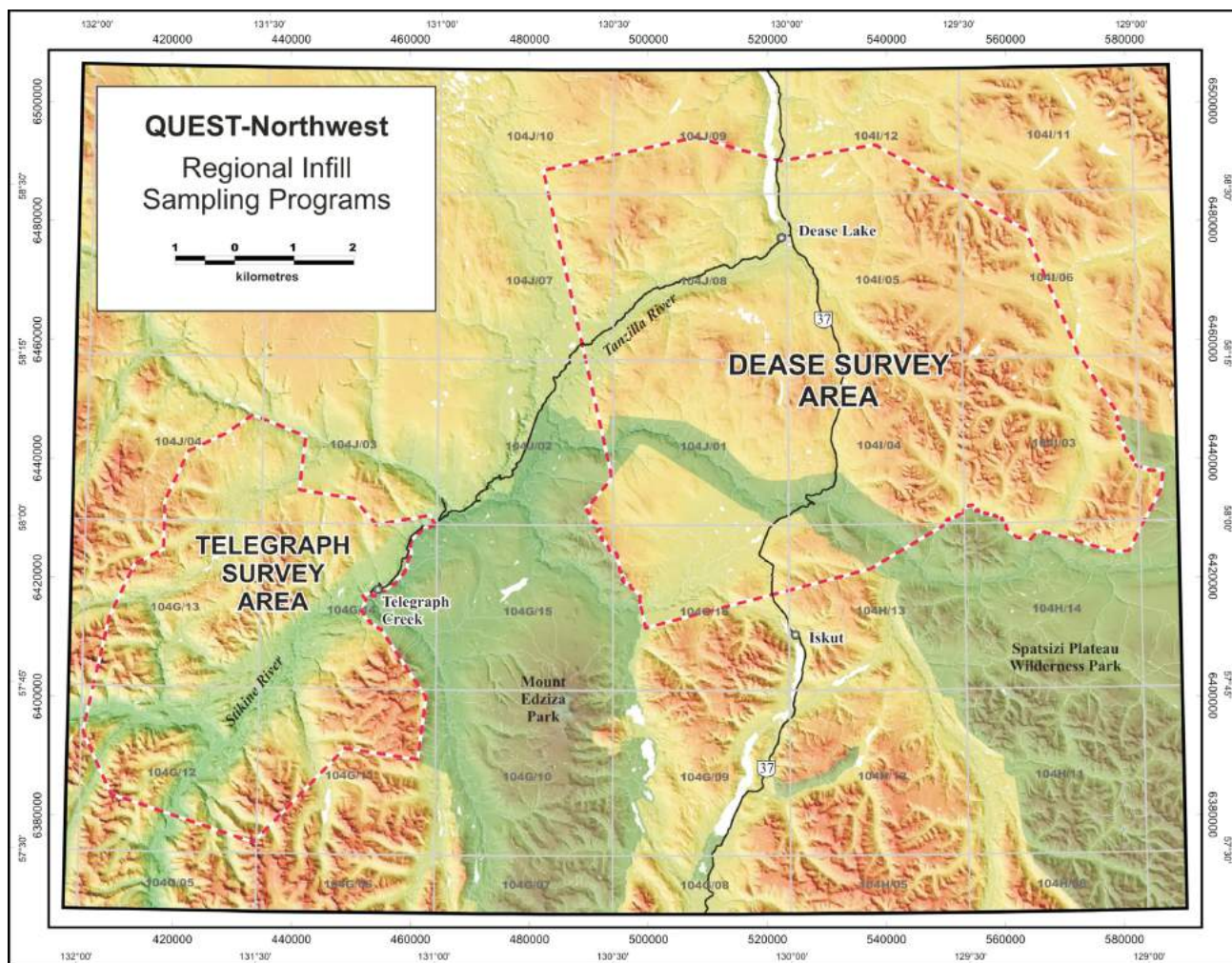


Figure 2. Locations of Telegraph Creek and Dease Lake infill sampling areas (indicated by the dashed red outlines), northwestern British Columbia.

Stikine River valley. To the west and south of the valley, the area is characterized by high rugged peaks of the Boundary Ranges, and to the north, the more subdued mountains of the Tahltan Highland (Holland, 1976). The Dease Lake survey covers more than 5500 km² and also includes parts of the Stikine River valley and the Tanzilla River valley. The area extends east into the Stikine Ranges of the Cassiar Mountains.

In low-lying regions of the survey areas (Figure 3), access was limited by thick tree cover. In addition, the availability of suitable sample material was often hampered by poorly developed stream drainages associated with extensive wetland cover. Exposed areas at higher elevations (Figure 4) provided excellent access to streams and numerous opportunities to improve the overall sample site coverage.

QUEST-Northwest Infill Surveys

Using helicopter support, stream-based sample collection was carried out in August 2011. A total of 441 stream sediment and water samples were systematically collected. Combined with previous survey results, the sample site density was increased to one site every 7 km². The sampling generally included approximately 2 kg of sediment material and 250 mL of clear water obtained from the active stream channel of first-order drainages. Field observations of location, sample information and site characteristics were recorded for each site. Samples were transported back to field camps in the community of Telegraph Creek and near Iskut along Highway 37, where the samples were catalogued and sediments were drip-dried in a contaminant-free structure and water bottles were stored in a cool, dark location.

At the completion of the field program, stream sediment samples were dried and sieved to –80 mesh (<177 µm) and were shipped to Eco Tech Laboratory Ltd. (Kamloops, British Columbia). To monitor and assess accuracy and precision of analytical results, control reference material, analytical duplicate and field duplicate samples are included in each block of 20 samples. Once processed, splits of the sediment samples will be forwarded to Acme Analytical Laboratories Ltd. (Vancouver, British Columbia) and Becquerel Laboratories Inc. (Mississauga, Ontario). The sample pulps will be analyzed for 53 analytes by inductively coupled plasma–mass spectrometry (ICP-MS) using an aqua-regia digestion and instrumental neutron activation analysis (INAA) for 32 elements. Loss-on-ignition and fluorine content will also be determined for stream sediment samples. Streamwater was measured for pH and conductivity at each site and fluoride will be determined from the raw streamwater samples.

All components of the survey are conducted to protocols maintained by the National Geochemical Reconnaissance (NGR) and BC Regional Geochemical Survey (RGS) programs (Ballantyne 1991; Friske and Hornbrook, 1991).

QUEST-Northwest Sample Reanalysis

As part of the NGR program, the map areas targeted for reanalysis were previously surveyed in 1987 as part of a joint federal-provincial initiative (Gravel and Matysek, 1988). At that time, sediment samples were analyzed for a limited range of metals by aqua-regia digestion–atomic absorption spectrometry (AAS), and for gold by lead collection fire assay. By design, samples have been routinely retained for all surveys completed in BC. The availability of these samples has provided the opportunity to generate up-to-date analytical information for samples collected during older surveys.

In co-operation with the BC Geological Survey (BCGS) and Natural Resources Canada (NRCan), samples from the 1987 surveys were retrieved from storage facilities in Ottawa. A total of 997 drainage-sediment pulps from NTS 104K plus quality-control samples have been recovered from storage and delivered to Acme Analytical Laboratories Ltd. (Vancouver, British Columbia) and are being analyzed by an ultratrace aqua-regia digestion (0.5 g) ICP-MS package for 53 elements. In addition, 1399 drainage-sediment pulps from NTS 104F and 104G plus quality-control samples have been recovered from storage and shipped to Becquerel Laboratories Inc. and are being analyzed by INAA for 34 elements.

Results of this reanalysis work will add up to 87 new elements to the existing geochemical database and will provide greater data continuity with more recent survey work and other data reanalysis initiatives such as the Geoscience



Figure 3. Thick forest coverage characteristic of the Stikine River valley, northwestern British Columbia.



Figure 4. Typical higher elevation valley in the Stikine Ranges, northwestern British Columbia.

BC-funded Northern BC Sample Reanalysis Project (Jackaman, 2011b).

Data Release Information

Results of the reanalysis work are scheduled to be published in January 2012 and the new infill survey results will be released in the late spring 2012. Prior to release, the analytical information is carefully scrutinized using established quality-control measures, such as blind duplicate samples and control reference materials. Approved analytical information is digitally merged with complete and accurate sample site location information and field observations. The final release packages include detailed descriptions of the work and will be publicly available free of charge from the Geoscience BC and the BCGS websites in a variety of digital data formats. In combination with other geoscience information, careful assessments of the published data will help identify exploration opportunities associated with regional geochemical trends and individual sample anomalies.

Acknowledgments

Acknowledgments are extended to E. Jackaman, S. Reichheld, J. Dimock, J. Faulkner and L. Quock for their contributions to the field program; M. McCurdy, S. Day and R. McNeil of NRCan for their ongoing support of the development and maintenance of the BC RGS program, Stikine Riversong Lodge and Tatogga Lake Resort for their excellent service and hospitality and R. Lett for his program support and for reviewing this paper.

References

- Ballantyne, S.B. (1991): Stream geochemistry in the Canadian Cordillera: conventional and future applications for exploration; *in* Exploration Geochemistry Workshop, Geological Survey of Canada, Open File 2390, p. 6.1–6.74.
- Friske, P.W.B. and Hornbrook, E.H.W. (1991): Canada's National Geochemical Reconnaissance programme; Transactions of the Institution of Mining and Metallurgy, Section B, v. 100, p. 47–56.
- Gravel, J. and Matysek, P.F. (1988): Regional Geochemical Survey 18–Iskut River (104B), RGS 19–Sumdum (104F) and Telegraph Creek (104F), RGS 20–Tulsequah (104K); *in* Geological Fieldwork 1987, BC Ministry of Energy and Mines, Paper 1988-1, p. 489–492, URL <<http://www.empr.gov.bc.ca/Mining/Geoscience/PublicationsCatalogue/Fieldwork/Documents/1987/489-492-gravel.pdf>> [November 2011].
- Holland, S.S. (1976): Landforms of British Columbia: a physiographic outline; BC Ministry of Energy and Mines, Bulletin 48, 138 p, URL <<http://www.empr.gov.bc.ca/Mining/Geoscience/PublicationsCatalogue/BulletinInformation/BulletinsAfter1940/Pages/Bulletin48.aspx>> [November 2011].
- Jackaman, W. (2011a): The British Columbia Regional Geochemical Survey: new analytical data and sample archive upgrades; *in* Geoscience BC Summary of Activities 2010, Geoscience BC, Report 2011-1, p. 181–187, URL <http://www.geosciencebc.com/i/pdf/SummaryofActivities2010/SoA2010_Jackaman.pdf> [November 2011].
- Jackaman, W. (2011b): Northern BC Sample Reanalysis Project; Geoscience BC, Report 2011-2, 11 p., URL <<http://www.geosciencebc.com/s/2011-02.asp>> [November 2011].
- Lett, R.E.W. (2005): Regional geochemical survey database on CD; BC Ministry of Energy and Mines, GeoFile 2005-17, CD-ROM, URL <<http://www.empr.gov.bc.ca/Mining/Geoscience/PublicationsCatalogue/GeoFiles/Pages/2005-17.aspx>> [November 2011].
- Logan, J.M., Diakow, L.J., van Straaten, B.I., Moynihan, D.P. and Iverson, O. (2012): QUEST-Northwest mapping: BC Geological Survey Dease Lake Geoscience Project, northern British Columbia (NTS 104I, J); *in* Geoscience BC, Summary of Activities 2011, Geoscience BC, Report 2012-1, p. 5–14.
- Simpson, K. (2012): QUEST-Northwest: Geoscience BC's new minerals project in northwestern British Columbia (NTS 104G, J, parts of NTS 104A, B, F, H, I, K, 103O, P); *in* Geoscience BC Summary of Activities 2011, Geoscience BC, Report 2012-1, p. 1–4.

Porphyry Integration Project: Bringing Together Geoscience and Exploration Datasets for British Columbia's Porphyry Districts

F. Devine, Merlin Geosciences Inc., Atlin, BC, fdevine@merlingeo.com

Devine, F. (2012): Porphyry Integration Project: bringing together geoscience and exploration datasets for British Columbia's porphyry districts; in Geoscience BC Summary of Activities 2011, Geoscience BC, Report 2012-1, p. 19–28.

Introduction

Understanding the geology of porphyry systems is necessary to focus exploration for porphyry mineralization. However, bridging the gap between conceptual ideas or focused scientific insights and practical exploration methods can be a challenge. Interpreting patterns, trends and features in geophysical and geochemical data from porphyry systems in the context of complex magmatic-hydrothermal systems can be difficult, particularly when data may be limited or restricted in aerial extent.

Geological models for porphyry systems have been developed over several decades by numerous researchers, providing guidance to explorers on both the regional and the more detailed levels of porphyry exploration (see Thompson, 1995). In BC, research related to porphyry systems has seen several periods of collaboration resulting in seminal volumes such as CIM Special Volume 15 (Sutherland Brown, 1976) and CIM Special Volume 46 (Schroeter, 1995), as well as integrated research projects on alkalic systems (e.g., research in the 1990s by the Mineral Deposit Research Unit [MDRU]; research in the 2000s by MDRU and the Centre for Ore Deposit Research [CODES], see Chamberlain et al., 2007; as well as research and mapping by the BC Geological Survey [BCGS], e.g., Preto et al., 2004; Logan et al., 2006, 2007). These projects have advanced the level of understanding of the tectonic and local magmatic-hydrothermal controls on BC's porphyry systems, as well as developed more detailed conceptual models for specific porphyry classes.

As explorers gain a better understanding of the details of porphyry systems, there is a need to review these models in the context of practical exploration methods. It is important not only to understand the variations within the models, but also to recognize what the variations within different porphyry systems look like in exploration datasets. Identifying which features of geological, geochemical and geophysical

datasets are linked to mineralized porphyry centres is the key to successful exploration.

The porphyry integration project is working to develop integrated geological, geophysical and geochemical maps and datasets for thirteen important porphyry districts in BC. The exploration data are drawn from public and, where possible, private company contributions. The goal is to develop an integrated model for porphyry discovery that links conceptual geological models with practical field exploration.

Porphyry Integration Project

Some of BC's more advanced porphyry districts have exploration datasets that span decades, and full compilation of these data has not yet been completed. Integrating the data and then interpreting the geological, geophysical and geochemical context for known mineralization in these districts, some of which have developed mines, will provide an excellent resource to aid in the development of focused exploration strategies for other porphyry occurrences in BC. Compiling examples of how porphyry system features manifest in exploration datasets and explaining the significance of the findings in the context of the current understanding of porphyry systems, is fundamental to strong science-based exploration and is the concept for the porphyry integration project. The porphyry integration project was outlined in detail in Devine (2011) and the following article is intended to provide a brief update on the progress to date.

Selected BC Porphyry Districts

The districts chosen for evaluation during this project reflect the variety in porphyry systems in BC (Figure 1). Porphyry deposits in BC may be grouped into 'pre-accretion' and 'post-accretion' settings, based on the timing of their emplacement relative to tectonic accretion to the North American continental margin (e.g., McMillan et al., 1995; Figure 1). The calcalkalic and alkalic classification is also reflected in this grouping by the direct links between tectonic processes and magma series. The pre-accretion porphyries are those developed in the Stikine and Quesnel arc terranes; they include both calcalkalic Cu-Mo-(Au) and alkalic Cu-Au systems, commonly found to occur within coeval magmatic and volcanic host rocks. The porphyry

Keywords: *porphyry, integration, district, exploration*

This publication is also available, free of charge, as colour digital files in Adobe Acrobat® PDF format from the Geoscience BC website: <http://www.geosciencebc.com/s/DataReleases.asp>.

districts in Quesnel and Stikine terrane include many of BC's richest Cu-porphyry deposits. The post-accretion deposits are more widespread across terrane boundaries and occur in magmatic suites emplaced into older rocks, in-board of the continental margin. They are calcalkalic Cu-Mo and Mo dominant systems formed from more evolved magmatic systems.

Variation within porphyry systems is also reflected in the earlier divisions of classic, volcanic and plutonic (McMillan and Panteleyev, 1988), which reflect the variety of emplacement settings for porphyry systems. The dominant controls include hostrock variation and resultant reactivity of hostrocks, as well as variable degrees of structural control, either pre-emplacement, synemplacement or post-

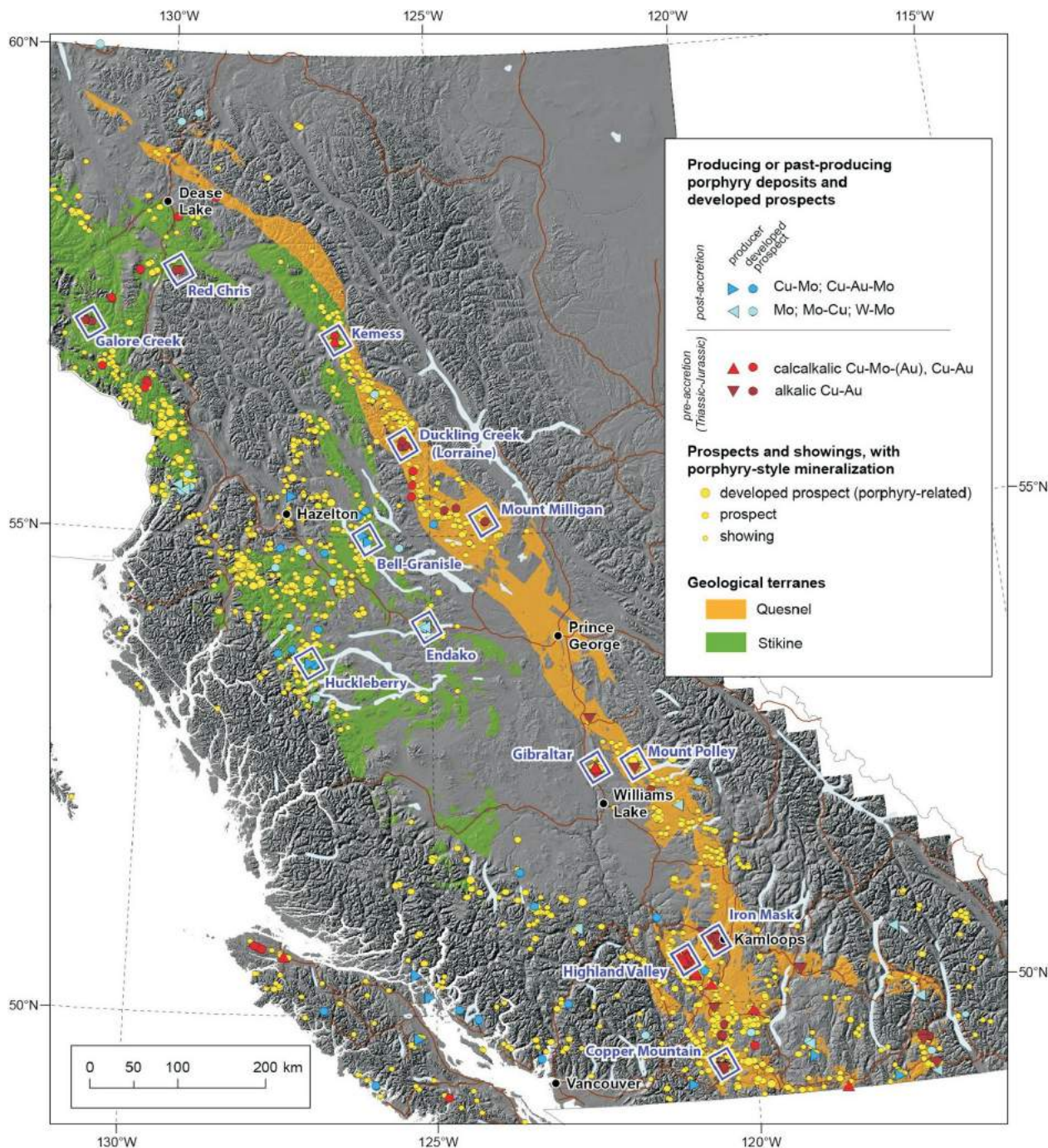


Figure 1. Locations of porphyry districts in British Columbia identified for compilation and integration by the Porphyry Integration Project (blue rectangles); digital elevation model developed by the Canadian Council on Geomatics (2004). The locations of porphyry showings, prospects and developed prospects are from the MINFILE database (BC Geological Survey, 2011).

emplacement. Together with the variations in magmatic and hydrothermal character of calcalkalic and alkalic systems these controls may lead to a variety of porphyry mineralization settings and styles.

The districts chosen for evaluation in the project represent these porphyry system variations within BC (Figure 1). Data availability, quality and quantity were also taken into consideration, and the result is a working list of 13 BC porphyry districts. They include Triassic and Jurassic alkalic and calcalkalic districts within the Stikine and Quesnel terranes, represented by Copper Mountain, Iron Mask, Mount Polley, Mount Milligan, Duckling Creek (Lorraine), Galore Creek, Red Chris, Kemess and Highland Valley. Post-accretion districts are represented by Endako, Huckleberry and Bell-Granisle. The list is somewhat weighted toward the alkalic class due to the high level of exploration interest in these gold-rich, potentially high-grade, although smaller footprint deposits. This interest in alkalic systems has been reflected in the recent research by the MDRU-CODES collaboration (Chamberlain et al., 2007), BCGS initiatives (e.g., Logan et al., 2006, 2007), as well as recent Geoscience BC Quesnellia Exploration Strategy (QUEST) initiatives to develop datasets over the Quesnel and Stikine terranes to encourage new exploration.

District-Scale Approach

The 'district-scale' approach is fundamental to the focus of the project. Encouragement for developing strong district-scale understanding of porphyry systems comes from the recognition that porphyry deposits commonly occur in clusters associated with certain magmatic suites and that deposits of different ages, mineralization styles and metal ratios may occur within a single district (e.g., Cadia Ridgeway, Wilson et al., 2003). Mineralization occurring peripheral to the main porphyry centres may also be economically significant and warrant inclusion in any district-scale model for porphyry exploration. The idea of adopting a porphyry 'footprints' approach to research and exploration recognizes that the alteration and hydrothermal manifestations of a porphyry systems may extend much farther outwards than the mineralized zones and provide a larger target area for exploration.

While deposit-scale variations within a district are important to understanding the intricacies of porphyry systems, the variations can be quite complex and dependent on a number of specific local factors. Significant effort has been put into understanding the geological details of many BC porphyry deposits (e.g., Sutherland Brown, 1976; Schroeter, 1995). The district-scale controls are certainly dependent on local characteristics; however, the step back in scale allows for the recognition of other magmatic and structural features that may be controlling porphyry mineralization within a wider region.

This district-scale challenge is familiar to explorers who commonly rely on broad aeromagnetic, electromagnetic, induced polarization (IP) and geochemistry surveys to focus their efforts. Insight into the manifestation of the more subtle features of porphyry systems within these data, at the district-scale, is highly useful to field exploration.

Development of Data Layers and Presentation

The approach for data collection and integration over the selected districts has been systematic and has followed the general order listed below:

- 1) collection of available public geochemical and geological data
- 2) review of assessment reports for historic soil geochemistry data, and digitizing when of value to the project
- 3) engagement with companies in the district of interest following a review of historic work
- 4) development of consistent maps and digital datasets by the project team
- 5) integration of spatial data and geological evaluation

Stage 1 compilation includes regional public data: BC regional geochemical survey (RGS), aeromagnetic surveys, QUEST electromagnetic and gravity data. Figure 2 is an example of a set of regional data presented in a consistent format at the district-scale for the Mount Polley area. The BC Geological Survey geological compilation for Mount Polley can be compared with the regional magnetic, radiometric (K-Th) and stream-sediment geochemistry data. By comparing these integrated data at a similar scale and format it is possible to develop interpretations of trends.

Stage 2 compilation includes more detailed, district-specific data such as ground geophysical surveys, for example local ground magnetic and IP surveys. Soil geochemistry surveys are also included in this compilation, many of which have been filed in historic assessment reports. The distribution and availability of these district-specific data is more limited than the government-developed regional datasets. Compilation of these data is on-going and will result in several new digital products.

Where possible, companies have been contributing digital data, such as detailed geophysical surveys or historic soil geochemistry data, to complete certain district datasets (stage 3 compilation).

During the course of the project, maps of the data are being produced in-house by the Geoscience BC project team. Figures 2 and 3 are examples of some of the GIS-based maps that are being used to organize and view the multi-layered, multi-disciplinary data. The concept of scale consistency between districts is important in the development of data layers. Not only are maps being used to evaluate datasets within the districts, but also to compare and con-

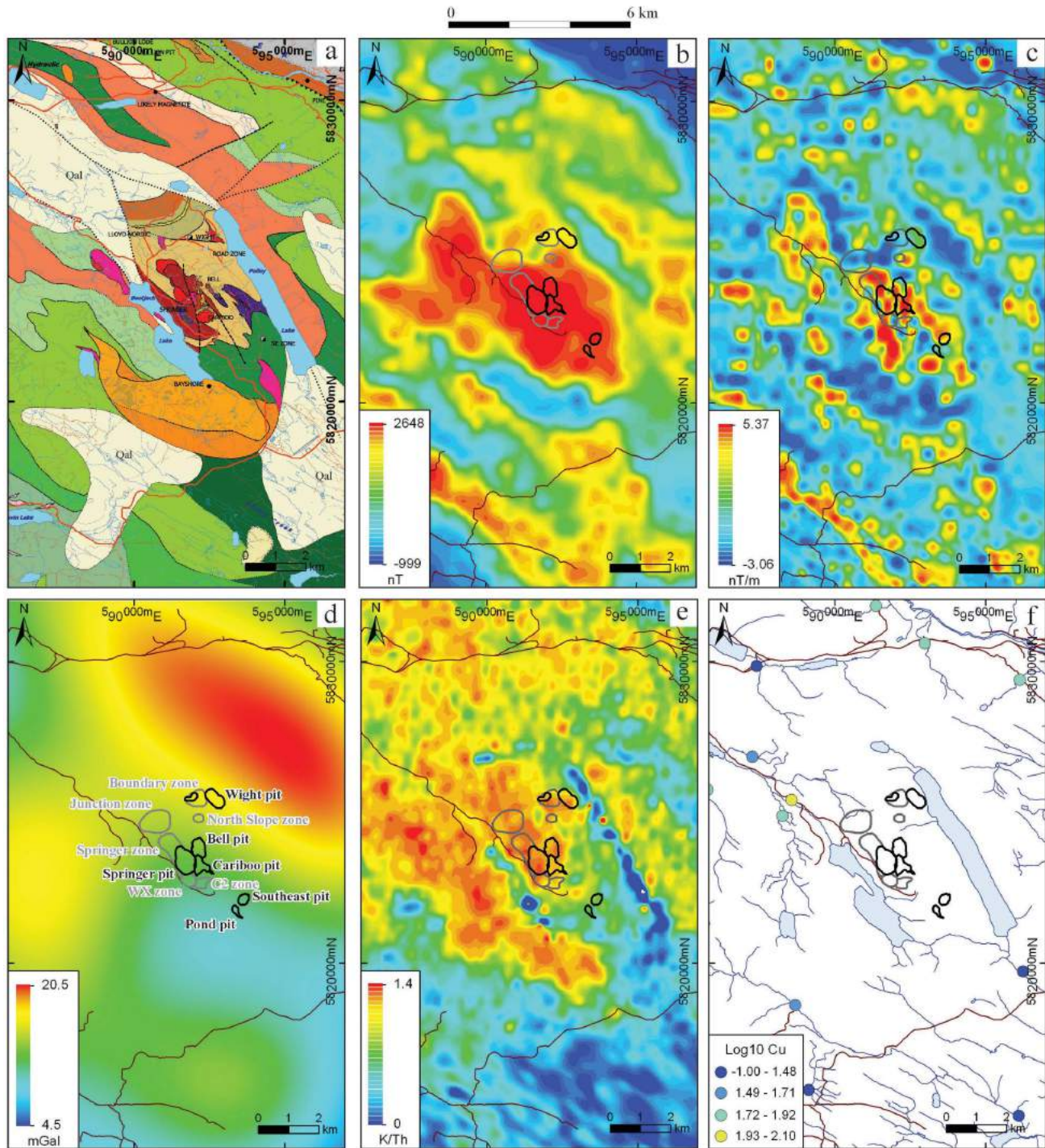


Figure 2. Examples of layers of regional data over the Mount Polley alkalic Cu-Au porphyry district, British Columbia; the locations of developed pits are shown in black outlines, and the locations of undeveloped mineralized zones are shown in grey outlines (taken from Imperial Metals Corporation (2011); **a**) geological map of Logan et al. (2007); the intrusive complex between Polley and Bootjack lakes is host to the mineralized zones that comprise the district; **b**) total magnetic field map generated by Geoscience BC (GBC) from the 2005 Geological Survey of Canada Hydraulic Survey (Carson et al., 2006); a more detailed magnetic survey of the Mount Polley area was undertaken by Shives et al. (2003); **c**) first vertical derivative of the total magnetic intensity (TMI) image generated by GBC from Carson et al. (2006); **d**) isostatic Bouguer gravity image from the Quesnellia Exploration Strategy (QUEST) project data (Sander Geophysics, 2008); **e**) radiometric image generated by GBC from Carson et al. (2006); **f**) compilation of Cu values in regional stream-sediment data (Jackaman, 2008). All geophysical data layers are produced by P. Kowalczyk on behalf of Geoscience BC; the regional stream-sediment data compilation is by D. Heberlein for Geoscience BC. All maps are in UTM NAD83 projection, Zone 10.

Legend for Mount Polley geology map

modified from Logan et al. (2007)

INTRUSIVE ROCKS

Middle Jurassic (~163 Ma)

 Hornblende-biotite quartz monzonite

Early Jurassic (~193-195 Ma)

 Hornblende quartz porphyritic monzonite

Late Triassic to Early Jurassic composite intrusions

 Pyroxenite-hornblende monzodiorite, hornblende-biotite monzonite and potassium feldspar megacrystic syenite

Late Triassic (205-200 Ma)

 Breccia: potassic-albitic-calcic altered, matrix to clast-supported, polymict intrusive-dominated pipes

 Biotite-pyroxene diorite

 Pyroxene/hornblende-biotite monzonite

 Melanocratic (pyroxene+hornblende) pseudoleucite syenite

 Orbicular pseudoleucite nepheline syenite

 Hydrothermal altered intrusive carapace holocrystalline monzonitic intrusions and volcanoclastic wall rock

 undivided polyolithic breccias

LAYERED ROCKS

Quaternary thick alluvium: Qal

Miocene to Pleistocene Chilcotin Group

 vesicular alkali olivine basalt breccia flows

Eocene Kamloops Group

 undivided calcalkaline volcanic rocks

 mudstone, siltstone, shale and fine clastic sedimentary rocks

Un-named Cretaceous Conglomerate

 Polymictic clast-supported cobble conglomerate, includes gneiss, marble, chert, granitoid and volcanic clasts

Middle Jurassic Dragon Mountain Formation

 Polymictic conglomerate, sandstone, graded siltstone

Un-named Sinemurian to Pliensbachian Sediments

 Brown-grey siltstone, sandstone and calcareous conglomerate

Sinemurian (196 Ma)

 Quartz-phyric latite tuff

Late Triassic to Early Jurassic

 Well-bedded and sorted, polymict volcanic conglomerate, pink monzonite to K-feldspar megacrystic syenite clasts

Late Triassic Nicola Group

 Massive, polymict breccia, feldspar and hornblende crystal tuff

 Hornblende-phyric andesitic basalt flows and breccias

 Plagioclase-phyric, pyroxene lapilli tuff, breccia and minor flows

 Limestone, ash and crystal-rich sandstone and maroon siltstone

 Analcime pyroxene+/-olivine basalt breccia, flows and tuffs

 Green and maroon pyroxene porphyry breccias, pyroxene-olivine basalt flows and crystal-rich sediments

 Massive, coarse polymict volcanic breccias, graded sandstones, siltstone and rare limestone breccia horizons

 Grey siltstone, normal graded sandstone and cherty shale with pyroxene and plagioclase-rich crystal sandstones

 Undivided mafic volcanic and volcanoclastic rocks

SYMBOLS

 roads

 BC MINFILE occurrences: developed prospect, showing

 Pit boundaries (2011)

 Zone boundaries, undeveloped (2011)

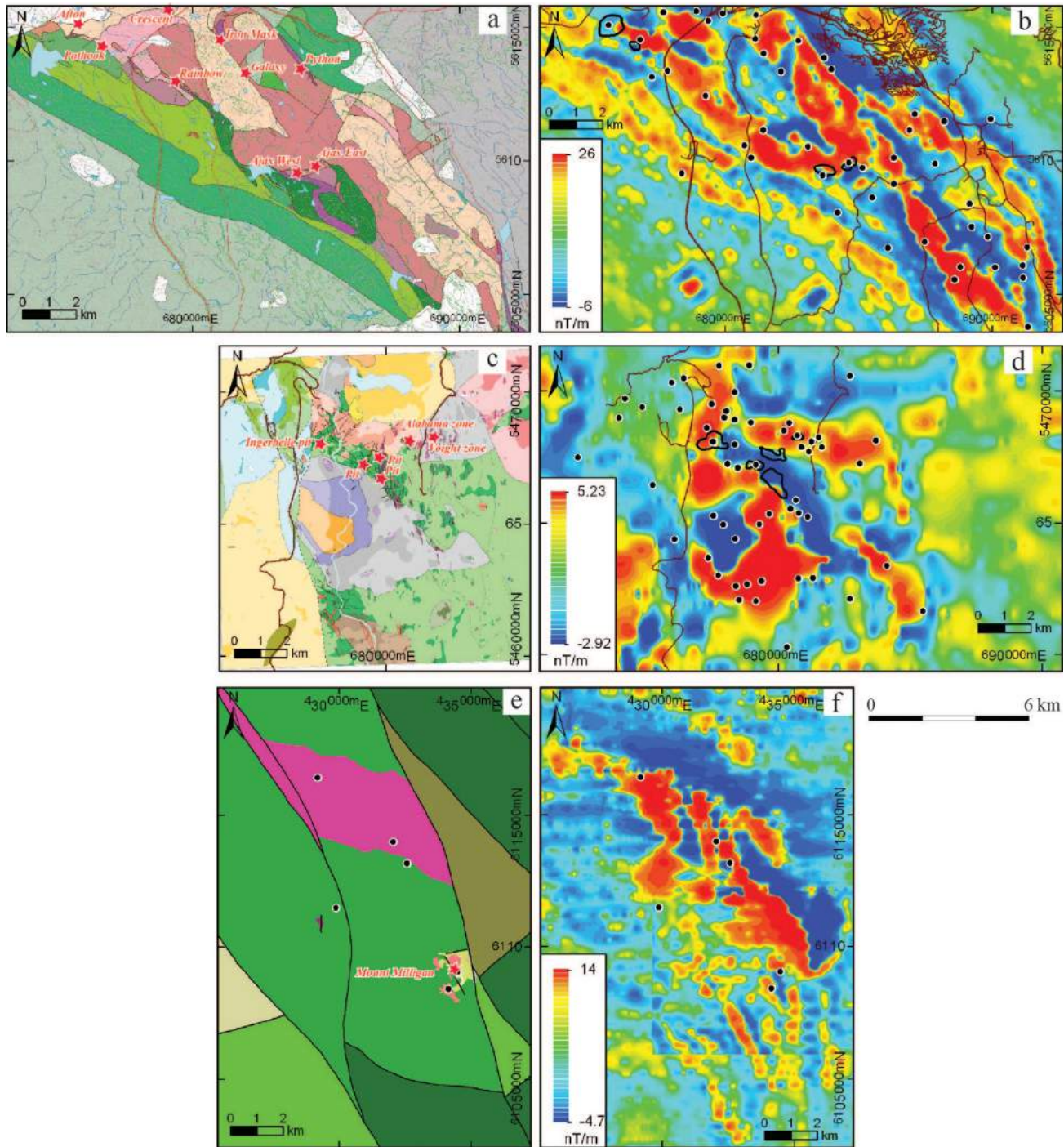


Figure 3. Examples of 1:50 000 scale compilation maps of geology and first-vertical derivative magnetic survey images generated from regional data over several alkalic Cu-Au districts in British Columbia. Maps are produced to the same scale using consistent colour ramps and legends to allow for comparing and contrasting data between districts: **a**) and **b**) geology map of Iron Mask batholith, compilation by Logan, et al. (2006), first vertical derivative magnetic survey map generated from the 1995 Iron Mask geophysical survey (Shives and Carson, 1995); **c**) and **d**) Copper Mountain geology compilation of Preto et al. (2004), first vertical derivative magnetic data generated from the 1971 Geological Survey of Canada aeromagnetic survey (Natural Resources Canada, 2011); **e**) and **f**) geology of the Mount Milligan area from the BC Digital Geology compilation (Massey et al., 2005), with more detailed geology in the vicinity of the deposit developed by Placer Dome Inc., published in Jago and Tosdal (2009), first vertical derivative magnetic survey map is generated from the 2005 Mount Milligan geophysical survey (Shives, 2005) and the 2008 Z-Axis Tipper Electromagnetic (ZTEM) survey test block over the Mt. Milligan area (Geotech Ltd., 2009). All levelled first vertical derivative products were produced by P. Kowalczyk for Geoscience BC.

Legend for Iron Mask geology map

modified from Logan et al. (2006)

INTRUSIVE ROCKS

Latest Triassic Iron Mask batholith

- Sugarloaf: porphyritic hornblende diorite
- Cherry Creek: biotite monzonite to monzodiorite
- Pothook: coarse biotite pyroxene diorite
- Hybrid: xenolith-rich Pothook or Sugarloaf phase

LAYERED ROCKS

Un-named Miocene volcanic rocks

- vesicular basalt flows and tuff

Eocene Kamloops Group

- undivided alkaline volcanic rocks

Late Triassic Nicola Group

- undivided volcanic and sedimentary rocks
- augite porphyry and polyolithic breccia
- feldspar>pyroxene-porphyritic lapilli tuff
- polyolithic lahar, including mineralized clasts
- picrite flow, breccia
- coarse augite porphyry
- feldspar>pyroxene volcanoclastic
- sediments with augite porphyry source
- Nicola sedimentary facies: mainly siltstone, lesser basalt, chert, minor limestone and ultramafite

Legend for Mount Milligan map

INTRUSIVE ROCKS

- hornblende-biotite monzonite
- diorite, lesser monzonite, syenite
- monzonite

LAYERED ROCKS

sedimentary rocks

- Nechako Plateau Group
- un-named

TAKLA GROUP volcanic rocks

- trachyte
- latite
- Witch Lake formation
- undivided andesitic rocks

- roads
- BC MINFILE occurrences
- Afton* Mines and developed prospects

Legend for Copper Mountain geology map

modified from Preto et al. (2004)

INTRUSIVE ROCKS

Post-Lower Cretaceous

- grey andesite feldspar porphyry dikes
- 'mine dikes': light grey and buff felsite, and quartz, quartz-feldspar and feldspar porphyry dikes

Late Lower Cretaceous

- Verde Creek Quartz Monzonite
- porphyritic biotite-hornblende quartz monzonite and/or granite

Late Triassic

COPPER MOUNTAIN INTRUSIONS

- Lost Horse Intrusions
- porphyritic augite and biotite-augite microdiorite, micromonzonite and microsyenite

Copper Mountain, Voigt, Smelter Lake stocks

- microdiorite and latite porphyry dikes
- pegmatite, syenite, and perthitic alkali feldspar syenite ("perthosite")
- monzonite
- gabbro and/or pyroxenite
- diorite

STRATIFIED ROCKS

Tertiary (Middle Eocene)

PRINCETON GROUP

- Allenby Formation
- dacite tuff, breccia
- Lower volcanic formation
- undivided basalts

Late Triassic

NICOLA GROUP

Sedimentary rocks

- conglomerates, minor sandstone
- calcareous siltstone, clastic limestone

Volcanic and volcanoclastic rocks

- massive andesite, pillow lava, volcanoclastic breccia
- Wolf Creek formation -massive andesite, minor basalt, volcanoclastic breccia

trast between districts (Figure 3). The development of consistent legends and scales is paramount to the value of the maps for further interpretation of the relationships of exploration data within and between districts.

Looking Forward

The porphyry integration project is ongoing and has made steady progress over the past year. The data compilation component of the project has taken longer than anticipated and is scheduled for completion over the winter of 2012. Data interrogation and interpretation has started and will ramp-up once the data compilation phase is complete. Maps and digital products developed during the course of the project will be made available publically through Geoscience BC's website (<http://www.geosciencebc.com/DataReleases.asp>) in 2012.

Acknowledgments

The other members of the Porphyry Integration Project team, including D. Heberlein, P. Kowalczyk and F. Ma along with K. Simpson for Geoscience BC, are acknowledged for their contribution. Mineral Deposit Research Unit (MDRU) participants F. Blaine, T. Bissig and D. Mitchinson are also thanked. The Porphyry Integration Project is grateful for the on-going contributions from company participants on specific porphyry districts.

References

- BC Geological Survey (2011): MINFILE BC mineral deposits database; BC Ministry of Energy and Mines, URL <<http://www.minfile.ca/>> [November 2011].
- Canadian Council on Geomatics (2004): Canadian digital elevation data; Natural Resources Canada, GeoBase[®], URL <<http://www.geobase.ca/geobase/en/data/cded/description.html>> [November 2011].
- Carson, J.M., Dumont, J.M., Potvin, R., Shives, R.B.K., Harvey, B.J.A. and Buckle, J.L. (2006): Geophysical series - NTS 93A/12 - Hydraulic, British Columbia; Geological Survey of Canada, Open File 5290, URL <<http://www.em.gov.bc.ca/Mining/Geoscience/MapPlace/thematicmaps/pages/geophys2005.aspx>> [November 2011].
- Chamberlain, C.M., Jackson, M., Jago, C.P., Pass, H.E., Simpson, K.A., Cooke, D.R. and Tosdal, R.M. (2007): Toward an integrated model for alkali porphyry copper deposits in British Columbia (NTS 093A, N; 104G); *in* Geological Fieldwork 2006, BC Ministry of Energy and Mines, Paper 2007-1, p. 259–273, URL <<http://www.em.gov.bc.ca/Mining/Geoscience/PublicationsCatalogue/Fieldwork/Documents/26-Chamberlain.pdf>> [November 2011].
- Devine, F. (2011): Porphyry Integration Project: combining British Columbia's wealth of datasets with modern exploration geoscience at the district scale to provide new insight into porphyry-deposit exploration strategies; *in* Geoscience BC Summary of Activities 2010, Geoscience BC, Report 2011-1, p. 1–4, URL <http://www.geosciencebc.com/i/pdf/SummaryofActivities2010/SoA2010_Devine.pdf> [November 2011].
- Geotech Ltd. (2009): Helicopter-borne Z-Axis Tipper Electromagnetic (ZTEM) and aeromagnetic survey, Mt. Milligan test block; Geoscience BC, Report 2009-7, URL <<http://www.geosciencebc.com/s/2009-07.asp>> [November 2011].
- Imperial Metals Corporation (2011): Mount Polley exploration, zone map; Imperial Metals Corporation, URL <<http://www.imperialmetals.com/i/pdf/zone-map-mount-polley-zone-map.pdf>> [November 2011].
- Jackaman, W. (2008): QUEST Project sample reanalysis; Geoscience BC, Report 2008-3, 4 p., URL <<http://www.geosciencebc.com/s/2008-03.asp>> [November 2011].
- Jago, C.J. and Tosdal, R.M. (2009): Distribution of alteration in an alkalic porphyry copper-gold deposit at Mount Milligan, central British Columbia (NTS 094N/01); *in* Geoscience BC Summary of Activities 2008, Geoscience BC, Report 2009-1, p. 33–48, URL <http://www.geosciencebc.com/i/pdf/SummaryofActivities2008/SoA2008-Jago_original.pdf> [November 2011].
- Logan, J.M., Bath, A., Mihalynuk, M.G., Rees, C.J., Ullrich, T.D. and Friedman, R. (2007): Regional geology of the Mount Polley area, central British Columbia; BC Ministry of Energy and Mines, Geoscience Map 2007-1, URL <<http://www.em.gov.bc.ca/MINING/GEOSCIENCE/PUBLICATI ONSCATALOGUE/MAPS/GEOSCIENCEMAPS/Pages/2007-1.aspx>> [November 2011].
- Logan, J.M., Mihalynuk, M.G., Ullrich, T.D. and Friedman, R. (2006): Geology of the Iron Mask batholith; BC Ministry of Energy and Mines, Open File 2006-11, URL <<http://www.empr.gov.bc.ca/Mining/Geoscience/PublicationsCatalogue/OpenFiles/2006/Pages/2006-11.aspx>> [November 2011].
- Massey N.W.D., MacIntyre, D.G., Desjardins, P.J. and Cooney, R.T. (2005): Digital geology map of British Columbia: whole province; BC Ministry of Energy and Mines, GeoFile 2005-1, URL <<http://www.em.gov.bc.ca/Mining/Geoscience/PublicationsCatalogue/GeoFiles/Pages/2005-1.aspx>> [November 2011].
- McMillan, W.J. and Panteleyev, A. (1988): Porphyry copper deposits; *in* Ore Deposit Models, R.G. Roberts and P.A. Sheahan (ed.), Geoscience Canada Reprint Series 3, Geological Association of Canada, p. 45–58 and Geoscience Canada, Geological Association of Canada, v. 7, no. 2, p. 52–63.
- McMillan, W.J., Thompson, J.F.H., Hart, C.J.R. and Johnston, S.T. (1995): Regional geological and tectonic setting of porphyry deposits in British Columbia and Yukon Territory; *in* Porphyry Deposits of the Northwestern Cordillera of North America, T.G. Schroeter (ed.), Canadian Institute of Mining, Metallurgy and Petroleum, Special Volume 46, p. 41–57.
- Natural Resources Canada (2011): Aeromagnetic data; Geological Survey of Canada, Geoscience Data Repository, Survey British Columbia – 82-40A, URL <<http://gdrdap.agg.nr.can.gc.ca/geodap/home/Default.aspx?lang=e>> [November, 2011].
- Preto, V.A., Nixon, G.T. and Macdonald, E.A.M. (2004): Alkaline Cu-Au porphyry systems in British Columbia: Copper Mountain; BC Ministry of Energy and Mines, Geoscience Map 2004-3, URL <<http://www.empr.gov.bc.ca/Mining/Geoscience/PublicationsCatalogue/Maps/GeoscienceMaps/Pages/2004-3.aspx>> [November 2011].
- Sander Geophysics (2008): Airborne gravity survey Quesnellia Region, British Columbia; Geoscience BC, Report 2008-8,

- URL <<http://www.geosciencebc.com/s/2008-08.asp>> [November 2011].
- Schroeter, T.G., editor (1995): Porphyry deposits of the northwestern Cordillera of North America; Canadian Institute of Mining and Metallurgy, Special Volume 46, 888 p.
- Shives, R.B.K. (2005): Helicopter-borne gamma ray spectrometric and magnetic total field geophysical survey, Mount Milligan Area, British Columbia (Parts of NTS 092N/01; 093N/02E; 093O/04W); BC Ministry of Energy and Mines, Open File 2005-09 and Geological Survey of Canada, Open File 2535, URL <<http://www.em.gov.bc.ca/Mining/Geoscience/MapPlace/thematicmaps/pages/milligan.aspx>> [November 2011].
- Shives, R.B.K. and Carson, J.M. (1995): Airborne geophysical survey, Iron Mask batholith, British Columbia; BC Ministry of Energy and Mines, Open File 2005-13 and Geological Survey of Canada Open File 2817, URL <<http://www.em.gov.bc.ca/Mining/Geoscience/MapPlace/thematicmaps/pages/IronMask.aspx>> [November 2011].
- Shives, R.B.K., Carson, J.M., Ford, K.L., Holman, P.B. and Cathro, M. (2003): Helicopter-borne gamma ray spectrometric and magnetic total field geophysical survey, Imperial Metals Corporation's Mount Polley Mine area, British Columbia (Part of NTS 93A/12); BC Ministry of Energy and Mines, Open File 2004-10 and Geological Survey of Canada, Open File 4619, URL <<http://www.em.gov.bc.ca/Mining/Geoscience/PublicationsCatalogue/OpenFiles/2004/Pages/2004-10.aspx>> [November 2011].
- Sutherland Brown, A., editor (1976): Porphyry deposits in the Canadian Cordillera; Canadian Institute of Mining and Metallurgy, Special Volume 15, 510 p.
- Thompson, J.F.H. (1995): Exploration and research related to porphyry deposits; *in* Porphyry Deposits of the Northwestern Cordillera of North America, T.G. Schroeter (ed.), Canadian Institute of Mining, Metallurgy and Petroleum, Special Volume 46, p. 857–870.
- Wilson, A.J., Cooke, D. R. and Harper, B.L. (2003): The Ridgeway gold-copper deposit: a high-grade alkalic porphyry deposit in the Lachlan Fold Belt, New South Wales, Australia; *Economic Geology*, v. 98, p. 1637–1666.

Geochemical-Exploration Models for Porphyry Deposits in British Columbia

F.A. Blaine, Mineral Deposit Research Unit, University of British Columbia, Vancouver, BC,
fredblaine@hotmail.com

C.J.R. Hart, Mineral Deposit Research Unit, University of British Columbia, Vancouver, BC

Blaine, F.A. and Hart, C.J.R. (2012): Geochemical-exploration models for porphyry deposits in British Columbia; *in* Geoscience BC Summary of Activities 2011, Geoscience BC, Report 2012-1, p. 29–40.

Introduction

Exploration geochemistry using surficial material has been used to great success in British Columbia for a number of years and is a commonly used tool in porphyry-deposit exploration. However, as deposits become scarcer and exploration focuses on areas under deeper and/or more complex cover, greater care has to be taken in the choice of sampling media and/or analytical method as well as in the interpretation of the resulting geochemical data to achieve maximum benefit. Exploration is further complicated by the introduction of newer techniques in recent years, including proprietary selective leaches and analytical methods, making it necessary to be aware of both the strengths and limitations of these various techniques and methods. In many cases, time or budget limitations or a lack of knowledge about an area preclude carrying out a proper site-specific orientation survey, which makes it very difficult to determine proper sampling media and analytical techniques. In these cases, it is necessary to turn to historical exploration studies of similar deposits covered by similar surficial environments to help predict the geochemical expressions of the deposit in the surficial material and maximize one's chances of success. Geochemical-exploration models, which are developed from known processes and deposits, can provide the necessary framework to develop successful geochemical-exploration programs.

Geochemical-exploration models were first developed and presented by Bradshaw (1975) for deposits in the Canadian Cordillera and Canadian Shield. Bradshaw (1975) created general, conceptual geochemical-exploration models for ore deposits in BC, based on fundamental scientific principles and a limited number of case histories. The exploration models summarized the potential controls on geochemical dispersion and dispersal, and the expected results on geochemical distribution.

Keywords: *geochemical-exploration models, geochemistry, regional geochemical survey, geochemical survey, orientation survey, porphyry deposits, soil, till, vegetation*

This publication is also available, free of charge, as colour digital files in Adobe Acrobat® PDF format from the Geoscience BC website: <http://www.geosciencebc.com/s/DataReleases.asp>.

Subsequently, much research has been done expanding on these models for varied environments in the Canadian Shield (Cameron et al., 2004) and areas outside of Canada, in arid (Butt, 2005; Aspandiar et al., 2008) and tropical environments (Butt and Zeegers, 1992), as well as for volcanogenic massive sulphide and shale-hosted Pb-Zn-Ag deposits in the Canadian Cordillera (Lett, 2000, 2001; Lett and Bradshaw, 2003). Although proposed by Lett and Bradshaw (2003), further refinement of models for porphyry deposits in the Canadian Cordillera has not been addressed until this time. This study expands on the general conceptual models presented by Bradshaw (1975) and develops empirically-defined geochemical-exploration models for specific surficial environments, specifically for porphyry deposits in BC. These empirically-defined models will be based on historical exploration data from both industry and government sources. The data necessary to complete this study have been captured from many sources, including regional geochemical surveys carried out by the Geological Survey of Canada and the BC Geological Survey (BCGS); the results of updated sampling and archival-sample analysis available from Geoscience BC; deposit- and area-specific studies carried out by the BCGS and Geoscience BC; and historical geochemical data generated through exploration by industry.

Industry-generated geochemical-exploration data have been collected and maintained in the BC assessment report indexing system (ARIS) since the early 1950s. There is a wealth of historical information available within this dataset for deposits that have been subsequently well characterized. However, the majority of this information has been submitted in paper form, and is stored and made available to the public in Adobe® Acrobat® PDF format; therefore, the geochemical data is not currently available in a readily-accessible digital format. A secondary purpose of this project was to capture this data digitally and produce a province-wide geochemistry database for porphyry deposits.

Objectives for the project include

- compiling a consistent and comprehensive geochemical database for porphyry deposits in BC through acquisi-

- tion of data from assessment reports and industry sources;
- categorizing deposits and geochemical data based on deposit and environmental variables likely to affect geochemical distribution;
- generating geochemical-exploration models for specific deposit types and surficial environments based on relevant classification criteria to provide
 - dominant geochemical dispersion and dispersal mechanisms;
 - typical or expected mineralization-element associations;
 - location, extent and magnitude of element enrichments or depletions;
 - potential sources of false anomalies or of element enrichments or depletions and, where possible, the means to identify them;
 - preferred sampling material and horizon, as well as preferred analytical method; and
 - guidelines for data interpretation.

Porphyry Selection and Data Collection

Of the 279 porphyry deposits listed within MINFILE (BC Geological Survey, 2011) and classified as ‘developed prospect’, ‘past producer’ or ‘current producer’, 73 were determined to have geochemical data contained within 273 assessment reports in ARIS. These geochemical reports present the results of industry-conducted, surficial geochemical surveys involving over 150 000 samples. However, the data contained within these reports are of highly variable quality and much of the data is of limited use or is not extractable due to poor print quality. The initial 73 porphyry deposits were subsequently reduced to 41 (Figure 1) and, to date, data for some 70 500 samples, summarized in Table 1, have been captured from assessment reports. To be selected for entry, reports must contain a minimum amount of information, including sample type and sampling horizon, digestion method, analytical finish and detailed spatial data. For inclusion into the porphyry geochemical database, it is necessary to convert local grid co-ordinates to UTM; where conversion is not possible, data are included for interpretation purposes only.

A combination of manual entry and optical character recognition (OCR) using ABBYY® FineReader® software was used to capture the data from the assessment reports. All OCR-collected data were manually verified against analytical certificates or submitted data tables to ensure the highest level of data quality and consistency. Due to the large

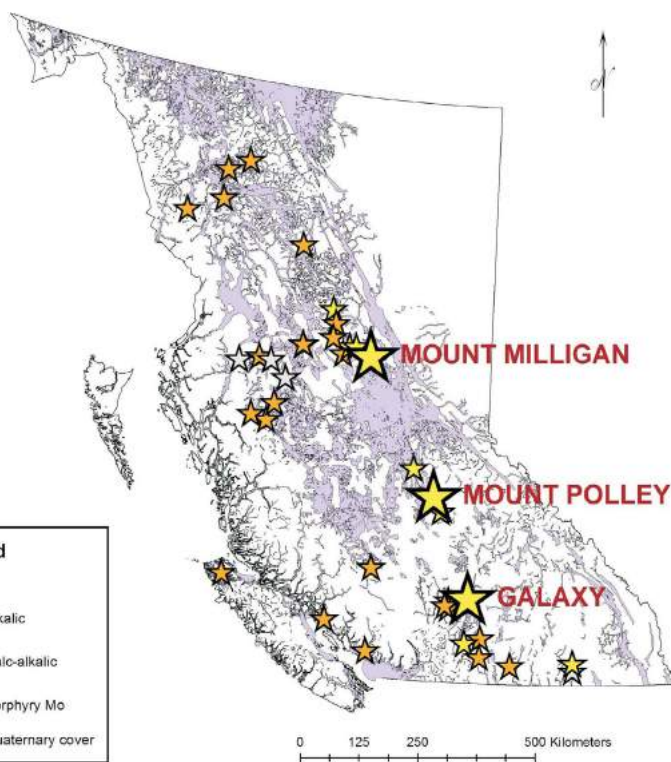


Figure 1. Location of selected porphyry deposits and distribution of Quaternary cover in British Columbia (from Massey et al., 2005).

amount of data, various data sources and often incomplete or missing quality-control data, full quality-assurance-quality-control procedures were not completed for all surveys; however, comments on data quality will eventually be included in the completed database. Where data were reported below the detection limit of the method, values were maintained in the database as the negative of the detection limit.

All geochemical data and metadata were converted to a consistent format, including column headings, units and projection method; metadata was added as required; and data were added to the master database, which was compiled using Microsoft® Access®. This database will be made available at the conclusion of the project and will be included with the final report.

Table 1. Summary of industry-generated geochemical data collected from the British Columbia assessment report indexing system (ARIS).

Sample Type	Current Totals
Soils (B-horizon)	61 000
Soils (other)	6 000
Tills	2 000
Streams	1 000
Vegetation	500
TOTAL	70 500

Controls on Geochemical Distribution and Porphyry-Classification Criteria

Although this study is restricted to porphyry deposits in a relatively restricted area, there are a number of variables that influence both the nature and geometry of the deposits and that also affect the development of the associated geochemical signature in the surficial material. These variations result in a unique set of conditions for each porphyry system and even for individual deposits in a single porphyry system. Therefore, in order to develop usable and appropriate geochemical-exploration models, deposits must be categorized based on a limited number of processes or deposit characteristics, which will control the dominant geochemical expressions of a porphyry deposit in the surficial environment, and on the factors that control or influence these processes, which can be broadly categorized as primary, secondary and postsecondary processes. Classification of the porphyry deposits of interest is found in Table 2 and explained below.

Primary Processes

In this paper, primary processes are deposit-specific mechanisms that control the geochemical distribution of elements within the deposit itself and relate to the ore-forming processes and/or mineralization styles. These primary processes control the inherent geochemical signature of the deposit itself and any associated alteration, which is subsequently modified or redistributed by secondary processes.

Moreover, to address primary processes, deposits are classified based on the porphyry-type classification developed by Lefebure and Ray (1995), which categorizes porphyry deposits as ‘alkalic’, ‘calc-alkalic’ and ‘porphyry Mo’ deposits. It is recognized that this is somewhat of a generalization since individual deposits will vary within these groupings and whenever possible, the characteristics of individual deposits that can affect the resulting surficial geochemistry are discussed.

Secondary Processes

Secondary processes result in the transfer or modification of the ore-deposit material and can include both physical and chemical mechanisms. These processes include the physical transport of material through geomorphological processes (colluvial, alluvial, fluvial, eolian and glacial), and weathering of the ore deposits and overlying bedrock. Glaciation is the secondary process that will perhaps exert the greatest control on the geochemical expression in BC, as widespread glaciation throughout the province has occurred most recently during the Late Wisconsinan (maxima circa 14 500 BP; Clague and James, 2002). This glacial event has caused widespread distribution of tills and other glacial deposits throughout BC (Figure 1), and the nature and distribution of these materials has had a profound effect on the geochemical signature of deposits. For the purpose of identifying secondary processes, surficial cover is divided into four categories based upon soil (terrain) mapping done by the BC Ministry of Environment (2011):

Table 2. Classification of selected British Columbia porphyry deposits, based on factors that can affect the surficial geochemical expression, as well as the dispersion and dispersal mechanisms. These factors are temperature, expressed in terms of periods of frost-free days (ffp) and amount of non-snow precipitation (nsp); relief, expressed in terms of topography; and porphyry type, as presented in Lefebure and Ray (1995).

		Warm (> 50 days ffp)			Cold (<50 days ffp)		
		Steep	Moderate	Slight	Steep	Moderate	Slight
Dry (<500 mm nsp)	Calc-alkalic	May Hearne Hill Morrison Indata Schaft Creek	Brenda HED Highmont Alwin Poplar	Getty South Jean	Takla (Redton-Rainbow) Kemess Red Chris	Gnat Pass Eaglehead	
	Alkalic	Mount Polley Col Mount Milligan	Prime Getty Mouse Mountain	Galaxy Ajax Woodjam	Chuchi Lake		
	Mo	Carmi Mo Stewart Davidson	Mineral Hill		Storie		
Wet (>500 mm nsp)	Calc-alkalic	OK North Hushamu	Louise Lake	Gambier Island	Taseko (Empress) Huckleberry New Nanik Whiting Creek		
	Alkalic	Kena Gold Kena (Gold Mountain)					
	Mo	Pitman					

Abbreviations: ffp, frost-free period; nsp, non-snow precipitation.

- Residual soils: soils developed directly from the weathering of the bedrock on which they reside
- Locally-derived transported cover (geochemically attached): these materials have a direct connection to the underlying bedrock and may be developed through glacial weathering and localized transport (a few tens of metres) or through colluvial processes (colluvium and some till veneers)
- Transported cover (geochemically detached): these materials have no direct geochemical connection to the underlying bedrock and are sourced from distal materials (i.e., till blankets, outwash, glaciolacustrine deposits)
- Blind deposits: the current surface of weathered bedrock has not reached these deposits and they are therefore blind to the surface

Postsecondary Processes

Postsecondary processes, for the purpose of this paper, are defined as those processes that modify or transport a geochemical signature after the deposition of the material, and which are generally independent of the physical transport of mineralized material. These processes include hydromorphic, phreatic, vadose zone and gaseous transport, as well as transportation by vegetation. Also included in these postsecondary processes are bio- and cryoturbation, as they are processes that modify the postdepositional distribution of material; however, these processes are not prevalent throughout most of BC.

Controlling Factors

Climate

The overall climate in BC during the last postglacial period has been fairly stable, becoming steadily cooler and wetter throughout approximately the past 14 000 years (Hebda, 2007). However, due to the broad range of climate zones within BC, climatic conditions can vary greatly between deposits, a factor which can have a considerable effect on the generation of geochemical anomalies by controlling the secondary and postsecondary processes (Butt, 2005; Aspandiar et al., 2008). The two dominant climatic controls are temperature and availability of water (precipitation). Climate data for deposit locations (from BC Geological Survey, 2011) were determined using the ClimateBC model developed at the University of British Columbia (2011) and based on the PRISM (Parameter-Elevation Regressions on Independent Slopes Model) climate-mapping system presented in Daly et al. (2002). Although climate can be an important factor, the influence of temperature and water availability decreases as relief increases; as a result, physical transport processes will dominate in areas of steep topography (Butt, 2005).

Temperature

Temperature can affect the geochemical signature of an ore deposit in the surficial environment through a number of different mechanisms. Warmer climates promote chemical weathering and increase the availability of elements liberated through weathering. Moreover, temperature controls the availability of water throughout the year as water is not available during winter months due to freezing. Low temperatures and long periods of frost can also promote frost-induced fracturing, leading to weathering and increased colluvial processes.

Porphyry deposits were classified based on temperature according to their frost-free period (ffp), which is the number of consecutive days that the area experiences temperatures above freezing. Two classifications were made, with deposits falling into period categories of either more or less than 50 frost-free days. Frost-free period was chosen over mean annual temperature, as it was considered a better indicator of the potential effects of temperature, highlighting the unavailability of water and frost-driven processes that prevail during winter months.

Precipitation

Precipitation, or the availability of water, is the main factor controlling postsecondary processes and it can also have an effect on secondary physical-transport mechanisms. Although the amount of precipitation (Butt, 2005) is an important factor, so is seasonality; therefore, the classification of the deposits falls into two categories based upon whether the amount of non-snow precipitation (nsp) is greater or lesser than 500 mm. Precipitation received as snow will more likely be introduced to the hydrological system as runoff, thus increasing alluviation, rather than, to any significant extent, to the local groundwater system, where the aforementioned postsecondary processes occur.

Increased availability of water in areas of low to moderate relief will generally cause a higher water table and increase the likelihood of phreatic and hydromorphic processes occurring, whereas in areas with lower water tables, the dominant processes will be gaseous transport and vadose zone processes.

Physiography

The relief of the area surrounding a deposit has strong control over the processes responsible for physical transport and soil development. Steep areas will prevent soil formation and result in physical transport (alluvial and colluvial processes) exerting the dominant control on geochemical dispersal. Moreover, in steep areas rainfall will be more likely to manifest itself in the form of runoff, decreasing the likelihood of water infiltration and increasing that of alluvial processes. Deposits are classified, generally based on topography, as being of slight (<100 m elevation-change/km), moderate (100–300 m elevation-change/km)

or steep (>300 m elevation-change/km) relief; however, local variations in relief are common and interpretation is based primarily on local assessment of elevation.

Development of Geochemical-Exploration Models

The geochemical-exploration models for this project were developed by determining the element associations and their distribution between sampled media and mineralization, and linking those distributions to the process generating the geochemical pattern. Relating the geochemical expression to mineralization and/or geology, and relating the expression to a process is a necessary exercise for each deposit as well as within each deposit. At the conclusion of the project, these geochemical expression-process relationships will be compiled into a generalized graphical representation of the individual geochemical-exploration models. At this stage, these models are incomplete and are also beyond the scope of this paper. Geochemical expressions and related processes for selected deposits are discussed below to highlight the importance of their study and that of the data extracted from assessment reports.

Discussion

This paper presents a preliminary discussion and interpretation of observed geochemical behaviour for the Mount Polley (MINFILE 093A 008; BC Geological Survey, 2011), Mount Milligan (MINFILE 093N 194) and Galaxy (MINFILE 092INE007) porphyry deposits, over which substantial B-horizon surveys were conducted and the results reported in ARIS; details of the deposits and surveys are summarized in Table 3.

The Mount Polley and Mount Milligan deposits are alkalic porphyry deposits characterized by a warm, dry climate (>50 days ffp and <500 mm nsp) and predominantly steep

topography (although locally variable). The mineralized areas at Mount Polley and Mount Milligan are covered with material of variable type and thickness (Figures 2, 3), with areas covered by predominantly colluvial material due to the steep topography. The Galaxy deposit is an alkalic porphyry deposit characterized by a warm, dry climate (>50 days ffp and <500 mm nsp) and predominantly slight topography. A relatively consistent till cover of variable thickness (up to 2–3 m) blankets the mineralized areas at Galaxy (Figure 4).

The results discussed here show that there is a broad range of potential anomaly-formation mechanisms, even in a limited number of deposits, illustrating the need for both properly-mapped surficial units and interpretation of the geochemistry based on this mapping. Many of the elements analyzed show an association with underlying geology, although this association is not discussed in this paper. Interpreted geochemical expressions are based on the analysis of multi-element geochemistry and element associations are explained in the text. However, due to length restrictions and to maintain clarity, only the data for copper (Figures 2–4) and gold (Figure 5) are presented; all geochemical data and maps will be included in the final report.

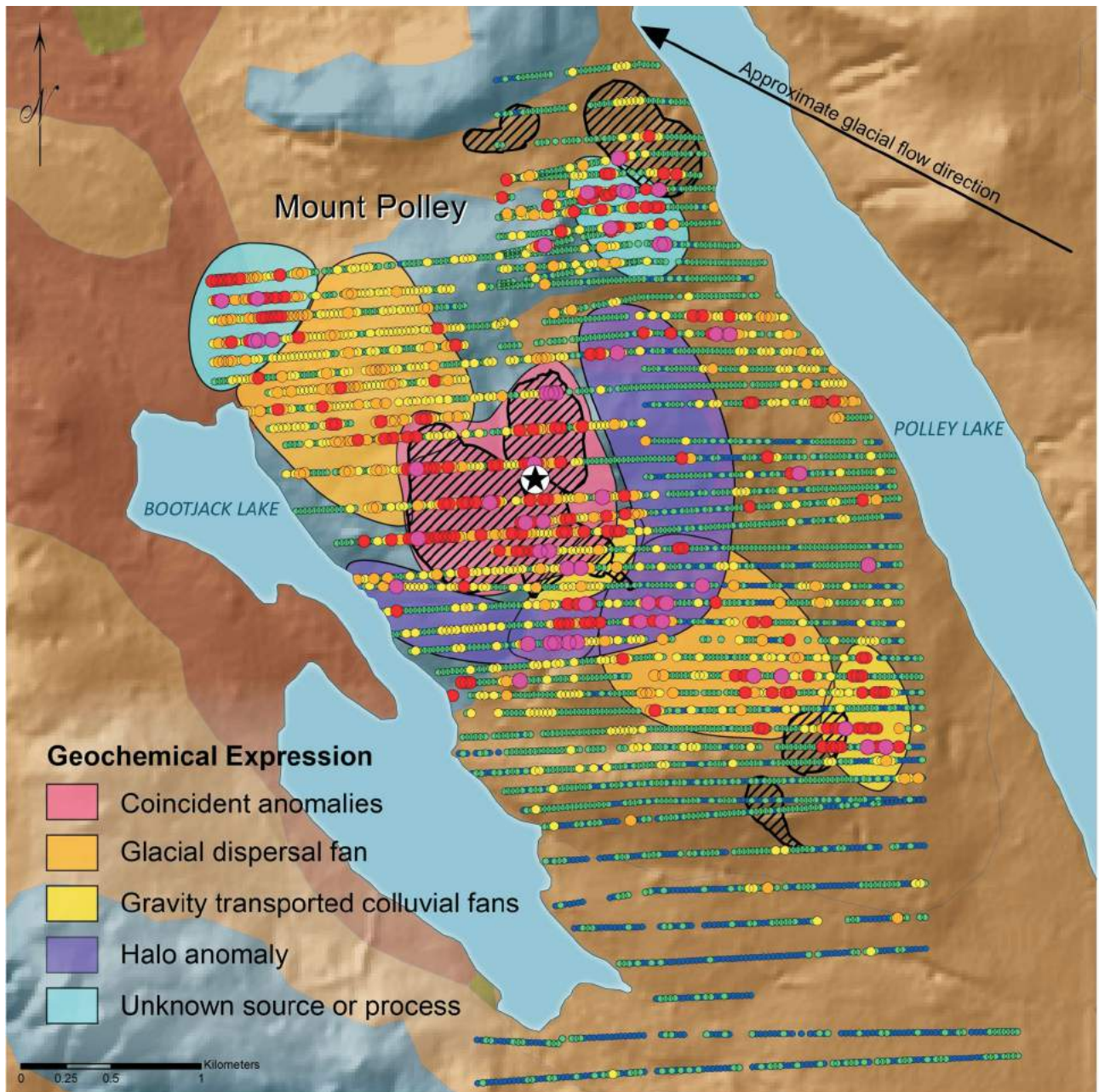
Shallow, Locally Derived Cover

The simplest case for interpreting geochemical signatures, aside from residual soils, is in those areas where the deposits are concealed beneath shallow (on the order of 1–3 m), locally-derived cover, such as basal-till veneers or colluvium, or areas that are characterized by predominantly locally-derived cover sediment (tens of metres). In this case, the soils are developed directly from material transported from the deposit and, as a result, the geochemical signature can be preserved and detected in B-horizon soils. Two locations where this is interpreted as occurring are the Galaxy

Table 3. Summary of B-horizon soil surveys at Mount Polley, Mount Milligan and Galaxy porphyry deposits.

	Mount Polley	Mount Milligan	Galaxy
ARIS number	16040 (McNaughton, 1987)	12912 (Heberlein et al., 1984)	29628 (Caron, 2007)
Availability of water	Dry	Dry	Dry
Temperature	Warm	Warm	Warm
Topography	Variable - steep	Variable - steep	Slight
Surficial material	Variable simple to complex Transported Till veneer Till blanket with colluvium	Variable simple to complex Transported Colluvium Till blanket Glaciofluvial	Simple Transported Till veneer or blanket
Geochemical survey	B-horizon soils, 80 mesh, aqua-regia digest, ICP-ES	B-horizon soils, 80 mesh, aqua-regia digest, ICP-ES finish	B-horizon soils, 80 mesh, aqua-regia digest, ICP-ES
Elements analyzed	Ag, As, Au, Cd, Co, Cr, Cu, Fe, La, Mg, Mo, Mn, Ni, Pb, V, W, Zn	Cu, Ti, P, K, Cr, La, B, Mg, Ca, Mo, Sr, Zn, Pb, Al, Sn, Cd, Th, U, Bi, V, Ba, W, Ni, Fe, Ag, Mn, Sb, As, Co, Au	La, P, Bi, Al, Zn, Na, Ba, Au, Cu, Ag, Mo, Co, Cd, Fe, Ni, Cr, As, Ca, Mg, V, Sr, Ti, Sb

Abbreviations: ARIS, BC assessment report indexing system; ICP-ES, inductively coupled plasma-emission spectrometry



Copper in B-Horizon soil

- 99th - 100th percentile: 1934 - 14337 ppm
- 95th - 99th percentile: 681 - 1933 ppm
- 90th - 95th percentile: 395 - 680 ppm
- 75th - 90th percentile: 163 - 394 ppm
- 25th - 75th percentile: 27 - 162 ppm
- 0 - 25th percentile: 2 - 26 ppm

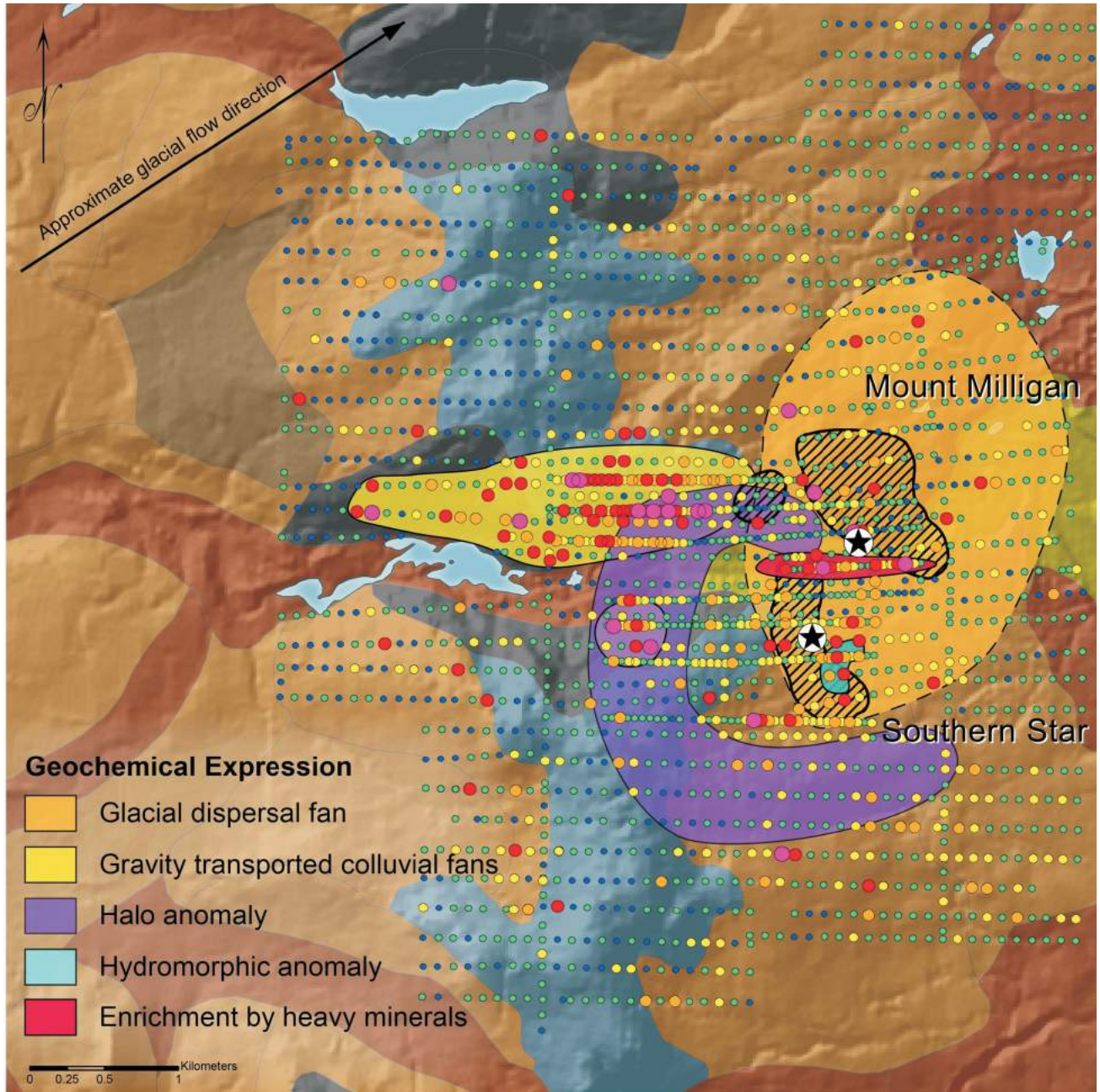
Dominant surficial material

- Shallow, locally-derived cover
- Thick, complex, multi-provenance cover
- Till and glaciofluvial material
- Other

Areas of known mineralization

-
- ★ **Mount Polley**
(5823580N, 592100E, NAD 83 Z10)

Figure 2. Copper distribution in B-horizon soils at the Mount Polley porphyry deposit, and illustration of associated geochemical expressions and distribution processes. Surficial material data modified from soil (terrain) mapping by the BC Ministry of Environment (2011); digital elevation data obtained from GeoBase® (Canadian Council on Geomatics, 2000); lake information obtained from Massey et al. (2005); and geochemical data from McNaughton (1987). Note: complete dataset extends beyond the limits of the map.



Copper in B-horizon soils

- 99th - 100th percentile: 554 - 5463 ppm
- 95th - 99th percentile: 241 - 553 ppm
- 90th - 95th percentile: 158 - 240 ppm
- 75th - 90th percentile: 84 - 157 ppm
- 25th - 75th percentile: 29 - 83 ppm
- 0 - 25th percentile: 7 - 28 ppm

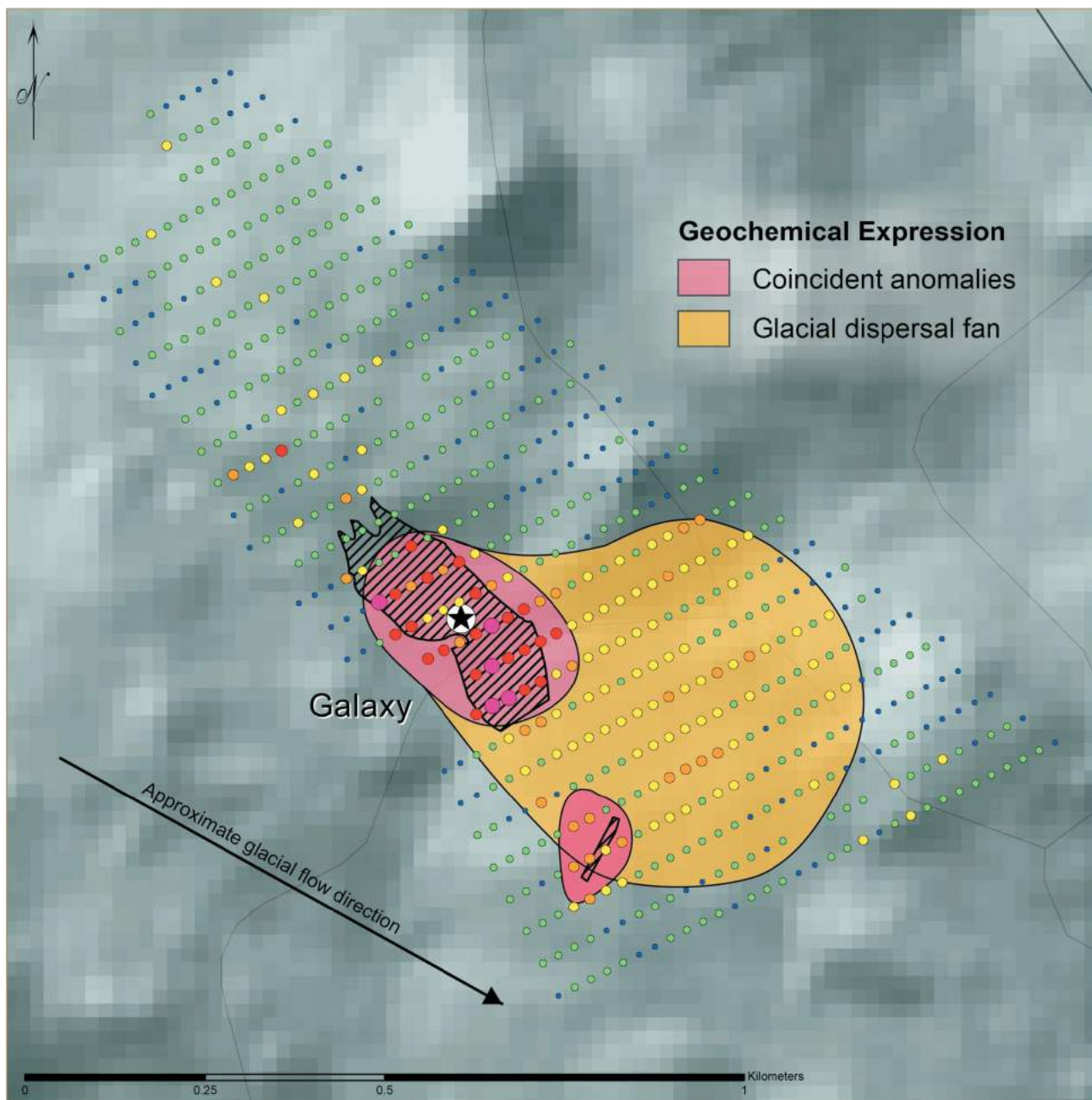
Dominant surficial material

- Glaciofluvial materials and till
- Colluvium over bedrock
- Shallow, locally-derived cover
- Fluvial materials
- Till blanket
- Thick, complex, multi-provenance cover

Approximate areas of known mineralization

- Mount Milligan (6109060N, 434476E, NAD 83 Z10)
- Mount Milligan - Southern Star (6108415N, 434148E, NAD 83 Z10)

Figure 3. Copper distribution in B-horizon soils at the Mount Milligan porphyry deposit, and illustration of associated geochemical expressions and distribution processes. Surficial material data modified from soil (terrain) mapping by the BC Ministry of Environment (2011). Digital elevation data obtained from GeoBase® (Canadian Council on Geomatics, 2000); lake information obtained from Massey et al. (2005); and geochemical data from Heberlein et al. (1984). Note: complete dataset extends beyond the limits of the map.



Copper in B-horizon Soil

- 99th - 100th percentile: 2616 - 5989 ppm
- 95th - 99th percentile: 600 - 2615 ppm
- 90th - 95th percentile: 314 - 599 ppm
- 75th - 90th percentile: 179 - 313 ppm
- 25th - 75th percentile: 91 - 178 ppm
- 0 - 25th percentile: 18 - 90 ppm

Dominant surficial material

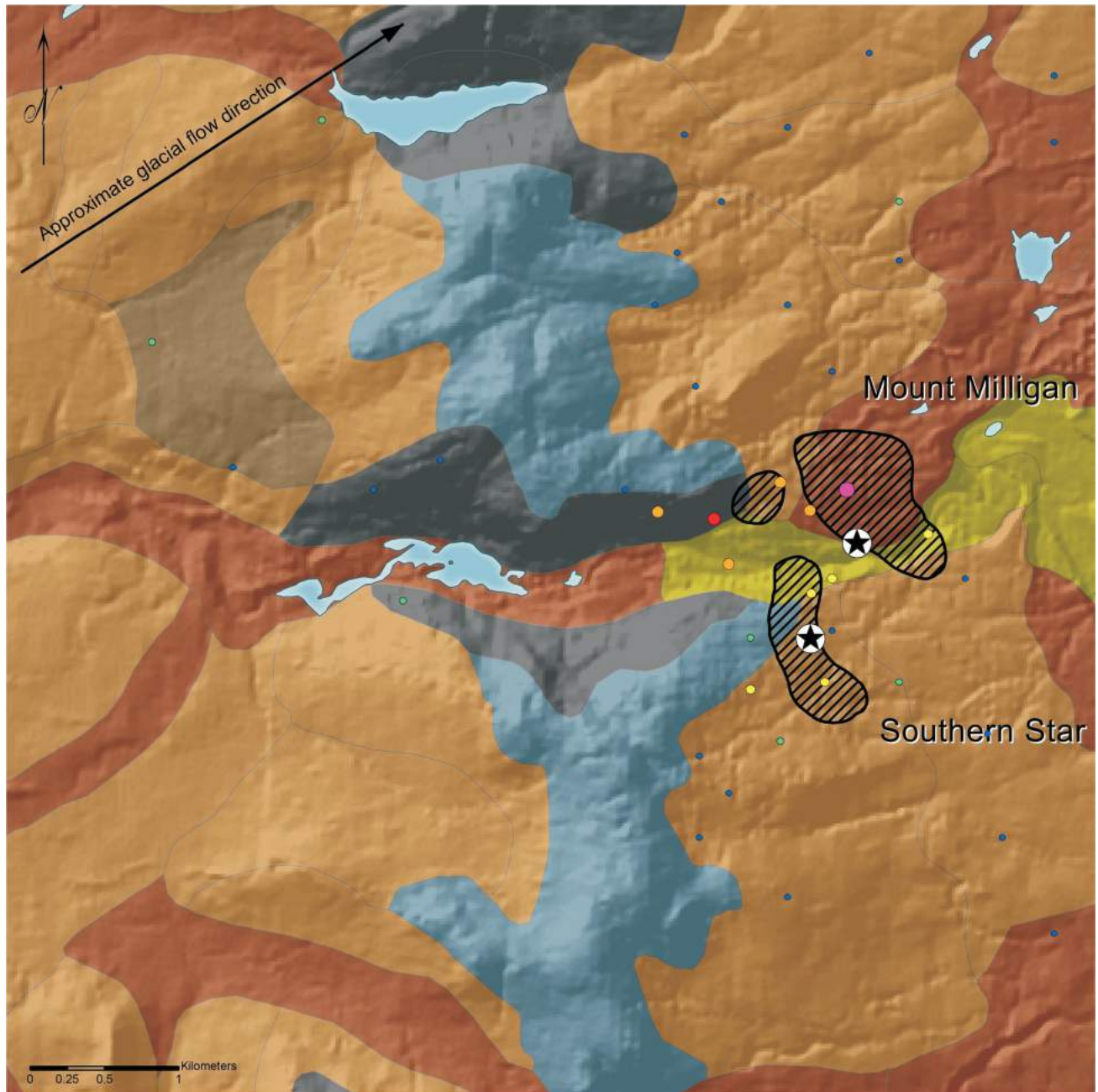
- Shallow, locally-derived cover

Areas of known mineralization



- ★ **Galaxy**
(5613329N, 682096E, NAD 83 Z10)

Figure 4. Copper distribution in B-horizon soils at the Galaxy porphyry deposit, and illustration of associated geochemical expressions and distribution processes. Surficial material data modified from soil (terrain) mapping by the BC Ministry of Environment (2011); digital elevation data obtained from GeoBase® (Canadian Council on Geomatics, 2000); and geochemical data from Caron (2007).



Gold in lodgepole pine bark

- 99th - 100th percentile: 144 - 185 ppm
- 95th - 99th percentile: 70 - 143 ppm
- 90th - 95th percentile: 33 - 69 ppm
- 75th - 90th percentile: 14 - 32 ppm
- 25th - 75th percentile: 5 - 13 ppm
- 0 - 25th percentile: < 5 ppm

Dominant surficial material

- Glaciofluvial materials and till
- Colluvium over bedrock
- Shallow, locally-derived cover
- Fluvial materials
- Till blanket
- Thick, complex, multi-provenance cover

Approximate areas of known mineralization

- ▨
- ★ **Mount Milligan**
(6109060N, 434476E, NAD 83 Z10)
- ★ **Mount Milligan - Southern Star**
(6108415N, 434148E, NAD 83 Z10)

Figure 5. Gold distribution in lodgepole-pine (*Pinus contorta latifolia*) bark at the Mount Milligan porphyry deposit, and illustration of associated geochemical expressions and distribution processes. Surficial material data modified from soil (terrain) mapping by the BC Ministry of Environment (2011); digital elevation data obtained from GeoBase® (Canadian Council on Geomatics, 2000); lake information obtained from Massey et al. (2005); and geochemical data from Dunn et al. (1997). Note: complete dataset extends beyond the limits of the map.

deposit and areas in the vicinity of the Mount Polley deposit.

At Mount Polley, in areas covered by a shallow till veneer (approximately 1 m or less), there are elevated (Cu, Mo, Au) and reduced (As) soil geochemical signatures coincident with the mineralization (Figure 2). This area is also bounded by elevated Pb and Zn in soil forming a halo around the mineralized bedrock (Figure 2). Compared to Mount Polley, the till cover at the Galaxy deposit is slightly thicker; however, the B-horizon soil geochemistry also exhibits elevated Cu, Mo and Au coincident with the mineralized zone (Figure 3). Evident at Galaxy, though not at Mount Polley, is a zone of depressed barium concentrations in soil also coincident with the mineralized zone, but this may be an effect related to the low solubility of some Ba minerals (e.g., barite) in the aqua-regia digestion of the soil samples. The geochemical analyses of soil samples at Galaxy did not generate reliable data for As, Pb and Zn, and therefore these elements cannot be compared with the data collected at the Mount Polley deposit.

Associated with the coincident soil geochemical anomalies discussed above at the Mount Polley and Galaxy deposits are glacial dispersal fans, in the shallow cover, which extend the soil anomalies in the direction of glacial transport. At Mount Polley (Figure 2), the glacial dispersal fan shows elevated Cu, Au and Mo, the highest values being coincident with mineralization. At Galaxy, the dispersal fan shows elevated Cu (Figure 4) and Au, but provides no conclusive evidence for glacial dispersal of Mo.

Another possibility for predominantly locally-derived cover is material transported by gravity or colluvial processes. Both the Mount Polley and Mount Milligan deposits have areas of steep relief proximal to mineralization, where colluvial processes have the potential to transport mineralized material. These areas of steep elevation show evidence of gravity-transported anomalies and geochemical analysis of B-horizon soils reveals elevated Cu, Au, \pm Mo and \pm Co values in soils overlying colluvium developed from mineralized zones (Figures 2, 3).

Complex, Multiprovenance Cover

Areas of the Mount Polley and Mount Milligan deposits are covered by complex multiprovenance till blankets, which may be intermixed with local colluvium. In most cases involving complex cover, B-horizon soils are inadequate to determine the location of mineralization and there is no conclusive, coincident, elevated geochemical signature in soil relating to the mineralization at these deposits. However, at Mount Milligan there is evidence of geochemical haloes in the B-horizon soils, which show elevated levels of As, Zn and Pb surrounding mineralization (Figure 3).

Although there are no coherent coincident geochemical indicators within the B-horizon soils overlying the thicker, complex transported cover at Mount Polley and Mount Milligan, there are patchy, elevated concentrations of Cu, Mo and Au in soils following the direction of glacial dispersal at both deposits, which may be related to the up-ice mineralization (Figures 2, 3). These elevated values could indicate the presence of lenses of locally-derived material in the till blankets or of small windows to the underlying till veneer.

Vegetation and Tills

The vegetation survey of lodgepole-pine (*Pinus contorta latifolia*)-bark conducted at the Mount Milligan deposit by Dunn et al. (1997) was successful in identifying areas of mineralization under areas of complex cover and revealed elevated Au (Figure 5), Cu, Mo and As in bark directly overlying or immediately adjacent to mineralization. A till survey by Sibbick et al. (1997) conducted at the same time as the sampling of lodgepole-pine bark, also found similar element-distribution patterns. The maximum Au value in bark (Figure 5), located over the northeastern area of mineralization, may reflect transported cover material from the southern mineralized area and may not be an in situ anomaly; this situation may also apply in the case of Cu, As and Mo.

Hydromorphic Anomalies

Hydromorphic anomalies are formed through transport and concentration of elements by an aqueous process and are generally recognized through the common association of elements that are enriched during these processes. An example of a hydromorphic anomaly interpreted from the soil geochemical data from the Mount Milligan deposit is shown in Figure 3; a small soil-Cu anomaly overlying a mineralized area has formed in a topographic depression and yielded elevated Mn, Fe and Co concentrations; these elements are generally found associated with hydromorphic anomalies.

Fluvial Concentration of Heavy Minerals

An elongate area of elevated Cu, Co and Fe concentration in soil labelled 'enrichment by heavy minerals' (Figure 3) is located along a valley bottom overlying fluvial sediments at the Mount Milligan deposit. It should be noted that the linear appearance of this anomaly is somewhat exaggerated due to a slight baseline shift in the geochemistry between the main survey lines and the infill lines; however, when comparing this anomaly to the adjacent infill lines, it remains readily apparent. The higher concentration of Cu, Co and Fe in the soil is also an association typical of a hydromorphic anomaly; however, Mn is not elevated and there are also elevated Ti and V associated with this area. The higher Ti and V can be indicative of elements concentrated by accumulation of heavy minerals; the proximity of

the soil anomaly to the fluvial sediments, in which heavy minerals (e.g., magnetite) might accumulate, supports this possibility.

Summary

Available data from multiple sources, including government, Geoscience BC, academic institutions and industry, have been compiled to allow the generation of empirically derived geochemical-exploration models. This compilation included geochemical data for over 70 000 surficial-material samples collected by industry; although publicly available, these data were only available in a largely unusable PDF format. The data were integrated into a comprehensive geochemical database for 41 porphyry deposits throughout BC (presented in Table 2). This database is being used, along with data for known mineralization, surficial-material mapping, digital elevation models, climate models, geology and geophysics, to generate geochemical-exploration models showing generalized or expected geochemical dispersion and dispersal patterns for porphyry deposits in BC. These models, developed for specific deposit types and climatic environments, provide the framework for the interpretation of geochemical-exploration-program design and data in areas not covered by proper orientation surveys, maximizing the potential for success in areas for which limited information is available.

The limited data presented here highlight the importance of integrating detailed surficial mapping and geochemical-distribution controls and processes into survey design and data interpretation. Without this integration, an area can easily be excluded, based on perceived negative results, or upgraded, based on false positive results. The selection of the proper sample media and method is the key to exploration success and, in many cases, one sample media may not be suitable to properly cover even a relatively small area.

Acknowledgments

The authors would like to thank Geoscience BC and the Mineral Deposit Research Unit at the University of British Columbia for providing funding for this project. Many thanks to the members of the project advisory committee for their discussion of ideas necessary to the success of this project, and especially to R. Lett and P. Bradshaw for spearheading it from the start. The authors would also like to thank N. Bueckert, L. Bueckert, C. Oliver and M. Tang for their help with data collection. Many thanks as well to R. Lett for his thorough and insightful review of this paper.

References

Aspandiar, M.F., Anand, R.R. and Gray, D.J. (2008): Geochemical dispersion mechanism through transported cover: implications for mineral exploration in Australia; CRC LEME Open File Report 246, p. 1–84.

- BC Geological Survey (2011): MINFILE BC mineral deposits database; BC Ministry of Energy and Mines, URL <<http://www.empr.gov.bc.ca/Mining/Geoscience/MINFILE/Pages/default.aspx>> [October 2011].
- BC Ministry of Environment (2011): BC terrain data; BC Ministry of Environment, Environmental Stewardship Division, URL <<http://www.env.gov.bc.ca/esd/distdata/ecosystems/>> [October 2011].
- Bradshaw, P.M.D. (1975): Conceptual models in exploration geochemistry – the Canadian Cordillera and Canadian Shield; *Journal of Geochemical Exploration*, v. 4, p. 1–213.
- Butt, C.R.M. (2005): Geochemical dispersion, process and exploration models; *in* *Regolith Expression of Australian Ore Systems*, C.R.M. Butt, I.D.M. Robertson, K.M. Scott and M. Cornelius (ed.), CRC LEME, Perth, p. 81–106.
- Butt, C.R.M. and Zeegers, H., editors (1992): *Regolith exploration geochemistry in tropical and subtropical terrains*; *in* *Handbook of Exploration Geochemistry*, Elsevier, Amsterdam, v. 4, 607 p.
- Cameron, E.M., Hamilton, S.M., Leybourne, M.I., Hall, G.E. and McClenaghan, M.B. (2004): Finding deeply buried deposits using geochemistry; *Geochemistry: Exploration, Environment, Analysis*, v. 4, p. 7–32.
- Canadian Council on Geomatics (2000): Canadian digital elevation data; Natural Resources Canada, GeoBase®, URL <<http://www.geobase.ca>> [October 2011].
- Caron, L. (2007): Grid work, soil geochemistry and geophysics on the Galaxy property located in the Afton area; BC Ministry of Energy and Mines, Assessment Report 29628, 88 p., URL <<http://www.empr.gov.bc.ca/Mining/Geoscience/ARIS/Pages/default.aspx>> [October 2011].
- Clague, J.J. and James, T.S. (2002): History and isostatic effects of the last ice sheet in southern British Columbia; *Quaternary Science Reviews*, v. 21, p. 71–87.
- Daly, C., Gibson, W.P., Taylor, G.H., Johnson, G.L. and Pasteris, P. (2002): A knowledge-based approach to the statistical mapping of climate; *Climate Research*, v. 22, p. 99–113.
- Dunn, C.E., Balma, R.G. and Sibbick, S.J. (1997): Biogeochemical survey using lodgepole pine bark: Mount Milligan central British Columbia; BC Ministry of Energy and Mines, Open File 1996-17, 115 p., URL <<http://www.empr.gov.bc.ca/Mining/Geoscience/PublicationsCatalogue/OpenFiles/1996/Pages/1996-17.aspx>> [October 2011].
- Hebda, R. (2007): Biodiversity: geological history in British Columbia; *in* Report on the Status of Biodiversity in BC, Biodiversity BC Technical Subcommittee, URL <<http://www.biodiversitybc.org/assets/Default/BBC%20Biodiversity%20and%20Geological%20History.pdf>> [October 2011].
- Heberlein, D., Rebagliati, C.M. and Hoffman, S.J. (1984): 1984 Geological and geochemical exploration activities, Phil A, B, and 1, claim groups; BC Ministry of Energy and Mines, Assessment Report 12912, 290 p., URLs <<http://aris.empr.gov.bc.ca/ArisReports/12912A.PDF>>, <<http://aris.empr.gov.bc.ca/ArisReports/12912B.PDF>> [October 2011].
- Lefebvre, D.V. and Ray, G.E., editors (1995): Selected British Columbia mineral deposit profiles, volume 1 – metallics and coal; BC Ministry of Energy and Mines, Open File 1995-20, 135 p., URL <<http://www.em.gov.bc.ca/Mining/>>

[Geoscience/PublicationsCatalogue/OpenFiles/1995/Pages/1995-20.aspx](http://www.empr.gov.bc.ca/Mining/Geoscience/PublicationsCatalogue/OpenFiles/1995/Pages/1995-20.aspx) [October 2011].

- Lett, R.E. and Jackaman, W. (2000): Geochemical exploration models, volume 1: VMS deposits in south central BC; BC Ministry of Energy and Mines, Open File 2000-31, 31 p., maps, CD-ROM.
- Lett, R.E. (2001): Geochemical exploration models, volume 2: shale-hosted Pb-Zn-Ag deposits in NE BC; BC Ministry of Energy and Mines, Open File 2001-7, 70 p., maps, appendices, URL <http://www.empr.gov.bc.ca/Mining/Geoscience/PublicationsCatalogue/OpenFiles/2001/Pages/2001-7.aspx> [October 2011].
- Lett, R.E.W. and Bradshaw, P. (2003): Atlas of landscape geochemical models for porphyry copper, VMS and gold deposits in the Cordillera from Alaska to Nevada; Association of Applied Geochemists, Explore newsletter, no. 118, p. 20–23.
- Massey, N.W.D., MacIntyre, D.G., Desjardins, P.J. and Cooney, R.T. (2005): Digital geology map of British Columbia: whole province; BC Ministry of Forests, Lands and Mines, GeoFile 2005-1, URL <http://www.empr.gov.bc.ca/Mining/Geoscience/PublicationsCatalogue/GeoFiles/Pages/2005-1.aspx> [October 2011].
- McNaughton, K (1987): 1986 geochemical, geophysical and drilling report on the BJ, Bootjack, CB and Polley mineral claims; BC Ministry of Energy and Mines, Assessment Report 16040, 494 p., URLs <http://aris.empr.gov.bc.ca/ArisReports/16040A.PDF>, <http://aris.empr.gov.bc.ca/ArisReports/16040B.PDF>, <http://aris.empr.gov.bc.ca/ArisReports/16040C.PDF> [October 2011].
- Sibbick, S.J., Balma, R.G. and Dunn, C.E. (1997): Till geochemistry of the Mount Milligan area; BC Ministry of Energy and Mines, Open File 1996-22, 18 p., URL <http://www.empr.gov.bc.ca/Mining/Geoscience/PublicationsCatalogue/OpenFiles/1996/Pages/1996-22.aspx> [October 2011].
- University of British Columbia (2011): ClimateBC: a program to generate climate normal data for geneecology and climate change studies in western Canada; University of British Columbia, Centre for Forest Conservation Genetics, URL <http://www.genetics.forestry.ubc.ca/cfcg/climate-models.html> [October 2011].

Fluid Controls on Ore Genesis in the Eskay Creek Deposit, Northwestern British Columbia (NTS 104B/09, /10)

T. Meuzelaar, Department of Geology and Geological Engineering, Colorado School of Mines, Golden CO, tmeuzela@mymail.mines.edu

T. Monecke, Department of Geology and Geological Engineering, Colorado School of Mines, Golden CO

Meuzelaar, T. and Monecke, T. (2012): Fluid controls on ore genesis in the Eskay Creek deposit, northwestern British Columbia (NTS 104B/09, /10); in Geoscience BC Summary of Activities 2011, Geoscience BC, Report 2012-1, p. 41–52.

Abstract

Geochemical modelling was performed to constrain fluid controls on the formation of the Eskay Creek sulphide and sulphosalt deposit in northwestern British Columbia. Using recently published H₂S solubility data, models of seafloor sulphide precipitation were developed for several modern seafloor vents of known fluid compositions. The modelling suggests that a fluid with a pH of 4.5–5.0 could have precipitated sphalerite at Eskay Creek at temperatures of 180–220°C. Such a fluid could have sufficient alkalinity to reach carbonate saturation, which is required to explain the origin of the carbonate-kaolinite alteration in the mudstone hosting the stratiform orebodies of clastic sulphide and sulphosalt deposits. The geochemical modelling demonstrates that the Eskay Creek deposit formed from a near-neutral and relatively reducing fluid. As the chemical character of the hydrothermal fluid is not unusual for submarine hydrothermal systems, exploration for volcanic-hosted, precious-metal deposits such as Eskay Creek can be guided by criteria not unlike those used in the search for conventional massive sulphide deposits.

Purpose of Research

The Eskay Creek deposit (MINFILE 104B 008; BC Geological Survey, 2011) in northwestern BC represents an unusual volcanic-hosted sulphide and sulphosalt deposit that is characterized by high precious-metal concentrations (average of 48.4 g/t Au and 132.2 g/t Ag), a geochemical association of the precious metals with the epithermal suite of elements, and low temperatures (<200°C) of sulphide and sulphosalt deposition (Roth et al., 1999). Based on these deposit attributes, Eskay Creek is considered to represent the type example of a new group of volcanic-hosted gold deposits that formed in relatively shallow water, submarine

environments, where phase separation of the hydrothermal fluids represented an important control on metal precipitation (Hannington et al., 1999).

Detailed mineralogical and geochemical investigations of the hostrocks of the Eskay Creek deposit resulted in the definition of a distinctive alteration halo surrounding the deposit (Ettlinger, 1992; Roth et al., 1999; Meuzelaar and Monecke, 2011). Most notable is an extensive zone of carbonate-kaolinite alteration in the carbonaceous mudstone hosting the stratiform clastic sulphide and sulphosalt orebodies. This style of alteration is largely restricted to areas overlying upflow zones of mineralizing hydrothermal fluids and associated discordant sulphide zones in the footwall rhyolite. The newly defined alteration signature and compositional trends within the carbonaceous mudstone can be used to parameterize models of fluid evolution aimed at understanding deposit genesis and the unique geochemical footprint of the Eskay Creek deposit.

Previous numerical simulations of submarine ore-forming processes have so far been impaired by a number of issues, including the quality of H₂S-solubility data in databases used for geochemical modelling. In this paper, it is shown that the data from Duan et al. (2007) provide reliable constraints on H₂S solubility. The quality of the data was tested by modelling sulphide precipitation at modern seafloor vent sites, where the compositions of the mineralizing chloride waters are known. The results indicate that predicted sulphide-precipitation temperatures are in agreement with seafloor observations. Based on published homogenization temperatures of fluid inclusions in sphalerite, it is possible for the first time to constrain the chemical nature of the fluids responsible for the formation of the Eskay Creek deposit. The findings of the geochemical modelling have significant implications for exploration as they show that gold-rich massive sulphide deposits, such as the Eskay Creek deposit, are not formed by hydrothermal fluids of unusual chemical character.

Geology

The Eskay Creek deposit is located on the western margin of the allochthonous Stikine terrane of the northern Cana-

Keywords: Eskay Creek deposit, massive sulphide deposits, gold, ore vectors, H₂S solubility, sulphide precipitation, geochemical modelling

This publication is also available, free of charge, as colour digital files in Adobe Acrobat® PDF format from the Geoscience BC website: <http://www.geosciencebc.com/s/DataReleases.asp>.

dian Cordillera (Figure 1). The hostrock succession of the deposit is part of the Upper Hazelton Group, which formed by extensional, continental-margin arc volcanism between 181 and 172 Ma (Barrett and Sherlock, 1996; Childe, 1996).

The hostrocks of the deposit are folded into a shallowly north-plunging, north-northeast-trending, upright open anticline (Figure 1). The ore zones of the Eskay Creek deposit occur on the western limb of the fold, near the fold closure, and dip gently 30–45° to the west. The metamorphic grade in the mine area is lower greenschist (Roth et al., 1999). The bulk of the mineralization consists of stratiform clastic beds and laminations of commonly graded sulphide and sulphosalt debris, which are hosted by a thick interval of carbonaceous mudstone at the contact between felsic volcanic rocks and overlying basalt (Britton et al., 1990; Ettlinger, 1992). In addition to the stratiform orebodies, economic concentrations of precious metals have been recognized in discordant zones of sulphide veins and disseminations in the footwall rhyolite.

The stratigraphic footwall of the deposit is composed of multiple rhyolite units and associated volcanoclastic deposits, reaching a maximum apparent thickness of approxi-

mately 100 m in the mine area (Britton et al., 1990). Hydrothermal alteration is widespread throughout the footwall rhyolite (Robinson, 1991; Barrett and Sherlock, 1996). Secondary potassium-feldspar formation and moderate silicification occurred in the periphery of the stratiform ores and in deeper parts of the footwall. Immediately underlying the stratiform ore zones, a tabular zone of more intense and texturally destructive chlorite and white mica alteration is recognized (Ettlinger, 1992; Roth et al., 1999). An unusual hydrocarbon alteration occurs locally below the stratiform ore zones (Ettlinger, 1992; Barrett and Sherlock, 1996; Roth et al., 1999).

The footwall rhyolite is overlain by carbonaceous mudstone, which hosts the stratiform ore zones of clastic sulphide and sulphosalt deposits. The carbonaceous mudstone has an apparent stratigraphic thickness that ranges from <1 to >60 m (Britton et al., 1990); it is laminated, thinly bedded or massive and contains abundant intercalated, tan-coloured beds of fine-grained volcanoclastic material. Calcareous and siliceous intervals are present, but not common. The carbon content generally decreases toward the top of the unit. The mudstone contains radiolarians, dinoflagellates, rare belemnites and corals, suggesting a marine depositional environment (Britton et al., 1990; Robinson,

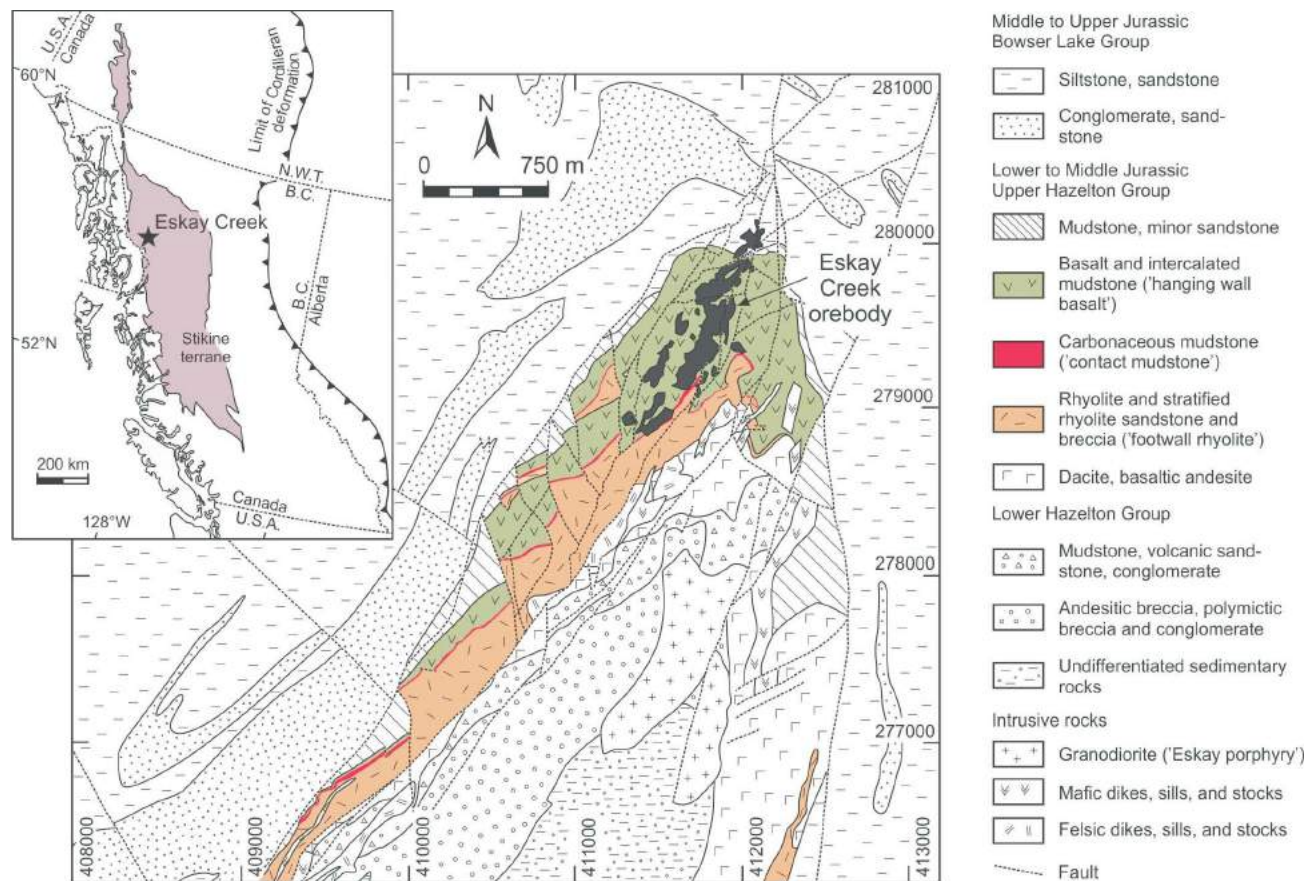


Figure 1. Geology of the Eskay Creek anticline, showing the location of the surface projection of the ore zones (modified from Alldrick et al., 2005). Inset shows the location of the deposit in the Stikine terrane (modified from Gabrielse et al., 1991).

1991; Nadaraju, 1993; Monecke et al., 2005). Thin pyrite laminations are common throughout the unit. The occurrence of flame structures at the base of the sulphide laminations indicates that the pyrite is clastic in origin (Britton et al., 1990; Monecke et al., 2005). In addition to the sulphide laminations, thin veins and veinlets of pyrite crosscutting bedding are widespread close to the contact with the underlying rhyolite.

Basalt sills and dikes occur throughout the carbonaceous mudstone unit. The occurrence of mudstone-matrix basalt breccia along the bottom and top margins of coherent basalt intervals indicates that the lava intruded the mudstone when it was still wet and unconsolidated (Monecke et al., 2005). The relative proportion of basalt increases in the upper part of the hostrock succession of the Eskay Creek deposit. Both intrusive and extrusive basalt units occur at this stratigraphic level, forming an interval up to 150 m thick, which generally thins southward, away from the deposit (Britton et al., 1990).

Previous work

Results of a detailed mineralogical and geochemical study of the carbonaceous mudstone hosting the Eskay Creek deposit (Meuzelaar and Monecke, 2011) revealed a number of important geochemical trends, which can be used both for numerical-model parameterization and target vectoring when exploring for precious and base metals. The occurrence of carbonate minerals appears to correlate with the distance to the mineralized zones, with higher dolomite-ankerite and magnesite-siderite abundances indicating proximity to the ore zones at the base of the mudstone unit. Magnesian calcite is abundant in the stratigraphic hanging-wall proximal to the stratiform ore zones.

In addition to carbonate alteration, which appears to be the most reliable vector of proximity within tens to hundreds of metres of mineralized zones, the composition of chlorite appears to vary systematically. Chlorite close to mineralization is characterized by an increased Mg content, which is consistent with compositional trends observed in the carbonate mineralogy. Local silicification of mudstone has been noted. Strongly altered mudstone samples collected close to the upflow zones of hydrothermal fluids are characterized by Na₂O depletion, which is caused by feldspar-destructive alteration commonly associated with submarine sulphide mineralization (e.g., Large, 1977; Schardt et al., 2001). Proximity to mineralization is also reflected in elevated F contents in sheet silicates, systematic changes in the Cs/Rb ratio of white mica and the Ni/V ratio in organic carbon.

The mudstone samples show increases in the galena, chalcopyrite and sphalerite contents with proximity to ore. Pyrite contained in background mudstone samples is mostly of diagenetic origin. However, pyrite that is distinctly en-

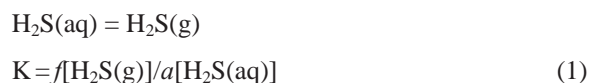
riched in As has also been recognized. This type of pyrite is interpreted to have formed in association with the sulphide and sulphosalt mineralization. Mineralogical variations in the mudstone samples in proximity to ore are reflected by increased Ag, As, Au, Cd, Cu, Sb, Pb, Te and Zn concentrations in whole-rock geochemical analyses. There is a strong correlation between the precious- and base-metal contents of the carbonaceous mudstone, which is reflective of the overall metal signature of the Eskay Creek deposit.

H₂S Solubility

Numerical simulation of the ore-forming processes at Eskay Creek and of those responsible for the formation of the associated carbonate-kaolinite alteration halo requires an adequate description of the H₂S solubility in the hydrothermal fluids.

Duan et al. (2007) summarized the results of previous experimental investigations, which have thus far been conducted only under a comparably narrow range of temperatures, pressures and salinities. Duan et al. (2007) also discussed the limitations of the various experimental studies and proposed a new thermodynamic model calculating the H₂S solubility in pure water and aqueous NaCl solutions. The model calculates the chemical potential of H₂S in the vapour phase using the equation of state presented in Duan et al. (1996), whereas the chemical potential of H₂S in the liquid phase is modelled using the approach described by Pitzer (1973). The proposed model is valid for solutions of varied electrolyte compositions, with ionic strengths (measured in terms of the NaCl molality) of 0–6 molal, at temperatures of 0–227°C, and H₂S fugacities of 0–200 bar (an online solubility calculator is available at <http://calc.geochem-model.org/>).

To conduct modelling for the present study, the H₂S-solubility data of Duan et al. (2007) was initially used to calculate the equilibrium constant *K* for the reaction and the corresponding mass-action equation



where *f* is the fugacity of the gas and *a* is the activity of H₂S in the solution. The fugacity of H₂S as a gas and the activity of H₂S in solution were made dimensionless based on the choice of an appropriate standard state (Bethke, 2008).

The values of the equilibrium-constant *K* for different temperatures calculated this way were inserted into the Lawrence Livermore National Laboratory (LLNL) thermochemical database (Delany and Lundeen, 1990), replacing the equilibrium constants originally given in the database. The original equilibrium constants for the LLNL and the extended LLNL thermochemical databases at temperatures ranging from 0 to 300°C are given in Figure 2.

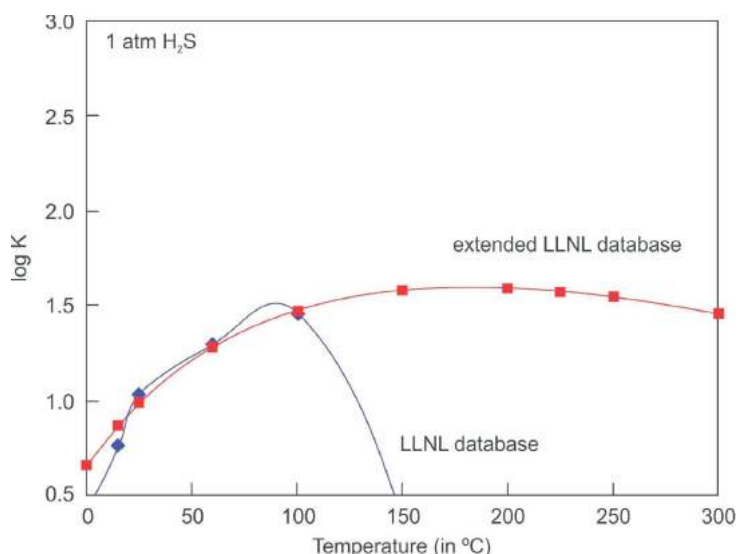


Figure 2. Temperature dependency of the equilibrium-constant K for the reaction $\text{H}_2\text{S}(\text{aq}) = \text{H}_2\text{S}(\text{g})$, according to the Lawrence Livermore National Laboratory (LLNL) thermochemical database (Delany and Lundeen, 1990) and the extended LLNL database.

The corrected equilibrium-constant data for the same temperature range, at ionic strengths of 0–2 molal and H_2S fugacities of 0–200 atm, are shown in Figure 3. Inspection of the data shows that the ionic strength has little influence on the equilibrium constant. Comparison with the original equilibrium constants in both LLNL databases reveals that they significantly underpredict H_2S solubility above 150°C at H_2S fugacities ranging from 1 to 40 atm. Duan et al. (2007) also noted that equilibrium constants calculated using the SUPCRT92 software (Johnson et al., 1992) underestimate H_2S solubility above 150°C. At 50 atm, the LLNL data underpredict solubility across the entire temperature range, whereas at higher fugacities of 100–200 atm both LLNL databases underpredict H_2S solubility below 100°C.

As a final step, the equilibrium constants describing the HS^- and H^+ partitioning were corrected in the LLNL database. The solubility data for dissolved H_2S and vapour-phase H_2S are given by the following two reactions:



Given that HS^- and H^+ partitioning data for the P-T- x_{NaCl} range of the solubility model from Duan et al. (2007) are not available, it is not possible to quantify equilibrium constants for these reactions. As reaction (1) is simply reaction (3) subtracted from reaction (2), the LLNL database was modified to calculate the equilibrium constant k_1 for reaction (1) from Duan et al. (2007) followed by the subtraction of k_1 from k_2 , the equilibrium constant for reaction (2). This yields k_3 , the equilibrium constant for reaction (3), which was used to replace the existing values in the LLNL database.

Following correction of the equilibrium-constant data, the LLNL database was used for modelling of the present study. It is important to note that the database is configured for modelling at 1 atm, temperatures of 0–300°C and activities calculated according to the B-dot equation of Helgeson et al. (1969) and Helgeson and Kirkham (1974). The 1 atm steam-saturation limitation appears somewhat troublesome given that seafloor hydrothermal venting occurs at a confining pressure corresponding to the hydrostatic pressure at a water depth of several hundreds to thousands of metres. However, Duan et al. (2007) pointed out that the fugacity coefficient of H_2S in the vapour phase of H_2S - H_2O mixtures differs little from that of pure H_2S within the temperature range of the model. As long as fluid temperature and hydrostatic confining pressure are below the two-phase curve for seawater (Bischoff and Rosenbauer, 1984), H_2S solubility can be estimated from H_2S fugacity apart from the saturation pressure of H_2O . Ohmoto (1996) showed that the two-phase curve of seawater is indeed an important control on the formation of modern, seafloor massive-sulphide accumulations. An additional constraint on modelling is imposed by the fact that the LLNL database is valid only for solutions with ionic strengths of up to 3.0 molal if Na and Cl are the dominant solutes. This condition is met in the case of most chloride waters sampled from modern seafloor vent sites (cf. Hannington et al., 2005).

Models of Sulphide Precipitation in Modern Vent Analogues

The quality of the equilibrium-constant data calculated above was evaluated by modelling sulphide precipitation from chloride waters of known compositions, which were sampled at modern seafloor vent sites. For this purpose, the

comprehensive compilation of modern seafloor fluid compositions by Hannington et al. (2005) was used. Although the database provides vent-fluid compositions for about 60 active vent sites worldwide, only 12 chloride waters were chosen for the present study. Most chloride waters either had temperatures exceeding the limits of the solubility model (227°C) by Duan et al. (2007) and the LLNL thermochemical database (300°C) or were not analyzed for all parameters required for geochemical modelling. In addition, the higher temperature vent fluids are likely poor analogues as sulphide and sulphosalt deposition at Eskay Creek occurred largely at temperatures below 200°C (Sherlock et al., 1999). The compositions of the 12 representa-

tive modern seafloor chloride waters are summarized in Table 1. Their pH values and contents of total dissolved solids are plotted in Figure 4.

The 12 chloride waters represent four different tectonic settings, including mid-ocean ridges, sedimented ridges, ridge-hotspot intersections and back-arc spreading centres and/or rifts; the latter is probably closest to the tectonic setting of the Eskay Creek deposit. Table 1 shows that the pH of the hydrothermal fluids broadly correlates with plate-tectonic setting and generally decreases from sedimented ridges (pH = 5.0–6.0), to ridge-hotspot intersections (pH = 4.0–4.5), mid-ocean ridges (pH = 3.0–4.0) and back-

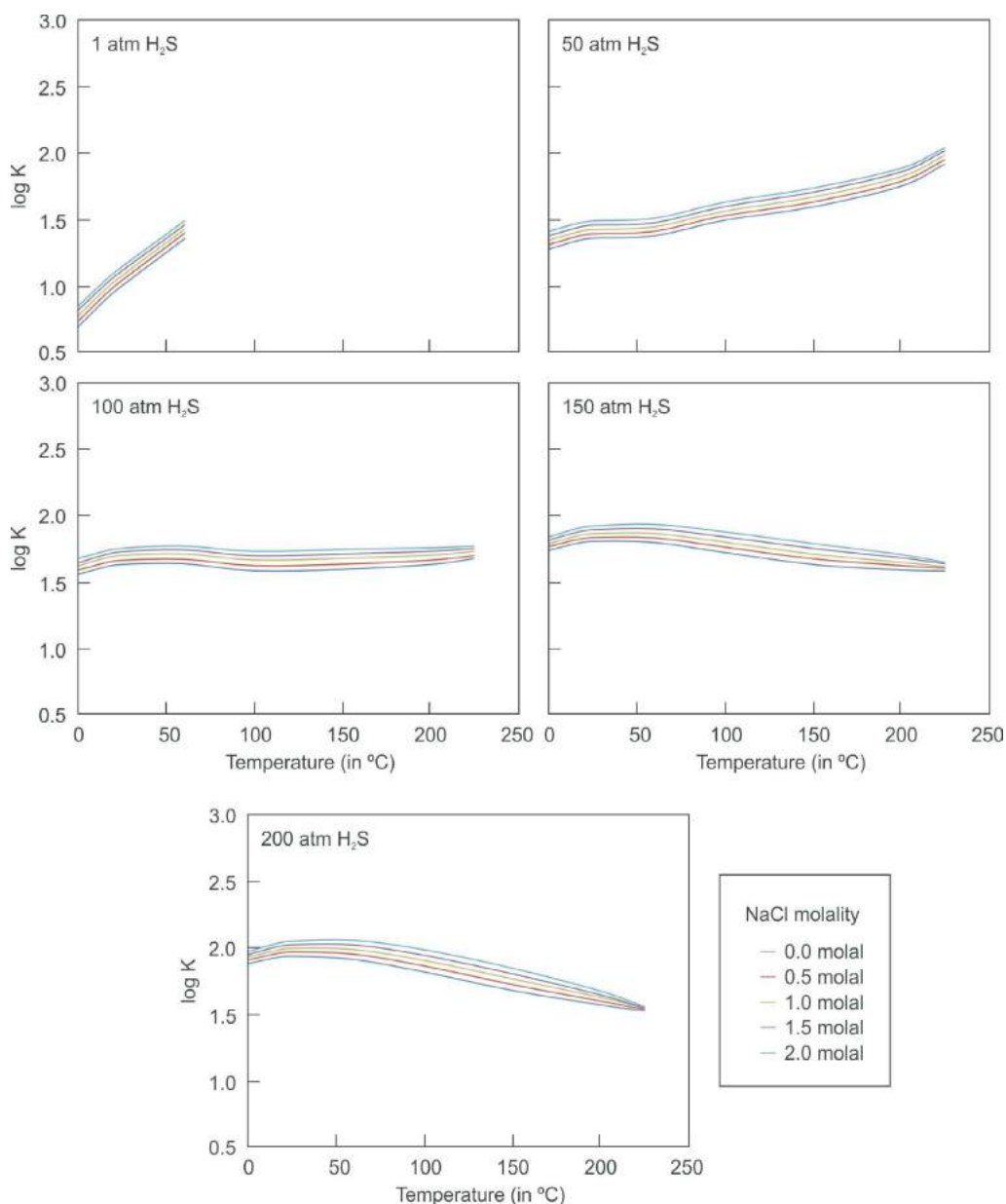


Figure 3. Temperature dependency of the equilibrium-constant K for the reaction $\text{H}_2\text{S}(\text{aq}) = \text{H}_2\text{S}(\text{g})$ at five selected H_2S fugacities and ionic strengths (NaCl molality) ranging from 0 to 2.0 molal (calculation is based on Duan et al., 2007).

Table 1. Composition of representative chloride waters from modern seafloor vent sites located in different tectonic settings (data compilation from Hannington et al., 2005).

	Seawater	North Cleft (NC)	South Cleft (SC)	21°N, EPR (EP)	17°S, SEPR (SE)	Guaymas (GY1)	Guaymas (GY2)
		Mid-ocean ridge	Mid-ocean ridge	Mid-ocean ridge	Mid-ocean ridge	Sedimented ridge	Sedimented ridges
Temperature (°C)	2	262	224	273	300	291	285
pH (25°C)	7.8	2.8	3.2	3.8	3.1	5.9	5.9
Total dissolved solids (mg/kg)	33183	87410	73900	44697	27318	46376	49474
Ionic strength (M)	0.6144	1.53	1.307	0.7591	0.4518	0.7799	0.8392
Composition:							
Cl (mM) ¹	541	1245	1087	579	323	589	637
Fe (µM)	<0.001	16400	18739	871	3600	49	180
Mn (µM)	<0.001	4250	3585	1002	740	222	236
Cu (µM)	<0.003	0.9	10	nd	10	nd	nd
Zn (µM)	<0.01	406	575	40	130	4	40
Pb (nM)	<0.01	1085	900	183	nd	265	653
Si (mM)	0.2	24	23	20	9	13	14
SO ₄ (mM)	27.9	0.01	0.01	0.01	0.01	0.01	0.01
Mg (mM)	52.7	0.01	0.01	0.01	0.01	0.01	0.01
Na (mM)	464	924	796	510	292	478	524
K (mM)	9.8	59	52	26	13	46	37
Ca (mM)	10.2	109	96	21	12	29	42
Sr (µM)	87	348	312	97	43	184	253
Li (µM)	26	2350	1718	1033	313	954	720

¹Concentrations are reported in M (moles), mM (millimoles), µM (micromoles) or nM (nanomoles) per kilogram (kg).

Abbreviation: nd, not detected

arc spreading centres and/or rifts (pH = 2.5–4.0). The higher pH of the chloride waters from sedimented ridges is likely a reflection of the neutralizing capacity of the sedimentary hostrocks. Figure 5 shows that the Zn and Pb concentrations for ten of the vent samples (data for two samples are either missing or below detection limit) are generally in-

versely proportional to pH, suggesting that the more acidic fluids have a higher capacity for transporting metals.

One representative chloride water sample from each of the four tectonic settings, generally representing a median content of total dissolved solids, was selected for numerical

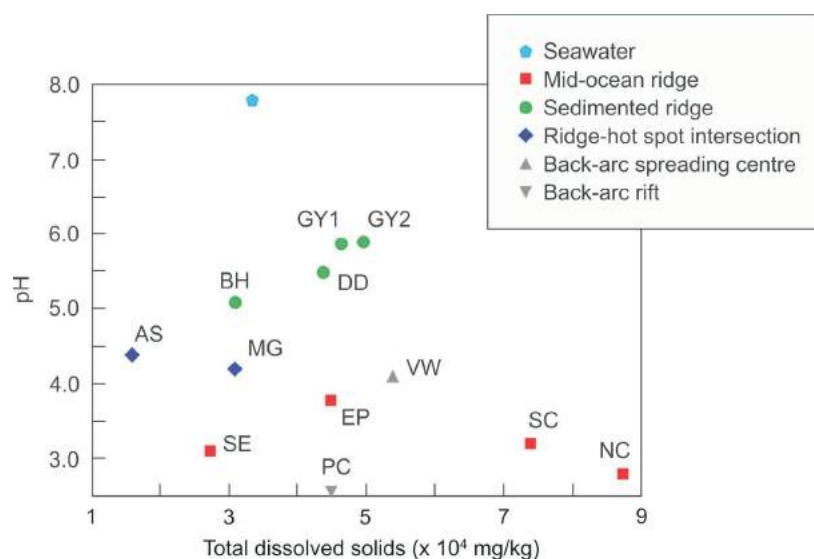


Figure 4. Scatter diagram of acidity (pH at 25°C) versus contents of total dissolved solids for representative chloride waters collected from different modern seafloor vent sites (data from Hannington et al., 2005). The composition of seawater is given for comparison. Abbreviations: AS, Axial Seamount; BH, Bent Hill; DD, Dead Dog; EP, 21°N, EPR; GY, Guaymas; MG, Menez Gwen; NC, North Cleft; PC, Pacmanus; SC, South Cleft; SE, 17°N, SEPR; VW, Vienna Wood.

Table 1 (continued)

	Dead Dog (DD)	Bent Hill (BH)	Axial Seamount (AS)	Menez Gwen (MG)	Vienna Wood (VW)	Pacmanus (PC)
	Sedimented ridge	Sedimented ridge	Ridge-hotspot intersection	Ridge-hotspot intersection	Back-arc spreading centre	Back-arc rift
Temperature (°C)	276	265	299	284	282	268
pH (25°C)	5.5	5.1	4.4	4.2	4.1	2.6
Total dissolved solids (mg/kg)	43530	30763	15593	30881	54010	44723
Ionic strength (M)	0.7361	0.5325	0.243	0.5155	0.9138	0.7446
Composition:						
Cl (mM) ¹	578	412	176	380	712	572
Fe (μM)	20	17	12	28	109	2404
Mn (μM)	63	78	142	59	348	3116
Cu (μM)	1.3	0.3	0.7	2.7	2	36
Zn (μM)	1.7	0.7	2.3	4.2	10	115
Pb (nM)	125	50	191	nd	4	7000
Si (mM)	10	nd	14	10	15	16
SO ₄ (mM)	0.01	0.01	0.01	0.01	0.01	0.01
Mg (mM)	0.01	0.01	0.01	0.01	1	0.01
Na (mM)	398	315	148	313	534	445
K (mM)	19	14	7	23	24	86
Ca (mM)	81	40	10	32	82	15
Sr (μM)	257	162	46	110	290	97
Li (μM)	500	370	184	270	1010	724

modelling. The four sites chosen were South Cleft (mid-ocean ridge), Dead Dog (sedimented ridge), Menez Gwen (ridge-hotspot intersection), and Pacmanus (back-arc rift). The four modelled vent fluids were speciated and cooled via simple, polythermal reaction-path models at fixed H₂S fugacities (constrained by aqueous-H₂S concentrations of the vent fluids) using The Geochemist's Workbench[®] software (Bethke, 2008) and the LLNL thermochemical database, modified using H₂S-solubility corrections from Duan

et al. (2007) at discrete pressures of 5–200 atm. Figure 6 shows an example output for one of the reaction-path models.

Modelling showed that the chalcopyrite mineral-solubility data in the LLNL database yielded incorrect results. Consequently, data from the MINTEQ database (Allison et al., 1991) was used. As H₂S-solubility data calculated according to Duan et al. (2007) are only slightly affected by

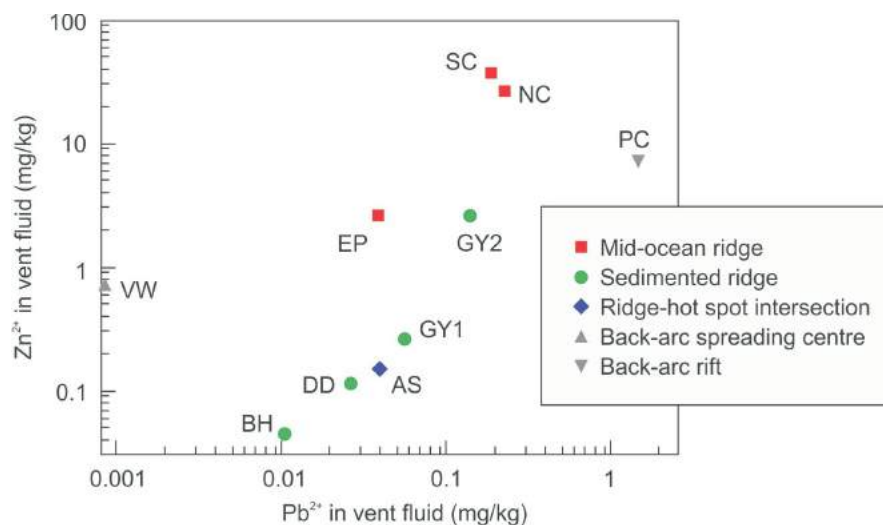


Figure 5. Scatter diagram of Zn versus Pb for representative chloride waters collected from different modern seafloor vent sites (data from Hannington et al., 2005). Abbreviations: AS, Axial Seamount; BH, Bent Hill; DD, Dead Dog; EP, 21°N, EPR; GY, Guaymas; NC, North Cleft; PC, Pacmanus; SC, South Cleft; VW, Vienna Wood.

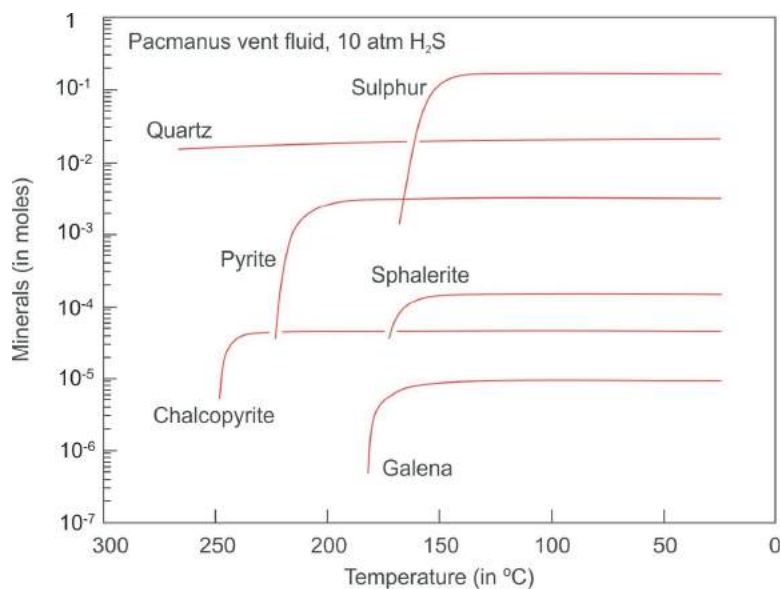


Figure 6. Results of a polythermal reaction-path model using The Geochemist's Workbench® software (Bethke, 2008) for chloride waters from the Pacmanus vent site. Chalcopyrite precipitation was modelled using thermodynamic data from the MINTEQ database (Allison et al., 1991). All other sulphides are modelled using data from the Lawrence Livermore National Laboratory database.

changes in ionic strength, a mid-range ionic strength of 1.0 molal (total dissolved solids of 55 g/kg) was chosen so that only H₂S corrections for temperature and pressure required evaluation. Figure 7 shows calculated dissolved H₂S concentrations at 1.0 molal ionic strength for discrete temperatures between 0 and 300°C, using the modified LLNL datasets at pressures between 5 and 200 atm. Solubility data above the temperature limit (227°C) of the model by Duan et al. (2007) and above boiling temperatures and below the boiling pressures were estimated using polynomial-trend fits.

Measured dissolved H₂S concentrations of the four vent fluids ranged from 0.0016 molal at Menez Gwen to 0.0068 molal at Pacmanus. Figure 7 can be applied to estimate H₂S fugacity using dissolved-H₂S concentrations and vent temperatures (the plot cannot be used to estimate mineralization depth as H₂S fugacity is independent of water-saturation pressure). In addition, there is a high uncertainty in the H₂S-solubility curves at high temperatures and low pressures, as solubility curves in this region contain extrapolated data. Nonetheless, first-order estimates suggest H₂S fugacities of 10–20 atm at South Cleft, and of 30–40 atm at Dead Dog, Menez Gwen and Pacmanus.

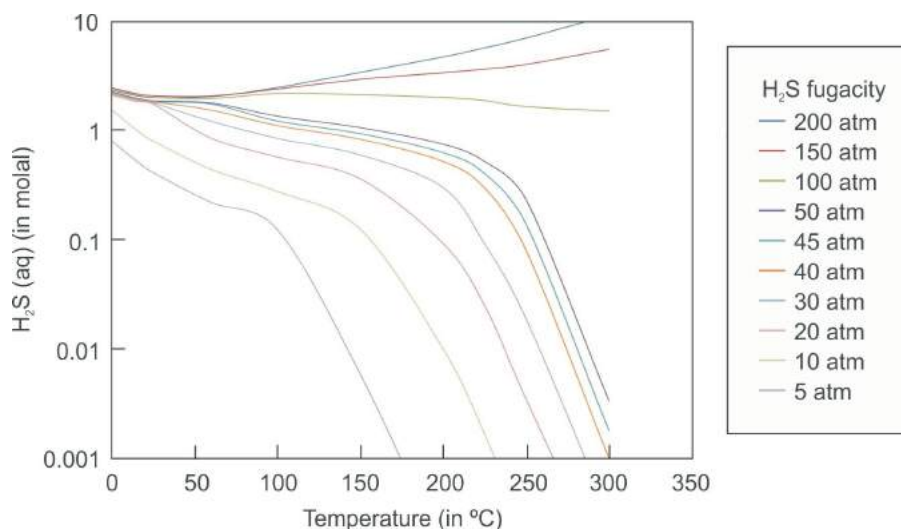


Figure 7. The H₂S-solubility data derived from the model presented in Duan et al. (2007) plotted as a function of temperature for different H₂S fugacities.

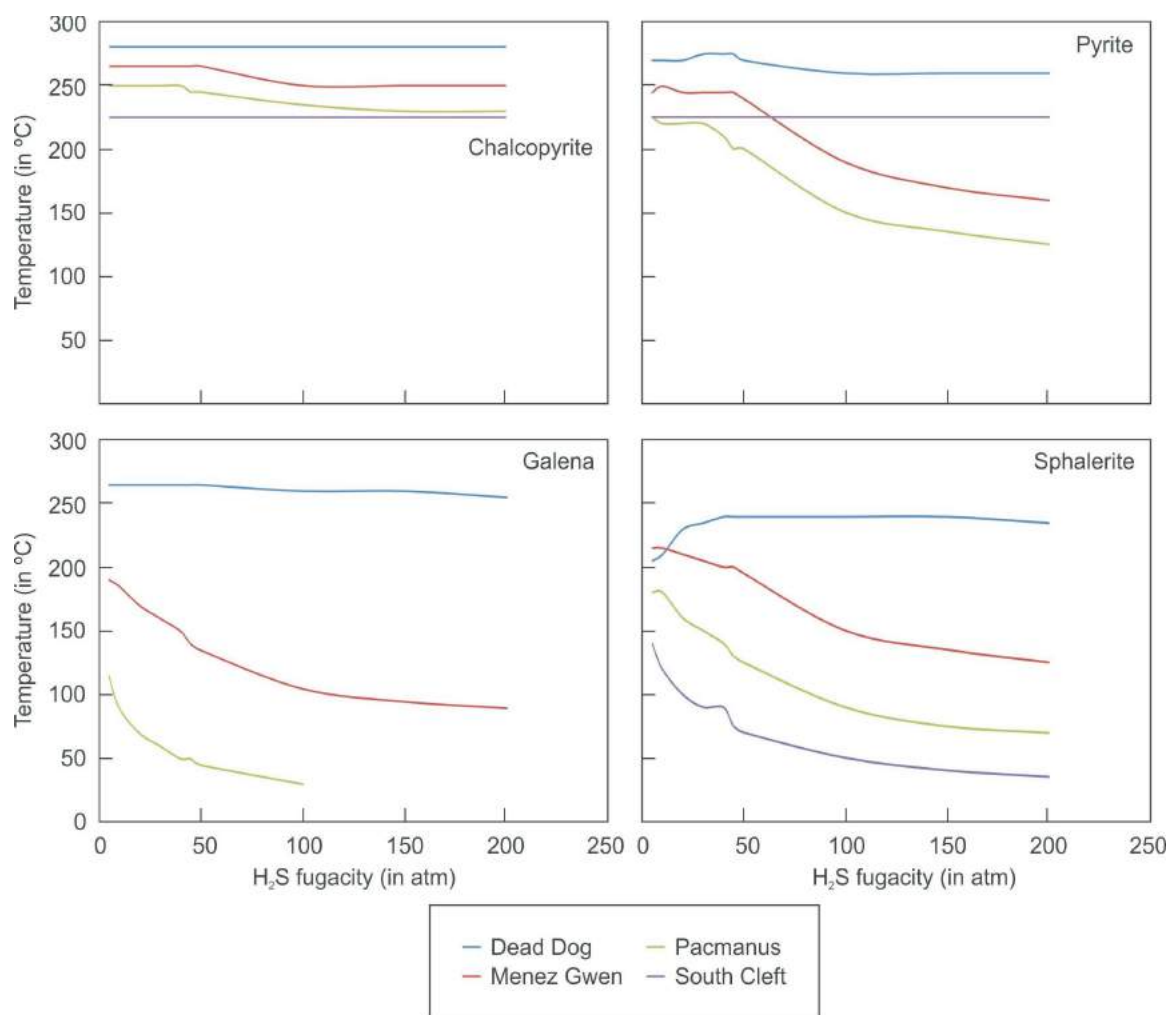


Figure 8. Temperatures of first precipitation of chalcopyrite, pyrite, galena and sphalerite for chloride waters sampled from the South Cleft, Dead Dog, Menez Gwen and Pacmanus vent sites at a range of H₂S fugacities.

Figure 8 shows the temperatures of first precipitation of chalcopyrite, pyrite, galena and sphalerite for H₂S fugacities ranging from 5 to 200 atm. In general, precipitation temperatures are proportional to fluid pH, with near-neutral fluids from Dead Dog precipitating sulphides at the highest temperatures, whereas the chloride waters at South Cleft and Pacmanus precipitate sulphides at distinctly lower temperatures (Table 2). The calculated sulphide-precipitation temperatures conform closely to observations made on the modern seafloor (cf. Hannington et al., 2005).

Homogenization temperatures of fluid inclusions in sphalerite from Eskay Creek range up to 180–220°C (Sherlock et al., 1999). Modelling of the present study suggests that a fluid with a pH of 4.0–5.0 is necessary to generate sphalerite at these temperatures (assuming that the homogenization temperatures are similar to the temperatures of formation). The crossover pH between CO₂ dissolved in chloride waters and the generation of bicarbonate waters is approximately 4.5 at 200°C (Bischoff and Rosenbauer, 1996). This suggests that a fluid with a pH somewhat higher

Table 2. Calculated sulphide-precipitation temperatures for four representative modern seafloor vent sites.

Vent site	Water depth (m)	Fluid temperature (°C)	pH	fH ₂ S(g) (atm)	Calculated sulphide-precipitation temperature (°C)			
					Chalcopyrite	Pyrite	Galena	Sphalerite
South Cleft	2300	224	3.2	10–20	224	224	80	130
Dead Dog	2425	276	5.5	30–40	276	276	265	235
Menez Gwen ¹	850	284	4.2	30–40	265	245	–	200
Pacmanus	1650	268	2.6	30–40	250	215	155	135

¹ Fluid does not contain Pb.

than that of the chloride waters from Menez Gwen would be capable of reaching carbonate saturation under those conditions, which would have been critical for generating the carbonate-kaolinite alteration halo at Eskay Creek. Although the hydrothermal fluids venting at Pacmanus represent the closest modern analogue to the mineralizing fluids at Eskay Creek in terms of tectonic setting and local host-rock composition, the numerical modelling shows that the alkalinity and pH of the chloride waters venting at Pacmanus are too low to explain the formation of the carbonate-kaolinite alteration halo observed at Eskay Creek. This alteration must have been caused by a bicarbonate water of higher alkalinity and near-neutral pH.

Future Modelling Work

The present modelling, largely based on thermochemical data from the LLNL database, successfully evaluated the role of simple cooling on sulphide precipitation in seafloor hydrothermal vents of different compositions. Predicted sulphide-precipitation temperatures closely conformed to seafloor observations, indicating that the data of Duan et al. (2007) provide a reliable approximation of H₂S solubility. Modelling of the present study also showed that chalcopyrite-solubility data from the MINTEQ dataset (Allison et al., 1991) is more reliable than that from the LLNL database. Future modelling will evaluate whether MINTEQ data are also more appropriate to describe solubility for other sulphide phases commonly precipitating at seafloor hydrothermal vents.

Following adequate description of sulphide precipitation, geochemical modelling will focus on the formation of the carbonate-kaolinite alteration at Eskay Creek, which represents for exploration the most useful vector to mineralization. This will require a better understanding of the controls on carbonate solubility, which is a direct function of dissolved and vapour-phase CO₂ concentrations. Similar to the H₂S-solubility data, CO₂ solubility in most thermochemical databases is currently only parameterized at low pressures and temperatures. To overcome this problem, the CO₂-solubility model of Duan and Sun (2003) and Duan et al. (2006), which is accurate over geologically relevant temperatures, pressures and fluid-solute levels, will be implemented using the approach established in this paper.

Once H₂S and CO₂ solubility in the mineralizing hydrothermal fluids is correctly described over the relevant pressure and temperature ranges, geochemical modelling will be able to show whether simple interaction with the wallrock and simple cooling of the chloride waters forming the sulphide and sulphosalt mineralization at Eskay Creek could have resulted in the generation of the bicarbonate waters responsible for the formation of the carbonate-kaolinite alteration. Future model calculations will also explore an alternative hypothesis that involves the effervescence of CO₂

from the chloride waters at higher temperatures, coupled with the subsequent take-up of the CO₂ by cooler, ambient pore waters, possibly producing waters of sufficient alkalinity and near-neutral pH to form the carbonate-kaolinite alteration halo.

Acknowledgments

The authors gratefully acknowledge the financial support provided by Geoscience BC, Barrick Gold Corporation, the Michael-Jürgen-Leisler-Kiep Foundation and the German Research Foundation. This study would not have been possible without the help provided by T. Roth, M.D. Hannington and R. Tosdal. R. Kleeberg is thanked for providing analytical support.

References

- Alldrick, D.J., Nelson, J.L., Barresi, T., Stewart, M.L. and Simpson, K. (2005): Geology of the Upper Iskut River area, British Columbia; BC Ministry of Energy and Mines, Open File 2006-2, scale 1: 100 000.
- Allison, J.D., Brown, D.S. and Novo-Gradac, K.J. (1991): User's manual for MINTQA2/PROFEFA2, version 3.0: a geochemical assessment model for environmental systems; United States Environmental Protection Agency, Environmental Research Laboratory, 107 p.
- Barrett, T.J. and Sherlock, R.L. (1996): Geology, litho-geochemistry and volcanic setting of the Eskay Creek Au-Ag-Cu-Zn deposit, northwestern British Columbia; Exploration and Mining Geology, v. 5, p. 339–368.
- BC Geological Survey (2011): MINFILE BC mineral deposits database; BC Ministry of Energy and Mines, URL <<http://www.empr.gov.bc.ca/Mining/Geoscience/MINFILE/Pages/default.aspx>> [November 2011].
- Bethke, C.M. (2008): Geochemical and Biogeochemical Reaction Modeling; Cambridge University Press, New York, 543 p.
- Bischoff, J.L. and Rosenbauer, R.J. (1984): The critical point and two-phase boundary of seawater, 200°–500°C; Earth and Planetary Science Letters, v. 68, p. 172–180.
- Bischoff, J.L. and Rosenbauer, R.J. (1996): The alteration of rhyolite in CO₂ charged water at 200 and 350°C: the unreactivity of CO₂ at higher temperature; Geochimica et Cosmochimica Acta, v. 60, p. 3859–3867.
- Britton, J.M., Blackwell, J.D. and Schroeter, T.G. (1990): #21 zone deposit, Eskay Creek, northwestern British Columbia; BC Ministry of Energy and Mines, Exploration in British Columbia 1989, p. 197–223.
- Childe, F. (1996): U-Pb geochronology and Nd and Pb isotope characteristics of the Au-Ag rich Eskay Creek volcanogenic massive sulfide deposit, British Columbia; Economic Geology, v. 91, p. 1209–1224.
- Delany, J.M. and Lundeen, S.R. (1990): The LLNL thermochemical database; Lawrence Livermore National Laboratory, Report URCL-21658, 150 p.
- Duan, Z., Møller, N. and Weare, J.H. (1996): Prediction of the solubility of H₂S in NaCl aqueous solution: an equation of state approach; Chemical Geology, v. 130, p. 15–20.
- Duan, Z. and Sun, R. (2003): An improved model calculating CO₂ solubility in pure water and aqueous NaCl solutions from

- 273 to 533 K and from 0 to 2000 bar; *Chemical Geology*, v. 193, p. 257–271.
- Duan, Z., Sun, R., Zhu, C. and Chou, I.M. (2006): An improved model for the calculation of CO₂ solubility in aqueous solutions containing Na⁺, K⁺, Ca²⁺, Mg²⁺, Cl⁻, and SO₄²⁻; *Marine Chemistry*, v. 98, p. 131–139.
- Duan, Z., Sun, R., Liu, R. and Zhu, C. (2007): Accurate thermodynamic model for the calculation of H₂S solubility in pure water and brines; *Energy and Fuels*, v. 21, p. 2056–2065.
- Ettlinger, A.D. (1992): Hydrothermal alteration and brecciation underlying the Eskay Creek polymetallic massive sulphide deposit; *in Geological Fieldwork 1991*, BC Ministry of Energy and Mines, Paper 1992-1, p. 535–541.
- Gabrielse, H., Monger, J.W.H., Wheeler, J.O. and Yorath, C.J. (1991): Morphogeological belts, tectonic assemblages and terranes; *in Geology of the Cordilleran Orogen in Canada*, H. Gabrielse and C.J. Yorath (ed.), Geological Survey of Canada, *Geology of Canada*, no. 4, p. 15–28 (also *Geological Society of America, Geology of North America*, v. G-2).
- Hannington, M.D., Poulsen, K.H., Thompson, J.F.H. and Sillitoe, R.H. (1999): Volcanogenic gold in the massive sulfide environment; *Reviews in Economic Geology*, v. 8, p. 325–356.
- Hannington, M.D., de Ronde, C.E.J. and Petersen, S. (2005): Seafloor tectonics and submarine hydrothermal systems; *Economic Geology*, 100th Anniversary Volume, p. 111–141.
- Helgeson, H.C., Garrels, R.M. and Mackenzie, F.T. (1969): Evaluation of irreversible reactions in geochemical processes involving minerals and aqueous solutions–II. Applications; *Geochimica et Cosmochimica Acta*, v. 33, p. 455–481.
- Helgeson, H.C. and Kirkham, D.H. (1974): Theoretical prediction of the thermodynamic behavior of aqueous electrolytes at high pressures and temperatures, II. Debye-Huckel parameters for activity coefficients and relative partial molal properties; *American Journal of Science*, v. 274, p. 1199–1261.
- Johnson, J.W., Oelkers, E.H. and Helgeson, H.C. (1992): SUPCRT92: a software package for calculating the standard molal thermodynamic properties of minerals, gases, aqueous species, and reactions from 1 to 5000 bar and 0 to 1000°C; *Computers and Geosciences*, v. 18, p. 889–947.
- Large, R.R. (1977): Chemical evolution and zonation of massive sulfide deposits in volcanic terrains; *Economic Geology*, v. 72, p. 549–572.
- Meuzelaar, T. and Monecke, T. (2011): Carbonaceous mudstone hosting the Eskay Creek deposit (NTS 104B/09, /10), northwestern British Columbia: multivariate statistical analysis of compositional trends; *in Geoscience BC Summary of Activities 2010*, Geoscience BC, Report 2011-1, p. 45–56.
- Monecke, T., Gale, D., Roth, T. and Hannington, M.D. (2005): The submarine volcanic succession hosting the massive sulfide and sulfosalt Eskay Creek deposit, Canada; *in Mineral Deposit Research: Meeting the Global Challenge*, Y. Mao and F.P. Bierlein (ed.), Proceedings of the 8th Biennial SGA (Society for Geology Applied to Mineral Deposits) Meeting, August 18–21, 2005, Beijing, Peoples Republic of China, Springer, p. 655–658.
- Nadaraju, G.D. (1993): Triassic–Jurassic biochronology of the eastern Iskut River map area, northwestern British Columbia, M.Sc. thesis, University of British Columbia, 268 p.
- Ohmoto, H. (1996): Formation of volcanogenic massive sulfide deposits: the Kuroko perspective; *Ore Geology Reviews*, v. 10, p. 135–177.
- Pitzer, K.S. (1973): Thermodynamics of electrolytes–I. Theoretical basis and general equations; *Journal of Physical Chemistry*, v. 77, p. 268–277.
- Robinson, H.M. (1991): Mineralisation and alteration patterns of the Central Lens (21B Zone), Eskay Creek, British Columbia, Canada; M.Sc. thesis, Imperial College, University of London, 129 p.
- Roth, T., Thompson, J.F.H. and Barrett, T.J. (1999): The precious metal-rich Eskay Creek deposit, northwestern British Columbia; *Reviews in Economic Geology*, v. 8, p. 357–373.
- Schardt, C., Cooke, D.R., Gemell, J.B. and Large, R.R. (2001): Geochemical modeling of the zoned footwall alteration pipe, Hellyer volcanic-hosted massive sulfide deposit, western Tasmania, Australia; *Economic Geology*, v. 96, p. 1037–1054.
- Sherlock, R.L., Roth, T., Spooner, E.T.C. and Bray, C.J. (1999): Origin of the Eskay Creek precious metal-rich volcanogenic massive sulfide deposit: fluid inclusion and stable isotope evidence; *Economic Geology*, v. 94, p. 803–824.

Development of a Database for Geoscience Field Observations, West-Central British Columbia (Part of NTS 093L)

A.J. Stumpf, Illinois State Geological Survey, Prairie Research Institute, University of Illinois Urbana-Champaign, Champaign, IL, USA, astumpf@illinois.edu

Stumpf, A.J. (2012): Development of a database for geological field observations, west-central British Columbia (part of NTS 093L); in Geoscience BC Summary of Activities 2011, Geoscience BC, Report 2012-1, p. 53–58.

Introduction

The recording, analysis and publication of field observations, measurements and interpretations are an integral part of developing geoscience investigations. Historically, these field-acquired data and associated research materials were recorded, compiled and maintained in hard copy by individual scientists using various schemas. At the completion of the study, field maps and notebooks are archived in data repositories and libraries (Schumacher, 2002). To date, there are only a few programs, such as Natural Resources Canada's Consolidating Canada's Geoscience Knowledge Program (http://ess.nrcan.gc.ca/2002_2006/ccgk/index_e.php), that have been developed to specifically catalogue and digitize geological information previously available only in hard copy.

Although recent technological advancements now allow geological information to be directly inputted into digital databases from the field (e.g., Brodaric, 2004), there remains a requirement that these custom databases be designed to allow data to be queried, appended and edited by the geoscientist. Furthermore, the databases must also be compatible with corporate data structures and readily converted to other file formats.

To this end, a database was developed to store observations made in the field for the Geoscience BC-supported project, Surficial Geochemistry and Lithology of the Bulkley River Valley, Central British Columbia, which is currently only available from the author in hard copy. This database will assist users of the accompanying till geochemistry and clast lithology data to explore and query other information collected at each sampling site (e.g., location, drainage class, topographic position, character of sampled material, lithology of clasts in the material and bedrock lithology if observed at the sampling site). This paper is a preliminary guide to the structure of the database, which will be re-

leased as part of the final project report in early 2012 through Geoscience BC.

Field Data

Field observations were made at a total of 146 sampling sites for a study of the till geochemistry and clast lithology in west-central BC (Stumpf, 2011) in an area approximately 340 km east of Prince Rupert and 400 km west of Prince George (Figure 1). The project area is centred along the Bulkley River valley and adjacent areas (encompassing parts of NTS map areas 093L/07, /08, /09, /10, /11, /15; Figure 1) within the Geoscience BC's QUEST-West Project area and the Mountain Pine Beetle-Impacted Zone.

In a similar manner to the till geochemistry surveys conducted by Levson (2002) and Ferbey (2011), the selection of field sample sites for this project was undertaken to provide as complete coverage of the project area as possible using existing access routes. The sites were also selected to set the greatest density of samples along transects perpendicular to the regional ice-flow direction. Along transects paralleling the ice flow, less dense sampling was carried out. Samples of various geological materials—predominantly glacial till, but also silt and clay (glacial lake sediment) or diamicton reworked by water and gravity—were collected from natural and manmade exposures such as roadcuts, cuts along the shore of rivers and lakes, borrow pits and hand-dug holes. The average sampling depth below land surface ranged from 0.20 to 22 m.

At each sample site, a series of observations were made describing the site location and conditions, landscape position and vegetation, and properties of the geological materials (Table 1). The field sites were marked with metal tags and flagging tape, both labelled with site numbers that were assigned in sequential order. The location of sample sites were plotted on 1:50 000 NTS base maps with the aid of air photographs and a handheld GPS unit. The co-ordinates from the GPS for each sample site were recorded in the field on a hard-copy card similar to the form shown in Figure 2. The co-ordinates were recorded in the UTM projection, referenced to NAD 83, Zone 9.

Keywords: *database, geoscience, Quaternary geology, mineral exploration, QUEST-West*

This publication is also available, free of charge, as colour digital files in Adobe Acrobat® PDF format from the Geoscience BC website: <http://www.geosciencebc.com/s/DataReleases.asp>.

Sedimentological data including sediment descriptions, primary and secondary structures, matrix texture, presence of fissility, compactness, sediment genesis and thickness, total percentage and modal size, rounding and presence of striated clasts were also collected at each site (Table 1). This information was used to identify geological materials with different processes of transportation and deposition. For example, the information was used to distinguish diamicton that was classified as till from deposits of glaciogenic debris flows, colluvial processes, proximal

glaciofluvial meltwater or subaqueous debris flows or ice-rafted debris in glacial lakes. This information is very important to the understanding of associated anomaly patterns because variations in geochemistry from local sources are reflected in some materials whereas regional trends are observed in others. Additional information was collected describing the soil horizons, local slope, drainage class, dominant tree species, bedrock striae and bedrock lithology (Table 1).

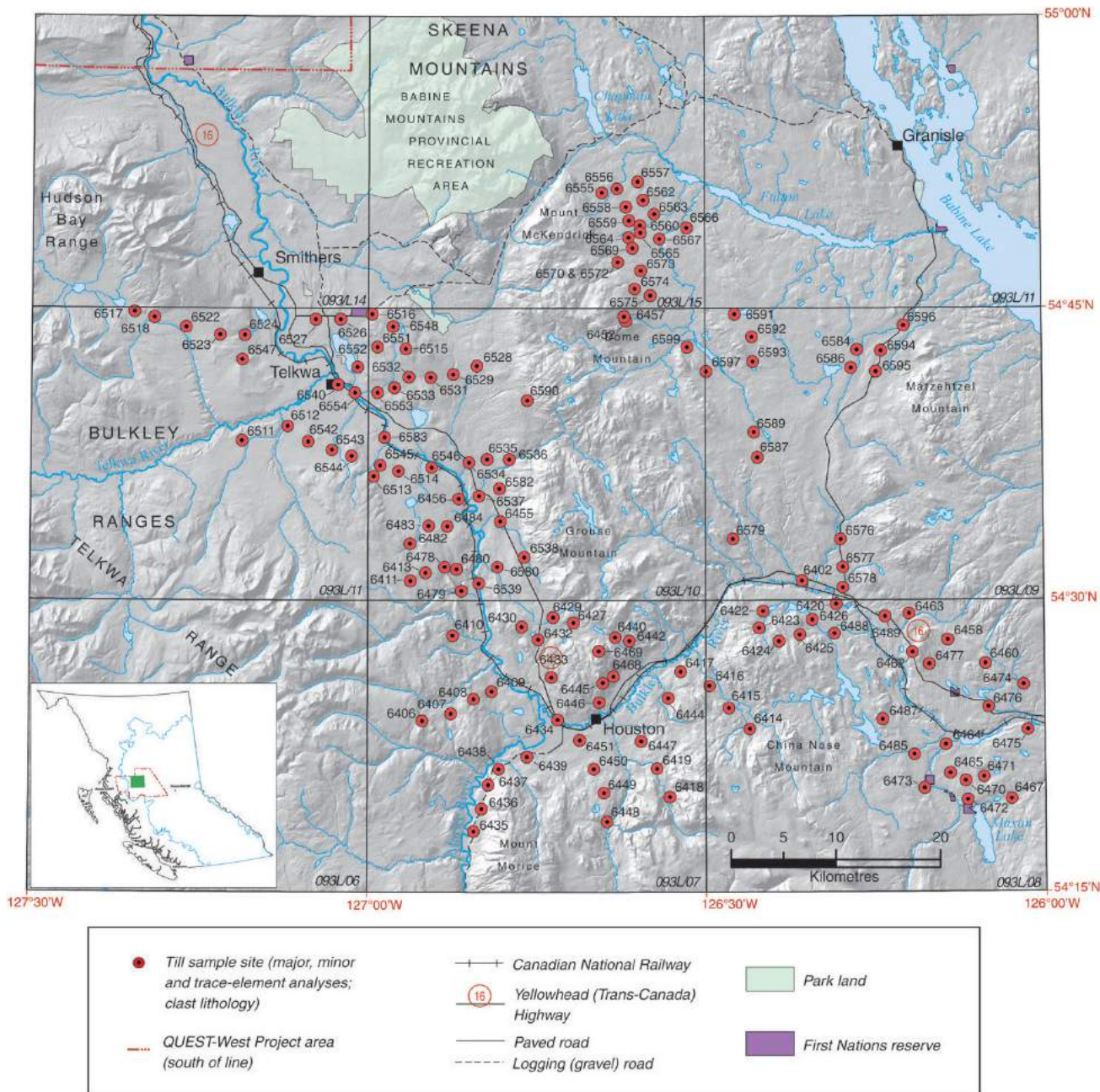


Figure 1. Location and till sample sites of the project area in west-central British Columbia (project area delineated by the green box on the inset map). Geoscience BC's QUEST-West Project area and the Mountain Pine Beetle-Impacted Zone are outlined by the red and light blue lines, respectively, on the inset map.

Table 1. Guide to field observations collected for the project along the Bulkley River valley (after Levson, 2002). The data is input into a relational database with a structure outlined in Tables 2–4. The 'Unit' field contains codes for deposit type, thickness and depositional processes (from Howes and Kenk, 1997).

Parameter	Description
Year	Year sample collected
Day_Month	Day and month sample collected
Type	Type of regional survey: LITH, clast lithology; TS, till
ID	Sample site number
Collector	Scientist(s) that collected the sample: AS, Andrew Stumpf; EB, Erin O'Brien; LV, Victor Levson; DM, Dan Meldrum; DH, David Huntley; CC, Craig
Map50	NTS 1:50 000 scale map (in 093L)
Status	Identifies the collection of multiple samples from a single site. Quality control identifier: 00, routine sample; 10, first field duplicate; 20, second field duplicate
UTMZ	Site location UTM zone
UTME83	Site location UTM easting (metres) referenced to NAD83 datum
UTMN83	Site location UTM northing (metres) referenced to NAD83 datum
Lat	Latitude (decimal degrees) calculated from NAD83 UTM coordinates
Long	Longitude (decimal degrees) calculated from NAD83 UTM coordinates
Elev	Elevation of land surface (in feet above mean sea level) taken from BC TRIM map
Depth	Depth of sample from land surface (in metres)
Unit*	Surficial deposit type and thickness/depositional process: b, blanket; C, colluvial; FG, glaciofluvial sediments; LG, glaciolacustrine sediments; M, morainal; R, bedrock map symbol: b, blanket; r, redeposited; v, veneer; ^, overlying; (e.g., FG^Mb, glaciofluvial sediments over morainal blanket)
Material	Sample material type: C, clay; Dmm, diamicton (massive, matrix-supported); G, gravel; S, sand; Z, silt; prefix: c, clayey, g, gravelly, s, sandy, z, silty (e.g., szDmm, sandy to silty diamicton)
Exposure	Sample material exposed in: 1, roadcut; 2, shore of river or lake; 3, borrow pit; 4, hand-dug hole
Terrain	Position of site location on slope: 1, flat; 2, lower slope; 3, midslope; 4, upper slope; 5, ridgecrest
Terrain_Com	Topographic position (description)
Aspect	Azimuth (direction) that the land surface is sloping
Slope	Inclination of the land surface at the site location
Drainage	Drainage class: 1, poor; 2, moderate; 3, well Note: 0.5 is intermediate between any two classes
Vegetation	Dominant tree species at site location: al, alder; as, aspen; b, birch; bf, balsam fir; cc, clearcut; d, deciduous; f, fir; j, juniper; p, lodgepole pine; pop, poplar; s, spruce; saf, subalpine fir; sw, swamp; ws, white spruce
Soil	Thickness (m) of soil horizon(s); X, disturbed ground
Fissility	0, none; 1, weak; 2, moderate; 3, strong
Density	1, loose; 2, stiff; 3, hard
Oxidation	0, none; 1, mild; 2, moderate; 3, high Note: 0.5 is intermediate between any two classes
Jointing	0, none; 1, few; 2, some; 3, many
Matrix	Proportion of matrix material in bulk sample: 60, 70, 80, 90
Matrix_Colour	Matrix colour: b, brown; bl, blue; bt, blue tinge; cb, chocolate brown; db, dark brown; dg, dark grey; dgr, dark green; dgb, dark greyish brown; dr, dark red; g, grey; gb, grey brown; gr, green; lb, light brown; lg, light grey; o, orange; ob, orange brown; ol, olive; p, purple; r, red; rb, reddish brown; y, yellow; t, tan; tb, tan brown
Matrix_Texture	Matrix texture: 1, sandy; 2, silty; 3, silty sand; 4, sandy silt; 5, other (see comments)
Clast_Mode	Size of pebbles: 1, small pebble; 2, medium pebble; 3, large pebble; Note: 0.5 is intermediate between any two mode classifications
Max_Clast_Size	Maximum clast size observed (b-axis dimension in cm)
Clast_Shape	Shape of clasts: 1, angular; 2, subangular; 3, subrounded; 4, rounded; 5, well rounded Note: 0.5 is an intermediate value between any two shape classifications
Clast_Striated	Proportion of striated clasts: 0, none; 1, rare (<1%); 2, common (1–10%); 3, abundant (>10%)
Bedrock_Lith	Bedrock lithology: n/v, not exposed; AND, andesite; B, basalt; CH, chert; COAL, coal; CONG, conglomerate; DIO, diorite; FP, feldspar porphyry; GR, granitic; GRD, granodiorite; GRN, greenstone; GW, greywacke; LAPT, lapilli tuff; LST, limestone; METSEDS, metasediments; MS, mudstone; RHY, rhyolite; SH, shale; SS, sandstone; SY, syenite;
Comments	Relevant information about the sedimentology, geology, location, or site characteristics

Database Construction

A database was developed using Microsoft® Access® 2010 to input field data including site information, observations and interpretations. The database was designed to facilitate retrieval, interpretation and analysis of information associated with the collection of till and clast lithology samples, and is based on a relational database using Microsoft Access forms and tables developed at the Illinois State Geological Survey (Stiff, 2002).

The data is input via either a write-access form or three database tables that allow researchers to query, append to and edit the data housed in the database. Each field site has a unique identification code ('Sys_ID'). This identification code is used to establish a 1:1 relationship between the 'Field ID' table and the other two tables containing location information and geographic descriptions ('Header' table) and geological observations and interpretations ('Descriptions' tables).

The 'Field_ID' table contains identification codes that have been assigned to a particular site (Table 2). The ID is a unique number for each sample site assigned by the project geologist. The 'Master_Num' field was created to follow the file structure of geochemical databases maintained by Geoscience BC (Jackaman, 2007) and the BC Geological Survey (Lett, 2008). This field is also a unique identifier containing sample identification information, a compound of the fields 'Type', 'Map50', the last two characters of 'Year' and the 'ID'. The 'Type' indicates the type of survey

DATE: 18-AUG-1996	ID: 6458
COLLECTOR: DM, AS	NTS MAP: 093L/08
STATUS: <input checked="" type="checkbox"/> Routine <input type="checkbox"/> First duplicate <input type="checkbox"/> Second duplicate	
Easting: 685250 Northing: 6039200	ELEV (ft.): 2523
MAP UNIT: Mb^R	MATERIAL: czDmm
DEPTH: 1.2 m	
EXPOSURE: <input checked="" type="checkbox"/> Roadcut <input type="checkbox"/> Str./Lake cut <input type="checkbox"/> Bor. pit <input type="checkbox"/> Dug hole	
TOPO POSITION: <input type="checkbox"/> Flat <input checked="" type="checkbox"/> L.slope <input type="checkbox"/> M.slope <input type="checkbox"/> U.slope <input type="checkbox"/> Crest	
ASPECT: NW	SLOPE (deg.): 2
DRAINAGE: <input checked="" type="checkbox"/> Poor <input checked="" type="checkbox"/> Moderate <input type="checkbox"/> Well	
VEGETATION: <input checked="" type="checkbox"/> Lodgepole Pine <input checked="" type="checkbox"/> Spruce <input type="checkbox"/> Other	
SOIL (cm): <input checked="" type="checkbox"/> Dist. <input type="checkbox"/> LFH <input type="checkbox"/> Ah <input type="checkbox"/> Ae <input type="checkbox"/> Bm <input type="checkbox"/> Bf <input type="checkbox"/> Bt	
FISSILITY: <input type="checkbox"/> None <input type="checkbox"/> Weak <input type="checkbox"/> Moderate <input checked="" type="checkbox"/> Strong	
DENSITY: <input type="checkbox"/> Loose <input type="checkbox"/> Stiff <input checked="" type="checkbox"/> Hard	
OXIDATION: <input type="checkbox"/> None <input checked="" type="checkbox"/> Mild <input checked="" type="checkbox"/> Moderate <input type="checkbox"/> High	
JOINTING: <input type="checkbox"/> None <input type="checkbox"/> Weakly <input checked="" type="checkbox"/> Moderate <input type="checkbox"/> Well	
MATRIX %:	<input type="checkbox"/> 60 <input type="checkbox"/> 70 <input checked="" type="checkbox"/> 80 <input checked="" type="checkbox"/> 90 <input type="checkbox"/> Other
COLOUR:	gb - grey brown
TEXTURE:	<input type="checkbox"/> S <input type="checkbox"/> Z <input type="checkbox"/> ZS <input type="checkbox"/> SZ <input checked="" type="checkbox"/> Other
CLASTS %:	Mode: <input type="checkbox"/> S <input type="checkbox"/> M <input checked="" type="checkbox"/> L <input type="checkbox"/> Pbl Max (cm): <input type="checkbox"/>
SHAPE:	<input type="checkbox"/> A <input type="checkbox"/> SA <input checked="" type="checkbox"/> SR <input type="checkbox"/> R <input checked="" type="checkbox"/> WR
STRIATED:	<input type="checkbox"/> none <input type="checkbox"/> <1 % <input type="checkbox"/> 1-10 % <input checked="" type="checkbox"/> >10 %
BEDROCK:	green- and maroon-coloured siltstone and sandstone
COMMENTS:	Site location at bottom of SE-trending (100°) fluted ridge; 50 m to east of site is exposed basalt (vesicular) with green amygdules and malachite staining; sampled bedrock

Figure 2. Example of the database input form.

Table 2. Structure of the 'Field ID' table (length in number of characters; abbreviations: CHAR, text field; NUM, numerical field).

TABLE_FIELD	TYPE	LENGTH	FORM EXPLANATION
SYS_ID	NUM	12	sequential, system-generated identifier
ID	CHAR	4	sample number in survey
YEAR	CHAR	4	year sample was collected
DAY_MONTH	CHAR	4	day and month sample was collected
MASTER_NUM	CHAR	15	unique samples identification combines type of regional sample, NTS map area, collection year and original sample site number (e.g., TILL93L09966402)
TYPE	CHAR	7	type of regional survey
STATUS	CHAR	2	sample quality control identifier

Table 3. Structure of the 'Header' table (length in number of characters; abbreviations: CHAR, text field; NUM, numerical field).

TABLE_FIELD	TYPE	LENGTH	FORM EXPLANATION
SYS_ID	NUM	12	sequential, system-generated identifier
COLLECTOR	CHAR	15	initials of field scientist(s) collecting the sample
MAP50	CHAR	5	NTS 1:50 000 scale map
UTME83	NUM	14	site location UTM easting (6 decimal places)
UTMN83	NUM	14	site location UTM northing (6 decimal places)
UTMZ	NUM	2	site location UTM zone
LAT	NUM	10	latitude in decimal degrees (6 decimal places)
LONG	NUM	10	longitude in decimal degrees (6 decimal places)
ELEV	NUM	5	elevation of site location (in feet)
DEPTH	NUM	3	depth of sample (m) (1 decimal place)

Table 4. Structure of the ‘Descriptions’ table (length in number of characters; abbreviations: CHAR, text field; NUM, numerical field).

TABLE_FIELD	TYPE	LENGTH	FORM EXPLANATION
SYS_ID	NUM	12	sequential, system-generated identifier
UNIT	CHAR	5	deposit type and thickness/depositional process
MATERIAL	CHAR	5	sampled material type and texture
EXPOSURE	NUM	1	condition that material is exposed
TERRAIN	NUM	1	position of site location on slope
TERRAIN_COM	CHAR	100	topographic position (description)
ASPECT	NUM	3	azimuth of slope (degrees)
SLOPE	NUM	2	inclination of land surface (degrees)
DRAINAGE	NUM	2	drainage class
VEGETATION	CHAR	10	predominant tree species
SOIL	NUM	3	thickness of soil horizon (m)
FISSILITY	NUM	1	degree of fissility developed
DENSITY	NUM	1	field measure of density, consistency or compaction
OXIDATION	NUM	1	degree of oxidation
JOINTING	NUM	1	density of joints and fractures
MATRIX	NUM	2	proportion of matrix material (percent)
MATRIX_COLOUR	CHAR	3	primary color of matrix material
MATRIX_TEXTURE	CHAR	15	in field estimate of matrix texture
CLAST_MODE	NUM	2	average size of pebbles
MAX_CLAST_SIZE	NUM	3	maximum size of clasts (cm)
CLAST_SHAPE	NUM	1	dominant shape of clasts
CLAST_STRIATED	NUM	3	proportion of striated clasts in bulk sample (percent)
BEDROCK_LITH	CHAR	8	bedrock lithology at site location (if exposed)
COMMENTS	CHAR	100	descriptive details relating to sedimentology, geology, site location, etc.

that was completed. For this project, only till geochemistry and clast lithology surveys were completed. The ‘Status’ is a unique quality-control identifier assigned to field duplicate samples sent for geochemical analyses. One field duplicate sample was collected for every 20 samples in the survey and the duplicate samples were collected at the same site of the preceding sample in the sampling sequence. This sampling protocol is adapted from similar QA-QC procedures used by Geoscience BC, the BC Geological Survey and the Geological Survey of Canada for geochemical surveys (e.g., Cook and Dunn, 2007). These duplicate samples were randomly submitted to the laboratory without any indication of their proximity.

The ‘Header’ table includes information about the site and its location (Table 3). A geoscientist can update fields in this table as more accurate or more complete data become available.

The ‘Descriptions’ table includes information describing the physical, chemical and engineering properties of the geological materials sampled, as well as the topography, drainage class, predominant tree species and soil formation at the land surface (Table 4). Additional detailed comments are included in the table describing specific aspects of sedimentology, geology and the site location that cannot be entered in the other fields (e.g., direction of glacier flow inferred from striated bedrock).

Conclusion

This digital database of descriptive sedimentology, geology and characteristics of the land surface, along with the associated geospatial information, will add to the functional data repositories available from Geoscience BC. The database structure will first be used to distribute the results of the Geoscience BC–supported project, Surficial Geochemistry and Lithology of the Bulkley River Valley, Central British Columbia, in early 2012. In addition, the database has a digital framework that is compatible with other data repositories maintained by Geoscience BC and the BC Geological Survey. The ‘open access’ structure permits database query and edit functions. Because the database was constructed using an industry-standard database system, data can easily be exported to other systems (e.g., Oracle[®], MySQL[®]) or linked with GIS software. This database will provide access to ancillary information collected as part of a geochemical survey that can be incorporated into a wide range of exploration and research activities and assist in the planning of detailed surveys and targeted studies.

Acknowledgments

The project along the Bulkley River valley is being funded by Geoscience BC. The author thanks B. Stiff and S. Brown at the Illinois State Geological Survey for their insightful information about database structures. The author thanks B. Bauer and R. Klass for their thorough review of an earlier version of the manuscript.

References

- Brodaric, B. (2004): The design of GSC FieldLog: ontology-based software for computer aided geological field mapping; *Computers and Geosciences*, v. 30, p. 5–20, URL <<http://dx.doi.org/10.1016/j.cageo.2003.08.009>> [October 2011].
- Cook, S.J. and Dunn, C.E. (2007): Final report on results of the Cordilleran geochemistry project: a comparative assessment of soil geochemical methods for detecting buried mineral deposits – 3Ts Au-Ag prospect, central British Columbia, Geoscience BC, Report 2007-7, 225 p., URL <http://www.geosciencebc.com/i/project_data/GBC_Report2007-7/2007-7_2007-7_Report.pdf> [October 2011].
- Ferbey, T. (2011): Till geochemistry of the Colleymount map area (093L/01), west-central British Columbia; BC Ministry of Energy and Mines, Open File 2011-06 and Geoscience BC, Report 2011-9, 51 p., URL <<http://www.empr.gov.bc.ca/Mining/Geoscience/PublicationsCatalogue/OpenFiles/2011/Documents/OF2011-6/OF2011-6.pdf>> [October 2011].
- Foerste, A.F. (2002): August F. Foerste's unpublished field notes for the area of the Serpent Mound disturbance; Ohio Department of Natural Resources, Division of Geological Survey, Open-File Report, Paper 2002-01, 21 p. (transcribed by G.A. Schumacher with assistance from M. Hackathorn), URL <<http://www.dnr.state.oh.us/Portals/10/pdf/foerste.pdf>> [October 2011].
- Howes, D.E. and Kenk, E. (1997): Terrain classification system for British Columbia (version 2); BC Ministry of Environment and Surveys and Resource Mapping Branch, MOE Manual 10, 102 p., URL <http://www.for.gov.bc.ca/hfd/library/ffip/Howes_DE1997.pdf> [October 2011].
- Jackaman, W. (2007): Geoscience BC MPB data repository (v1.0); Geoscience BC, Report 2007-9, 8 p., URL <http://www.geosciencebc.com/i/project_data/GBC_Report2007-9/2007-9_README.pdf> [October 2011].
- Lett, R.E. (2008): British Columbia till geochemical survey data compilation; BC Ministry of Energy and Mines, GeoFile 2008-13, 7 p., URL <<http://www.empr.gov.bc.ca/Mining/Geoscience/PublicationsCatalogue/GeoFiles/Pages/2008-13.aspx>> [October 2011].
- Levson, V.M. (2002): Quaternary geology and till geochemistry of the Babine porphyry copper belt, British Columbia (NTS 093L/9, 16; M/1, 2, 7 & 8); BC Ministry of Energy and Mines, Bulletin 110, 278 p., URL <<http://www.empr.gov.bc.ca/Mining/Geoscience/PublicationsCatalogue/BulletinInformation/BulletinsAfter1940/Documents/00-cover.pdf>> [October 2011].
- Stiff, B.J. (2002): Developing a working database for mapping and modeling in Illinois; *in* Digital Mapping Techniques '02–Workshop Proceedings, D.R. Soller (ed.), United States Geological Survey, Open-File Series 02-370, p. 21–28, URL <<http://pubs.usgs.gov/of/2002/of02-370/stiff.html>> [October 2011].
- Stumpf, A.J. (2011): Quaternary geology and till geochemistry of the Bulkley River valley, west-central British Columbia (part of NTS 093L); *in* Geoscience BC Summary of Activities 2010, Geoscience BC, Report 2011-1, p. 57–64, URL <http://www.geosciencebc.com/i/pdf/SummaryofActivities2010/SoA2010_Stumpf.pdf> [October 2011].

Heavy Mineral Analysis of Till Samples within the QUEST Project Area, Central British Columbia (NTS 093J)

B.C. Ward, Department of Earth Sciences, Simon Fraser University, Burnaby, BC, bcward@sfu.ca

M.I. Leybourne, GNS Science, 1 Fairway Drive, Avalon, Lower Hutt, New Zealand

D.A. Sacco, Department of Earth Sciences, Simon Fraser University, Burnaby, BC

Ward, B.C., Leybourne, M.I. and Sacco, D.A. (2012): Heavy mineral analysis of till samples within the QUEST Project area, central British Columbia (NTS 093J); in Geoscience BC Summary of Activities 2011, Geoscience BC, Report 2012-1, p. 59–68.

Introduction

The McLeod Lake map area (NTS 093J), within Geoscience BC's Quesnellia Exploration Strategy (QUEST) Project area, has shown good potential for Cu and Au porphyry and volcanogenic massive sulphide (VMS) mineralization (Ward et al., 2011). Previously, mineral exploration activity has been hindered in this area due to the thick cover of surficial deposits, therefore, regional-scale till sampling has been carried out to target potential zones of mineralized bedrock. Detailed investigations of regional-scale till samples with elevated or anomalous values help identify potentially mineralized zones within covered bedrock units (e.g., Levson, 2001; McClenaghan et al., 2002; McClenaghan, 2005). The preferred sampling medium for till geochemical surveys is basal till, as it is commonly considered a first derivative of bedrock (Dreimanis, 1989; Levson, 2001). In its entirety, this Quaternary geology project is designed to provide both regional and detailed till geochemical surveys and the Quaternary framework necessary to interpret these data. Geochemical data from this project provide new exploration targets and also provide geological context for companies to interpret their own geochemical and geological datasets. This report adds to previous Geoscience BC publications that have dealt with the Quaternary geology (Ward et al., 2009; Sacco et al., 2010) and analysis of the clay and silt+clay fractions of basal till by inductively coupled plasma–mass spectrometry (ICP-MS) following aqua-regia digestion and induced neutron activation analysis (INAA; Ward et al., 2011). This paper discusses INAA results from the heavy mineral fraction of 136 samples from six 1:50 000 map areas in the QUEST Project area (Figure 1).

Keywords: *geochemistry, regional till geochemical survey, heavy minerals, Cu-Au porphyry, VMS*

This publication is also available, free of charge, as colour digital files in Adobe Acrobat® PDF format from the Geoscience BC website: <http://www.geosciencebc.com/s/DataReleases.asp>.

Physiography, Bedrock and Quaternary Geology

The study area occurs in the heart of the QUEST Project area, northwest of Prince George. The majority of this area lies in the relatively low relief area of the Interior Plateau (Mathews, 1986), including its subdivisions, the Fraser Basin and Nechako Plateau. It is characterized by glacial lake deposits, drumlinized drift and glaciofluvial outwash and esker deposits (Holland, 1976).

The majority of the study area straddles four of the terranes that make up the Canadian Cordillera (Cache Creek, Slide Mountain, Quesnel, Kootenay) whereas the most north-eastern corner of it extends into the Rocky Mountain assemblage. The Quesnel terrane dominates the study area and is composed primarily of Late Triassic to Early Jurassic arc volcanic rocks of the Witch Lake succession and volcanoclastic rocks of the Cottonwood River succession, both part of the Nicola Group (Logan et al., 2010). The Cache Creek terrane is composed of Pennsylvanian and Permian limestone in the southwestern portion of the study area, with basalts occurring just to the south of the study area. A complex assemblage of intrusive and extrusive rocks of the Slide Mountain terrane occurs in the east. The Rocky Mountain assemblage in the northeastern corner of the study area comprises Silurian to Devonian sandstone and quartzite. Stratigraphically overlying these terranes are a series of overlap assemblages ranging from Upper Cretaceous to Miocene sedimentary rocks and Cretaceous to Pliocene volcanic rocks (Struik, 1994; Logan et al., 2010). See Figure 1 for a more comprehensive presentation of the bedrock units of the study area.

The study area was repeatedly affected by the Cordilleran Ice Sheet over approximately the last two million years (Armstrong et al., 1965; Clague, 1989), the most recent being during the Fraser glaciation. The major sources of regional ice that covered the study area advanced from accumulation centres in the Coast, Skeena and Cariboo mountains (Tipper, 1971; Levson and Giles, 1997; Plouffe, 1997, 2000). The dominant ice flow direction in the study area, and thus main sediment transport, was northeasterly

with minor deviations to a more northerly direction in the north and a more easterly direction in the southern portions of the study area. Little information exists on ice flow during the glacier's advance into the area, but it is likely that ice flowed eastward from the Coast Mountains and was subsequently deflected to the northeast by interaction with ice flowing north from sources in the Coast and Cariboo mountains to the south (Plouffe, 1997, 2000).

The regional Quaternary framework and bedrock geology are described in more detail in Sacco et al. (2010) and Ward et al. (2011).

Field and Analytical Methods

Field Sampling

Basal till samples were collected at a total of 712 sites. The sampling regime included collecting three separate 800–900 g samples at each sample site for: 1) analysis of the clay-sized (hereafter referred to as clay) fraction by aqua-regia digestion followed by ICP-MS at Acme Analytical Laboratories Ltd. (Vancouver); 2) analysis of the clay plus silt-sized (hereafter referred to as clay+silt) fraction by INAA at Activation Laboratories Ltd. (Ancaster, Ontario); and 3) archiving at the Geological Survey of Canada. In addition, at every 4–5 sites (136 samples in total), a 10–15 kg sample was collected for heavy mineral separation and gold grain counts. The heavy mineral separations and counts were conducted at Overburden Drilling Management Limited (Nepean, Ontario). The <0.25 mm fraction of the heavy mineral concentrates were then analyzed by INAA at Becquerel Laboratories Inc. (Mississauga, Ontario). Results of the ICP-MS analysis, INAA and some heavy mineral grain counts were reported and discussed in Ward et al. (2011), and heavy mineral INAA results and selected grain counts from the large samples are reported here.

Analytical Methods

Heavy mineral concentrates were separated on large till samples at Overburden Drilling Management Limited. One hundred and thirty-six samples, 10–15 kg each, were panned for gold grains, platinum group metals (PGM) and uraninite. Bulk samples were disaggregated, followed by separation of the >2 and <2 mm fractions. The <2 mm fraction was then pre-concentrated on a shaking table, with the finest, heaviest fraction being panned. Gold, uraninite and PGM were then examined under optical microscope to provide grain counts as well as grain morphology. More detailed descriptions of the methods are provided in Averill (2001). Sulphide and cinnabar grains were also counted, although where the number of grains was >20, these counts are estimates.

The table concentrate was then sieved and the <0.25 mm fraction subsequently separated using heavy liquid at

3.2 g/cm³. This <0.25 mm fraction was then analyzed by INAA at Becquerel Laboratories Inc. under their BQ-NAA-1 package with the addition of Hg. Samples were placed in vials and were stacked into 30 cm long bundles for irradiation at the McMaster Nuclear Reactor (Hamilton, Ontario), which has flux of 8×10^{12} neutrons/cm²/sec. After a typical decay period of six days, the irradiated samples were loaded onto a high resolution, coaxial germanium detector that constructed a spectrum of gamma-ray energies versus intensities. The counting time was twenty to thirty minutes per sample. Quantitative elemental contents were derived by comparison of peak positions and area with library standards. Several elements, such as Hg, Ni, Zr, Rb, Au, had variable and higher than usual detection limits because of very high Cr, REE and Th contents (S. Simpson, personal communication, 2011). For example, Au usually has a detection limit of 2 ppb but here it ranges from 5 to 42 ppb depending on the sample.

Results

Au, As and Hg Contents

All till samples processed for heavy minerals ($n = 136$) contain visible gold (Figure 2a; Ward et al., 2011). Not surprisingly, the distribution of Au contents in the heavy mineral concentrates (Figure 2b), determined by INAA, mimics the Au contents in the silt+clay fraction, previously determined by INAA (Ward et al., 2011, Figure 4b). In the heavy mineral analysis, Au ranges from below detection (5–42 ppb depending on the sample) to 2630 ppb. Gold contents show clearly anomalous values around the 95th percentile (~750 ppb), although there is also a subtle change in the slope around the 80th percentile (~400 ppb). The highest values correspond to the area identified as having potential porphyry Cu-Au-style mineralization (cf. Ward et al., 2011). The highest gold grain numbers and INAA contents are associated with the margin between gravity lows and higher values (Figure 2b). This likely represents the contact between the felsic intrusions of the Wolverine metamorphic complex and the more mafic rocks of Quesnel terrane.

Arsenic is typically considered a pathfinder element for Au. Arsenic contents range from 9 to 414 ppm, show clearly anomalous values around the 95th percentile (60 ppm). The spatial distribution of As contents mimic those of Au and most anomalous values are in the north-western part of the study area, coincident with the margin of low gravity values with higher values, with slightly lower contents in the northwest (Figure 3a).

Cinnabar counts range from 0 to 400 grains. Anomalous cinnabar grain counts (>60 grains) occur in the western part of the study area, and mark the start of a trend of decreasing values to the southeast (Figure 3c). Because of the large number of cinnabar grains identified, the samples were also

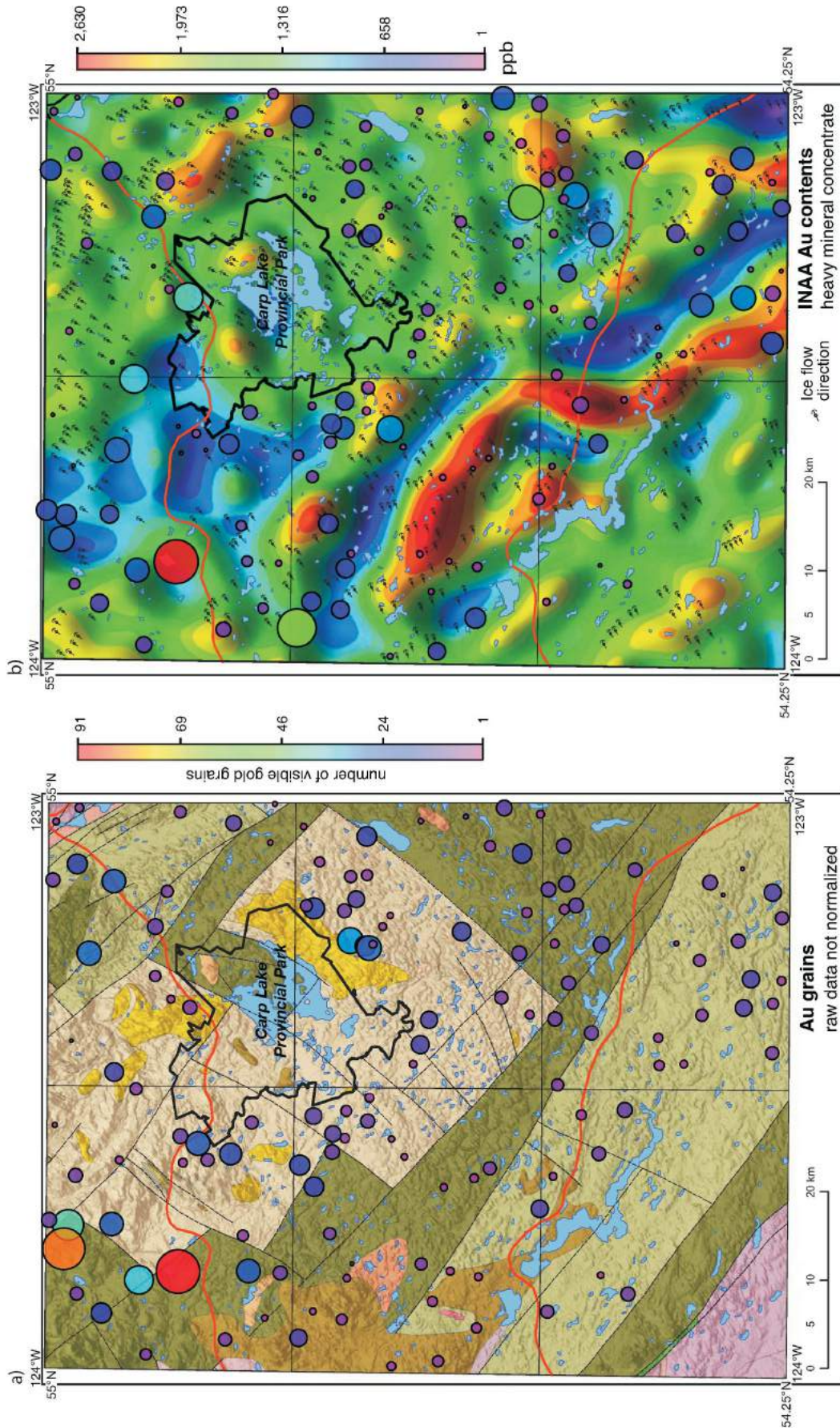


Figure 2. Proportional dot maps of Au contents in heavy mineral separates from till samples: **a)** Au grain counts, with data overlain on the bedrock geology map presented in Figure 1, and **b)** Au contents by instrumental neutron activation analysis (INAA), with data overlain on a gravity geophysical map (gravity highs in red; lows in blue) modified from Sanders Geophysical Limited (2008) with ice flow from Tipper (1971).

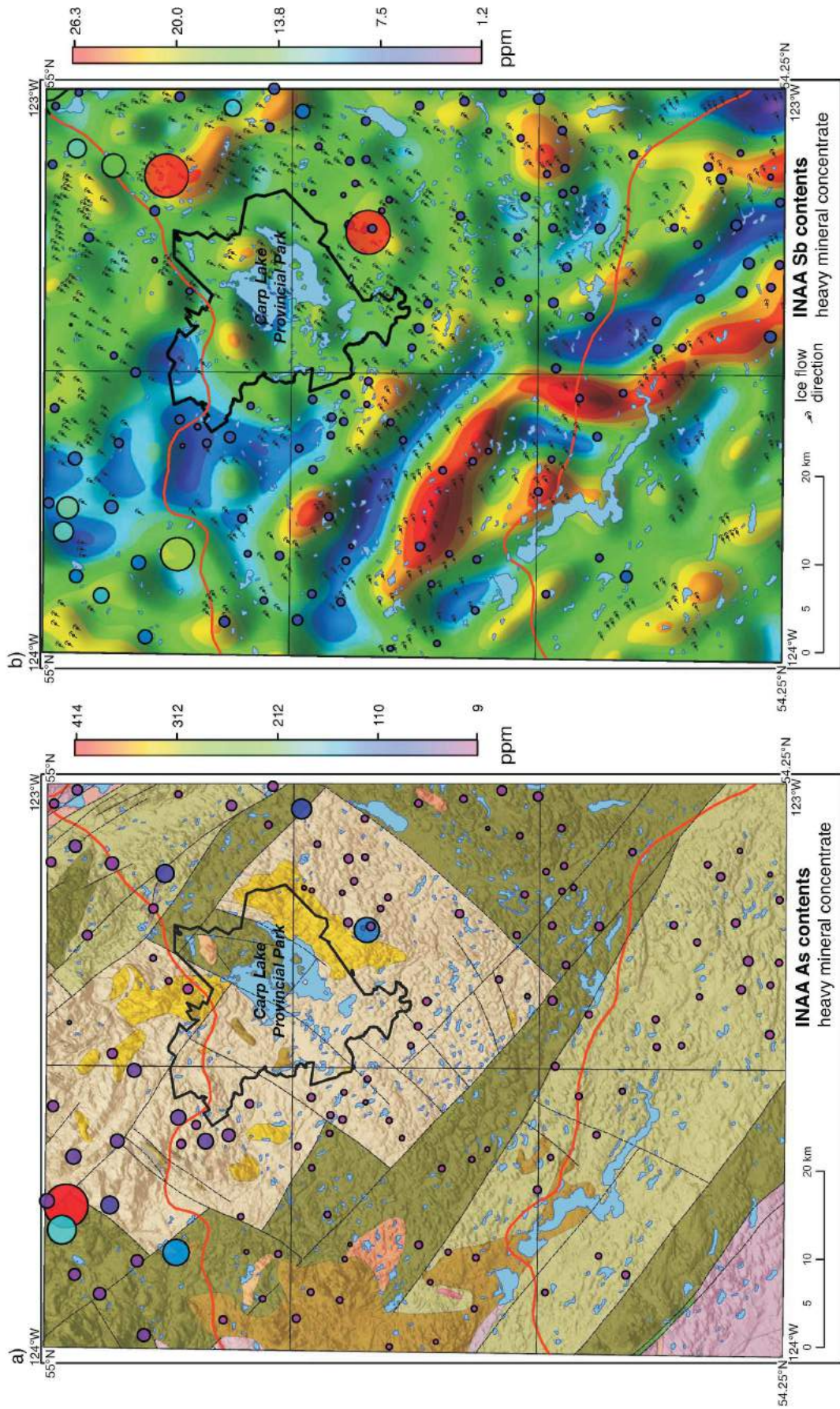


Figure 3. Proportional dot maps of selected elements in heavy mineral separates from till samples: **a)** As contents by instrumental neutron activation analysis (INAA), with data overlain on the bedrock geology map presented in Figure 1, and **b)** Sb contents by INAA, with data overlain on a gravity geophysical map (gravity highs in red; lows in blue) modified from Sanders Geophysical Limited (2008) with ice flow from Tipper (1971).

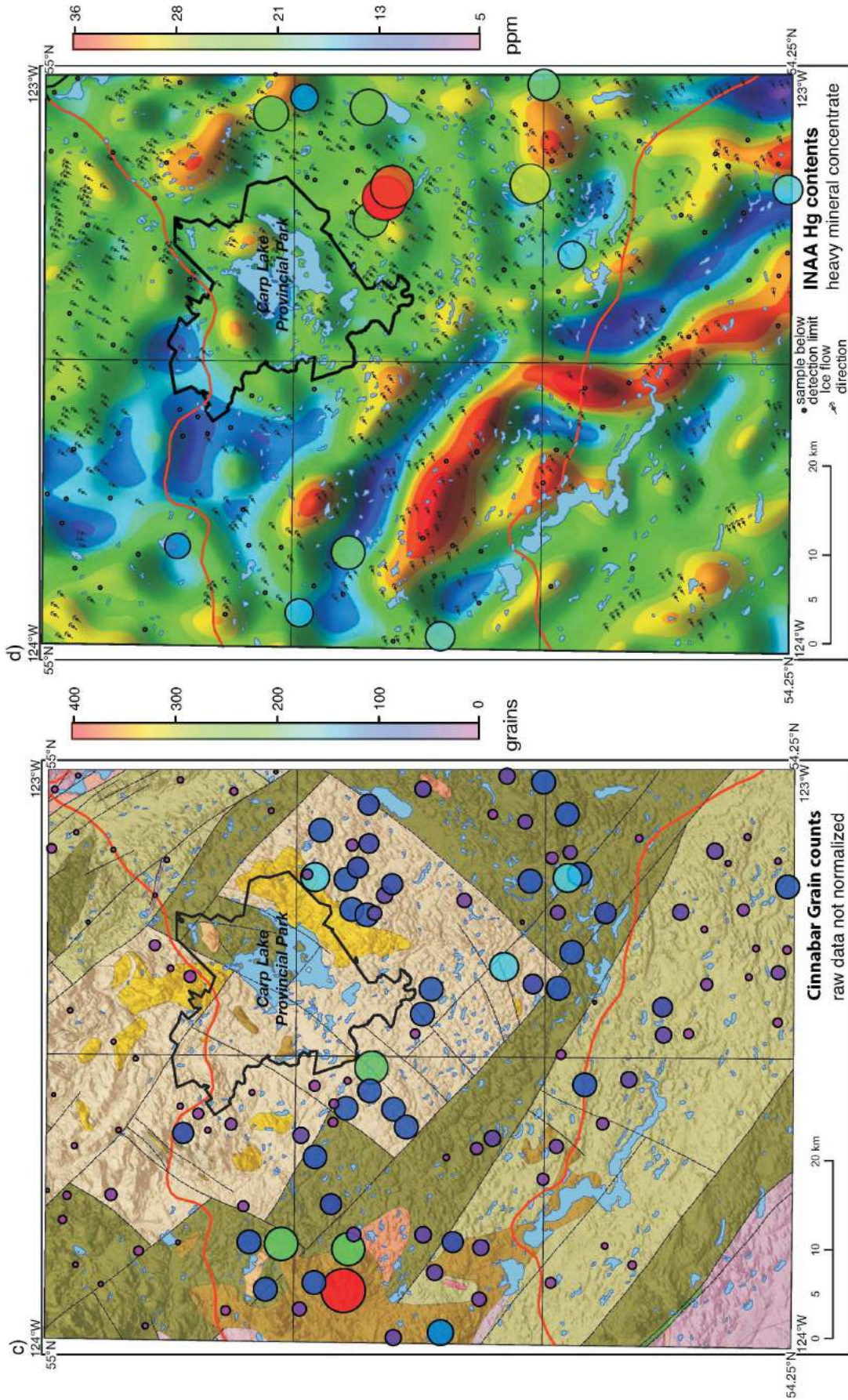


Figure 3 (continued). Proportional dot maps of selected elements in heavy mineral separates from till samples: **c)** cinnabar grain counts, with data overlain on the bedrock geology map presented in Figure 1, and **d)** Hg contents by instrumental neutron activation analysis (INAA), with data overlain on a gravity geophysical map (gravity highs in red; lows in blue) modified from Sanders Geophysical Limited (2008) with ice flow from Tipper (1971).

analyzed for Hg by INAA (Figure 3d); unfortunately, because of detection limit issues, due to interference with other elements, only 14 samples have values above detection limit. These samples are on the western and eastern sides of the study area and do mimic highs in the cinnabar grain counts. Also plotted are Sb contents as Sb is commonly associated with Hg (Figure 3b). Antimony is also a common pathfinder element of porphyry Cu-Au and VMS mineralization. The two highest values are to the southeast and northeast of Carp Lake, with intermediate values in the northwest, the zone of potential porphyry Cu-Au-style mineralization.

Ce, Th, Cr and Ta Contents

The basal till geochemical results presented by Ward et al. (2011) show that values for rare earth elements (REE), U, Th, K, Ca, Mg, Na, Ni and Cr have spatial relationships that are consistent with changes in the dominant underlying bedrock lithology. Thus, incompatible elements that are enriched in felsic rocks (i.e., REE, U, Th, K and Hf) are elevated in the northern part of the study area coincident with the Wolverine metamorphic complex, which contains felsic rocks such as granitic pegmatite, granite, granodiorite and rhyolite (Struik, 1994). Ni and Cr contents are highest in the south-southwestern portion of the study area where mafic and volcanoclastic rocks of the Quesnel terrane occur (Struik, 1994). The INAA determinations on the heavy mineral fraction presented here show a similar spatial distribution of elements. High Ce, Th and Ta contents in the north to northwest suggest more felsic rocks, likely the granitic pegmatite, granite, granodiorite and rhyolite and/or more enriched mafic rocks; whereas high Cr contents in the south indicates more primitive mafic rocks (Figure 4a–d). There is the possibility that the Cr could be derived from ultramafic rocks to the southwest in the Cache Creek terrane (Struik, 1994; Logan et al., 2010). If the Cr contents were derived from these ultramafic rocks, this would represent the longer distance of glacial transport associated with the thicker till in this area. The thinner till in the northern portion of the study area is thought to have a more local signature, reflecting local bedrock with a shorter distance of glacial transport.

Till Geochemical Exploration

The INAA determinations on heavy mineral concentrates presented here add to the previously published data and begin to build a coherent story on the potential for metallic mineralization in the study area. The spatial distribution of Au, As and Sb contents confirm the potential for epigenetic Au-Cu mineralization and to a lesser extent porphyry Cu-Au in the northeastern and northwestern areas of the study area, respectively. With >30 samples having Au contents >400 ppb, there is the potential for mineralized bedrock to occur there. Gold anomalies commonly coincide with

anomalies in other pathfinder elements, such as As and Sb. Although only a limited number of values are above detection limit, the spatial distribution of Hg values from the heavy mineral concentrate does mimic the distribution of cinnabar grains. Areas with elevated INAA values and grain counts may be associated with faults similar to the Pinchi Lake fault.

Elevated light REE and Th in the northern part of the study area are coincident with, and located down-ice from, granite pegmatite, granite and granodiorite suggesting the possibility of REE mineralization being associated with felsic porphyry bodies in the area, especially in the zone of gravity lows in the northwestern portion of the study area. Previous studies by the authors on the clay+silt and clay fractions of tills in the study area and the presence of large numbers of pyrite/marcasite grains in some of the heavy mineral concentrate samples suggest possible VMS mineralization (Ward et al., 2011). However, the inherent limitations of the INAA method (e.g., lack of Cu and Pb determinations and high detection limits for Zn, Cd and Ag) mean that INAA determinations presented here on heavy mineral concentrates do not add any insight into the potential for VMS-style mineralization within the study area.

Conclusions

The INAA of the <0.25 mm fraction of the heavy mineral concentrate of till samples adds insight into the interpretation of regional till geochemistry for the McLeod Lake map area. The potential for epigenetic Au-Cu mineralization, and to a lesser extent porphyry Cu-Au mineralization, in the northeastern and northwestern areas of the study area, respectively, is confirmed by the distribution of Au, As and Sb contents presented here. The few samples with Hg contents above detection limit mimic the distribution of cinnabar grains, implying there could be mineralization along faults in the area. Elevated Th and light REE in the northern part of the study area suggest the possibility of REE mineralization in association with felsic intrusions. The INAA data from heavy mineral concentrates does not add any insight in to potential VMS mineralization in the study area due to inherent limitations of the INAA method. All geochemical data from the Quaternary project will be released in early 2012 as a Geoscience BC report.

Acknowledgments

Geoscience BC provided the funding for this project and the authors extend many thanks to C. Anglin and C. Sluggett for helping to make this project happen. M. Casola, M. Dinsdale, K. Kennedy, J. McDonald, C. Pennimpede, S. Reichheld, I. Sellers and D. Vis, provided able assistance in the field. Geochemical reference standards were provided by R.E. Lett, who extensively discussed till geochemistry with the senior author. Review by T. Ferbey improved the manuscript.

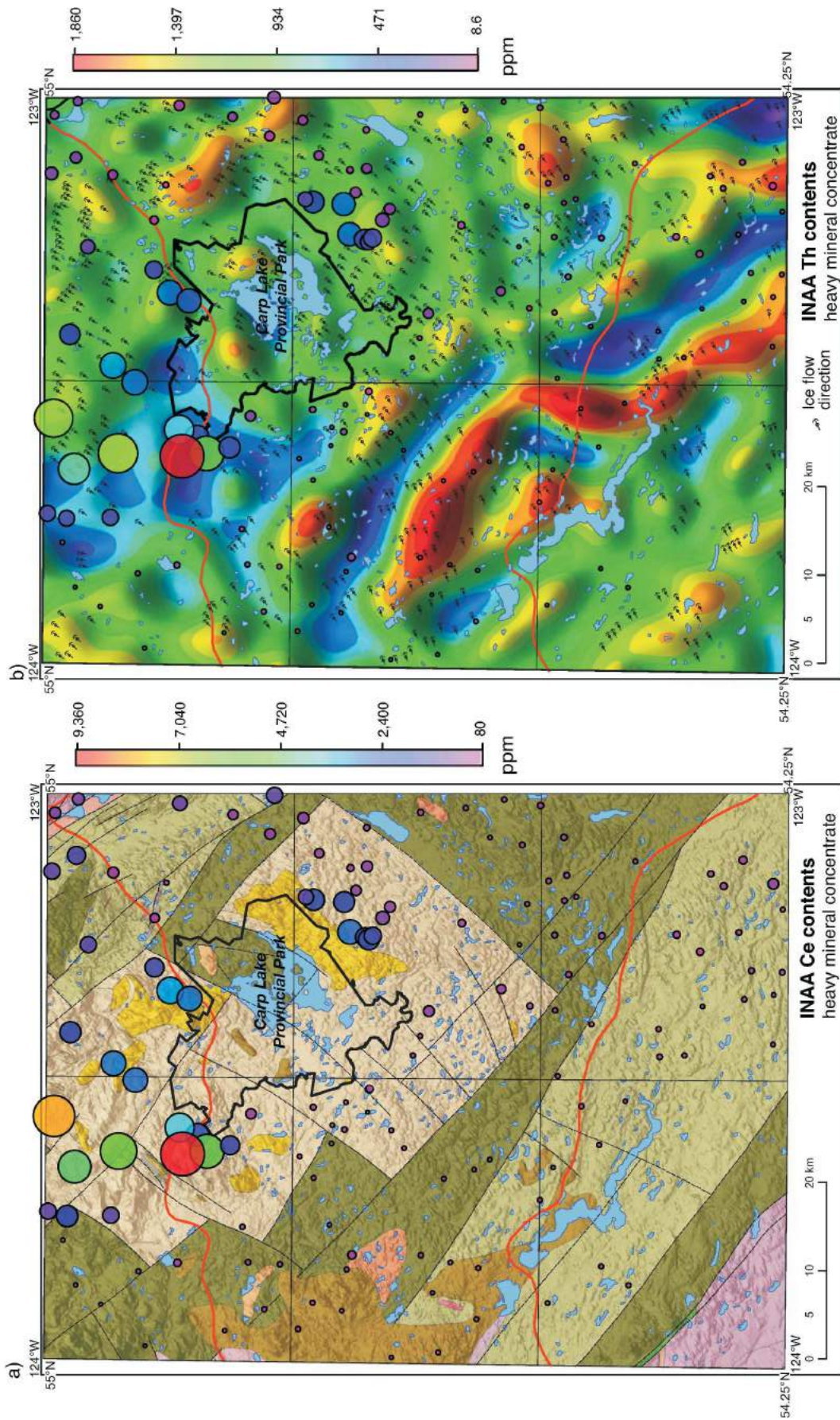


Figure 4. Proportional dot maps of selected elements in heavy mineral separates from till samples: **a)** Ce contents by instrumental neutron activation analysis (INAA), with data overlain on the bedrock geology map presented in Figure 1, and **b)** Th contents by INAA, with data overlain on a gravity geophysical map (gravity highs in red; lows in blue) modified from Sanders Geophysical Limited (2008) with ice flow from Tipper (1971).

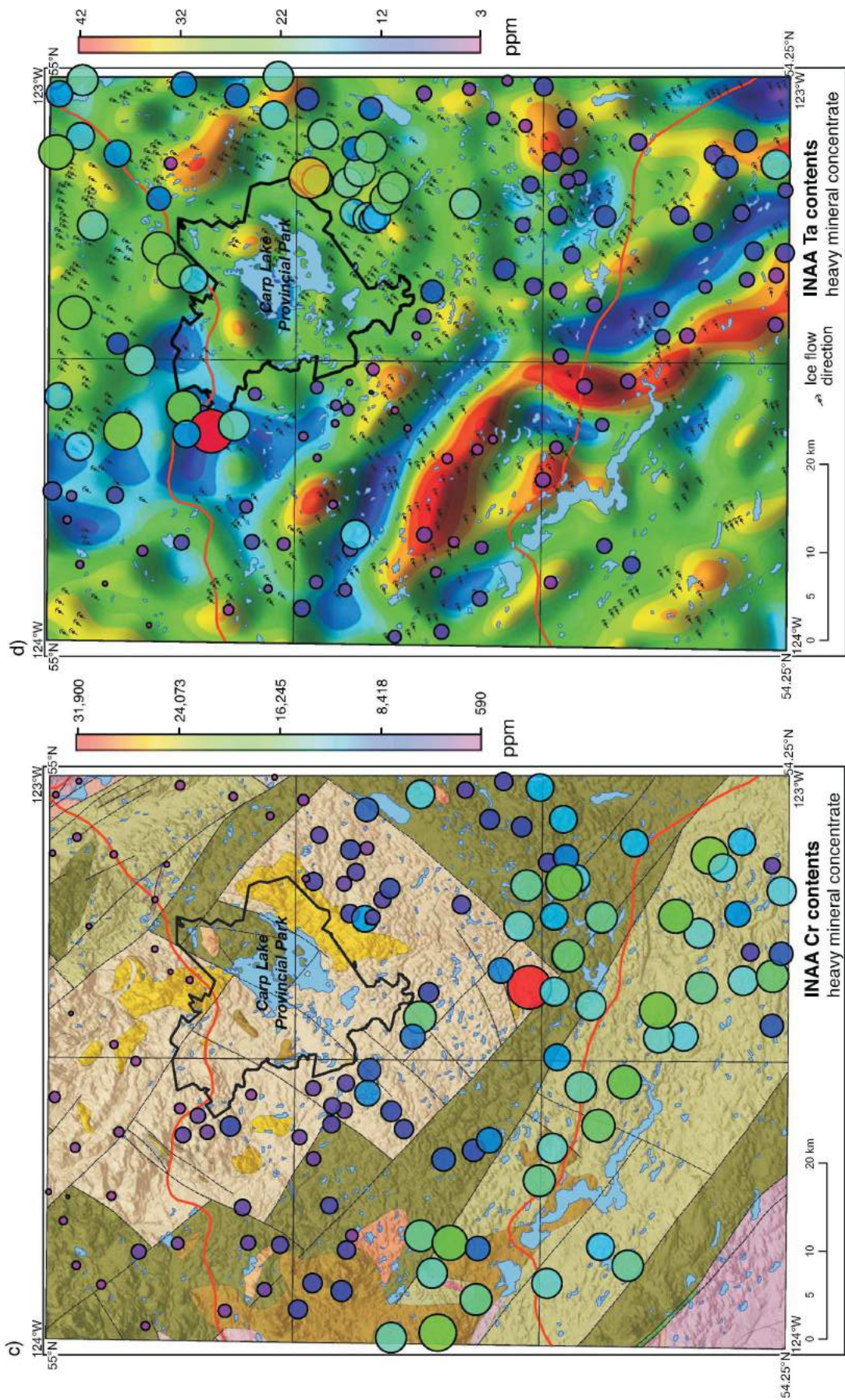


Figure 4 (continued). Proportional dot maps of selected elements in heavy mineral separates from till samples: **c)** Cr contents by instrumental neutron activation analysis (INAA), with data overlain on the bedrock geology map presented in Figure 1, and **d)** Ta contents by INAA, with data overlain on a gravity geophysical map (gravity highs in red; lows in blue) modified from Sanders Geophysical Limited (2008) with ice flow from Tipper (1971).

References

- Armstrong, J.E., Crandell, D.R., Easterbrook, D.J. and Noble, J.B. (1965): Late Pleistocene stratigraphy and chronology in south-western British Columbia and north-western Washington; *Geological Society of America Bulletin*, v. 72, p. 321–330.
- Averill, S.A. (2001): The application of heavy indicator mineralogy in mineral exploration with emphasis on base metal indicators in glaciated metamorphic and plutonic terrains; *Geological Society Special Publications*, v. 185, p. 69–81.
- BC Geological Survey (2011): MINFILE BC mineral deposits database; BC Ministry of Energy and Mines, URL <<http://minfile.ca>> [September 2011].
- Clague, J.J. (1989): Chapter 1: Quaternary geology of the Canadian Cordillera; *in* Quaternary Geology of Canada and Greenland, R.J. Fulton (ed.), *Geology of Canada Series No. 1.*, p. 17–96.
- Dreimanis, A. (1989): Tills: their genetic terminology and classification; *in* Genetic Classification of Glacigenic Deposits, R.P. Goldthwait and C.L. Matsch (ed.), A.A. Balkema, Rotterdam, p. 17–83.
- Holland, S.S. (1976): Landforms of British Columbia – a physiographic outline; BC Ministry of Energy and Mines, *Bulletin* 48, 138 p.
- Levson, V.M. (2001): Regional till geochemical surveys in the Canadian Cordillera: sample media, methods and anomaly evaluation; *in* Drift Exploration in Glaciated Terrain, M.B. McClenaghan, P.T. Bobrowsky, G.E.M. Hall and S.J. Cook (ed.), *The Geological Society, Special Publication no. 185*, p. 45–68.
- Levson, V.M. and Giles, T.R. (1997): Quaternary geology and till geochemistry studies in the Nechako and Fraser plateaus, central British Columbia; *in* Interior Plateau Geoscience Project: Summary of Geological, Geochemical and Geophysical Studies, L.J. Diakow, P. Metcalfe and J. Newell (ed.), BC Ministry of Energy and Mines, Paper 1997-2, p. 121–145.
- Logan, J.M., Schiarizza, P., Struik, L.C., Barnett, C., Nelson, J.L., Kowalczyk, P., Ferri, F., Mihalynuk, M.G., Thomas, M.D., Gammon, P., Lett, R., Jackaman, W. and Ferbey, T. (2010): Bedrock geology of the QUEST map area, central British Columbia; Geoscience BC, Report 2010-5 and BC Ministry of Energy and Mines, Geoscience Map 2010-1 and Geological Survey of Canada, Open File 6476, URL <<http://www.geosciencebc.com/s/2010-005.asp>> [November 2010].
- Mathews, W.H. (1986): Physiographic map of the Canadian Cordillera; Geological Survey of Canada, “A” Series Map 1710A, scale 1:5 000 000.
- McClenaghan, M.B. (2005): Indicator mineral methods in mineral exploration; *Geochemistry: Exploration, Environment, Analysis*, v. 5, p. 233–245.
- McClenaghan, M.B., Ward, B.C., Kjarsgaard, I.M., Kjarsgaard, B.A., Kerr, D.E. and Dredge, L.A. (2002): Indicator mineral and till geochemical dispersal patterns associated with the Ranch Lake kimberlite, Lac de Gras region, NWT, Canada; *Geochemistry: Exploration, Environment, Analysis*, v. 2, p. 299–320.
- Plouffe, A. (1997): Ice flow and late glacial lakes of the Fraser glaciation, central British Columbia; *in* Current Research 1997-A, Geological Survey of Canada, p. 133–143.
- Plouffe, A. (2000): Quaternary geology of the Fort Fraser and Manson River map areas, central British Columbia; Geological Survey of Canada, *Bulletin* 554, 62 p.
- Sacco, D.A., Ward, B.C., Maynard, D., Geertsema, M. and Reichheld, S. (2010): Terrain mapping, glacial history and drift prospecting in the northwest corner of McLeod Lake map area (part of NTS 093J), central British Columbia; *in* Geoscience BC Summary of Activities 2009, Geoscience BC, Report 2010-1, p. 33–42, URL <http://www.geosciencebc.com/i/pdf/SummaryofActivities2009/SoA2009_Sacco.pdf> [November 2011].
- Sander Geophysics Limited (2008): Airborne gravity survey, Quesnellia Region, British Columbia; Geoscience BC, Report 2008-08, 121 p., URL <<http://www.geosciencebc.com/s/2008-08.asp>> [November 2011].
- Struik, L.C. (1994): Geology of the McLeod Lake map area (93J), British Columbia; Geological Survey of Canada, Open File 2439, 18 p.
- Tipper, H.W. (1971): Glacial geomorphology and Pleistocene history of central British Columbia; Geological Survey of Canada, *Bulletin* 196, 89 p.
- Ward, B.C., Leybourne, M.I. and Sacco, D.N. (2011): Drift prospecting within the QUEST Project area, central British Columbia (NTS 093J): potential for porphyry copper-gold, volcanogenic massive sulphide mineralization and gold-copper veins; *in* Geoscience BC Summary of Activities 2011, Geoscience BC, Report 2011-1, p. 73–96, URL <http://www.geosciencebc.com/i/pdf/SummaryofActivities2010/SoA2010_Ward_et al.pdf> [November 2011].
- Ward, B., Maynard, D., Geertsema, M. and Rabb, T. (2009): Ice-flow history, drift thickness and drift prospecting for a portion of the QUEST Project area, central British Columbia (NTS 093G, H [west half], J); *in* Geoscience BC Summary of Activities 2008, Geoscience BC, Report 2009-1, p. 25–32, URL <http://www.geosciencebc.com/i/pdf/SummaryofActivities2008/SoA2008-Ward_original.pdf> [November 2011].

Chemical Variations of Pyroxene and Fe-Ti–Oxide Crystals in Basalts Hosting Cu-Au Porphyry Mineralization in the Quesnel Terrane, Interior British Columbia (NTS 092H, I, P, 093A, J, N)

S. Vaca, Mineral Deposit Research Unit, University of British Columbia, Vancouver, BC, svaca@eos.ubc.ca

T. Bissig, Mineral Deposit Research Unit, University of British Columbia, Vancouver, BC

M. Raudsepp, Department of Earth and Ocean Sciences, University of British Columbia, Vancouver, BC

C.J.R. Hart, Mineral Deposit Research Unit, University of British Columbia, Vancouver, BC

Vaca, S., Bissig, T., Raudsepp, M. and Hart, C.J.R. (2012): Chemical variations of pyroxene and Fe-Ti–oxide crystals in basalts hosting Cu-Au porphyry mineralization in the Quesnel terrane, interior British Columbia (NTS 092H, I, P, 093A, J, N); *in* Geoscience BC Summary of Activities 2011, Geoscience BC, Report 2012-1, p. 69–78.

Introduction

The Late Triassic Quesnel terrane is mainly composed of rocks of the Nicola Group and its along-strike equivalent Takla Group, both of which are largely composed of alkalic and lesser calcalkalic basalts, derivative volcanic products and associated arc-fringing sedimentary strata (Dawson, 1879; Preto, 1979; Mortimer, 1987). Hereafter, these two groups are referred to as the Nicola Group. The Quesnel terrane in British Columbia is known to host several alkalic porphyry Cu-Au deposits, including (from north to south) Lorraine, Mount Milligan, Mount Polley, Afton/Ajax and Copper Mountain (Figure 1).

Variation in the magnetic susceptibility values and Fe^{2+}/Fe^{3+} ratios in basalts from different localities in central Quesnel terrane have been previously documented by Bissig et al. (2010) and Vaca et al. (2011). These authors showed that the volcanic arc can be subdivided on the basis of variation in oxidation state and magnetic susceptibility. Porphyry Cu-Au deposits broadly coeval with volcanism at Mount Polley are hosted in a relatively oxidized and alkaline part of the arc when compared to areas devoid of coeval porphyry style of mineralization. Although the least altered basalts were studied, the magnetic susceptibility and Fe^{3+} content may be influenced by low temperature alteration processes. Thus, in this paper we present an alternate way to estimate oxidation state and alkalinity of magmas using the chemistry of effectively unaltered phenocrysts.

Keywords: Nicola Group, alkalic porphyry, microprobe, pyroxene, basalt

This publication is also available, free of charge, as colour digital files in Adobe Acrobat® PDF format from the Geoscience BC website: <http://www.geosciencebc.com/s/DataReleases.asp>.

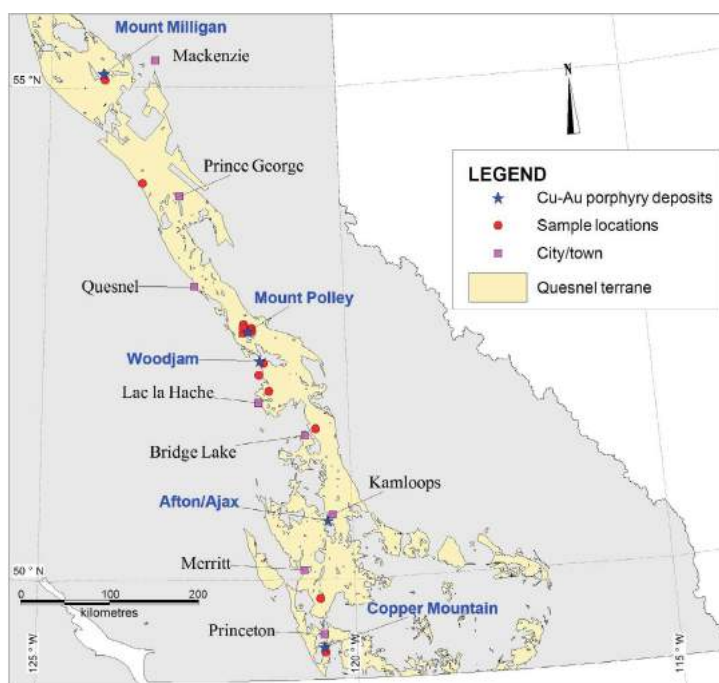


Figure 1. Spatial distribution of Cu-Au porphyry deposits in the Quesnel terrane of interior British Columbia (the Lorraine deposit is located north of the area covered by the figure).

Clinopyroxene is the most common phenocryst in basalts of the Quesnel terrane. Pyroxenes from different Nicola Group map units around the Mount Polley Cu-Au porphyry deposit (Logan and Bath, 2005; Logan et al., 2007) were selected for microanalytical geochemistry. Clinopyroxene compositions from these areas were compared with those from other localities, along strike but still within the arc (Figure 1).

Scanning electron microscopy (SEM) and electron microprobe (EMP) analyses were performed to obtain qualitative and quantitative analyses of the chemical variations within and between pyroxene crystals. In addition, the composi-

tion of the Fe-Ti-oxide inclusions within pyroxene was determined.

Pyroxene and Fe-Ti-oxide chemistry records the alkalinity and oxidation state of parent magma (Kushiro, 1960; LeBas, 1962; Taylor, 1964). High oxidation state is an important characteristic of igneous rocks related to porphyry Cu-Au mineralization (e.g., Seedorff et al., 2005; Chamberlain et al., 2007). Thus, studying chemical changes of minerals within basalts will lead to a more complete understanding of the magmatic evolution of the arc. This might generate new ideas on the prospectivity for comagmatic Cu-Au porphyry mineralization in different arc segments.

Samples

Sampling was conducted during the 2009 and 2010 summer field seasons and was focused on coherent volcanic

rocks from different localities along the Quesnel terrane (Figure 1).

The areas studied in this research include

- Mount Polley, where host volcanic rocks are interpreted to be broadly coeval with the mineralization (Bailey and Hodgson, 1979; Logan and Bath, 2005); three different map units of volcanic host rocks around this alkalic silica-undersaturated Cu-Au porphyry deposit were sampled (see Figure 2);
- Mount Milligan, where basaltic host rocks are cut by silica-saturated alkalic porphyry Cu-Au mineralization that is approximately 20 m.y. younger (Nelson and Bellefontaine, 1996);
- Copper Mountain, where silica-saturated alkalic Cu-Au porphyry deposits are interpreted to be coeval with the volcanic host rocks, paleontological data of the south-

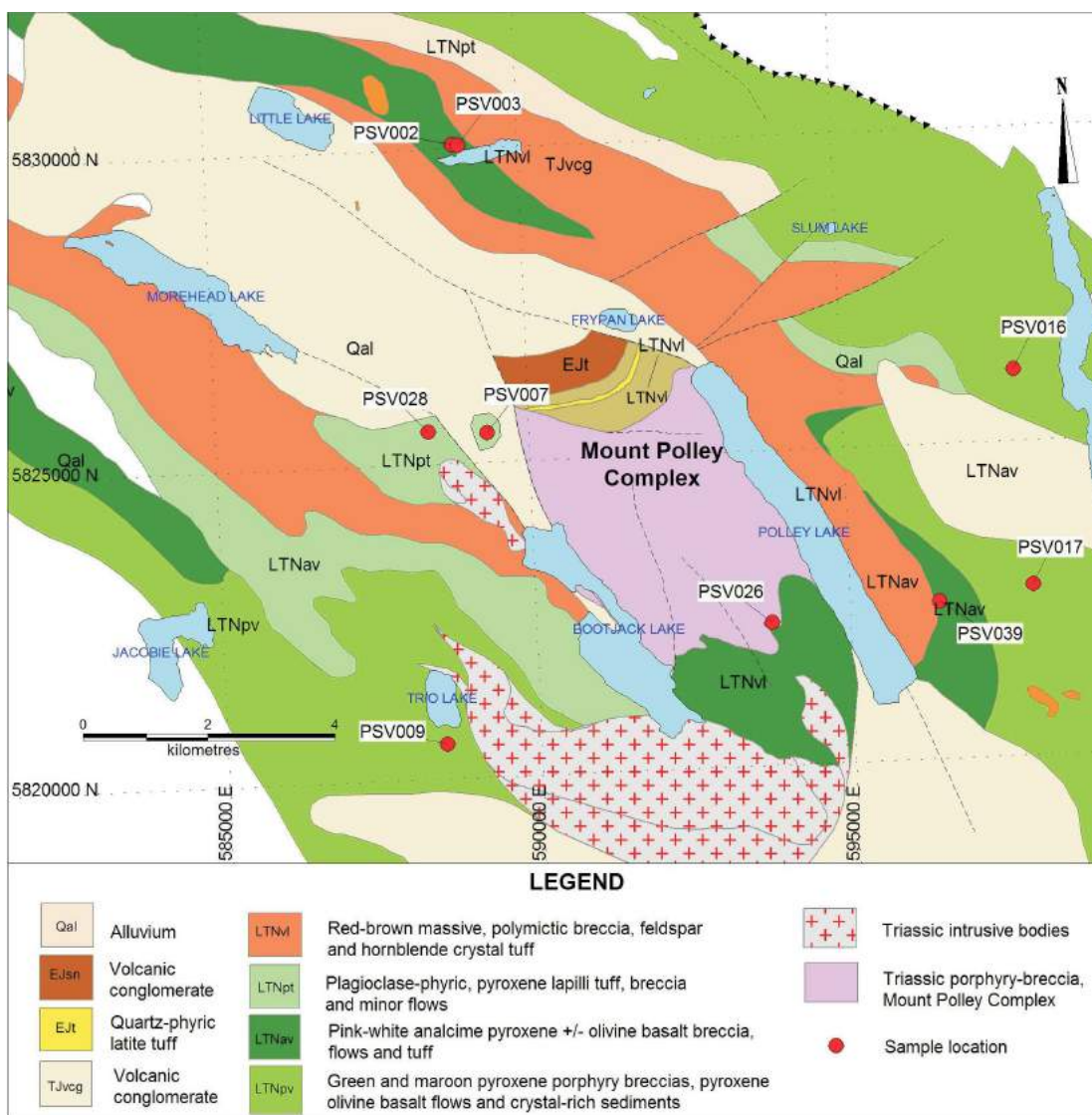


Figure 2. Different map units at the Mount Polley area, showing the location of the samples used in this research (Modified from Logan et al., 2007).

eastern part of the Nicola Group is Late Norian, ca. 204 Ma and intrusive bodies in the Copper Mountain complex date to ca. 200–205 Ma (Carter et al., 1991; Mortensen et al., 1995);

- Woodjam prospect, which features silica-saturated porphyry Cu-Au-Mo mineralization; recent detailed mapping by Blackwell et al. (2010) revealed that a rock unit previously mapped as a plagioclase porphyry stock is actually part of the volcanic succession, presenting an age of ca. 204 Ma, while the age of the intrusion is ca. 196.84 Ma (Schiarizza unpublished zircon ages in Logan et al., 2011), thus, volcanic rocks here are approximately 7 m.y. older than the fertile intrusions;
- Lac la Hache prospect, where Cu-Au mineralization is interpreted to be related to alkalic intrusions (Schiarizza et al., 2008), both host rock and mineralization ages are unknown; and
- exposures around Prince George, Bridge Lake and south of Merritt, that represent apparently barren arc segments (Figure 1).

Analytical Procedures

Magnetic susceptibility was measured in the field using a KT-9 Kappameter handheld instrument. The values reported are the average of 10 readings over the outcrop. Polished thin sections were prepared from 17 rock samples from different locations in the study area, for petrography, SEM and EMP analyses. All analyses were conducted in the laboratories at the Department of Earth and Ocean Sciences, University of British Columbia.

Detailed petrographic observations were made using transmitted and reflected light microscopy. Polished thin sections were carbon coated in an Edwards Auto 306 carbon-coater instrument. The SEM analyses were done with a Philips™ XL-30 scanning electron microscope/Bruker Quantax™ 200 energy-dispersion X-ray microanalysis system. Chemical compositions of pyroxene and Fe-Ti oxides were determined using a fully automated CAMECA™ SX-50

electron microprobe. Pyroxene compositions were measured with the following operating conditions: excitation voltage, 15 kV; beam current, 20 nA; peak count-time, 20 s; background count-time, 10 s; spot diameter, 5 μm. The Fe-Ti-oxide analyses were obtained using the same operating conditions as pyroxene. Standards for pyroxene and Fe-Ti-oxide analyses are indicated in Table 1.

Data reduction for was done using the ‘PAP’ $\phi(\rho Z)$ method (Pouchou and Pichoir, 1985). The structural formulas of pyroxene were calculated on the basis of 6 O; for Fe-Ti oxides, structural formulas were calculated on the basis of 32 O. The Fe³⁺ content was calculated using the method proposed by Droop (1987).

Petrography

Detailed petrographic study shows that all samples are basalts, except for one sample collected from the Woodjam property, which is a basaltic andesite. The rocks are porphyritic, with a visual estimation of 30–60% phenocrysts per sample, ranging from 1 to 5 mm in diameter. Phenocrysts are mainly euhedral to subhedral clinopyroxene, tabular plagioclase and, in the most alkaline basalts, euhedral to anhedral analcime is present. Mineral proportions vary according to sample location as demonstrated in Table 2. Groundmass in all samples consists of fine-grained plagioclase, clinopyroxene, opaque minerals and products of volcanic glass devitrification.

The rocks are weakly altered, with a chlorite-calcite-epidote assemblage, overprinting the fine-grained groundmass; hematite is also locally present.

Scanning Electron Microscopy and Electron Microprobe Analyses

Clinopyroxene

In all samples, clinopyroxene crystals are colourless to pale green in transmitted light, ≤4 mm, euhedral to subhedral,

Table 1. Standards, analysis lines and crystals used for pyroxene and Fe-Ti-oxide analyses.

Pyroxene	Fe-Ti oxides
albite, Na _{Kα} , TAP	synthetic spinel, Al _{Kα} , TAP
kyanite, Al _{Kα} , TAP	synthetic magnesiochromite, Mg _{Kα} , TAP
diopside, Mg _{Kα} , TAP	diopside, Si _{Kα} , TAP
diopside, Si _{Kα} , TAP	diopside, Ca _{Kα} , PET
diopside, Ca _{Kα} , PET	rutile, Ti _{Kα} , PET
rutile, Ti _{Kα} , PET	synthetic magnesiochromite, Cr _{Kα} , LIF
synthetic magnesiochromite, Cr _{Kα} , LIF	synthetic rhodonite, Mn _{Kα} , LIF
synthetic rhodonite, Mn _{Kα} , LIF	synthetic fayalite, Fe _{Kα} , LIF
synthetic fayalite, Fe _{Kα} , LIF	synthetic Ni ₂ SiO ₄ , Ni _{Kα} , LIF
synthetic Ni ₂ SiO ₄ , Ni _{Kα} , LIF	vanadium metal, V _{Kα} , PET

Abbreviations: LIF, lithium fluoride; PET, pentaerythritol; TAP, thallium acid phthalate

Table 2. List of samples showing the amounts of the most important phenocryst phases and the occurrence of Fe-Ti oxides and hematite within the basalts. Magnetic-susceptibility values indicate the presence and amount of magnetite. All of the samples have been affected by weak epidote-chlorite-calcite alteration.

Sample ID	UTM: NAD 83, Zone 10S		Location	Main phenocryst phases			Fe-Ti oxide (%)	Hem ¹	Magnetic susceptibility ² (SI units)
	Easting	Northing		Cpx (%)	Plag (%)	Anl (%)			
PSV002	588966	5830062	Mount Polley-LTN	30	14	12	1	x	21.5
PSV003	589059	5830056	Mount Polley-LTN	30	15		1		41.9
PSV007	589328	5825476	Mount Polley-LTNpt	10	50		1 2		70.1
PSV009	588497	5820559	Mount Polley-LTNpv	25	35		1 2		70
PSV016	597756	5826139	Mount Polley-LTNpv	25	4		1		23.7
PSV017	597925	5822708	Mount Polley-LTNpv	30	3	7	<1	x	1.16
PSV026	593744	5822273	Mount Polley-LTN	35	25		2 3		86.1
PSV028	588392	5825520	Mount Polley-LTNpt	20	30		2 3		111
PSV039	596426	5822502	Mount Polley-LTN	20	15	30	1 2	x	60.9
MTB031	433079	6105548	Mount Milligan	27	5		<1		0.4
CMSV203	681762	5461207	Copper Mountain	40	5		<1		1.2
WTB085	611019	5786299	Woodjam	25	30		1	x	1.55
LTB073	606030	5773254	Lac la Hache north	33	13		1 2		83.5
LTB067	617760	5755186	Lac la Hache south	35	25		2	x	40
PGTB074	474874	5989106	Prince George	12	30		<1		15.4
BTB051	670097	5712526	Bridge Lake	37	5		<1		1.29
SSV128	676083	5521435	South of Merritt	25	5	10	1	x	0.27

¹ within the matrix (primary and/or alteration)

² values are multiplied by 10⁻³ (e.g., 21.50 x 10⁻³)

Abbreviations: Anl, analcime; Cpx, clinopyroxene; Hem, hematite; Plag, plagioclase

and typically display concentric zonation. Magnetite and apatite inclusions are common (Figure 3). They are variably fractured and locally chloritized, but only effectively unaltered crystals were analyzed in this study. Generally, clinopyroxene spans a narrow overall chemical variation from core to rim. The average composition of the pyroxene phenocrysts in basalts along the Quesnel terrane is (Ca_{0.89},Fe²⁺_{0.08},Na_{0.03})(Al^{VI}_{0.03},Fe³⁺_{0.11},Fe²⁺_{0.05},Ti_{0.02},Mg_{0.79},Mn_{0.01})(Si_{1.85},Al^{IV}_{0.15})O₆, falling in the diopside field of the pyroxene quadrilateral (Figure 4). Most analy-

ses plot in the diopside field, except for some data from the Mount Polley, Prince George and Woodjam areas, which straddle the border of the augite field (Figure 4).

Pyroxene compositions comprise two populations (Figure 4). The more crowded population (right) ranges between 10–20 mol % Fe content and corresponds to analyses performed from core through interior to rim in the crystals from all localities, except Woodjam. The other population (left, circled by brown dashed line) lies within 0–10 mol %

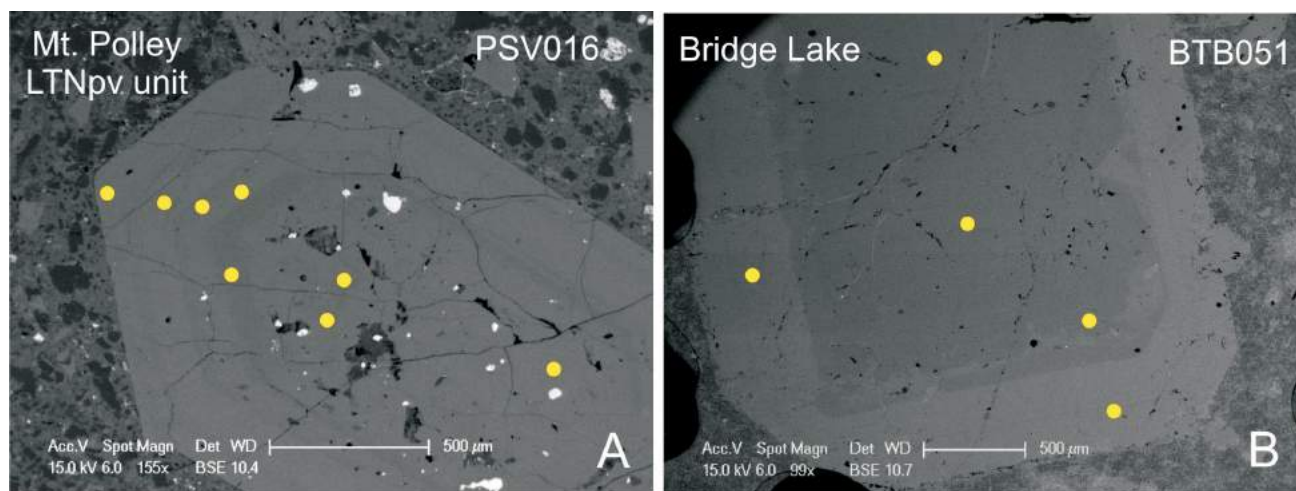


Figure 3. Representative backscattered electron images of clinopyroxene, electron microprobe (EMP) analysis spots are shown in yellow: **A)** clinopyroxene showing concentric zonation and Fe-Ti-oxide inclusions (bright gray); **B)** zoned clinopyroxene evidencing a sharp transition between the core/interior (dark gray) and rim (light gray). Note that magnetite inclusions are present only within pyroxene A. Zonation suggests rapid changes in the temperature-composition (T-X) parameters during crystallization.

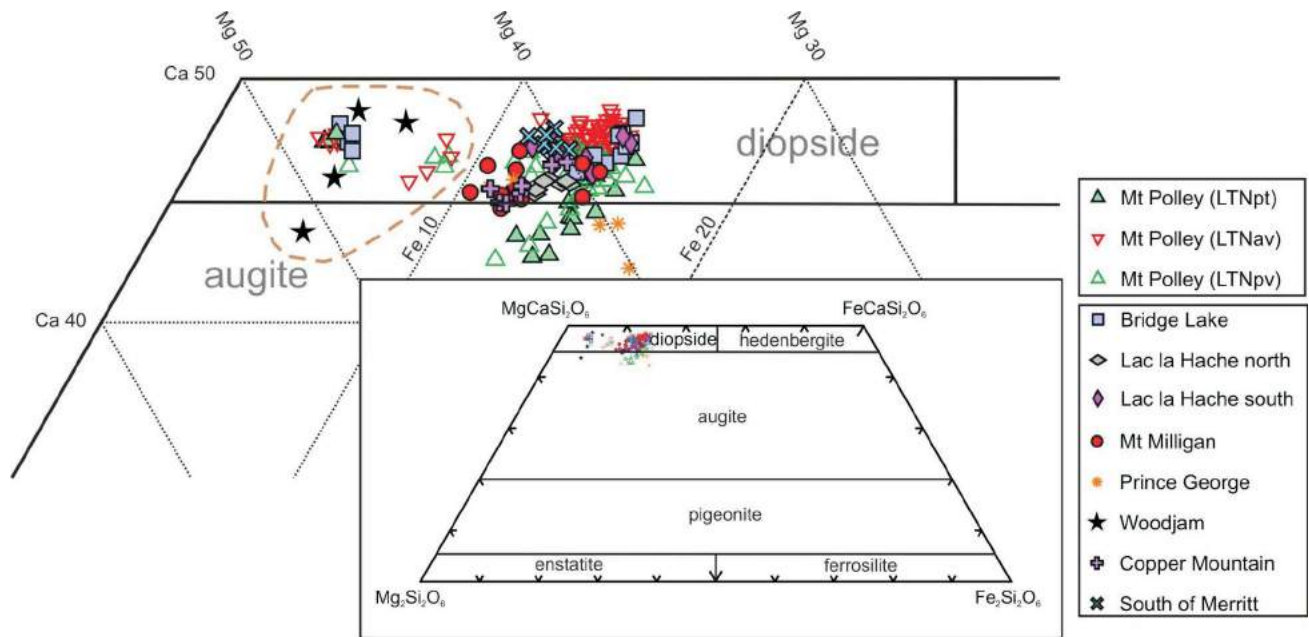


Figure 4. Pyroxene quadrilateral compositions for basalts of the Quesnel terrane. The circled field corresponds to pyroxene from core to rim of the Woodjam sample, and some spots from cores and interiors of pyroxene crystals from samples collected near Bridge Lake and Mount Polley. The pyroxene quadrilateral is that of Morimoto (1988).

Fe, and includes the Woodjam sample and some spots from cores and interiors only (no rims) of the Bridge Lake sample and Mount Polley samples (PSV007, PSV016, PSV017, PSV026 and PSV039, refer to Figure 2).

Chemical composition of pyroxene is characterized by a nearly constant Ca content of ~0.9 cations per formula unit (cpfu); the Mg# ($100 * Mg^{2+} / (Mg^{2+} + Fe^{2+})$) ranges from

76.27 to 98.12, showing an overlap among the different rock units (Figure 5). Most spot analyses from Copper Mountain, Lac la Hache north, South of Merritt and unit LTNav at Mount Polley fall above an empirically defined division line at Mg# of 85, whereas pyroxene from Mount Milligan, Lac la Hache south, Bridge Lake, Prince George and unit LTNpt at Mount Polley fall mostly below this line. Analy-

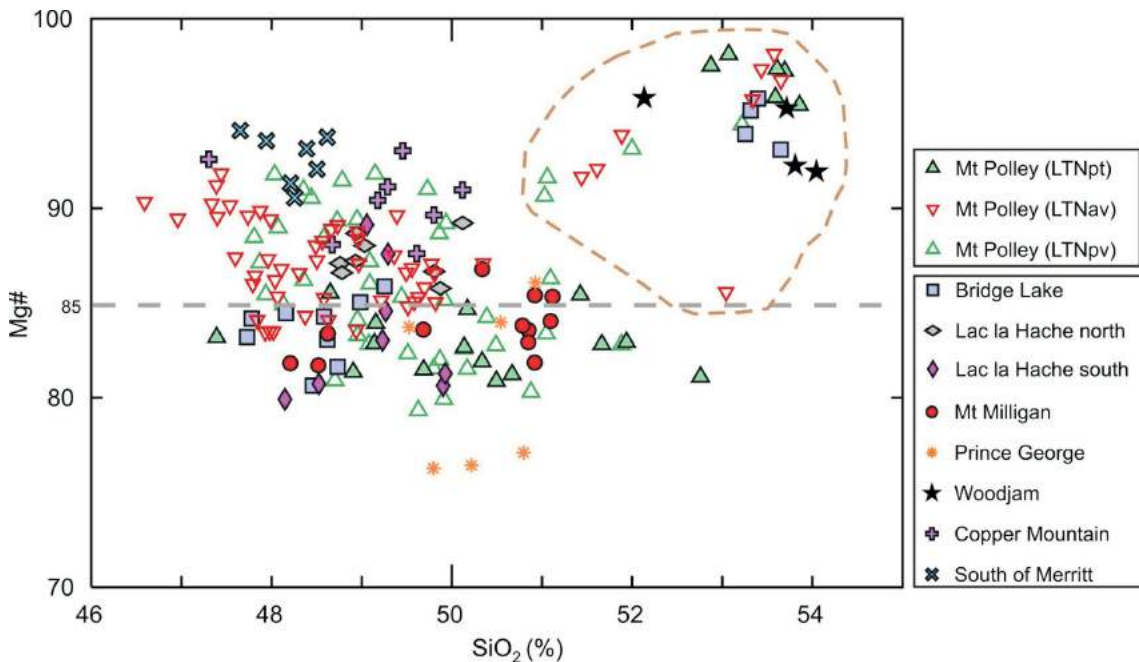


Figure 5. Chemical distribution based on the content of SiO₂ and Mg# from electron microprobe (EMP) analyses of pyroxene crystals in basalts of the Nicola Group. High Mg# is indicative of primitive melts. Dashed brown line outlines pyroxene analyses from Woodjam, with some core and interior analyses from Bridge Lake and Mount Polley.

ses from the unit LTNpv plot both above and below this reference line.

Another group of spots with high Mg# (85.56–98.12) and SiO₂ (51.03–54.05%) content (Figure 5, top right, dashed brown line) corresponds to core and interiors of pyroxene analyses from Woodjam and some from Bridge Lake and Mount Polley. This group matches with the group with lower Fe values in Figure 4. Pyroxene crystals contain sufficient Si and Al to fill the tetrahedral site (Al^{IV}), except for a few analyses from Bridge Lake and Mount Polley sam-

ples, which require addition of Fe³⁺ (0.03–0.018 cpfu). This group also coincides with the analyses outlined in the Figure 4 (top left) and Figure 5 (top right).

Overall calculated Fe³⁺ within clinopyroxene present values ranging from 0.002 to 0.19 cpfu and Al^{IV} numbers between 0.006 and 0.25 cpfu (Figure 6A); overlap among the different localities is common, however, some trends in the data can be recognized. Pyroxene from Copper Mountain, Bridge Lake, Lac la Hache north, units LTNpv and LTNpv at Mount Polley and south of Merritt have a consistently

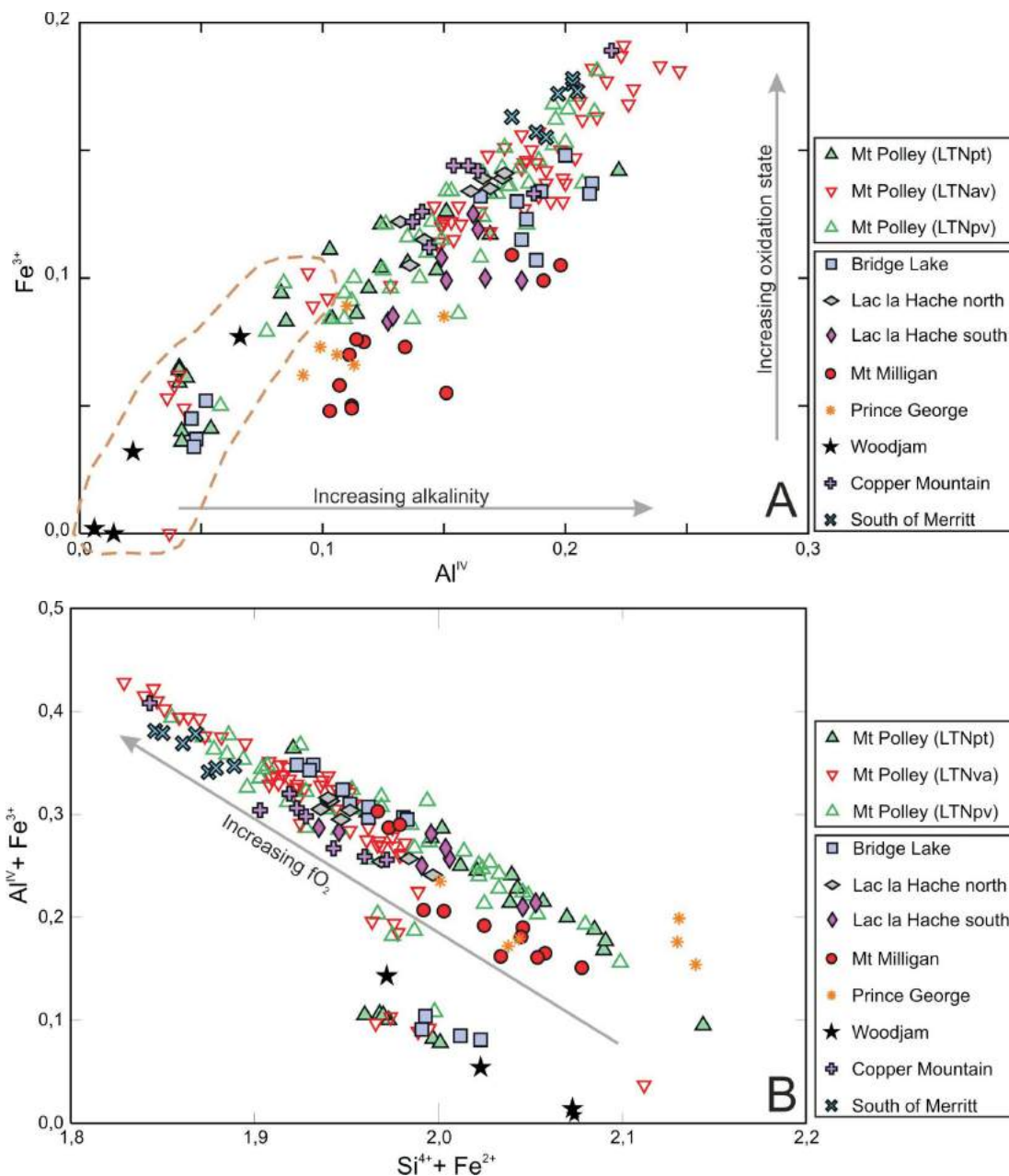


Figure 6. Cation relationships for clinopyroxene crystals from samples of Nicola Group basalts: **A)** direct relationship between Al^{IV} and Fe³⁺ in pyroxene composition from core to rim; **B)** negative correlation between (Si⁴⁺ + Fe²⁺) and (Al^{IV} + Fe³⁺) in pyroxene indicating higher oxygen fugacity (fO₂) with lower Si⁴⁺ + Fe²⁺. Dashed brown line outlines pyroxene analyses from Woodjam, with some core and interior analyses from Bridge Lake and Mount Polley.

higher calculated Fe^{3+} (~0.10–0.19 cpfu) and Al^{IV} (~0.13–0.25 cpfu) content, compared with Fe^{3+} (0.002–0.13 cpfu) and Al^{IV} (0.006–0.15 cpfu) from the Mount Milligan, Mount Polley unit LTNpt, Lac la Hache south, Prince George and Woodjam samples. Some analyses (core and interiors) of clinopyroxene from Bridge Lake and from all units at Mount Polley also belong to this latter group (Figure 6A, bottom left).

The Al^{IV} values increase directly proportional to Fe^{3+} contents (Figure 6A), but $(\text{Si}^{4+} + \text{Fe}^{2+})$ and $(\text{Al}^{\text{IV}} + \text{Fe}^{3+})$ show negative correlation (Figure 6B). These data suggest that clinopyroxene from samples obtained from Copper Mountain, Bridge Lake (rims), Lac la Hache north, LTNpv and LTNpv units near Mount Polley and south of Merritt crystallized from a melt with higher relative oxygen fugacity than the others.

Fe-Ti-Oxide Minerals

Primary Fe-Ti-oxide minerals are commonly present as inclusions within clinopyroxene in the study area. These oxides exhibit subsolidus exsolution features, and distinctive compositions and textures (Figure 7). Representative analyses of primary Fe-Ti oxides show variable Fe^{3+} , Ti and Fe^{2+} contents (Figure 8). A few spot analyses in exsolution lamellae within crystals from the LTNpt unit at Mount Polley (Figure 7C), Lac la Hache south and Prince George are depleted in Fe^{3+} and relatively enriched in Ti. The former plots within the ferropseudobrookite and ilmenite fields respectively; the latter plots within the ulvoespinel field (Figure 8).

The remaining spot analyses from Lac la Hache south and Prince George samples show titanomagnetite compositions, while the remaining spots from the LTNpt unit span from titanomagnetite to maghemite (cation-deficient spinel) compositions (Figure 8). The Fe-Ti oxides from Mount Milligan plot as a relatively Fe^{2+} -rich magnetite. The other crystals analyzed from samples of Mount Polley LTNpv and LTNpv units, Bridge Lake, Lac la Hache north, Copper Mountain, south of Merritt and Woodjam tend to increase the ferric iron content, falling in the titanomagnetite, magnetite and maghemite fields.

Discussion and Conclusions

The results presented above show some systematic differences among the basalts studied, on the basis of pyroxene and Fe-Ti-oxide chemistry. The EMP analyses from core to rim in clinopyroxene from the Woodjam area presents high Mg# and $\text{SiO}_2\%$, low Fe and Al cpfu values (Figures 5 and 6A) relative to those from samples collected in the other areas. This denotes a relatively homogeneous, primitive and reduced magma chamber. Some spot analyses in the core and interiors of pyroxene crystals from the Bridge Lake and Mount Polley areas are similar in composition to those at

Woodjam. However, at Bridge Lake and Mount Polley the chemistry varies from core to rim, indicating a pyroxene fractionation trend, where the cores are richer in Mg and Si and poorer in Fe, Ti and Al than the rims, which suggests a rapid change in the temperature-composition (T-X) param-

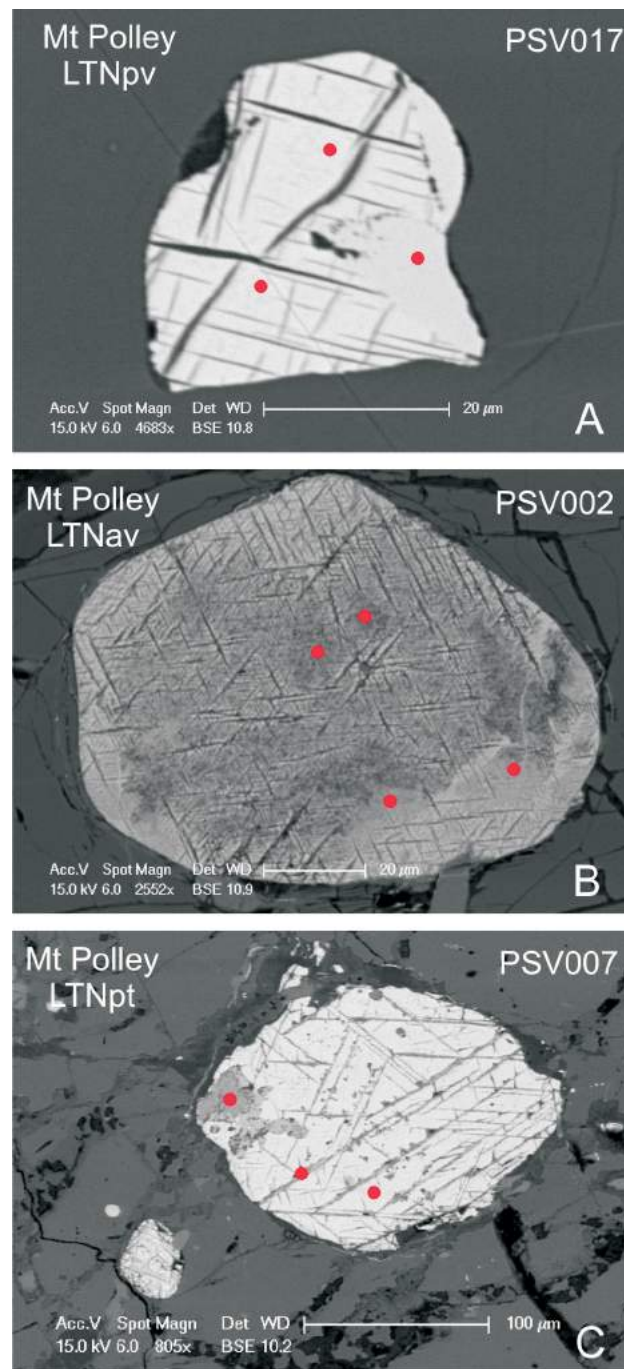


Figure 7. Representative backscattered electron images of Fe-Ti-oxide minerals; electron microprobe (EMP) analysis spots are shown in red: **A)** magnetite with lamellae of titanomagnetite, maghemite at the border of the grain (right side of the crystal); **B)** magnetite composition in the core (dark gray) and titanomagnetite composition at the border (light gray) of the crystal; **C)** Ferropseudobrookite lamellae (dark gray) within titanomagnetite grain (light gray).

eters during crystallization. Thus, the Bridge Lake sample and a few samples from Mount Polley suggest a transition from a primitive, relatively reduced and less alkaline magma, to a less primitive, relatively oxidized and more alkaline one.

The Al and Fe^{3+} contents in pyroxene are indicators of the alkalinity and the oxygen fugacity of magma (Kushiro, 1960; LeBas, 1962), respectively. Pyroxene from Copper Mountain, Bridge Lake, Lac la Hache north, LTN_{av} and LTN_{pv} units at Mount Polley and south of Merritt, is more alkaline, and crystallized at higher oxygen fugacity, than the pyroxene crystals around the Mount Milligan, unit LTN_{pt} at Mount Polley, Lac la Hache south, Prince George and Woodjam areas (Figure 6A and B). This is consistent with the findings of Mortimer (1987), where pyroxenes from his alkalic type 1 basalts plot in the diopside field and thus in the same area as most samples presented herein, whereas calcalkalic and transitional tholeiitic lavas contain augitic clinopyroxene.

Chemistry of Fe-Ti-oxide inclusions in pyroxene can be grouped into two populations. The first one corresponds to crystals relatively rich in Fe^{3+} , such as magnetite and maghemite from LTN_{pv} and LTN_{av} units at Mount Polley, Bridge Lake, Lac la Hache north, Copper Mountain, south of Merritt and Woodjam (Figure 8). The second group corresponds to grains relatively rich in Ti and Fe^{2+} , typically titanomagnetite, showing subsolidus exsolution lamellae

of ferropseudobrookite, ilmenite and ulvoespinel, denoting relatively reduced conditions of formation. Samples from unit LTN_{pt} at Mount Polley, Mount Milligan, Lac la Hache south and Prince George belong to this group (Figure 8).

The results presented above are consistent with the oxidation states inferred from the pyroxene composition, with the exception of Fe-Ti oxides at Woodjam, which are Fe^{3+} rich, potentially due to a late alteration process as indicated by secondary hematite affecting the groundmass of the rock (Table 2).

This research shows that the oxidation state predicted from Fe-Ti-oxide chemistry is not proportional to the magnetic susceptibility of the rock (Table 2). The Fe-Ti-oxide minerals have variable magnetic susceptibility values (Hunt et al., 1995; Peters and Dekkers, 2003) because the magnetic susceptibility of the rock depends on the abundance as well as type of Fe-Ti minerals.

Comparing the petrographic description of the collected samples with the chemical composition of pyroxene and Fe-Ti oxides, it can be concluded that pyroxene and pyroxene-analcime-bearing basalts of the Quesnel terrane were produced from a more oxidized magma than pyroxene-plagioclase-rich basalts.

Considering the petrography and pyroxene plus Fe-Ti-oxide geochemistry, it can be implied that basalts of Copper

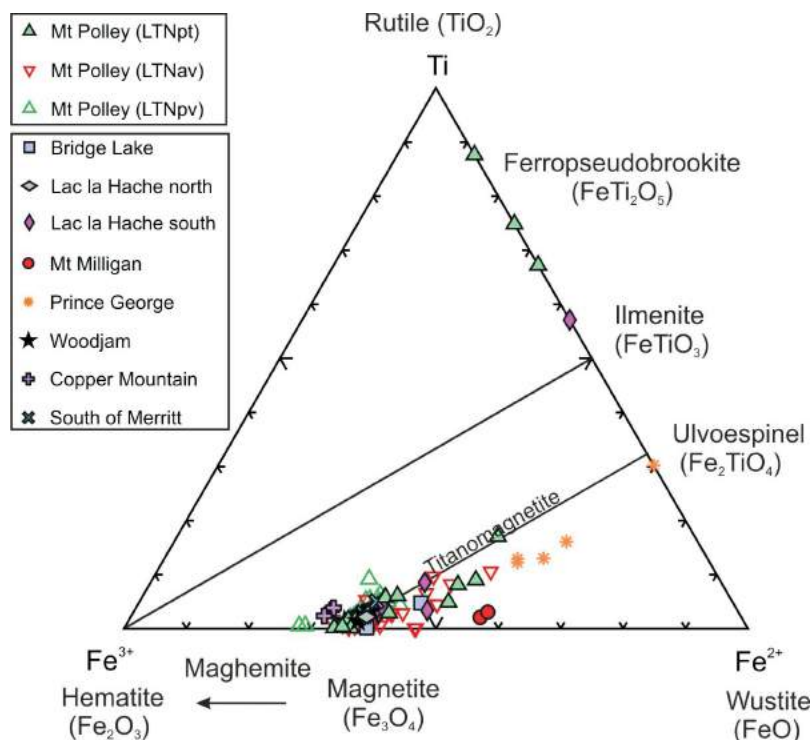


Figure 8. The Fe^{3+} -Ti- Fe^{2+} cpfu (cations per formula unit) contents of Fe-Ti-oxide minerals as inclusions in pyroxene crystals of the Nicola Group, British Columbia, plotted in FeO - Fe_2O_3 - TiO_2 space after the method of Taylor (1964).

Mountain, Lac la Hache north, units LTNav and LTNpv at Mount Polley, and south of Merritt represent similar magma-generating conditions that were likely oxidized and relatively alkaline. Such rocks are found in spatial and temporal proximity to porphyry mineralization at Mount Polley and Copper Mountain. Thus, the magmatic chambers source of the volcanic rocks around south of Merritt, and Lac la Hache north, may also have had the potential to develop comagmatic porphyry-style mineralization.

The Bridge Lake area might represent a transition between reduced and oxidized magma, while the unit LTNpt at Mount Polley, Lac la Hache south, Prince George and Woodjam may be the evidence of a reduced magma-generating environment. The sources of these lavas had probably less potential to evolve in a fertile intrusion.

This research is based on the mineral chemistry of basalt. To produce porphyry mineralization, a change in the tectonic setting that results in intrusive rather than extrusive magmatism is necessary. However, our work suggests that indications for a favourable magma-generating environment are also recorded in the precursor volcanic rocks in prospective arc segments.

Acknowledgments

Geoscience BC is thanked for the economic support to this project. The authors also acknowledge E. Czech and J. Lai for their help in the SEM-EMP laboratory during sample preparation and data acquisition. The peer review and comments provided by M. Mihalynuk helped to improve clarity of this paper.

References

Bailey, D.G. and Hodgson C, J. (1979): Transported altered wall rock in laharic breccias at the Cariboo-Bell Cu-Au porphyry deposit, British Columbia; *Economic Geology*, v. 74, p. 125–12, URL <<http://econgeol.geoscienceworld.org/cgi/reprint/74/1/125.pdf>> [November 2011].

Bissig, T., Vaca, S., Schiarizza, P. and Hart, C. (2010): Geochemical and physical variations in the Late Triassic Nicola Arc and metallogenic implications, central British Columbia (NTS 092P, 093A, N): preliminary results; *in* Geoscience BC Summary of Activities 2009, Geoscience BC, Report 2010-1, p. 49–52, URL <http://www.geosciencebc.com/i/pdf/SummaryofActivities2009/SoA2009_Bissig.pdf> [November 2011].

Blackwell, J., Lesage, G., Skinner, T., Eckfeldt, M., Hamilton, J., Hertel, J., Laird, B., Madsen, J., Rainbow, A., Sherlock, R. and Sepp, M. (2010): Woodjam property mapping 2010 interpretation, geology of the Woodjam property core area; unpublished internal report, Gold Fields Canada Exploration.

Carter, E.S., Orchard, M.J., Ross, C.A., Ross, J.R.P., Smith, P.L. and Tipper, H.W. (1991): Geology of the Cordillera Orogen in Canada, Part B, paleontological signatures of terranes; Chapter 2 *in*, H. Gabrielse and C.J. Yorath (ed.), *Geological Survey of Canada, Geology of Canada*, no. 4, p. 28–38 and

The Geology of North America; Geological Society of America, v. G-2.

Chamberlain, C.M., Jackson, M., Jago, C.P., Pass, H.E., Simpson, K.A., Cooke, D.R. and Tosdal, R.M. (2007): Toward an integrated model for alkalic porphyry copper deposits in British Columbia (NTS 093A, N; 104G); *in* Geoscience BC Summary of Activities 2006, Geoscience BC, Report 2007-1, p. 259–274, URL <<http://www.empr.gov.bc.ca/Mining/Geoscience/PublicationsCatalogue/Fieldwork/Documents/26-Chamberlain.pdf>> [November 2011].

Dawson, G.M. 1879: Preliminary report on the physical and geological features of the southern portion of the interior of British Columbia, 1877; Geological Survey of Canada, Progress Report, 1877–1878, p. 96B-101B.

Droop, G.T.R. (1987) A general equation for estimating Fe³⁺ concentrations in ferromagnesian silicates and oxides from microprobe analyses, using stoichiometric criteria; *Mineralogical Magazine*, v. 51, p 431–435.

Hunt, C.P., Moskowitz, B. M. and Banerjee, S. K. (1995): Magnetic properties of rocks and minerals; *in* Rock Physics and Phase Relations: A Handbook of Physical Constants, T.J. Ahrens (ed.), AGU Reference Shelf 3, American Geophysical Union, p. 189–204.

Kushiro, I. (1960): Si-Al relations in clinopyroxenes from igneous rocks; *American Journal of Science*, v. 258, p. 548–554.

LeBas, M.J. (1962): The role of aluminum in igneous clinopyroxenes with relation to their parentage; *American Journal of Science*, v. 260, p. 267–288.

Logan, J.M. and Bath, A.B. (2005): Geochemistry of Nicola Group basalt from the central Quesnel trough at the latitude of Mount Polley (NTS 093A/5, 6, 11, 12), central British Columbia; *in* Geological Fieldwork, BC Ministry of Energy and Mines, Paper 2006-1, p. 83–98, URL <<http://www.empr.gov.bc.ca/Mining/Geoscience/PublicationsCatalogue/Fieldwork/Documents/2005/Paper09.pdf>> [November 2011].

Logan, J.M., Bath, A., Mihalynuk, M.G. and Rees, C.J. (2007): Regional geology of the Mount Polley area, central British Columbia; BC Ministry of Energy and Mines, Geoscience Map 2007-1, scale 1:50 000, URL <http://www.em.gov.bc.ca/Mining/Geoscience/PublicationsCatalogue/Maps/GeoscienceMaps/Documents/GM2007-1_Mount_Polley.pdf> [November 2011].

Logan, J.M., Mihalynuk, M.G., Friedman, R.M. and Creaser, R.A. (2011): Age constraints of mineralization at the Brenda and Woodjam Cu-Mo±Au porphyry deposits - an Early Jurassic calcalkaline event, south-central British Columbia; *in* Geological Fieldwork 2010, BC Ministry of Energy and Mines, Paper 2011-1, p. 129–144, URL <<http://www.fjordlandex.com/Research/2010Fieldwork.pdf>> [November 2011].

Morimoto, N., Fabries, J., Ferguson, A.K., Ginzburg, I.V., Ross, M., Seifert, F.A., Zussman, J., Aoki, K. and Gottardi, G. (1988): Nomenclature of pyroxenes; *American Mineralogist*, v. 173, p. 1123–1133, URL <http://www.minso.cam.org/ammin/AM73/AM73_1123.pdf> [November 2011].

Mortensen, J.K., Ghosh, D.K. and Ferri, F. (1995): U-Pb geochronology of intrusive rocks associated with copper-gold porphyry deposits in the Canadian Cordillera; *in* Porphyry Deposits of the Northwestern Cordillera of North America, T.G. Schroeter (ed.), Canadian Institute of Mining, Metallurgy and Petroleum, Special Volume 46, p. 142–158.

- Mortimer, N. (1987): The Nicola Group: Late Triassic and Early Jurassic subduction-related volcanism in British Columbia; *Canadian Journal of Earth Sciences*, v. 24, p. 2521–2536.
- Nelson, J.L. and Bellefontaine, K.A. (1996): The geology and mineral deposits of north-central Quesnellia; Tezzeron Lake to Discovery Creek, central British Columbia; BC Ministry of Energy and Mines, Bulletin 99, 100 p, URL <http://www.empr.gov.bc.ca/Mining/Geoscience/PublicationsCatalogue/BulletinInformation/BulletinsAfter1940/Documents/Bulletin_099.pdf> [November 2011].
- Peters, C. and Dekkers, M.J. (2003): Selected room temperature magnetic parameters as a function of mineralogy, concentration and grain size; *Physics and Chemistry of the Earth*, v. 28, no. 16–19, p. 659–667.
- Pouchou, J.L. and Pichoir, F. (1985): “PAP” $\phi(\rho Z)$ procedure for improved quantitative microanalysis; *in* *Microbeam Analysis -1985*, J.T. Armstrong (ed.), San Francisco Press, p. 104–106.
- Preto, V.A. (1979): Geology of the Nicola Group between Merritt and Princeton; BC Ministry of Energy and Mines, Bulletin 69, 90 p., URL <http://www.em.gov.bc.ca/Mining/Geoscience/PublicationsCatalogue/BulletinInformation/BulletinsAfter1940/Documents/Bulletin_069.pdf> [November 2011].
- Schiarizza, P., Bligh, J., Bluemel, B. and Tait, D. (2008): Geology of the Timothy Lake Area (NTS 092P/14); BC Ministry of Energy and Mines, Open File, 2008-5, 1:50 000 scale, URL <<http://www.empr.gov.bc.ca/Mining/Geoscience/PublicationsCatalogue/OpenFiles/2008/Pages/2008-5.aspx>> [November 2011].
- Seedorff, E., Dilles, J.H., Proffett, J.M., Jr., Einaudi, M.T., Zurcher, L., Stavast, W.J.A., Johnson, D. and Barton, M.D. (2005): Porphyry deposits: characteristics and origin of hypogene features; *Economic Geology*, 100th Anniversary Volume, p. 251–298.
- Taylor, R. W. (1964): Phase equilibria in the system FeO-Fe₂O₃-TiO₂ at 1300°C; *American Mineralogist*, v. 49, no. 7–8, p. 1016–1030.
- Vaca, S., Bissig, T., Mitchinson, D.F., Barker, S. and Hart, C.J.R. (2011): Variability in the basaltic rocks hosting Cu-Au porphyry mineralization in the Quesnel terrane, south-central British Columbia (NTS 092, 093): geochemistry, stable isotopes and physical properties; *in* *Geoscience BC Summary of Activities 2010*, Geoscience BC, Report 2011-1, p. 123–132, URL <http://www.geosciencebc.com/i/pdf/SummaryofActivities2010/SoA2010_Vaca_et_al.pdf> [November 2011].

Geological Mapping, Regional Data Compilation and Mineral Evaluation of the Burrell Creek Map Area, Southeastern British Columbia (NTS 082E/09)

T. Höy, consultant, Sooke, BC, thoy@shaw.ca

W. Jackaman, Noble Exploration Services Ltd., Sooke, BC

Höy, T. and Jackaman, W. (2012): Geological mapping, regional data compilation and mineral evaluation of the Burrell Creek map area, southeastern British Columbia (NTS 082E/09); in Geoscience BC Summary of Activities 2011, Geoscience BC, Report 2012-1, p. 79–80.

Project Summary

The Burrell Creek project involves geological mapping and compilation of a large part of the area covered by the 1:50 000 scale Burrell Creek map sheet (NTS 082E/09), located in the Columbia Mountains of southeastern British Columbia (Figure 1). The project is a northward extension of the Deer Park mapping project completed in 2009 (Höy, 2010; Höy and Jackaman, 2010), which focused on the potential for Tertiary mineralization within the southern Monashee Mountains along the northern margins of the Grand Forks gneiss complex (Preto, 1970; Höy and Jackaman, 2005), and recognized and defined a variety of base-metal and precious-metal mineral deposits seemingly related to prominent north- and northwest-trending regional structures. The Burrell Creek project will extend this work into an area that has attracted considerable historical exploration, due in large part to development of the Franklin mining camp (Drysdale, 1915; Keep and Russell, 1989), but that has seen little university- or government-led research since a regional (1:250 000 scale) mapping project by Little in the 1950s (Little, 1957) and a regional (1:250 000 scale) compilation map done in the late 1980s (Tempelman-Kluit, 1989).

The Burrell Creek map sheet is located along the eastern edge of the Pentiction map sheet (NTS 082E), 60 km northwest of the Rosslund Gold mining camp and approximately 50 km northeast of the Greenwood camp. The Franklin mining camp in the southern part of the Burrell Creek map sheet includes numerous deposits and past producers related to an alkalic, mafic to ultramafic complex. Styles of mineralization include platinum-palladium-copper mineralization, contact-metamorphic skarns and precious- and base-metal quartz veins. A few other mineral occurrences, of largely unknown character and age, are scattered throughout the rest of the map area. Recent exploration ac-

tivity, largely concentrated in the immediate vicinity of the Franklin mining camp and in the Deer Park map area immediately to the south, and the results of the Geoscience BC 2009 mapping project have highlighted the Tertiary mineral potential in the southern Columbia Mountains.

The Burrell Creek project will include approximately 40 days of geological mapping, which will concentrate on areas of higher mineral potential or mineral occurrences as well as on the evaluation and upgrading of the mineral occurrence database (MINFILE; BC Geological Survey, 2011). It will also include compilation in digital format of all regional geological, geophysical and geochemical data collected under the National Geochemical Reconnaissance (NGR) Program and the BC Regional Geochemical Survey (RGS) Program, which information will be combined with mineral occurrence and geology databases to produce several 1:20 000 and 1:50 000 scale geological maps suitable for directing and focusing mineral exploration. An important focus of the project is mapping and evaluation of Tertiary intrusive activity and faulting and their relationships to mineralization. Höy and Jackaman (2010) have shown that several styles of mineralization in the adjacent Deer Park map area, including base- and precious-metal veins and porphyry molybdenite, are in part controlled by Tertiary extensional tectonics; these models will be further developed and evaluated in the Burrell Creek map area, again with the goal of defining exploration targets and regional controls to mineralizing trends.

Geological mapping of the southern part of the Burrell Creek map area began in late 2011 and will be completed during the 2012 field season. Data, including integrated geological maps, poster displays and articles for the *Geoscience BC Summary of Activities* series, will be released on completion of the project in the winter of 2012–2013.

Keywords: *geology, regional compilations, Grand Forks gneiss complex, Tertiary extensional faulting, mineral deposit evaluation, Franklin mining camp*

This publication is also available, free of charge, as colour digital files in Adobe Acrobat® PDF format from the Geoscience BC website: <http://www.geosciencebc.com/s/DataReleases.asp>.

References

BC Geological Survey (2011): MINFILE BC mineral deposits database; BC Ministry of Energy and Mines, URL <<http://www.empr.gov.bc.ca/Mining/Geoscience/MINFILE/Pages/default.aspx>> [October 2011].

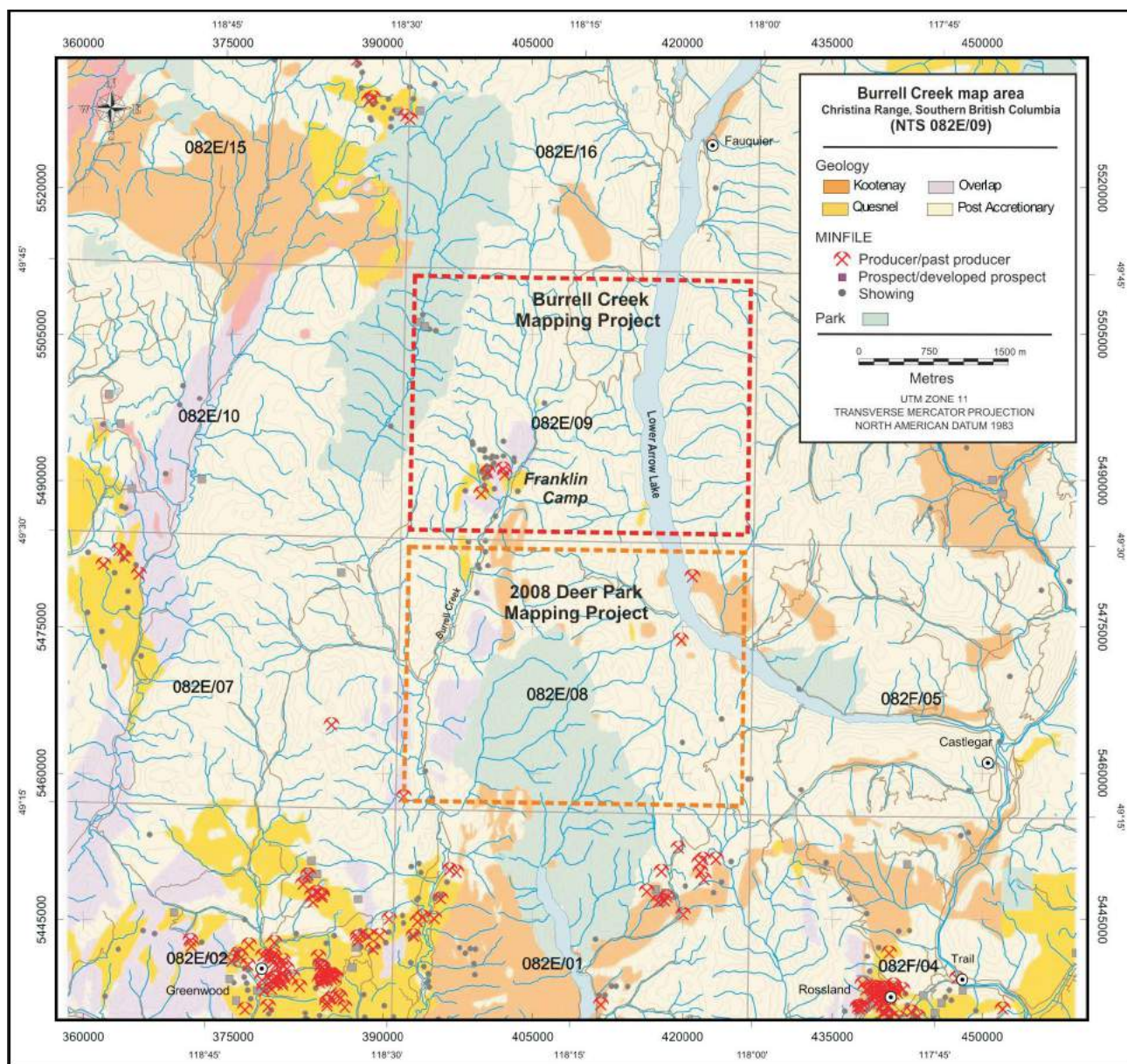


Figure 1. Location of Burrell Creek map area, southeastern British Columbia.

Drysdale, C.W. (1915): Geology of Franklin Mining Camp, British Columbia; Geological Survey of Canada, Memoir no. 56, 246 p.

Höy, T. (2010): Geology of the Deer Park map area, southeastern British Columbia (NTS 082E/08); in Geoscience BC Summary of Activities 2009, Geoscience BC, Report 2010-1, p. 127–140.

Höy, T. and Jackaman, W. (2005): Geology of the Grand Forks map sheet; BC Ministry of Energy and Mines, Geoscience Map 2005-2, scale 1:50 000.

Höy, T. and Jackaman, W. (2010): Geology of the Deer Park map sheet (NTS 82E/08); Geoscience BC Report 2010-7-1, scale 1:50 000.

Keep, M. and Russell, J.K. (1989): The geology of the Averill plutonic complex, Grand Forks, British Columbia (82E/9W); in Geological Fieldwork 1988, BC Ministry of Energy and Mines, Paper 1989-1, p. 27–31.

Little, H.W. (1957): Kettle River, British Columbia; Geological Survey of Canada, Map 6-1957.

Preto, V.A. (1970): Structure and petrology of the Grand Forks Group, BC; Geological Survey of Canada, Paper 69-22, 80 p.

Tempelman-Kluit, D. J. (1989): Geology, Penticton, British Columbia; Geological Survey of Canada, Map 1736A.

Hydrological Modelling and Decision-Support Tool Development for Water Allocation, Northeastern British Columbia

A. Chapman, BC Oil and Gas Commission, Victoria, BC, Allan.Chapman@BCOGC.ca

B. Kerr, Foundry Spatial Ltd., Victoria, BC

D. Wilford, BC Ministry of Forests, Lands and Natural Resource Operations, Smithers, BC

Chapman, A., Kerr, B. and Wilford, D. (2012): Hydrological modelling and decision-support tool development for water allocation, north-eastern British Columbia; in Geoscience BC Summary of Activities 2011, Geoscience BC, Report 2012-1, p. 81–86.

Introduction

In northeastern British Columbia, unconventional gas development requires large quantities of water, with the largest volumes of water used for hydraulic fracturing for well stimulation and completion. The management of water for industrial uses is the responsibility of the BC Oil and Gas Commission (OGC), through short-term water use approvals, and the BC Ministry of Forests, Lands and Natural Resource Operations (FLNRO), through long-term water licenses. For much of northeastern BC, there is a dearth of hydrometric measurements to directly support decision-making under the Water Act. As a result, there is a strong need for hydrological modelling to provide quantified estimates of monthly, seasonal and annual runoff thus allowing estimations of water availability for water use approvals. A hydrological modelling pilot project (Chapman and Kerr, 2011), utilizing available gridded climate data and land cover/vegetation data, and encompassing the Horn River Basin and Liard Basin gas play areas, concluded that there is utility in pursuing a monthly water balance modelling approach. Following the pilot project, the OGC, in partnership with Geoscience BC and FLNRO, is now extending and fine-tuning the hydrological modelling to all of northeastern BC. This paper summarizes the current status of the modelling project as of November 2011. The project is anticipated to be completed in early 2012.

Objectives

The project will complete overview hydrological modelling for northeastern BC, and will produce a decision-support tool (in Arc Server format) to be used by the OGC and FLNRO for water use approvals and water licenses under the Water Act. The modelling information and decision-support tool will be available to industry, First Nations and others, and will be valuable in helping communicate and

understand the water resources of northeastern BC. The model will provide estimates of monthly and annual natural runoff, and will provide guidance on hydrological thresholds necessary for the maintenance of environmental flows.

Study Area

This study within northeastern BC includes the unconventional gas play areas of the Montney Trend, Liard Basin, Horn River Basin and the Cordova Embayment, from south of Dawson Creek to the Yukon and Northwest Territories boundaries in the north, and east of the Rocky Mountains to the Alberta border (Figure 1). Adjacent areas of Alberta, the Yukon and NWT have been incorporated to facilitate the hydrological modelling in BC. The total area in BC under study is approximately 175 500 km². The climate varies from cold continental in the south to cold subarctic in the north, characterized by sustained cold winters and warm summers. Average monthly temperatures for November to March are below freezing. There are few climate stations with long-term records, however, Fort Nelson has a measured 30-year Normal precipitation of 451 mm, while Fort St. John has a Normal precipitation of 465 mm. Precipitation amounts increase to the west of the study area, in the higher elevation terrain of the Rocky Mountain foothills.

The streamflow regime is typically nival (snowmelt dominated), with a sustained cold winter period characterized by low rates of streamflow and competent river ice. This is followed by a spring freshet from approximately mid-April to late June, characterized by high rates of streamflow as the winter's accumulated snow melts. After the spring freshet period, river levels generally recede slowly through the summer and autumn until the winter freeze-up. Frontal or convective storm systems bring varying amounts of rain from late spring to autumn, often resulting in increases in river levels and discharge, and occasionally producing flooding. The timing of the annual peak flow usually coincides with the timing of the annual freshet snowmelt runoff, except for small river basins, which, on occasion, can experience their largest peak flows from summer frontal or convective rain storms.

Keywords: hydrological modelling, hydrology, water allocation, northeastern British Columbia

This publication is also available, free of charge, as colour digital files in Adobe Acrobat® PDF format from the Geoscience BC website: <http://www.geosciencebc.com/s/DataReleases.asp>.

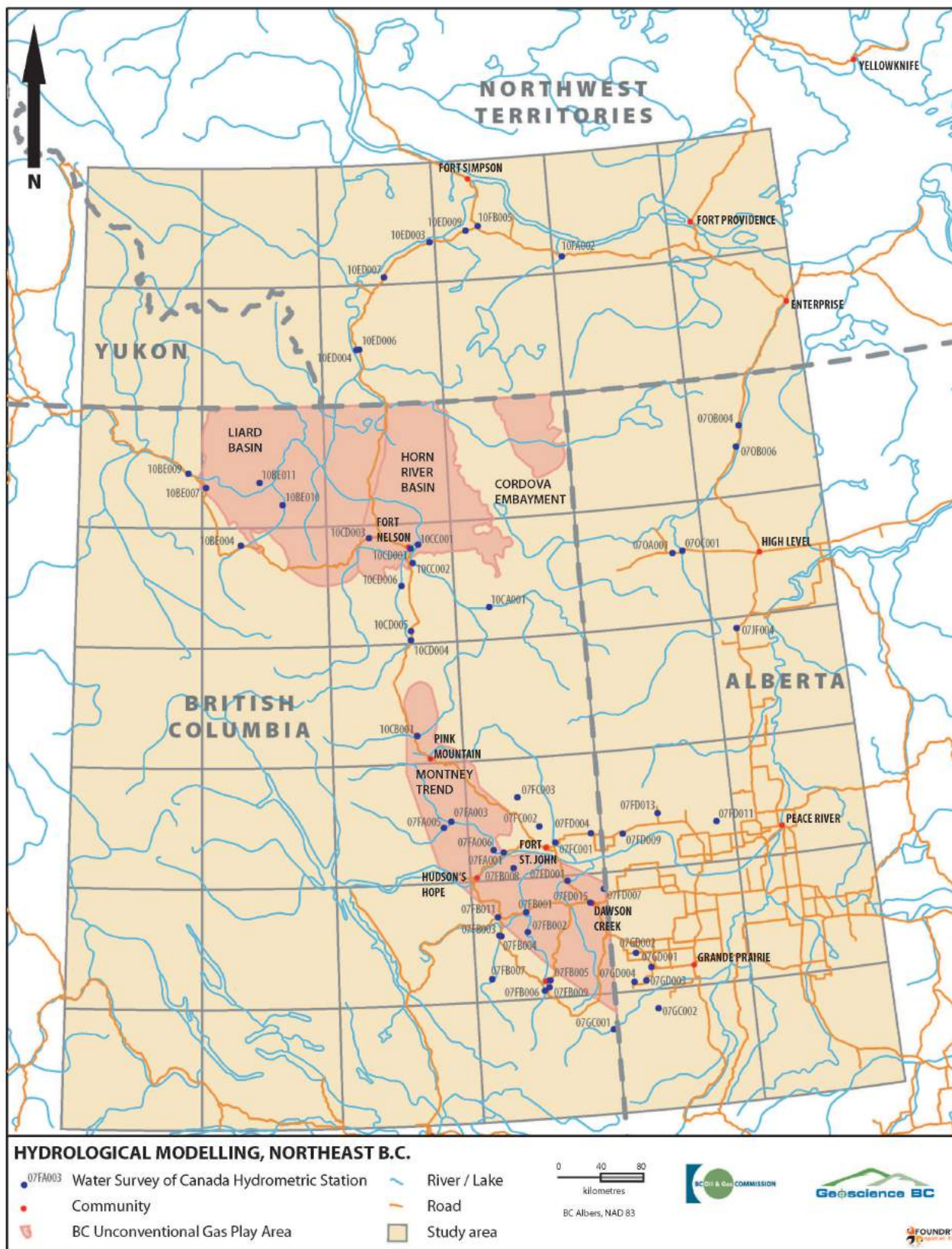


Figure 1. Modelling study area in northeastern British Columbia, showing natural gas play areas and hydrometric stations used in the model calibration.

Data

The water balance model takes a conservation of mass approach and follows on a concept originally applied by other researchers (Solomon, 1968; Moore et al., in press). Key inputs to the application for northeastern BC are

- monthly and annual precipitation and temperature grids from the ClimateWNA program (Wang et al., in press), which are derived from the PRISM methodology (Daly et al., 2008),
- gridded evapotranspiration data produced by the Consultative Group on International Agricultural Research (CGIAR),
- land cover and vegetation mapping from Natural Resources Canada and the Province of British Columbia, and
- hydrometric data from the Water Survey of Canada (WSC).

An interim product resulting from the model development is a gridded dataset representing actual evapotranspiration (AET), incorporating both climate and vegetative controls.

Actual evapotranspiration data produced by CGIAR accounts for water availability using a modified Hargreaves approach and takes climate inputs from the WorldClim database, a 1 km gridded climate surface representing the time period 1950–2000 (Hijmans et al., 2005; Trabucco and Zomer, 2010). Within the CGIAR data, evapotranspiration is adjusted according to soil moisture content factors and assumes agronomic land cover. The authors have transformed this estimate of evapotranspiration by incorporating a vegetation factor for northeastern BC. For this procedure, a vector coverage of vegetation and land cover was converted to raster values numerically equivalent to the ratio of the actual evapotranspiration for the land cover or vegetation type to that of the estimated agronomic evapotranspiration rate in the region. The evapotranspiration values used for each land-cover type were determined from several sources (Chapman, 1988; Spittlehouse, 1989; Liu et al., 2001; Barr et al., 2007) and were adjusted within the model.

Model Calibration

Estimates of monthly and annual runoff, the ultimate end product of the modelling component of the project, were not produced by running a defined routine through a piece of software. Instead, routines and components of other modelling projects (Solomon et al., 1968; Hock, 2003; McCabe and Markstron, 2007; Moore et al., in press) were evaluated, tested and incorporated by closely monitoring regional data inputs and results. These were evaluated against prior knowledge of the study region, using the simple continuity equation: $Q = P - ET$, where Q = annual runoff (mm), P = annual precipitation (mm) and ET = annual evapotranspiration (mm). Exploratory spatial data analysis

was a large component of this work, and as such, the end result will be a product that represents the hydrology of northeastern BC as effectively as possible given available data.

The results of the annual runoff modelling were calibrated against hydrometric data collected by the WSC. Fifty-three hydrometric stations were selected for calibration (Table 1). Not included were gauges on very large drainages (Peace River, Liard River), lake outlet stations or stations on drainages with man-made controls. The size of drainage area ranges from 38 to over 43 200 km². The stations are located in BC, western Alberta and the southern Northwest Territories and in several cases the watersheds cross provincial/territorial borders. Although the objective of this work was only to create estimates for ungauged drainages in BC, these transborder stations and stations wholly located in adjacent jurisdictions provided critical representation of portions of BC that are ungauged.

A GIS was used to generate statistics for each watershed used in the calibration through a simple overlay operation. Once precipitation and climate-adjusted evapotranspiration for each of the gauged watersheds were calculated, these values were collated into a spreadsheet for further analysis and incorporation of the vegetation component of evapotranspiration. The percentage of each type of vegetative cover was determined for each watershed through a GIS overlay and added to the calculation.

Significant variability, as well as error, exists in the natural processes represented by all components of the model and also in the hydrometric data to which model results are compared. Preliminary results for the annual runoff modelling indicate a mean error of 5.5%, with 75% of the calibration basins having estimates within $\pm 20\%$ of the measured mean annual runoff. Unlike Moore et al. (in press) who used a water balance modelling approach to estimate monthly runoff, the authors used a statistical model based on a multivariate regression technique to distribute the modelled annual runoff to individual months over the year. Monthly runoff (as a percentage of annual runoff) is estimated as a function of grid cell elevation, UTM northing, UTM easting, monthly mean temperature and monthly mean precipitation. Adjusted R² values range from 0.50 to 0.76, with the lowest values for July, August and September, and the highest values for October to June. In general, the monthly runoff modelling is quite good, with hydrograph fits that are visually accurate (Figure 2), and with reasonable statistics (median Nash-Sutcliffe efficiency = 0.94, with 65% of the calibration basins having Nash-Sutcliffe efficiency statistics of >0.90).

Summary

The hydrology modelling approach outlined in this paper is yielding consistent and reliable estimates of annual and

Table 1. Water Survey of Canada hydrometric stations used for model calibration.

Watershed	Name	Drainage area (km²)	Years of record	Annual mean runoff measured (mm)
07FA001	Halfway River near Farrell Creek (lower station)	9351	23	256
07FA003	Halfway River above Graham River	3764	19	298
07FA005	Graham River above Colt Creek	2139	26	388
07FA006	Halfway River near Farrell Creek	9296	25	253
07FB001	Pine River at East Pine	11906	48	503
07FB002	Murray River near the mouth	5558	32	474
07FB003	Sukunka River near the mouth	2591	32	667
07FB004	Dickebusch Creek near the mouth	85	31	220
07FB005	Quality Creek near the mouth	38	24	165
07FB006	Murray River above Wolverine River	2383	32	756
07FB007	Sukunka River above Chamberlain Creek	928	9	818
07FB008	Moberly River near Fort St. John	1522	29	239
07FB009	Flatbed Creek at kilometre 110 Heritage Highway	479	27	270
07FC001	Beaton River near Fort St. John	16059	48	106
07FC002	St. John Creek near Montney	212	13	87
07FC003	Blueberry River below Aitken Creek	1775	45	95
07FD001	Kiskatinaw River near Farmington	3601	54	91
07FD004	Alces River at 22nd Base Line	313	25	59
07FD007	Pouce Coupe River below Henderson Creek	2856	36	73
07FD009	Clear River near Bear Canyon	2876	39	56
07FD011	Hines Creek above Gerry Lake	373	36	42
07FD013	Eureka River near Worsley	755	35	32
07GC002	Pinto Creek near Grande Prairie	494	24	106
07GD001	Beaverlodge River near Beaverlodge	1621	42	46
07GD002	Beavertail Creek near Hythe	678	27	40
07GD003	Redwillow River near Beaverlodge	1605	11	94
07GD004	Redwillow River near Rio Grande	1240	17	142
07JF004	Boyer River near Paddle Prairie	140	29	19
07OA001	Sousa Creek near High Level	820	40	62
07OB004	Steen River near Steen River	2598	36	73
07OB006	Lutose Creek near Steen River	292	33	68
07OC001	Chinchaga River near High Level	10370	41	89
10BE004	Toad River above Nonda Creek	2549	48	537
10BE007	Trout River at kilometre 783.7 Alaska Highway	1191	39	434
10BE009	Teeter Creek near the mouth	210	30	177
10BE010	Toad River near the mouth	6890	13	490
10BE011	Grayling River near the mouth	1760	13	297
10CA001	Fontas River near the mouth	7439	17	132
10CB001	Sikanni Chief River near Fort Nelson	2181	65	374
10CC001	Fort Nelson River at Fort Nelson	43200	19	244
10CC002	Fort Nelson River above Muskwa River	22560	27	193
10CD001	Muskwa River near Fort Nelson	20250	65	332
10CD003	Raspberry Creek near the mouth	275	30	135
10CD004	Bougie Creek at kilometre 368 Alaska Highway	334	28	251
10CD005	Adsett Creek at kilometre 386.0 Alaska Highway	109	26	252
10CD006	Prophet River above Cheves Creek	7277	8	324
10ED003	Birch River at Highway No. 7	563	36	156
10ED004	Rabbit Creek below Highway No. 7	122	6	161
10ED006	Rabbit Creek at Highway No. 7	110	7	162
10ED007	Blackstone River at Highway No. 7	1381	19	243
10ED009	Scotty Creek at Highway No. 7	137	15	159
10FA002	Trout River at Highway No. 1	9111	41	141
10FB005	Jean-Marie River at Highway No. 1	1351	38	122

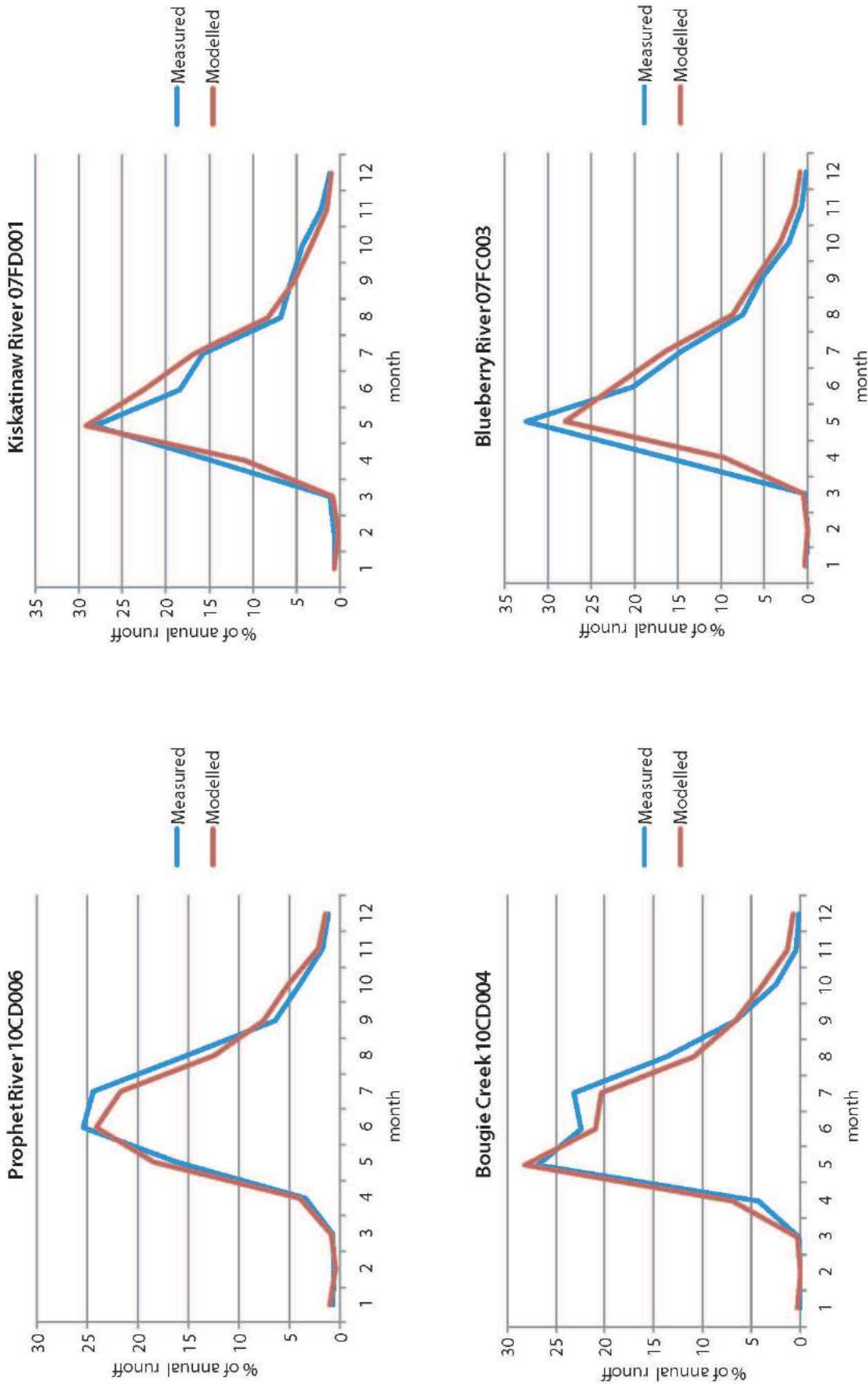


Figure 2. Examples of monthly hydrographs for four river basins in northeastern British Columbia.

monthly runoff for rivers in northeastern BC. At the time this paper was prepared, the modelling was not complete, and further enhancements are being tested. It is anticipated that the modelling will be completed by the end of 2011, with the development of a decision-support tool in early 2012.

Acknowledgments

This project was funded by Geoscience BC, the BC Ministry of Forests, Lands and Natural Resource Operations and the BC Oil and Gas Commission. The authors offer thanks to C.D. Anglin, N. Crisp and H. Madill for their support.

References

- Barr, A.G., Black, T.A., Hogg, E.G., Griffis, T.J., Morgenstern, K., Kljun, N., Theede, A. and Nestic, Z. (2007): Climatic controls on the carbon and water balances of a boreal aspen forest, 1994–2003; *Global Climate Biology*, v. 13, p. 561–576.
- Chapman, A.R. (1988): Some hydrological and hydrochemical characteristics of boreal forest watersheds in the subarctic of west-central Canada; M.Sc. thesis, Trent University, 234 p.
- Chapman, A. and Kerr, B. (2011): Development of a hydrology decision support tool; Unconventional Gas Technical Forum, Victoria, April 7, 2011, (slide presentation), URL <<http://www.empr.gov.bc.ca/OG/oilandgas/petroleumgeology/UnconventionalGas/Documents/2011Documents/A%20Chapman.pdf>> [November 2011].
- Daly, C., Halbleib, M., Smith, J.I., Gibson, W.P., Doggett, M.K., Taylor, G.H., Curtis, J. and Pasteris, P.P. (2008): Physiographically sensitive mapping of climatological temperature and precipitation across the conterminous United States; *International Journal of Climatology*, v. 28, p. 2031–2064.
- Hijmans, R.J., Cameron, S.E., Parra, J.L., Jones, P.G. and Jarvis, A. (2005): Very high resolution interpolated climate surfaces for global land areas; *International Journal of Climatology*, v. 25, p. 1965–1978.
- Hock, R. (2003): Temperature index melt modeling in mountain areas; *Journal of Hydrology*, v. 182, p. 104–115.
- Liu, J., Chen, J.M. and Cihlar, J. (2003): Mapping evapotranspiration based on remote sensing: an application to Canada's landmass; *Water Resources Research*, v. 39, p. 1189–1200.
- McCabe, G.J. and Markstron, S.L. (2007): A monthly water balance model driven by a graphical user interface; United States Geological Survey, Open-File Report 2007-1088, 6 p.
- Moore, R.D., Trubilowicz, J. and Buttle, J. (in press): Prediction of streamflow regime and annual runoff for ungauged basins using a distributed water balance model; *Journal of the American Water Resources Association*.
- Solomon, S.I., Denouvilliez, J.P., Chart, E.J., Wooley, J.A. and Cadou, C. (1968): The use of a square grid system for computer estimation of precipitation, temperature and runoff; *Water Resources Research*, v. 4, p. 919–929.
- Spittlehouse, D.L. (1989): Estimating evapotranspiration from land surfaces in British Columbia; *in* Estimation of Aerial Evapotranspiration, International Association of Hydrological Sciences, Publication no. 177, p. 245–253.
- Trabucco, A. and Zomer, R.J. (2010): Global high-resolution soil-water balance geospatial database; Consultative Group on International Agricultural Research – Consortium for Spatial Information, URL <<http://www.cgiar-csi.org/component/k2/item/60-global-high-resolution-soil-water-balance>> [November 2011].
- Wang, T., Hamann, A., Spittlehouse, D. and Murdock, T. (in press): ClimateWNA - high-resolution spatial climate data for western North America; *Journal of Applied Meteorology and Climatology*.

Geological Controls on Matrix Permeability of the Doig-Montney Hybrid Shale-Gas-Tight-Gas Reservoir, Northeastern British Columbia (NTS 093P)

G.R.L. Chalmers, University of British Columbia, Vancouver, BC, gchalmer@eos.ubc.ca

R.M. Bustin, University of British Columbia, Vancouver, BC

A.A.M. Bustin, University of British Columbia, Vancouver, BC

Chalmers, G.R.L., Bustin, R.M. and Bustin, A.A.M. (2012): Geological controls on matrix permeability of the Doig-Montney hybrid shale-gas-tight-gas reservoir, northeastern British Columbia (NTS 093P); in Geoscience BC Summary of Activities 2011, Geoscience BC, Report 2012-1, p. 87–96.

Introduction

Exploration and development of the hybrid shale-gas-tight-gas play of the Lower Triassic Montney Formation in northeastern British Columbia in recent years has led to attention being focused on the overlying Doig Formation, with the objective to coproduce the Doig and Montney plays. The Doig Formation has proven production from the Doig sandstone tight-gas play within the Groundbirch-field area (Walsh et al., 2006) and, currently, positive tests are reported from the Doig phosphate zone shale-gas play (Proust, 2010). The majority of production is associated with the middle Doig Formation and, to a lesser extent, with the upper Doig Formation within the Groundbirch area (D. Ross, personal communication). As very large gas-in-place estimates are common for shale-gas plays (i.e., 250 tcf for the Montney Formation; Adams, 2010), a better understanding of the geological controls on matrix permeability is needed. Fluid flow and the production rates of a shale-gas play are influenced by the matrix permeability of the reservoir and the length of the flow path, and hence, by the size of matrix blocks. Sedimentology has a large impact on the mineralogy, total organic carbon (TOC) content, fabric and texture of shale. The combination of these characteristics governs the pore-size distribution and the matrix permeability of the reservoir, which directly affects the productivity of the shale-gas play and development strategies.

As part of this study to quantify and interpret the reservoir characteristics of gas-shale units in northeastern BC, a detailed study of the Montney–Doig interval in the productive Groundbirch area, south of Fort St. John, will be conducted. This preliminary report describes the results of

Keywords: pulse-decay permeability, mineralogy, total organic carbon content, porosity and pore-size distribution

This publication is also available, free of charge, as colour digital files in Adobe Acrobat® PDF format from the Geoscience BC website: <http://www.geosciencebc.com/s/DataReleases.asp>.

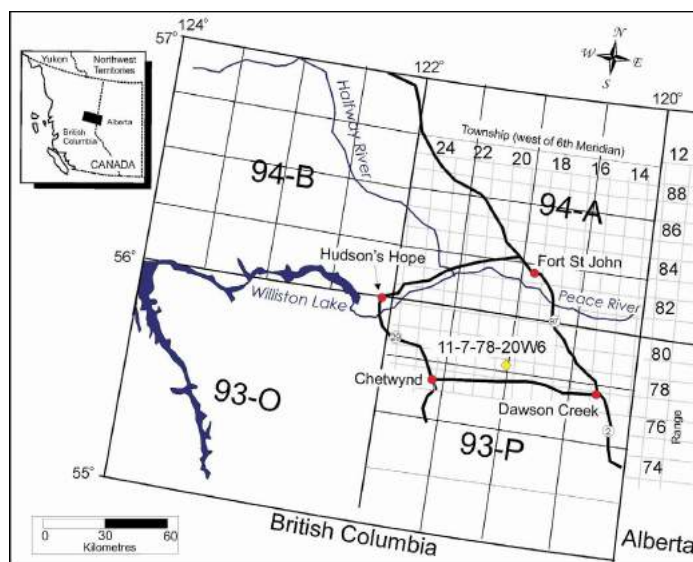


Figure 1. Index map showing the location of the 11-7-78-20W6 well sampled for this project (yellow diamond) and area cities and towns (red circles).

high-resolution stratigraphic analyses of the mineralogy and pore system of strata in the 11-7-78-20W6 well (Figure 1). The objectives of this study are to

- determine the influence sedimentology has on the TOC-content distribution, the mineralogy, the porosity and the pore-size distribution;
- resolve the influence mineralogy has on the porosity and the pore-size distribution; and
- identify the controls on matrix permeability.

Geological Background

The Daiber Group within the Peace River plains area of northeastern BC consists of the Lower Triassic Montney and the Middle Triassic Doig formations (Figure 2). The Montney and Doig formations were deposited along a passive continental margin and consist of a westward-thickening, siliciclastic, prograding wedge (Edwards et al., 1994; Davies, 1997; Walsh et al., 2006; Dixon, 2009a, b); they represent the first and second of three transgressive-regres-

sive (T-R) cycles, respectively, that deposited the Triassic strata in northeastern BC (Edwards et al., 1994). The depositional setting for the Montney and Doig formations is described as an open-shelf marine environment (Edwards et al., 1994). Paleogeographic reconstruction for Triassic sedimentation interprets a paleoshoreline that prograded during sea-level regressions to just east of Fort St. John and the BC-Alberta border (Kent, 1994). Throughout that period, shallow shelf mud covered the study area and deeper marine mud was deposited to the west of the study area.

In this study, the Montney and Doig formations are subdivided into units A to D (Figure 2) to simplify descriptions and comparison. The Montney Formation consists of variable amounts of interbedded shale, siltstone and sandstone. Dixon (2000) subdivided the Montney Formation within BC into the lower siltstone-sandstone and the upper shale members based on lithostratigraphy. The two members are separated by a basin-wide unconformity resulting from tectonic uplift of the basin margin (Dixon, 2009b) and are interpreted as the result of two higher-order T-R couplets (Uttings et al., 2005). The upper shale member of the Montney Formation (unit A in this study) is absent within Alberta and progressively becomes thicker (up to 159 m) to the west, towards the foothills of BC (Dixon, 2000).

Overlying the Montney Formation is the second T-R cycle, which deposited the Doig (units B to D of this study), Halfway (unit E) and Charlie Lake formations (Figure 2). The

Doig Formation is informally subdivided by Davies (1997) into three distinct lithological units: the lowermost phosphate zone (unit B); middle siltstone (unit C); and the upper regressive, coarsening-upward sequence (unit D). Thickness of the Doig Formation varies from 790 m, southwest of Fort St. John, to 80 m, toward the northeast, at the BC-Alberta border. Unit B is a highly radioactive unit, which consists of phosphatic nodules and granules within argillaceous siltstone, interbedded with calcareous siltstone and dark-grey shale (Riediger et al., 1990). The Doig Formation was deposited in a distal- to mid-shelf setting during a marine transgression. The middle Doig (unit C) is a medium to dark-grey argillaceous siltstone and shale unit deposited in a distal-shelf setting, which locally contains a shoreface sandstone up to 25 m thick (Evoy, 1998). This sandstone unit, interpreted as deltaic to shoreface sandstone, is part of the highstand-systems tract that deposited unit C (Harris and Bustin, 2000); highstand-systems tracts contain aggradational to progradational parasequence sets, which are bounded by a downlap surface and a sequence boundary. Unit D contains siltstone and fine sandstone, and the boundary with the overlying unit E lies between a mudrier Doig sandstone and an overlying cleaner Halfway sandstone (Figure 2; Evoy, 1998). Unit D is interpreted as having been deposited in a proximal-shelf to lower-shoreface environment. The Doig Formation is overlain by the prograding beach-barrier sandstone of unit E (Figure 2).

Methods

To evaluate the reservoir characteristics of the Montney and Doig formations, sidewall cores and core plugs were collected from the 11-7-78-20W6 well. Samples were analyzed to determine the TOC content, T_{max} , organic geochemistry, mineralogy, porosity, pore-size distribution (PSD) and permeability. The TOC content, organic geochemistry and T_{max} values were collected using a Rock Eval™ II apparatus with a TOC module.

A normal-focus cobalt X-ray tube was used on a Siemens D5000 diffractometer generated at 40 kV and 40 mA for X-ray diffraction analysis. Crushed samples (<250 µm) were mixed with ethanol, hand-ground in a mortar and pestle and smear-mounted on glass slides. The mineral composition was quantified by Rietveld analysis (Rietveld, 1967) using Bruker AXS TOPAS V3.0 software.

Porosity was calculated from the bulk density and the skeletal density. Mercury immersion determined the bulk density of a sample. Skeletal density was obtained by helium pycnometry on oven-dried samples (i.e., $S_w = 0$) with a grain size between 0.841 mm (sieve size of 20 mesh) and 0.595 mm (sieve size of 30 mesh). Pore-size distribution, pore area and porosity were measured by a Micromeritics AutoPore porosimeter on crushed samples (sieve size of

		This Study		
Jurassic		Fernie Fm		
Triassic	Upper	Pardonet Fm		
		Baldonnel Fm		
		Charlie Lake Fm		
		Halfway Fm	Unit E	
		Doig Fm	Unit C & D	
	Middle	Phosphate Zone	Unit B	
		Montney Fm	Unit A	
	Lower			
	Permian		Belloy Fm	

Figure 2. Stratigraphic columns for the Triassic strata within the Peace River plains area of northeastern British Columbia and the five units referred to within this study (modified from Davies, 1997). Abbreviations: Fm., Formation; Gp., Group.

20–30 mesh). To measure the pore-size distribution, cylindrical pore geometry is assumed and the pore radius is calculated from the applied pressure using the Washburn equation (Washburn, 1921). The porosimetry-derived porosity is the ratio between the total intrusion volume of the sample and the bulk volume of the sample. As a requirement of the analytical procedure of degassing and evacuating samples prior to analysis, the latter were oven dried at 110°C, which results in the water saturation being zero ($S_w = 0$). The pore-size detection limit of this analysis is 3 nm (approximate boundary between mesopore and micropore¹), with the pore size being calculated from the Washburn equation. Therefore the porosimetry-derived porosity results do not consider water saturation or the microporosity of the sample.

Permeability was determined by a pulse-decay permeameter using helium on core plugs and sidewall cores 2.5 cm in diameter and length. Permeability was measured with an

effective stress of 22.8 MPa (3300 psi, in situ reservoir pressure).

Results

Mineralogy

The Doig and Montney formations are dominated by carbonate (calcite and dolomite), quartz and feldspar (albite and microcline) with minor quantities of illite, pyrite and apatite (Figure 3; Bustin et al., 2011, Figure 6), although illite content can be locally important. In the case of well 11-7-78-20W6, the quartz content ranges between 13 and 74%, with an average of 31%, and increases from unit B to the base of unit E (Figure 3). Carbonate content averages 23% and ranges between 2 and 51%, whereas that of dolo-

¹ Micropores (<2 nm), mesopores (2–50 nm) and macropores (>50 nm) are defined by the physical gas-adsorption characteristics of microporous and mesoporous media.

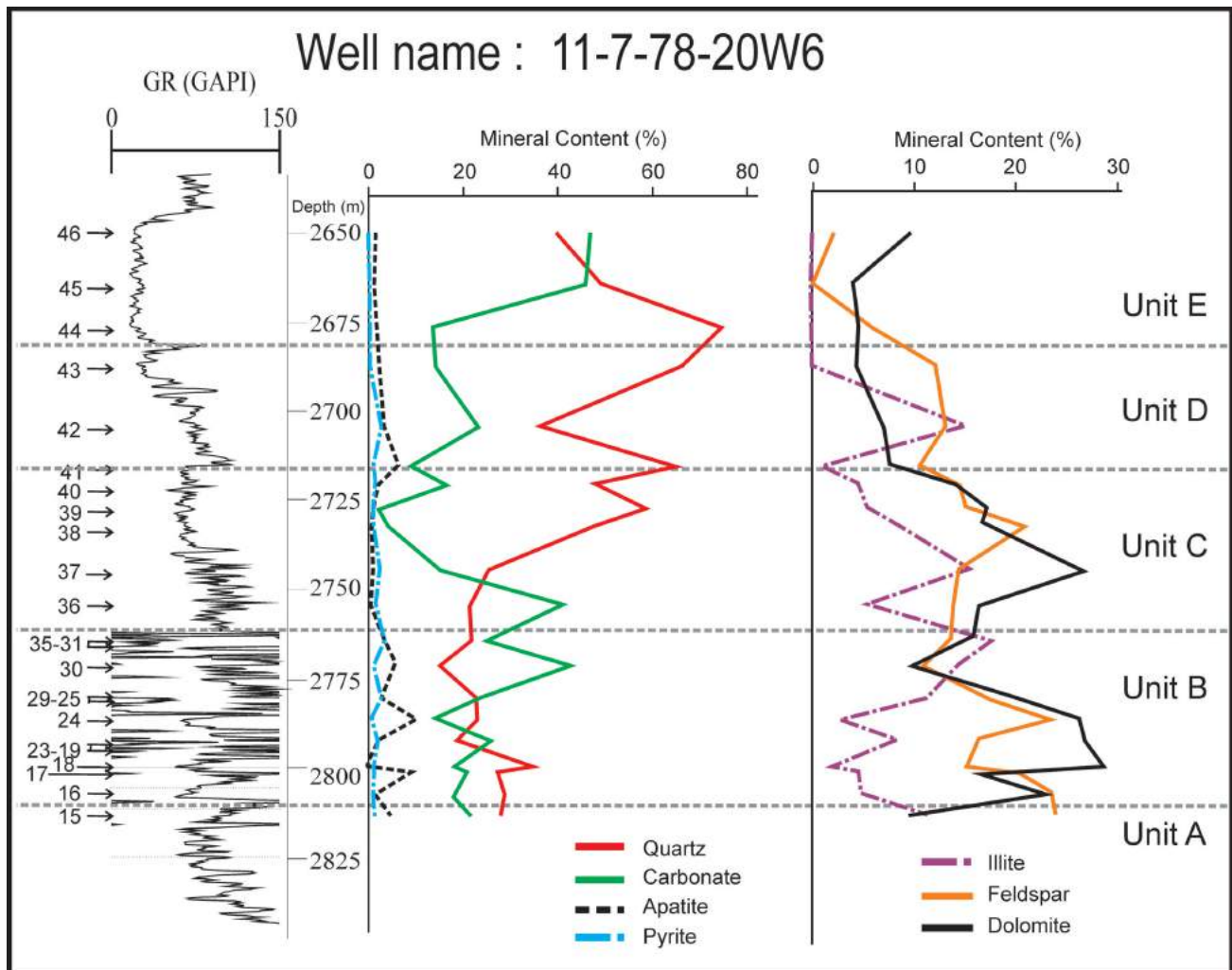


Figure 3. Mineralogical trends for the 11-7-78-20W6 well in northeastern British Columbia. Carbonate includes calcite and ankerite, although calcite dominates (i.e., ankerite averages 1.4%, and ranges between 0 and 7.2%). GR represents the geophysical gamma-log profile measured in American Petroleum Institute units (GAPI). Sample locations are shown on the left side of the diagram.

mite averages 17% and varies between 4 and 34%. The feldspar content averages 15% and ranges between 0 and 24%. The basal portion of unit B is carbonate- and/or dolomite-rich, which content decreases from the upper portion of unit C toward unit E, mirroring the quartz trends (Figure 3). The average illite content is 9% and ranges between 0 and 20%; higher illite contents are found within the upper portion of unit B and the lower (finer-grained) portions of units C and D. Pyrite averages 1.8% and varies between 1 and 5%. The Pearson product-moment correlation shows that the strongest relationships occur between total carbonate (calcite, ankerite and dolomite) and quartz ($r = -0.71$), illite and pyrite ($r = 0.74$), and between quartz+feldspar and carbonate (calcite+ankerite, $r = -0.62$).

Porosity

Porosity was determined by helium pycnometry and mercury porosimetry, with the former measuring pore sizes greater than the kinetic diameter of helium (0.26 nm) and the latter restricted to measuring pore sizes greater than 3 nm. Although the 3 nm boundary is derived from the Washburn equation and the assumption that all pores are cylindrical may not be correct, the relative difference between the two methods does indicate that pores present within some samples are undetectable using porosimetry. Therefore, any differences seen in the results obtained from these two methods (i.e., pycnometry-derived porosity and porosimetry-derived porosity) are considered an indication that there are pores within the size range of 0.26 to 3 nm (microporosity and fine mesoporosity). Pycnometry-derived porosity for the 11-7-78-20W6 well varies between 1.6 and 6.7%, with an average of 4.2%, and porosimetry-derived porosity varies between 1.9% and 6.5%, with an average of 3% (Figure 4). The two porosity profiles show a large difference within unit B and within unit D (Figure 4), indicating an increase in the fine meso- and microporosity (i.e., 0.26–3 nm) within these intervals. Above average porosity occurs within the coarser sections of the Doig Formation—at the base of unit B, and at the top of units C and D. Unit E and finer-grained intervals of units B, C and D have below-average porosity (Figure 4). Positive Pearson product-moment correlation coefficients exist between porosity and quartz content ($r = 0.58$), as well as between porosity and quartz+feldspar content ($r = 0.59$). Negative correlation coefficients exist between porosity and carbonate content ($r = -0.71$), and between porosity and total carbonate content ($r = -0.55$).

Pore-Size Distribution

Pore-size distribution (PSD) is illustrated by pore volume and by pore area for well 11-7-78-20W6 (Figures 5, 6). Unit B samples contain a high volume of pores within the 10 000–100 000 nm macropore size range and within the 3–50 nm mesopore size range. Variations in the proportion of

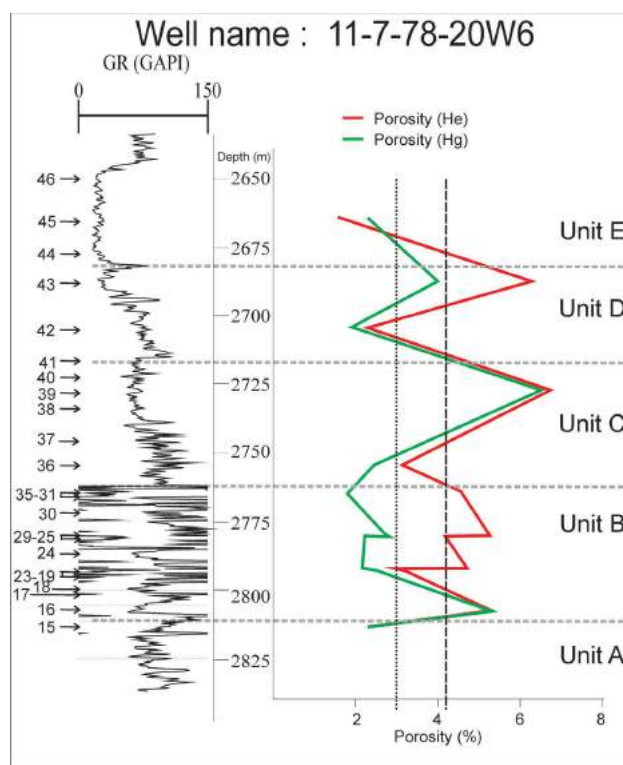


Figure 4. Pycnometry- and porosimetry-derived porosity profiles of the 11-7-78-20W6 well. The dotted line represents the average porosimetry-derived porosity and the dashed line represents the average pycnometry-derived porosity. Samples are oven dried to compare between methods as moist samples cannot be used for porosimetry (i.e., $S_w = 0$). GR represents the geophysical gamma-log profile measured in American Petroleum Institute units (GAPI). Sample locations are shown on the left side of the diagram.

macro- and mesopores exist between samples; those from units C, D and E (Figure 5a, b) have smaller proportions of mesopores compared to those from unit B (Figure 5c, d). Siltstone and very fine sandstone samples (e.g., sample 11-7-33; Figure 5c) from unit B also contain lower proportions of mesopores compared to finer-grained samples (e.g., sample 11-7-27; Figure 5c). Macropores, particularly in the 10 000–100 000 nm size fraction, do not significantly contribute to the pore area in comparison to mesopores and fine macropores (Figure 6).

Organic Geochemistry

The TOC content for the 11-7-78-20W6 well varies from 0.5 to over 7 wt %, with an average content of 3.2% (Figure 7). Samples from unit E and the top of unit D yielded TOC values below the detection limit of the Rock Eval™ apparatus (<0.5 wt %) and are therefore not included on the profile. Unit A (sample 11-7-15), the upper two-thirds of unit B, and unit C (sample 11-7-37) all register above average TOC-content values, which show high variability throughout the profile, the largest variation occurring in unit B (i.e., samples 11-7-25 to 11-7-29). A positive corre-

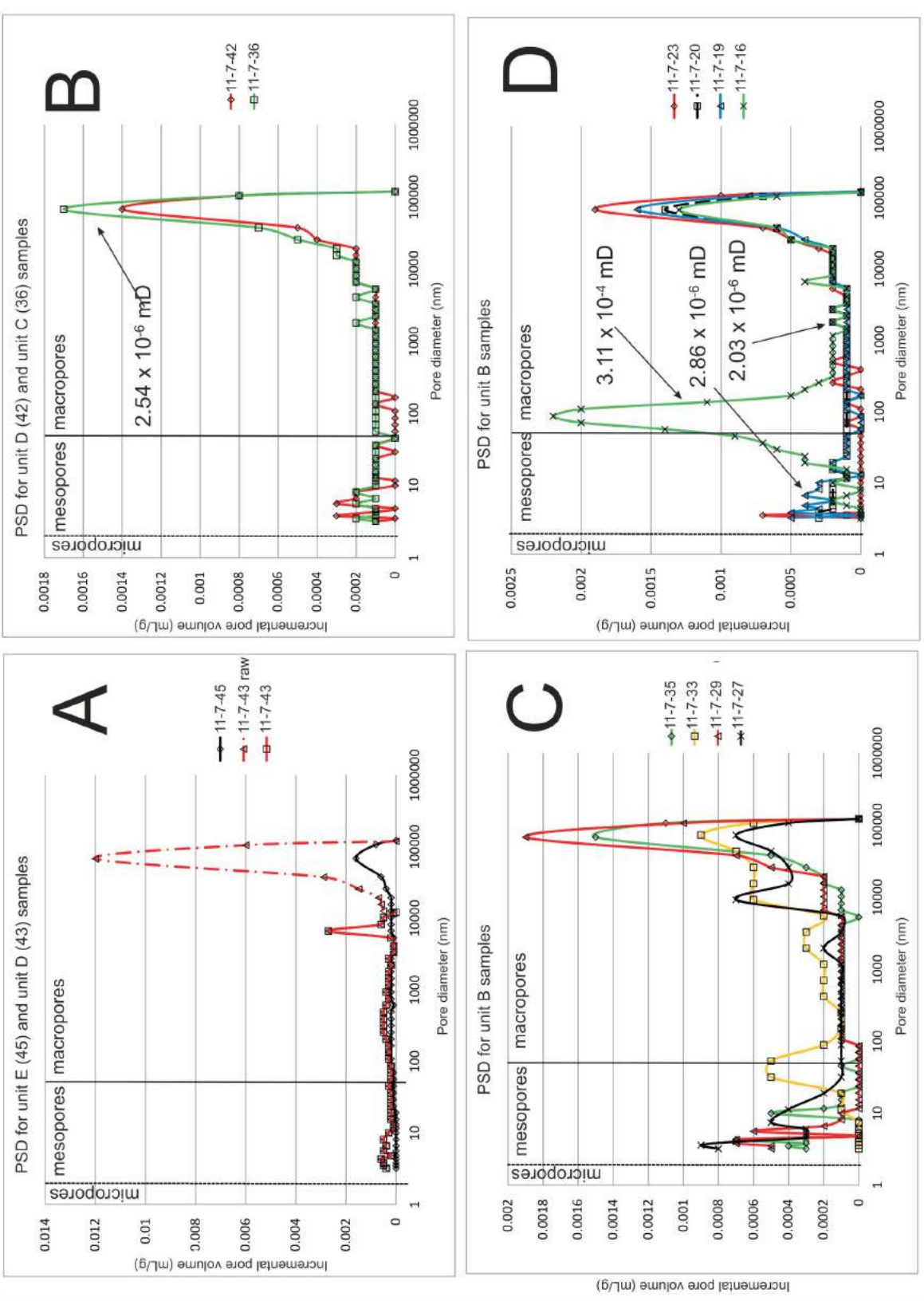


Figure 5. Pore-size distribution (PSD) for the 11-7-78-20W6 well, expressed using the incremental pore volume (mL/g). The dashed line represents the boundary between micro- and mesopores (2 nm) and the solid line demarcates the boundary between meso- and macropores (50 nm). Helium pulse-decay permeability (in mD) is also shown for some samples. Coarser-grained samples from units C, D and E show less mesopore volumes (Figure 5a, b) compared to samples from unit B (Figure 5c, d). Samples were crushed to a sieve size of 20–30 mesh. Sample locations can be found on Figure 4.

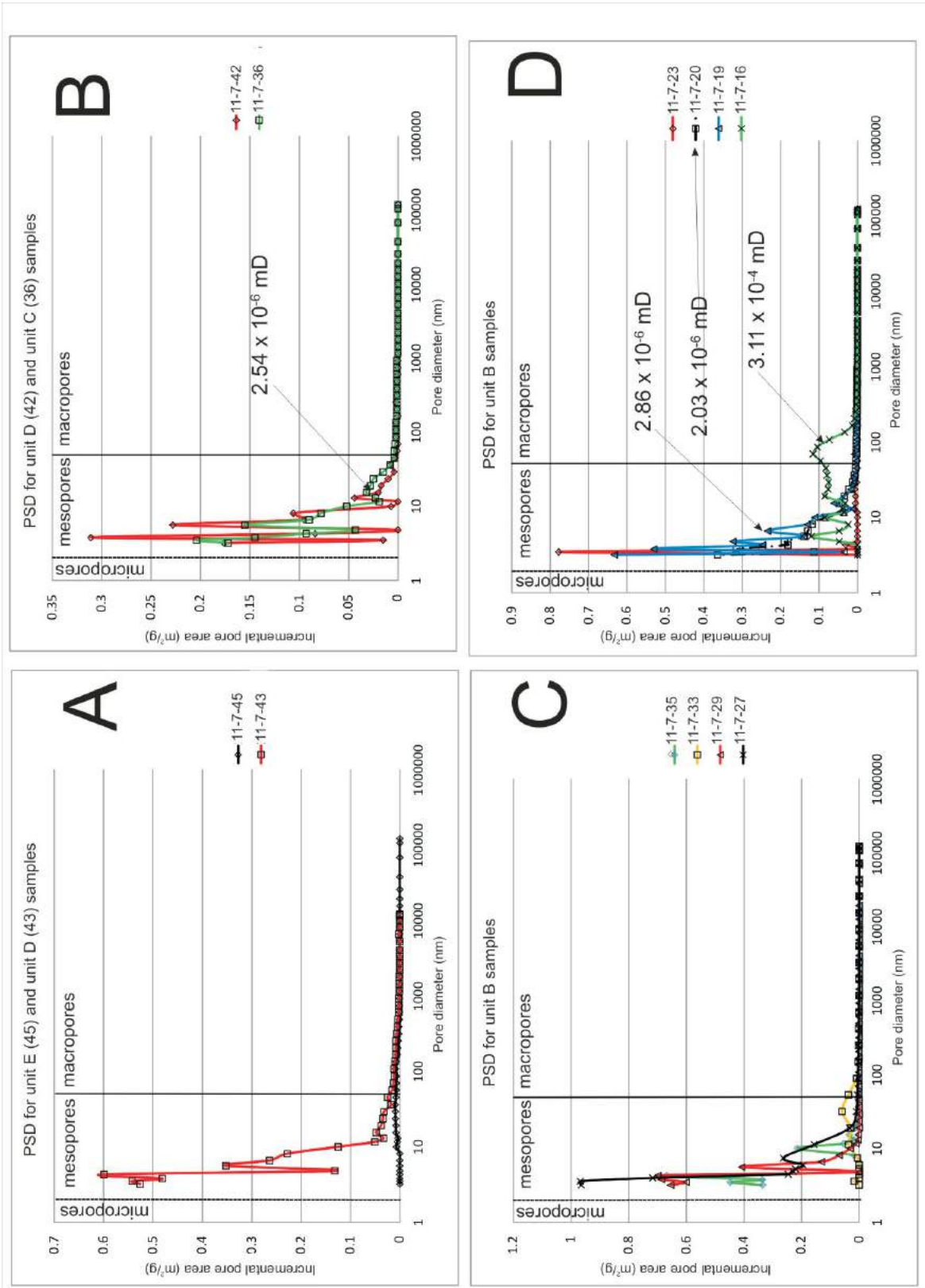


Figure 6. Pore-size distribution (PSD) for the 11-7-78-20W6 well, expressed using the incremental pore area (m^2/g). The dashed line represents the boundary between micro- and mesopores (2 nm) and the solid line represents the boundary between meso- and macropores (50 nm). Helium pulse-decay permeability (in mD) is also shown for some samples. Greater pore area is found in the finer-grained unit B samples (Figure 6c, d) compared to the coarser-grained units C to E samples (Figure 6a, b). Samples were crushed to a sieve size of 20–30 mesh. Sample locations can be found on Figure 4.

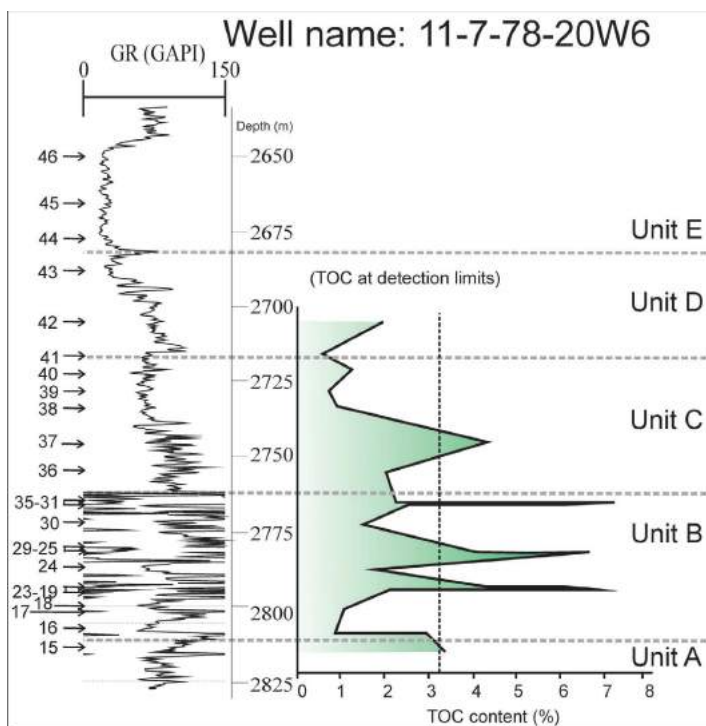


Figure 7. Total organic content (TOC) profile for the 11-7-78-20W well. TOC-content values were below the detection limit of the Rock Eval™ apparatus for samples collected within the Halfway Formation (unit E) and lower Doig member (unit D) and are therefore not included. The dashed line represents the average TOC content of 3.2 wt %. GR represents the geophysical gamma-log profile measured in American Petroleum Institute units (GAPI). Sample locations are shown on the left side of the diagram.

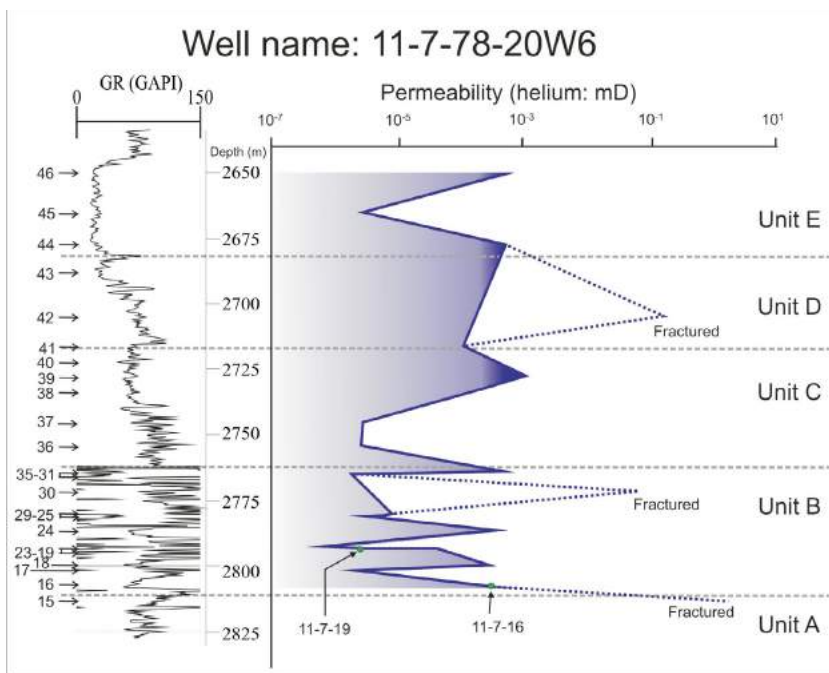


Figure 8. Downhole permeability trend for the 11-7-78-20W6 well, including the matrix permeability (solid line) and fracture permeabilities (dashed lines). The low frequency alternation within units C and D compared to unit B may be an artefact of their lower sampling resolution. GR represents the geophysical gamma-log profile measured in American Petroleum Institute units (GAPI). Sample locations are shown on the left side of the diagram.

lation exists between TOC and pyrite ($r = 0.68$) whereas a negative trend exists between quartz and TOC content ($r = -0.56$).

The hydrogen index (HI) for the 11-7-78-20W6 well averages 20 mg HC/g TOC, and ranges between 1 and 76 mg HC/g TOC. The oxygen index (OI) averages 34 mg CO₂/g TOC, and ranges between 5 and 172 mg CO₂/g TOC. The average T_{max} value is 457°C, and ranges between 443 and 478°C, placing the reservoirs within the gas window.

Pulse-Decay Permeability

The matrix permeability ranges between 10⁻⁴ and 10⁻⁷ mD (Figure 8); it also varies by two orders of magnitude between samples 11-7-16 and 11-7-19 (Figure 8), in part due to the difference in their PSD (see discussion for details). The higher matrix permeabilities in the 11-7-78-20W6 well are located in the top of unit C and scattered throughout unit B (solid line, Figure 8). The high alternation of permeability values within unit B may be due to the lithological and/or mineralogical changes and the lack of similar trends within units C, D and E could be an artefact of their lower sampling resolution compared to unit B. Samples that contain fractures (dashed lines, Figure 8) exhibit permeabilities that are four to five orders of magnitude greater than the lower permeabilities.

Discussion

Controls on Mineralogy

Unit B is carbonate and/or clay-rich and quartz-poor with units C and D being quartz-rich and carbonate and/or clay-poor (well 11-7-78-20W6; Figure 3). The Montney Formation (unit A) is carbonate-poor and quartz-rich compared to the Doig phosphate zone (unit B). The contrasting mineralogical character of the quartz-rich units C and D and carbonate-rich unit B in well 11-7-78-20W6 indicates a change in the sedimentary environment, accommodation space and/or tectonic activity within the study area as the depositional conditions shifted from carbonate deposition to clastic deposition. A greater influx of clastic rocks in the upper Doig Formation is either due to increasing tectonic activity or to a reduction in accommodation space (shore-line progradation) as a sea-level regression progressed. Clay deposition occurred when quartz and feldspar influx was low and pyrite deposition, high. The higher pyrite content (i.e., greater than 4%) indicates that the depositional conditions were dysoxic² to anoxic during periods of clay deposition. A negative relationship between quartz+feldspar and total carbonate contents indicates that during periods of quartz- and feldspar-rich detritus influx, carbonate

and dolomite deposition was low, whereas when influx of quartz and feldspar diminished, carbonate production relatively increased. Carbonate and clay sedimentation does not occur simultaneously (i.e., during low influx of quartz and feldspar), as indicated by the strong negative correlation between illite and carbonate. The deposition of the quartz, feldspar and clay minerals may be a result of turbiditic events, with fining-upward sequences ending in clay deposition; it therefore appears that carbonate deposition was restricted to the quiescent, non-turbiditic periods.

Controls on Porosity and Pore-Size Distribution

An increase in the difference between the pycnometry- and porosimetry-derived porosity occurs within unit B, indicating an increase in the fine meso- and microporosity (<3 nm) in the more carbonate/clay- and TOC-rich unit B compared to the other units (Figure 4).

The negative correlation between porosity and carbonate content could be an indication that porosity is low due to carbonate cementation, to recrystallization or to micritic mud deposition. Carbonate cementation of the pore network may be responsible for the porosity reduction within unit E (sample 11-7-45) with a high carbonate content and low porosity (Figure 4). The positive correlation between porosity and the quartz+feldspar content is indicative of an enhancement in the intergranular porosity. Higher porosity intervals within unit B are due to the localized increase in quartz content in an otherwise clay- and/or carbonate-rich unit.

Siltstone samples have a high volume of macropores and large mesopores (20–50 nm), high quartz content and low TOC and clay contents (e.g., sample 11-7-42 in unit D or sample 11-7-16 in unit B; Figures 3, 5, 6) compared with other samples characterized by low quartz, high clay and high TOC contents (e.g., samples 11-7-27 and 11-7-29 of unit B; Figures 3, 5, 6). Clay- and TOC-rich samples contain a higher proportion of mesopores, which results in a higher proportion of surface areas compared with siltstone samples; surface area provides gas storage in the sorbed state within the reservoir (Chalmers and Bustin, 2008).

Controls on the Distribution of the TOC Contents

Unit B contains the highest TOC contents, the lowest quartz contents and the highest contents of carbonate and/or clay compared to the other units. This observation is highlighted by the negative correlation between quartz and TOC contents. Higher TOC contents (Figure 7) in unit B are likely due to the increase in accommodation space, an increase in bottom-water anoxia, organic productivity and a reduction in clastic-rock influx. The positive correlation between TOC and pyrite indicates the bottom waters were anoxic to

² having a very low oxygen content (i.e., between anoxic and hypoxic)

euxinic during the deposition of unit B. A large variation in the TOC content can occur between closely-spaced samples (i.e., 20 cm for samples 11-7-31 to -35), which may be an indication that changes were occurring in the depositional environment or that turbiditic or storm events affected the preservation and accumulation of the organic matter. Low HI and OI values indicate that either the kerogen has experienced a high degree of hydrocarbon generation or that it originally came from oxidized plant material. The Montney and Doig formations are thermally mature to overmature (Riediger et al., 1990).

Controls on Matrix Permeability

The PSD, which controls the matrix permeability of the Doig and Montney reservoirs, was compared between samples that differed in matrix permeability by two orders of magnitude (Figure 5d, samples 11-7-16 and 11-7-19). Sample 11-7-16, which is characterized by a higher permeability, has a greater proportion of pores at the mesopore–macropore boundary compared with sample 11-7-19, which contains a greater volume of pores at the micropore–mesopore boundary. Both high- and low-permeability samples have bimodal pore-size distribution. The degree of separation between the two populations of pore sizes of the low-permeability samples (e.g., sample 11-7-19) is four orders of magnitude greater than that of the higher permeability samples (e.g., sample 11-7-16), whose degree of separation of only three orders of magnitude suggests a greater degree of communication within the matrix. The contrast-

ing PSD are due to the differences between the mineralogy and TOC contents. The difference between the high (10^{-4} mD) and low ($<10^{-6}$ mD) permeabilities of samples from well 11-7-78-20W6 (Figure 8) is due, in part, to the mineralogy; as shown on Figure 9, carbonate-rich samples have lower permeability than quartz-rich samples. Carbonate cementation during diagenesis and/or deposition of fine-grained micritic mud reduces both the porosity and permeability of the Doig and Montney formations.

Conclusions

Ongoing evaluation of the Doig and Montney reservoirs within the Groundbirch area of northeastern BC includes characterizing the mineralogy, porosity, pore-size distribution, organic geochemistry and matrix permeability. Downhole profiles illustrate the small-scaled heterogeneity in the mineralogy, TOC content and porosity. The finer-grained, high TOC-content, carbonate- and/or clay-rich intervals have lower permeability than the coarser-grained, lower TOC-content, carbonate- and/or clay-poor and quartz-rich intervals. Higher TOC contents in finer-grained intervals mean larger volumes of sorbed gas would be stored but its delivery to the wellbore would be slower, due to the lower permeability of these intervals compared with the higher permeability of the quartz-rich intervals.

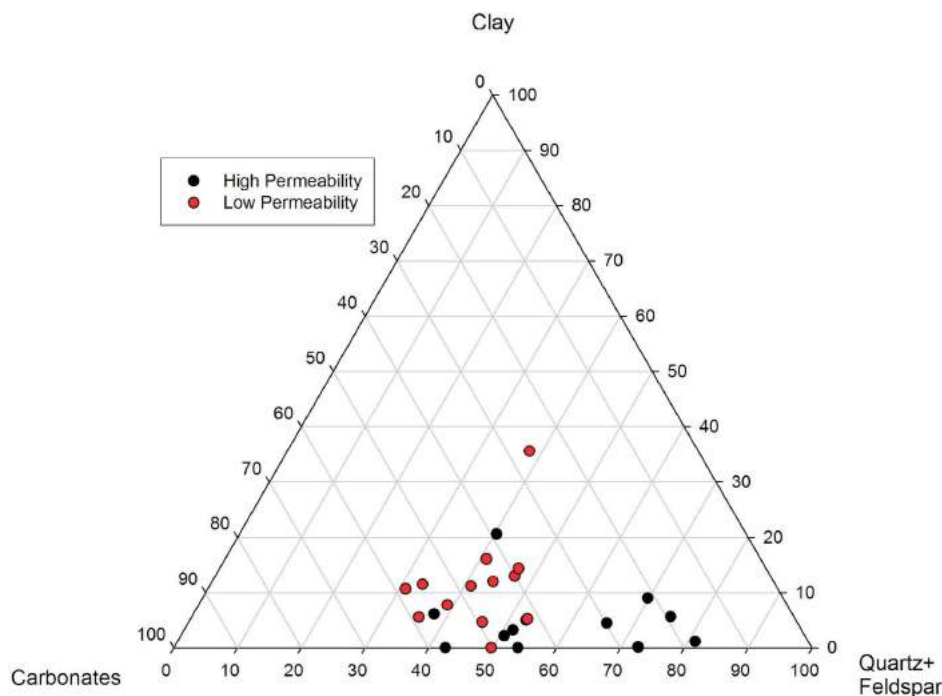


Figure 9. Mineralogical ternary diagram showing the difference between high and low matrix permeabilities.

Future Work

Data is currently being collected and interpreted from three more wells within the Groundbirch area. Inorganic petrology is to be conducted to examine the relationships between fabric, mineralogy, porosity and permeability. Organic petrology will also be performed to gain an understanding of the controls on organic sedimentation (i.e., terrestrial- versus marine-sourced organic materials).

Acknowledgments

The authors would like to thank Geoscience BC for its financial support of this ongoing research. They would also like to thank D. Ross who reviewed an earlier version of this manuscript.

References

- Adams, C. (2010): Shale gas activity in British Columbia: Exploration and Development of BC's shale gas areas (abstract); BC Ministry of Energy and Mines, 4th Annual Unconventional Gas Technical Forum, April 8–9, 2010, Victoria, BC, URL <<http://www.em.gov.bc.ca/OG/oilandgas/petroleumgeology/UnconventionalGas/Documents/C%20Adams.pdf>> [October, 2011].
- Bustin, R.M., Chalmers, G., Bustin, A.A.M. (2011): Quantification of the gas-in-place and flow characteristics of tight gas-charged rocks and gas-shale potential in British Columbia; *in* Geoscience BC Summary of Activities 2010, Geoscience BC, Report 2011-1, p. 201–208, URL <http://www.geosciencebc.com/i?pdf?SummaryofActivities2010/SoA2010_Bustin_etal.pdf> [October, 2011].
- Chalmers, G.R.L. and Bustin, R.M. (2008): Lower Cretaceous gas shales in northeastern British Columbia, Part I: geological controls on methane sorption capacity; *Bulletin of Canadian Petroleum Geology*, v. 56, p. 1–21.
- Davies, G.R. (1997): The Triassic of the western Canadian sedimentary basin: Tectonic and stratigraphic framework, palaeogeography, palaeoclimate and biota; *Bulletin of Canadian Petroleum Geology*, v. 45, p. 434–460.
- Dixon, J. (2000): Regional lithostratigraphic units in the Triassic Montney Formation of western Canada; *Bulletin of Canadian Petroleum Geology*, v. 48, p. 80–83.
- Dixon, J. (2009a): The Lower Triassic Shale member of the Montney Formation in the subsurface of northeast British Columbia; Geological Survey of Canada, Open File 6274, 9 p.
- Dixon, J. (2009b): Triassic stratigraphy in the subsurface of the plains area of Dawson Creek (93P) and Charlie Lake map areas (94A), northeast British Columbia; Geological Survey of Canada, Bulletin 595, 78 p.
- Edwards, D.E., Barclay, J.E., Gibson, D.W., Kville, G.E. and Halton, E. (1994): Triassic Strata of the Western Canada Sedimentary Basin; *in* Geological Atlas of the Western Canada Sedimentary Basin, G.D. Mossop and I. Shetsen (comp.), Canadian Society of Petroleum Geologists and Alberta Research Council, Special Report 4, URL <http://www.ags.gov.ab.ca/publications/wcsb_atlas/atlas.html> [August, 2011].
- Evoy, R.W. (1998): Reservoir sedimentology of the Doig Formation, Buick Creek Field, Northeastern British Columbia; *in* Oil and Gas Pools of the Western Canada Sedimentary Basin, J.R. Hogg (ed.), Canadian Society of Petroleum Geologists, Canada, Special Publication S-51, p. 127–135.
- Harris, R.G. and Bustin, R.M. (2000): Diagenesis, reservoir quality and production trends of Doig Formation sand bodies in the Peace River of western Canada; *Bulletin of Canadian Petroleum Geology*, v. 48, no. 4, p. 339–359.
- International Union of Pure and Applied Chemistry, (1997): Compendium of Chemical Terminology (2nd edition); A.D. McNaughton and A. Wilkinson (comp.), Blackwell Scientific Publications, Oxford, doi: 10.1351/goldbook.M03906, URL <<http://goldbook.iupac.org/M03906.html>> [November 2011].
- Kent, D.M. (1994): Paleogeographic evolution of the cratonic platform – Cambrian to Triassic; *in* Geological Atlas of the Western Canada Sedimentary Basin, G.D. Mossop and I. Shetsen (comp.), Canadian Society of Petroleum Geologists and Alberta Research Council, Special Report 4, URL <http://www.ags.gov.ab.ca/publications/wcsb_atlas/atlas.html> [August 4, 2010].
- Proust, J. (2010): Canada Energy Partners announces successful horizontal Montney test; Canada Energy Partners, press release, July 6, 2010, URL <http://www.canadaenergypartners.com/news/2010/index.php?&content_id=107> [October 2011].
- Riediger, C.L., Brooks, P.W., Fowler, M.G. and Snowdon, L.R. (1990): Lower and Middle Triassic source rocks, thermal maturation, and oil-source rock correlations in the Peace River embayment area, Alberta and British Columbia; *Bulletin of Canadian Petroleum Geology*, v. 38A, p. 218–235.
- Utting, J., MacNaughton, R.B., Zonneveld, J.P. and Fallas, K.M. (2005): Palynostratigraphy, lithostratigraphy and thermal maturity of the Lower Triassic Toad and Grayling, and Montney formations of western Canada, and comparisons with coeval rocks of the Sverdrup basin, Nunavut; *Bulletin of Canadian Petroleum Geology*, v. 53, p. 5–24.
- Walsh, W., Adams, C., Kerr, B. and Korol, J. (2006): Regional “shale gas” potential of the Triassic Doig and Montney formations, northeastern British Columbia; BC Ministry of Energy and Mines, Petroleum Geology Open File 2006-2.
- Washburn, E.W. (1921): Note on a method of determining the distribution of pore sizes in a porous material; *Proceeding of the National Academy of Sciences of the United States of America*, v. 7, p. 115–116.

Biostratigraphy and Sedimentary Provenance of Lower and Middle Triassic Natural Gas-Bearing Rocks in Northeastern British Columbia (parts of NTS 093P, 094A, B, K): Progress Report

M.L. Golding, University of British Columbia, Vancouver, BC, mgolding@eos.ubc.ca

J.K. Mortensen, University of British Columbia, Vancouver, BC

J-P. Zonneveld, University of Alberta, Edmonton, AB

M.J. Orchard, Geological Survey of Canada Pacific, Natural Resources Canada, Vancouver, BC

Golding, M.L., Mortensen, J.K., Zonneveld, J-P. and Orchard, M.J. (2012): Biostratigraphy and sedimentary provenance of Lower and Middle Triassic natural gas-bearing rocks in northeastern British Columbia (parts of NTS 093P, 094A, B, K): progress report; *in* Geoscience BC Summary of Activities 2011, Geoscience BC, Report 2012-1, p. 97–114.

Introduction

The Triassic natural gas-bearing rocks of the Western Canada Sedimentary Basin (WCSB) in British Columbia have been the subject of a multiyear interdisciplinary study designed to improve the biostratigraphic correlation of the gas-producing formations and to assess changes in sediment distribution patterns within this biostratigraphic framework. Initially, the focus of the work was on surface outcrop equivalents to the subsurface gas-producing formations, but it has since extended to encompass subsurface sections as well. Biostratigraphic correlation has been conducted through the identification of conodonts, and to a lesser extent, ammonoids and bivalves. Changes in sediment transport, including the sediment source and direction of input, have been formulated by the dating of detrital zircons, which gives an age for the protoliths from which the sediment was derived. Although the majority of sediment entering the WCSB during the Triassic came from the North American craton to the east, it is becoming more apparent that at least some of the sediment was derived from rocks to the north and west, and that this began to occur during the Triassic. This has implications not only for the source of sediment and therefore for the transport pathways of that sediment into the basin, but also for the timing of terrane accretion along the western margin of ancestral North America. Evidence from detrital zircon analyses in the Yukon (Beranek, 2009) and in this study points towards Permian-Triassic accretion of the Yukon-Tanana terrane, as first suggested by Nelson et al. (2006). This is much earlier than the Jurassic age that has previously been accepted for this event (e.g., Monger and Price, 2002).

Keywords: *Triassic, Western Canada Sedimentary Basin, correlation, conodont, detrital zircon, sedimentary provenance, Doig phosphate zone, Williston Lake, Alaska Highway*

This publication is also available, free of charge, as colour digital files in Adobe Acrobat® PDF format from the Geoscience BC website: <http://www.geosciencebc.com/s/DataReleases.asp>.

Previous progress reports on this study have described the sampling and analysis of samples from surface localities at South Halfway and Williston Lake (both in the Halfway River map area, NTS 094B), and subsurface samples from an oil well in the Dawson Creek map area (NTS 093P; Figure 1; Golding et al., 2010, 2011). These sections encompass an age range from the Smithian up to the Rhaetian. This report presents the results from those analyses, and describes a new round of fieldwork that was designed to build upon the results from previous field seasons. As such, outcrop was examined on the Alaska Highway in the summer of 2011, and six new subsurface cores were examined (Figure 1). The sections on the Alaska Highway cover an interval from the Anisian to Ladinian, which has previously been poorly covered by the sampling of this study. This time period was one of anomalous sediment thickness in the WCSB (Gibson, 1975) and also includes an unusual, highly phosphatic interval that is equivalent to the Doig phosphate zone in the subsurface. Additionally, these sections extend the area of study to the north. The extra subsurface sections cover an interval from the Spathian to the Anisian, and are therefore of a similar age to that from the previously studied borehole. They contain rocks belonging to the Doig phosphate zone, part of the Doig Formation that shows promise for producing natural gas (Walsh et al., 2006). Study of these cores will allow concepts derived from surface outcrop studies to be tested in the subsurface.

This interdisciplinary study has involved collaboration between the University of British Columbia, the University of Alberta, the Geological Survey of Canada, the BC Ministry of Energy and Mines, Geoscience BC and the petroleum industry.

Geological Setting

Triassic rocks of northeastern BC were deposited in the WCSB, along the western margin of the North American

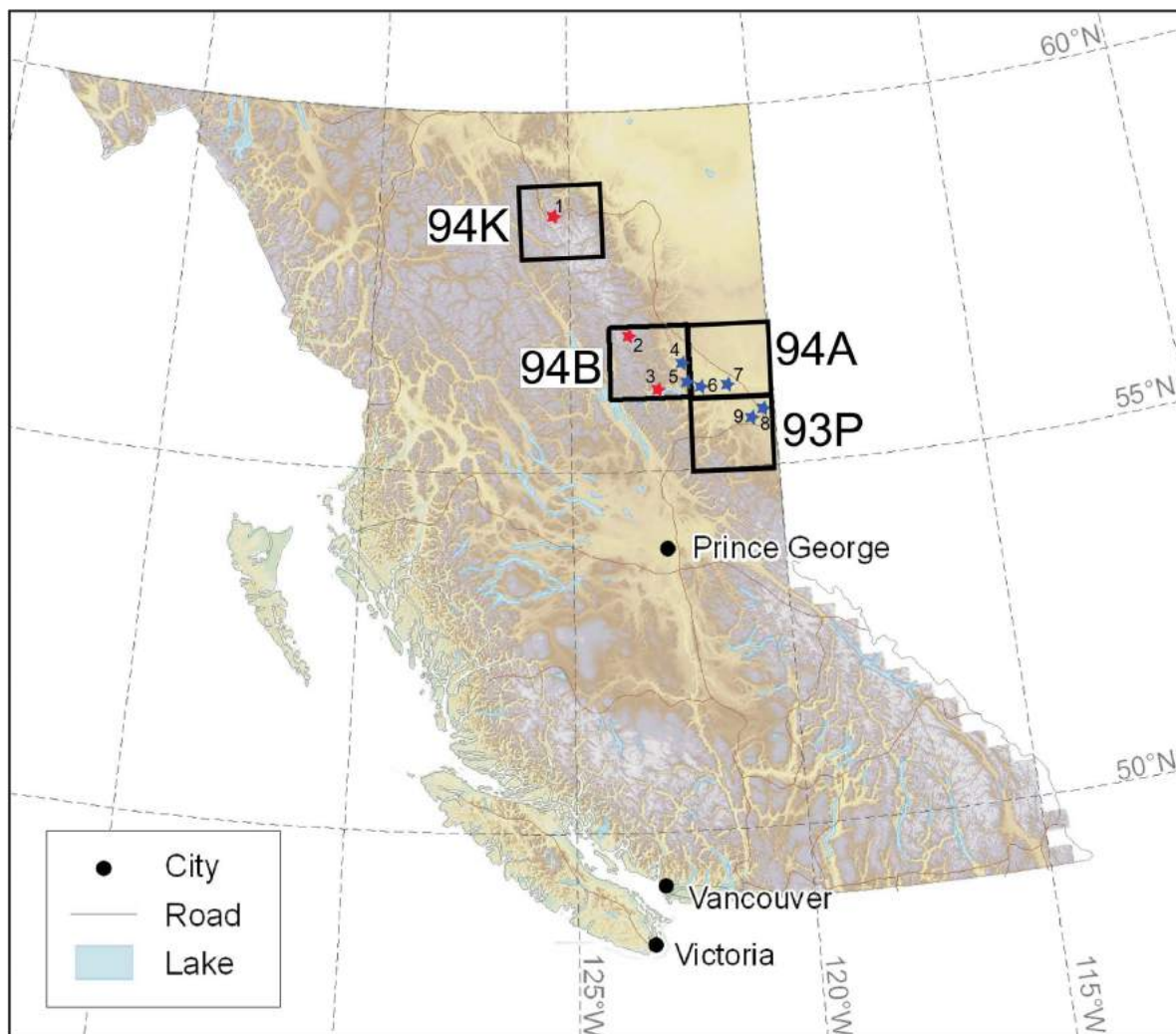


Figure 1. Location of map areas (NTS 093P, 094A, B, K), as well as the sampling localities: 1, Alaska Highway; 2, South Half-way; 3, Williston Lake; 4, Petro-Canada Kobes d-048-A/094-B-09; 5, Talisman Altares c-085-I/094-B-01; 6, Talisman Altares 16-17-083-25W6; 7, Rocor Monias 08-22-82-20W6; 8, Arc Dawson 07-13-79-15W6; and 9, Murphy Swan d-54-B/93-P-9. Red stars indicate outcrop localities, blue stars indicate subsurface wells.

continent. The WCSB at this time was at a latitude of around 30°N and the environment was arid (Davies, 1997). Sediment was deposited on the continental shelf, and consists primarily of a mixture of clastic and carbonate sediments. Windblown sediments are thought to have been a major constituent of the sediment deposited at this time (Davies, 1997), and storm reworking has been shown to have an important role in the distribution of sediment (Zonneveld et al., 1997). Although sediments were mainly deposited below normal wave base, some of the rocks show evidence of subaerial deposition (Zonneveld, 2010). Paleocurrent data is sparse for this time period, but that which is available indicates transport from the east, northeast and north (Pelletier, 1965).

Lithology varies from east to west, and from north to south along the belt of preserved Triassic rocks, as shown in Figure 2. In this study, rocks from the Toad, Liard, Baldonnel,

Pardonet, Montney and Doig formations have been observed and sampled.

The oldest observed unit in the study area is the Toad Formation. This is exposed in surface outcrop, and consists of argillaceous to calcareous siltstone, silty shale, silty limestone and dolostone, as well as very fine grained sandstone (Thompson, 1989). It spans the Smithian to the Ladinian, and it is equivalent to the Montney and lower Doig formations in the subsurface (Zonneveld, 2010). Above the Toad Formation lies the Liard Formation, which consists of fine to coarse sandstone, calcareous and dolomitic siltstone and sandy to silty dolostone and limestone (Thompson, 1989). It ranges in age from the Ladinian to the Carnian, and is the surface equivalent of the upper Doig and Halfway formations (Zonneveld, 2010).

		NW			SE
		Foothills - Halfway to Pine Rivers		Peace River Subsurface	Foothills - Bow to Sukunka Rivers
Jurassic		Fernie Fm			
Triassic	Upper	Rhaetian	Bocock Fm		
		Norian	Pardonet Fm	Pardonet Fm	
	Middle	Carnian	Baldonnell Fm	Baldonnell Fm	Winnifred Mbr
			Charlie Lake Fm	Charlie Lake Fm	Brewster Mbr
		Ladinian	Liard Fm	Halfway Fm	Starlight Evaporite Mbr
	Lower	Anisian	Toad Fm	Doig Fm	Llama Mbr
		Spathian	Grayling Fm	Montney Fm	Whistler Mbr
		Smithian			Vega-Phroso Mbr
		Dienerian			
	Griesbachian				
Permian		Fantasque Fm/Belloy Fm			

Figure 2. Triassic formations in British Columbia and their correlations with those in the subsurface and in southern Alberta. Modified from Ferri (2009). Abbreviations: Fm, Formation; Gp, Group; Mbr, Member; Mtn, Mountain.

The Baldonnell Formation, overlying the Liard Formation, is characterized by a sequence of limestone, dolostone and siltstone (Zonneveld, 2010). This unit is named after its subsurface equivalent. The age of this formation is diachronous and ranges from upper Carnian to lower Norian in the east, and from lower Carnian to upper Carnian in the west (Zonneveld, 2010). The Baldonnell Formation is typically succeeded by the Pardonet Formation, which consists of limestone, dolostone, calcareous silt and shale (Zonneveld, 2010). This unit can be traced into the subsurface, and it is Norian to Rhaetian in age (Zonneveld, 2010).

In the subsurface, shale and siltstone of the Montney Formation is overlain by the Doig Formation, with the boundary marked by a distinctive *Glossifungites* surface (indicative of a firmground surface). The basal part of the formation consists of a phosphatic pebble lag, which gives way to shale, siltstone, sandstone and occasional carbonate (Zonneveld, 2010). Deposition of this formation may extend as far back as the Spathian in age (Zonneveld, 2010) with its upper boundary in the Ladinian (Hunt and Ratcliffe, 1959). This makes it the subsurface equivalent of the upper part of the Toad Formation and the lower part of the Liard Formation.

Williston Lake Study Area (NTS 094B)

Williston Lake is located in the Halfway River map area (NTS 094B; Figure 1). In 2010, six sections were examined and sampled for conodont and detrital zircon geochronology (Golding et al., 2011; Tables 1, 2). From west to east, the sections are: Ursula Creek; Ne-parle-pas Point; Black Bear Ridge; Glacier Spur; East Carbon Creek and Beattie Ledge (Figure 3). These sections have been described and illustrated by Zonneveld (2010), and they range in age from Smithian to Rhaetian.

Results To Date

Ursula Creek

The Ursula Creek section contains shale and siltstone belonging to the Toad Formation. The sampled interval is Smithian to Ladinian. Four samples were collected for detrital zircon analysis, however, all were barren.

Ne-parle-pas Point

The Ne-parle-pas Point section contains shale, siltstone and sandstone of the Pardonet Formation. The sampled interval is Rhaetian. Three samples were collected for detrital zircon analysis, however, all were barren.

Black Bear Ridge

The Black Bear Ridge section contains siltstone and sandstone belonging to the Pardonet Formation. The sampled

Table 1. Detrital zircon samples collected from outcrop sites in the study area, northeastern British Columbia, in 2010 and 2011.

Outcrop sample number	Locality	Distance from base of section (m)	Formation	Analysis
MG-10-UC01	Ursula Creek	78.9	Toad	complete
MG-10-UC02	Ursula Creek	85.2	Toad	complete
MG-10-UC03	Ursula Creek	124.9	Toad	complete
MG-10-UC04	Ursula Creek	129.55	Toad	complete
MG-10-NPP01	Ne-parle-pas Point	41.2	Pardonet	complete
MG-10-NPP02	Ne-parle-pas Point	41.5	Pardonet	complete
MG-10-NPP03	Ne-parle-pas Point	51	Pardonet	complete
MG-10-BBR01	Black Bear Ridge	242	Pardonet	in progress
MG-10-GS01	Glacier Spur	122.6	Liard	complete
MG-10-GS02	Glacier Spur	149	Liard	complete
MG-10-GS03	Glacier Spur	255	Liard	complete
MG-10-GS04	Glacier Spur	293.8	Liard	complete
MG-10-GS05	Glacier Spur	304	Liard	complete
MG-10-ECC01	East Carbon Creek	76	Baldonnel	complete
MG-11-MP386-Z1	Mile Post 386	10.25	Toad	in progress
MG-11-MP386-Z2	Mile Post 386	17.5	Toad	in progress
MG-11-NTP-Z1	North Tetsa Phosphate	2.6	Toad	in progress
MG-11-NTP-Z2	North Tetsa Phosphate	2.7	Toad	in progress
MG-11-NTP-Z3	North Tetsa Phosphate	2.8	Toad	in progress
MG-11-NTP-Z4	North Tetsa Phosphate	10.6	Toad	in progress
MG-11-NTP-Z5	North Tetsa Phosphate	11.85	Toad	in progress
MG-11-OS-Z1a	Oyster Springs	3.3	Liard	in progress
MG-11-YB-Z1	Yellow Bluffs	1.7	Toad/Liard	in progress
MG-11-YB-Z2	Yellow Bluffs	3	Toad/Liard	in progress
MG-11-YB-Z3	Yellow Bluffs	3.75	Toad/Liard	in progress
MG-11-YB-Z4	Yellow Bluffs	10	Toad/Liard	in progress
MG-11-YB-Z5	Yellow Bluffs	13	Toad/Liard	in progress
MG-11-MP375W-Z1	Mile Post 375 West	n/a	Toad	in progress

interval is Rhaetian in age. Four samples were collected for conodonts, however, they contain only unidentifiable fragments. One sample was collected for detrital zircon analysis, and this contains Norian euhedral zircons. Work is ongoing to confirm the reliability of this result.

Glacier Spur

The Glacier Spur section contains sandstones and carbonate rocks of the Liard Formation, which span the Ladinian–Carnian boundary. Six samples were collected for conodonts, and all were productive. They contain a relatively abundant fauna, including representatives of *Budurovignathus mungoensis*, *Paragondolella inclinata*, *Metapolygnathus polygnathiformis* and *Neogondolella liardensis*. *Paragondolella willistonensis* was recovered for the first time from this section. These conodonts are indicative of the upper Ladinian and lower Carnian, which is in line with previous estimates for the age of this section. Five samples were collected for detrital zircon analysis, and all were productive. The lowest four samples are dominated by zircons of Proterozoic age, but also contain zir-

cons of lower Paleozoic age. The highest sample is lacking the lower Paleozoic population.

East Carbon Creek

The East Carbon Creek section consists of siltstone, sandstone and carbonate belonging to the Baldonnel Formation. The sampled interval is Carnian. One sample was collected for detrital zircon analysis, and it contains zircons of Proterozoic and lower Paleozoic age.

Beattie Ledge

The Beattie Ledge section consists of sandstone and carbonate belonging to the Liard Formation and is Ladinian. Two samples were collected for conodonts, and although neither contain conodonts, they do contain an abundant ichthyolith fauna. Work is ongoing to identify these elements and to determine their stratigraphic significance.

Discussion

The presence and spectra of detrital zircons of Proterozoic age is consistent with derivation from the North American

Table 2. Conodont samples collected from outcrop sites in the study area, northeastern British Columbia, in 2010 and 2011.

Outcrop sample number	Locality	Distance from base of section (m)	Formation	Analysis
MG-10-BBR02	Black Bear Ridge	242.8	Pardonet	complete
MG-10-BBR03	Black Bear Ridge	242.8	Pardonet	complete
MG-10-BBR04	Black Bear Ridge	243.8	Pardonet	complete
MG-10-BBR05	Black Bear Ridge	244.05	Pardonet	complete
MG-10-GS06A	Glacier Spur	129	Liard	complete
MG-10-GS06B	Glacier Spur	235	Liard	complete
MG-10-GS07	Glacier Spur	312.3	Liard	complete
MG-10-GS08	Glacier Spur	312.7	Liard	complete
MG-10-GS09	Glacier Spur	313	Liard	complete
MG-10-GS10	Glacier Spur	319.3	Liard	complete
MG-10-BL36	Beattie Ledge	36	Liard	complete
MG-10-BL48.5	Beattie Ledge	48.5	Liard	complete
MG-11-MP386-C1	Mile Post 386	3.5	Toad	in progress
MG-11-MP386-C2	Mile Post 386	8	Toad	in progress
MG-11-MP386-C3	Mile Post 386	12	Toad	in progress
MG-11-MP386-C4	Mile Post 386	14.1	Toad	in progress
MG-11-MP386-C5	Mile Post 386	17.5	Toad	in progress
MG-11-NTPW-C1	North Tetsa Phosphate West	n/a	Toad	in progress
MG-11-NTPW-C2	North Tetsa Phosphate West	n/a	Toad	in progress
MG-11-NTP-C0	North Tetsa Phosphate	-0.3	Toad	in progress
MG-11-NTP-C1	North Tetsa Phosphate	0.45	Toad	in progress
MG-11-NTP-C2	North Tetsa Phosphate	2.6	Toad	in progress
MG-11-NTP-C3	North Tetsa Phosphate	2.7	Toad	in progress
MG-11-NTP-C4	North Tetsa Phosphate	2.8	Toad	in progress
MG-11-NTP-C5	North Tetsa Phosphate	3.18	Toad	in progress
MG-11-NTP-C6	North Tetsa Phosphate	3.4	Toad	in progress
MG-11-NTP-C7	North Tetsa Phosphate	4.3	Toad	in progress
MG-11-NTP-C8	North Tetsa Phosphate	5.6	Toad	in progress
MG-11-NTP-C9	North Tetsa Phosphate	7.55	Toad	in progress
MG-11-NTP-C10	North Tetsa Phosphate	9.55	Toad	in progress
MG-11-NTP-C11	North Tetsa Phosphate	10.6	Toad	in progress
MG-11-NTP-C12	North Tetsa Phosphate	11.35	Toad	in progress
MG-11-NTP-C13	North Tetsa Phosphate	n/a	Toad	in progress
MG-11-OS-C1a	Oyster Springs	3.3	Liard	in progress
MG-11-OS-C4	Oyster Springs	17.9	Liard	in progress
MG-11-YB-C1	Yellow Bluffs	1.7	Toad/Liard	in progress
MG-11-YB-C2	Yellow Bluffs	1.7	Toad/Liard	in progress
MG-11-YB-C3	Yellow Bluffs	3	Toad/Liard	in progress
MG-11-YB-C4	Yellow Bluffs	3	Toad/Liard	in progress
MG-11-YB-C5	Yellow Bluffs	3.75	Toad/Liard	in progress
MG-11-YB-C6	Yellow Bluffs	3.75	Toad/Liard	in progress
MG-11-YB-C7	Yellow Bluffs	n/a	Toad/Liard	in progress
MG-11-YB-C8	Yellow Bluffs	10	Toad/Liard	in progress
MG-11-YB-C9	Yellow Bluffs	10	Toad/Liard	in progress
MG-11-YB-C10	Yellow Bluffs	8	Toad/Liard	in progress
MG-11-YB-C11	Yellow Bluffs	13	Toad/Liard	in progress
MG-11-YB-C12	Yellow Bluffs	13	Toad/Liard	in progress
MG-11-YB-Cfloat	Yellow Bluffs	n/a	Toad/Liard	in progress
MG-11-SL-C1	Sanitary Landfill	n/a	Toad	in progress
MG-11-SL-C2	Sanitary Landfill	n/a	Toad	in progress
MG-11-MP375W-C1	Mile Post 375 West	n/a	Toad	in progress
MG-11-MP375W-C2	Mile Post 375 West	n/a	Toad	in progress
MG-11-MP375W-C3	Mile Post 375 West	n/a	Toad	in progress
MG-11-MP375W-C4	Mile Post 375 West	n/a	Toad	in progress

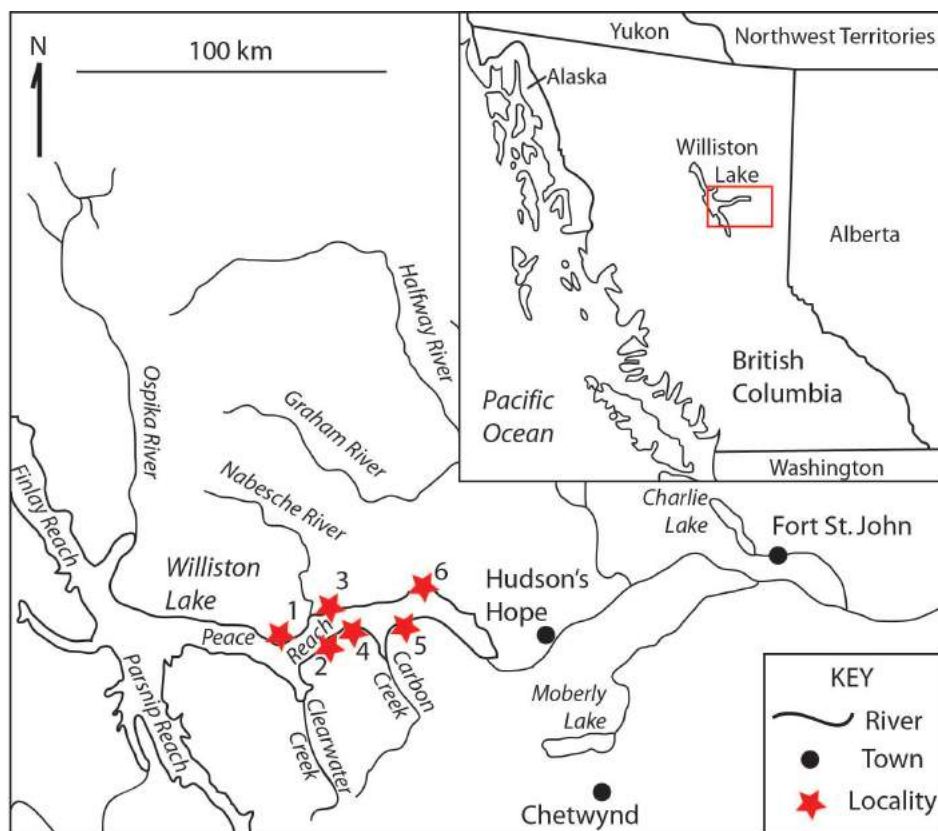


Figure 3. Location of Williston Lake sections: 1, Ursula Creek; 2, Ne-parle-pas Point; 3, Black Bear Ridge; 4, Glacier Spur; 5, East Carbon Creek; 6, Beattie Ledge. Modified from Zonneveld et al. (2001).

craton, and zircons of this age are present in all of the productive samples from Williston Lake. The detrital zircons of lower Paleozoic age (Ordovician–Devonian) imply initial derivation from the Innuitian/Ellesmerian Orogen to the north, likely by longshore drift. However, with the available data it is impossible to tell if these zircons were sourced directly from the orogen during the Triassic, or if they had been previously incorporated into older sediments near Williston Lake, before being reworked by more local systems during the Triassic. The zircons of Norian age from Black Bear Ridge could imply that pericratonic terranes with Triassic igneous rocks were in close proximity to the North American continent during the Rhaetian, and they were shedding some of this material into the WCSB. However, the euhedral nature of these zircons may suggest that they are primary, and represent deposition from contemporaneous volcanic activity during the Norian. This signal will be sought in other time equivalent sections on Williston Lake and elsewhere in northeastern BC. The absence of Mississippian and Permian detrital zircons is notable, as zircons of this age were identified in the Triassic of the Yukon by Beranek (2009), and interpreted as evidence for the Late Permian to Early Triassic accretion of the Yukon-Tanana terrane with North America. This conclusion is neither supported nor disproved by the data collected so far from BC.

Subsurface Correlation (NTS 093P)

In order to correlate the observations made at Williston Lake with equivalents in the subsurface, samples were collected from one subsurface core, taken from the Murphy Swan d-54-B/93-P-9 well. This is located to the southeast of the sections on Williston Lake and at South Halfway (Golding et al., 2011), in the Dawson Creek map area (NTS 093P; Figure 1, locality 9).

The Murphy Swan d-54-B/93-P-9 well intercepts the Montney and Doig formations, and eight core samples were processed for conodont and subsequent detrital zircon analysis (Tables 3, 4). These samples were processed for conodonts, and were productive, with the exception of material from 2556.90 m. The conodonts have not been identified to species level, but many appear to belong to the *Neogondolella constricta* group and are probably Anisian. Two of the samples (from 2551.80 and 2553.80 m) also produced enough detrital zircon to be dated, and as of November 2011 they were in the process of being analyzed.

These samples are slightly older than those that provided datable zircons from Williston Lake and South Halfway (Golding et al., 2011), and therefore may provide a test for the tectonic model suggested above. However, these are the most easterly of the samples studied so far, and may display

Table 3. Detrital zircon samples collected from subsurface wells in the study area, northeastern British Columbia, in 2010 and 2011.

Subsurface sample number	Locality	Distance from top of well (m)	Formation	Analysis
MG-10-JPZ1	d-54-B/93-P-9	2548.45	Doig	complete
MG-10-JPZ2	d-54-B/93-P-9	2549.66	Doig	complete
MG-10-JPZ3	d-54-B/93-P-9	2551.8	Doig	in progress
MG-10-JPZ4	d-54-B/93-P-9	2553.4	Doig	complete
MG-10-JPZ5	d-54-B/93-P-9	2553.8	Doig	in progress
MG-10-JPZ6	d-54-B/93-P-9	2556.25	Doig	complete
MG-10-JPZ7	d-54-B/93-P-9	2556.9	Doig	complete
MG-10-JPZ8	d-54-B/93-P-9	2557.3	Doig	complete
MG-11-C1	16-17-083-25W6	2258.30–2257.43	Montney	in progress
MG-11-C2	16-17-083-25W6	2256.22–2255.98	Doig	in progress
MG-11-C3	16-17-083-25W6	2255.30–2254.44	Doig	in progress
MG-11-C4	16-17-083-25W6	2248.52–2248.05	Doig	in progress
MG-11-C5	16-17-083-25W6	2247.75–2247.21	Doig	in progress
MG-11-C6	16-17-083-25W6	2245.79–2244.62	Doig	in progress
MG-11-C7	16-17-083-25W6	2242.35–2241.46	Doig	in progress
MG-11-C8	16-17-083-25W6	2239.75–2238.74	Doig	in progress
MG-11-C9	16-17-083-25W6	2237.05–2236.09	Doig	in progress
MG-11-C10	16-17-083-25W6	2234.57–2234.10	Doig	in progress
MG-11-C11	16-17-083-25W6	2233.61–2233.08	Doig	in progress
MG-11-C12	c-085-I/094-B-01	2374.17–2373.25	Doig	in progress
MG-11-C16	c-085-I/094-B-01	2315.22–2314.50	Doig	in progress
MG-11-C17	c-085-I/094-B-01	2310.89–2310.00	Doig	in progress
MG-11-C18	c-085-I/094-B-01	2306.82–2306.01	Doig	in progress
MG-11-C19	c-085-I/094-B-01	2295.92–2295.36	Doig	in progress
MG-11-C20	07-13-79-15W6	2056.35–2055.68	Montney	in progress
MG-11-C22	07-13-79-15W6	2054.30–2054.05	Doig	in progress
MG-11-C23	08-22-82-20W6	1779.61–1779.38	Doig	in progress
MG-11-C24	08-22-82-20W6	1778.98–1778.70	Doig	in progress
MG-11-C25	08-22-82-20W6	1775.20–1774.81	Doig	in progress
MG-11-C26	08-22-82-20W6	1774.16–1774.00	Doig	in progress
MG-11-C28	d-048-A/094-B-09	1968.25	Montney	in progress
MG-11-C29	d-048-A/094-B-09	1967.85	Montney	in progress
MG-11-C30	d-048-A/094-B-09	1967.50–1967.30	Doig	in progress
MG-11-C31	d-048-A/094-B-09	1967.00–1966.00	Doig	in progress
MG-11-C32	d-048-A/094-B-09	1965.90–1964.80	Doig	in progress
MG-11-C33	d-048-A/094-B-09	1965.40–1965.00	Doig	in progress

a detrital zircon signature dominated by the more proximal North American continent.

Alaska Highway Study Area (NTS 094K)

Seven sections were examined on the Alaska Highway during the summer of 2011 and sampled for detrital zircons and conodonts (Tables 1, 2). All sections are roadcuts on the Highway near to where it crosses the Tetsa River, and are situated in the Tuchodi Lakes map area (NTS 094K; Figure 4). From west to east, the sections are: Mile Post 386, North Tetsa Phosphate West, North Tetsa Phosphate, Oyster Springs, Yellow Bluffs, Sanitary Landfill and Mile Post 375 West. Of these sections, Mile Post 386, North Tetsa

Phosphate, Yellow Bluffs and Mile Post 375 West have been studied before, although detailed logs were not available. Mile Post 375 West is the only one of these sections to have been mentioned in press (McLearn, 1946; Tozer, 1967). The North Tetsa Phosphate West, Oyster Springs and Sanitary Landfill sections are new. These sections span most of the Middle Triassic, from the Mulleri Zone (base Anisian) to the Meginae Zone (upper Ladinian).

Sampling

Mile Post 386

The Mile Post 386 section is located at mile post 386 on the Alaska Highway, with its base at Zone 10, 410890E,

Table 4. Conodont samples collected from subsurface wells in the study area, northeastern British Columbia, in 2010 and 2011.

Subsurface sample number	Locality	Distance from top of well (m)	Formation	Analysis
MG-10-JPZ1	d-54-B/93-P-9	2548.45	Doig	complete
MG-10-JPZ2	d-54-B/93-P-9	2549.66	Doig	complete
MG-10-JPZ3	d-54-B/93-P-9	2551.8	Doig	complete
MG-10-JPZ4	d-54-B/93-P-9	2553.4	Doig	complete
MG-10-JPZ5	d-54-B/93-P-9	2553.8	Doig	complete
MG-10-JPZ6	d-54-B/93-P-9	2556.25	Doig	complete
MG-10-JPZ7	d-54-B/93-P-9	2556.9	Doig	complete
MG-10-JPZ8	d-54-B/93-P-9	2557.3	Doig	complete
MG-11-C1	16-17-083-25W6	2258.30–2257.43	Montney	in progress
MG-11-C3	16-17-083-25W6	2255.30–2254.44	Doig	in progress
MG-11-C7	16-17-083-25W6	2242.35–2241.46	Doig	in progress
MG-11-C8	16-17-083-25W6	2239.75–2238.74	Doig	in progress
MG-11-C9	16-17-083-25W6	2237.05–2236.09	Doig	in progress
MG-11-C10	16-17-083-25W6	2234.57–2234.10	Doig	in progress
MG-11-C13	c-085-I/094-B-01	2370.61–2369.96	Doig	in progress
MG-11-C14	c-085-I/094-B-01	2368.88–2368.04	Doig	in progress
MG-11-C15	c-085-I/094-B-01	2366.75–2366.06	Doig	in progress
MG-11-C16	c-085-I/094-B-01	2315.22–2314.50	Doig	in progress
MG-11-C18	c-085-I/094-B-01	2306.82–2306.01	Doig	in progress
MG-11-C21	07-13-79-15W6	2054.68–2054.48	Doig	in progress
MG-11-C22	07-13-79-15W6	2054.30–2054.05	Doig	in progress
MG-11-C24	08-22-82-20W6	1778.98–1778.70	Doig	in progress
MG-11-C27	08-22-82-20W6	1773.65–1773.21	Doig	in progress
MG-11-C28	d-048-A/094-B-09	1968.25	Montney	in progress
MG-11-C29	d-048-A/094-B-09	1967.85	Montney	in progress
MG-11-C30	d-048-A/094-B-09	1967.50–1967.30	Doig	in progress
MG-11-C31	d-048-A/094-B-09	1967.00–1966.00	Doig	in progress
MG-11-C32	d-048-A/094-B-09	1965.90–1964.80	Doig	in progress
MG-11-C33	d-048-A/094-B-09	1965.40–1965.00	Doig	in progress

6503721N (NAD 83). It consists of 17.75 m of siltstone and sandstone belonging to the Toad Formation. Five conodont samples were collected (Table 2) and two detrital zircon samples were collected (Table 1). M. Balini (University of Milan) was present in the summer of 2011 and collected ammonoids from horizons at 8.0, 12.0 and 14.0 m above the base of the section, as well as from isolated outcrop 0.45 m above the top of the section. Previous unpublished ammonoid collections indicate that this section encompasses the Meginae Zone of the Ladinian.

North Tetsa Phosphate West

The North Tetsa Phosphate West section is located to the west of the North Tetsa Phosphate section and it consists of siltstone and sandstone belonging to the Toad Formation. Two conodont samples were collected, one from in situ, the other from talus. The in situ collection was also associated with ammonoids that were collected by M. Balini. The age of this section is uncertain.

North Tetsa Phosphate

The base of the North Tetsa Phosphate section is located at Zone 10, 416937E, 6503965N. It consists of 17.85 m of siltstone and sandstone belonging to the Toad Formation. This section contains a high proportion of phosphate, and is thought to be equivalent at least in part to the Doig phosphate zone that can be identified in the subsurface. Twelve conodont samples were collected from the section (Table 2). Another sample was collected from 0.3 m below the base of the measured section, and a final sample was collected from isolated outcrop above the top of the section. Five detrital zircon samples were also collected (Table 1). M. Balini collected ammonoids from horizons at 2.7, 3.18, 5.5, 17.2 and 17.5 m above the base of the section, as well as from one bed 0.3 m below the base of the section. Eight samples were collected from throughout the section for total organic carbon (TOC) analysis. Previous unpublished fossil collections indicate that this section is probably early Anisian in age.

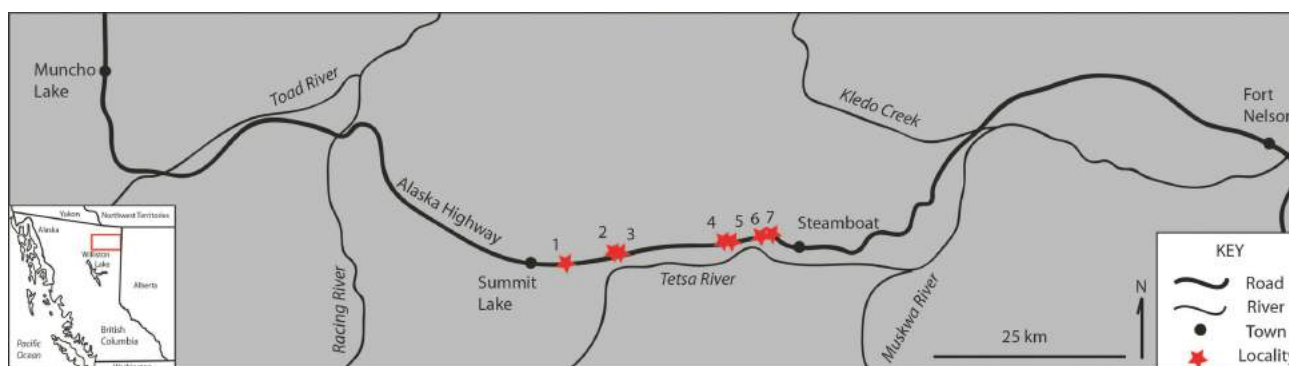


Figure 4. Location of Alaska Highway sections: 1, Mile Post 386; 2, North Tetsa Phosphate West; 3, North Tetsa Phosphate; 4, Oyster Springs; 5, Yellow Bluffs; 6, Sanitary Landfill; 7, Mile Post 375 West. Inset map modified from Zonneveld et al. (2001).

Oyster Springs

The base of the Oyster Springs section is located at Zone 10, 425012E, 6502735N and it consists of 18.53 m of siltstone, sandstone and carbonate belonging to the Liard Formation. Two conodont samples were collected (Table 2) and one detrital zircon sample was collected (Table 1). As this section has not been studied previously, its age is uncertain.

Yellow Bluffs

The base of the Yellow Bluffs section is located at Zone 10, 426835E, 6502265N and it consists of 92.5 m of siltstone and sandstone belonging to both the Toad and Liard formations. Eleven conodont samples were collected from the section (Table 2). A further two samples were collected from talus. Five detrital zircon samples were collected (Table 1). In the summer of 2011, M. Balini collected ammonoids from horizons at 1.7, 8.0 and 10.0 m above the base of the section. Previous unpublished fossil collections indicate that this section encompasses the Deleeni through Chischa zones of the Anisian.

Sanitary Landfill

The Sanitary Landfill section is located to the east of Yellow Bluffs near to an abandoned sanitary landfill. It consists of siltstone and sandstone belonging to the Toad Formation. Two conodont samples were collected, one from in situ and the other from talus (Table 2). The in situ collection was associated with ammonoids that were collected by M. Balini in the summer of 2011. The age of the section is uncertain.

Mile Post 375 West

The Mile Post 375 West section is located at mile post 375 on the Alaska Highway and is part of the Toad Formation. It was mentioned in Tozer (1967) and is the type section for the Caurus, Minor and Deleeni ammonoid zones. Four conodont samples were collected, one from Bed 1 of Tozer (1967), one from just above, one from Bed 2, and one from Bed 4 (Table 2). Bed 3 could not be located. One detrital zircon sample was collected from between the second and

third conodont samples (Table 1). M. Balini also collected ammonoids from Bed 4. Previous fossil collections indicate that this section encompasses the Caurus, Hagei, Hayesi, Minor and Deleeni Zones of the lower, middle and upper Anisian.

Subsurface Studies (NTS 093P, 094A, B)

In order to improve the correlation between surface and subsurface, five cores from wells drilled in northeastern BC were logged and sampled for conodont analysis (Table 4). Detrital zircon samples were also collected in order to ascertain whether the results from the surface sections can be replicated from the subsurface farther to the east (Table 3). The cores were selected for their geographic coverage and also because they all covered the interval of the Doig phosphate zone. This part of the Doig Formation is poorly dated but economically important as a source rock. It is thought to be anywhere from Spathian to Anisian (Zonneveld, 2010), and therefore covers the interval in which Beranek (2009) discovered evidence for sediment being derived from pericratonic terranes to the west. Recognizing such a signal in the subsurface of BC would have implications for understanding the Doig Formation and would alter the current understanding of sediment input into the WCSB at this time. The samples collected span the same interval (the boundary between the Montney and Doig formations) as those processed from the Murphy Swan well (see above). The processing of these samples is currently underway. Well locations are shown on Figure 1.

Sampling Methodology

Talisman Altares 16-17-083-25W6 Well

From the Talisman Altares 16-17-083-25W6 well, 34.00 m of core were logged, from 2267.00 to 2233.00 m below the surface (Figure 5). Six conodont samples were collected (Table 4) and 11 samples were collected for detrital zircon analysis (Table 3). The conodont sample from 2258.30 to 2257.43 m comes from the Montney Formation, all of the other samples come from the Doig Formation. This well is located in the Charlie Lake map area (NTS 094A).

Talisman Altares c-085-I/094-B-01 Well

From the Talisman Altares c-085-I/094-B-01 well, 85.00 m of core were logged, from 2375.00 to 2290.00 m below the surface (Figure 6). Five conodont samples (Table 4) and five detrital zircon samples were collected (Table 3). All of these samples come from the Doig Formation. This well is located in the Halfway River map area (NTS 094B).

Arc Dawson 07-13-79-15W6 Well

From the Arc Dawson 07-13-79-15W6 well, 5.00 m of core were logged, from 2059.00 to 2054.00 m below the surface (Figure 7). Two conodont samples (Table 4) and two detrital zircon samples were collected (Table 3). The zircon sample from 2056.35 to 2055.68 m is from the Montney Formation, all of the others come from the Doig Formation. This well is located in the Dawson Creek map area (NTS 093P).

Rocor Monias 08-22-82-20W6 Well

From the Rocor Monias 08-22-82-20W6 well, 10.60 m of core were logged, from 1781.00 to 1770.40 m below the surface (Figure 8). Two conodont samples (Table 4) and four detrital zircon samples were collected (Table 3). All the samples are from the Doig Formation. This well is located in the Charlie Lake map area (NTS 094A).

Petro-Canada Kobes d-048-A/094-B-09 Well

From the Petro-Canada Kobes d-048-A/094-B-09 well, 9.80 m of core were logged, from 1970.00 to 1960.20 m below the surface (Figure 9). Six samples were collected, with each one to be processed for both conodonts and detrital zircons (Tables 3, 4). The two samples, at 1968.25 and 1967.85 m, are from the Montney Formation, all of the others come from the Doig Formation. This well is located in the Halfway River map area (NTS 094B).

Conclusions and Future Work

Detrital zircon ages collected from the Ladinian–Carnian boundary at Glacier Spur on Williston Lake indicate derivation of at least some of the sediment from the Ellesmerian/Innuitian Orogen to the north, supporting the hypothesis of Ross et al. (1997) and Beranek (2009). None of the sections have produced any Mississippian or Permian zircons, such as those found by Beranek (2009) in the Yukon, and so as yet the hypothesis of early pericratonic terrane accretion cannot be confirmed in BC. However, the Late Triassic dates from zircon recovered from Rhaetian rocks at Black Bear Ridge indicate the possibility of a nearby Triassic igneous rock source, or perhaps even primary volcanism in the region of BC during the latest Triassic. This is significant as there is no evidence for Triassic volcanism on the craton, and so would imply a source from a pericratonic terrane to the west, possibly the Yukon-Tanana terrane. The absence of a western detrital zircon signature in particular sections may therefore be due to the

architecture of the WCSB, with these zircons not being transported to some parts of the basin.

All of this indicates a more complex pattern of sedimentation in the WCSB during the Triassic than has previously been assumed, it is not just a simple case of sediment being deposited from the east to the west. This has implications both for sedimentological analysis of the natural gas-bearing Montney and Doig formations, as well as for the tracing of facies within the basin.

Conodonts have already proved their worth in correlating beds within the Triassic (see Orchard and Tozer, 1997), and this study should contribute to a further refinement of the biostratigraphic scheme and enhanced correlation across the basin, improving the understanding of the timing of geological events during this period in BC.

The remainder of this study will focus on trying to find the Mississippian–Permian detrital zircon signal found in the Yukon. Work will be concentrated in the north of the province, to avoid the possible effects of entrainment by the Peace River embayment. This study will also try to confirm the Late Triassic detrital zircon signal found at Black Bear Ridge by examining and sampling other Rhaetian and Norian sections throughout the foothills. Analysis of whole rock geochemistry may help to determine the origin of the Late Triassic zircons; are they primary zircons from volcanic ash or are they reworked from older igneous intrusions on pericratonic terranes? The final goal of this study will be to improve the correlation of events between the surface and subsurface and further demonstrate the utility of this work in natural gas exploration.

This study provides the opportunity to understand the distribution of sedimentary facies in the WCSB in a way that is not possible simply by looking at subsurface core samples. Correlation between outcrop and the subsurface using biostratigraphy allows these facies to be traced into the subsurface where the equivalent formations contain important natural gas reserves. Understanding the distribution of sedimentary facies is important for the economic extraction of natural gas. The detrital zircon part of this study allows the provenance of the natural gas-bearing sediments to be determined. This in turn indicates the direction of transport of these sediments, which exerts an important control on the architecture of the sediments deposited in the basin. Understanding the direction of transport and therefore the architecture of the basin will also aid the extraction of natural gas. Finally, refinements that are being made to the biostratigraphic framework will allow more precise correlation of units both within the subsurface and from the subsurface to outcrop, which will in turn enable fine-scale mapping of facies across the basin and will also aid in finding more natural gas reservoirs of similar age to those already known.

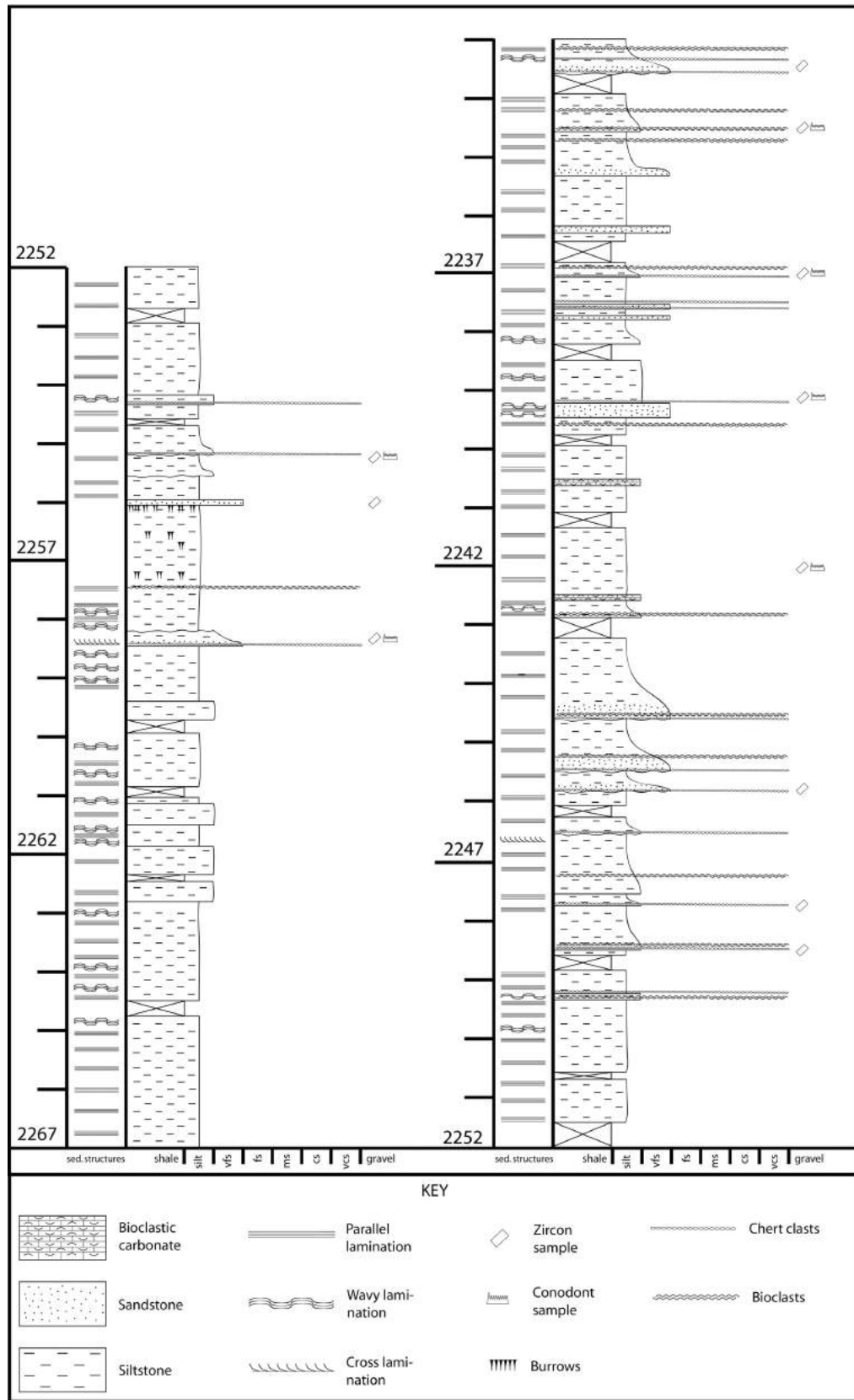
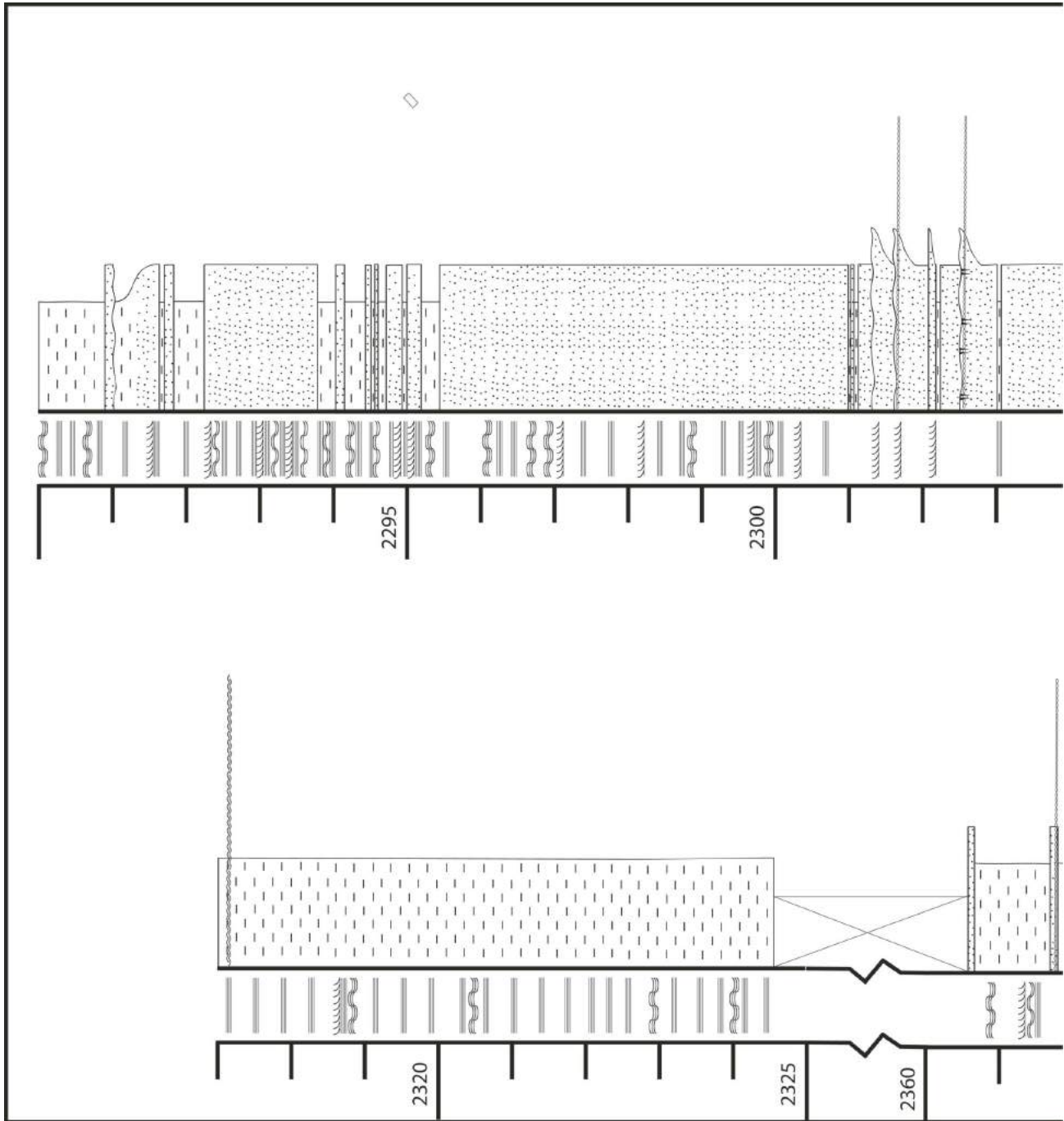


Figure 5. Sedimentary log of core from the Talisman Altares 16-17-083-25W6 well, showing location of sampled intervals. Vertical depths are shown in metres below surface. Abbreviations: cs, coarse-grained sand; fs, fine-grained sand; ms, medium-grained sand; sed, sedimentary; vcs, very coarse grained sand; vfs, very fine grained sand.



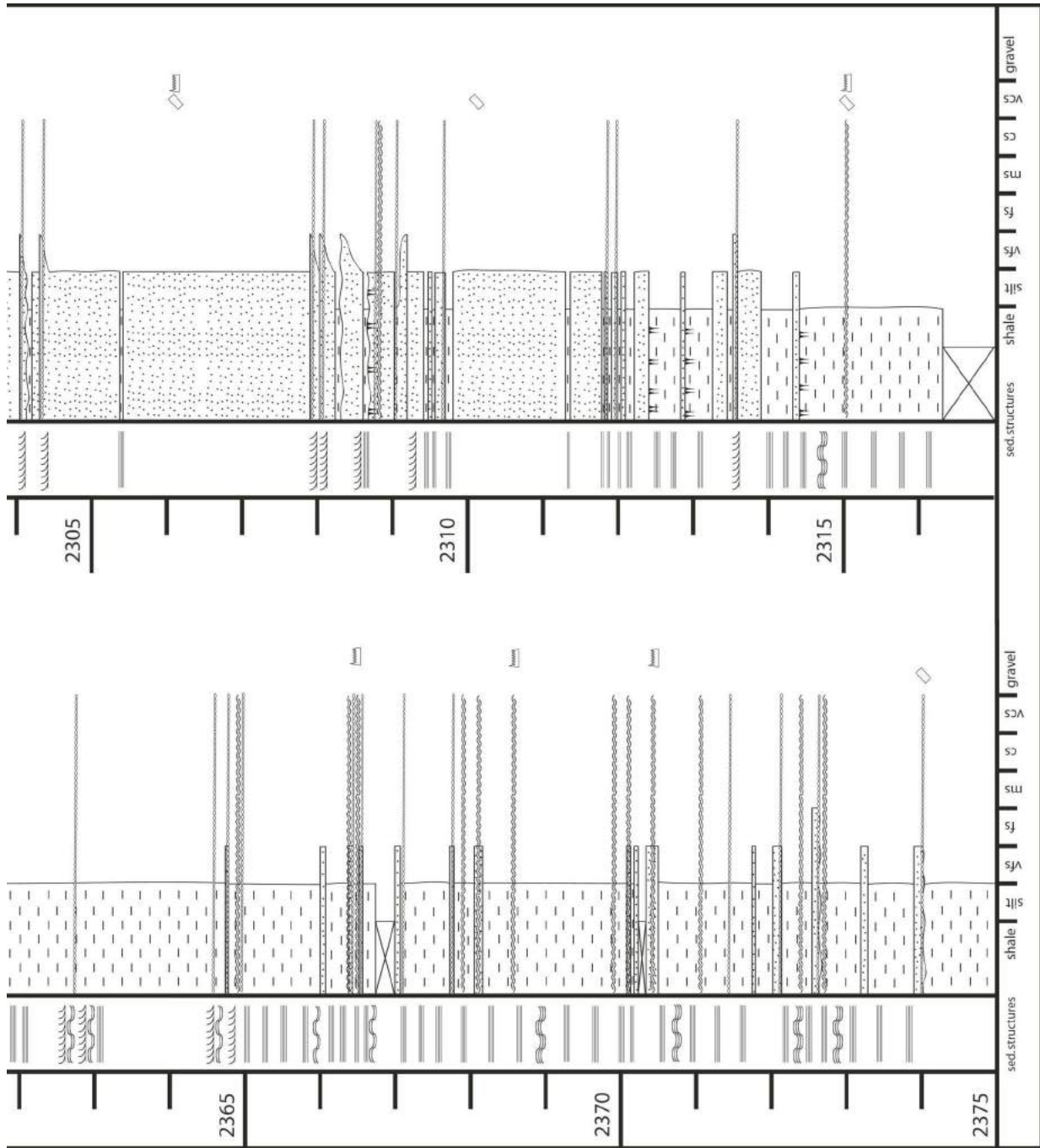


Figure 6. Sedimentary log of core from the Talisman Altares c-085-1/094-B-01 well, showing location of sampled intervals. Vertical depths are shown in metres below surface. See Figure 5 for the key to symbols. Abbreviations: cs, coarse-grained sand; fs, fine-grained sand; ms, medium-grained sand; sed, sedimentary; vcs, very coarse-grained sand; vfs, very fine-grained sand.

Acknowledgments

Funding for this project was provided by Geoscience BC. Core material was supplied by Murphy Oil Corporation. The staff at the BC Ministry of Energy and Mines core facility in Charlie Lake are thanked for their help and patience. F. Ferri provided a helpful review of the manuscript.

References

- Beranek, L. (2009): Provenance, paleotectonic setting, and depositional framework of North American Triassic strata in Yukon: the sedimentary record of pericratonic terrane accretion in the northern Canadian Cordillera; Ph.D. thesis, University of British Columbia, 338 p.
- Davies, G.R. (1997): The Triassic of the Western Canada Sedimentary Basin: tectonic and stratigraphic framework, paleogeography, paleoclimate and biota; *in* Triassic of the Western Canada Sedimentary Basin, T.F. Moslow and J. Wittenberg (ed.), Bulletin of Canadian Petroleum Geology, v. 45, p. 434–460.
- Ferri, F. (2009): Geology of the Jones Peak area (NTS 94B/02 and 07), Halfway River map sheet (94B); *in* Geoscience Reports 2009, BC Ministry of Energy and Mines, p. 5–24.
- Gibson, D.W. (1975): Triassic rocks of the Rocky Mountain Foot-hills and Front Ranges of northeastern British Columbia and

west-central Alberta; Geological Survey of Canada, Bulletin 247, 37 p.

- Golding, M.L., Ferri, F., Mortensen, J.K., Zonneveld, J-P. and Orchard, M.J. (2010): Biostratigraphic and sedimentological studies of natural gas-bearing Triassic strata in the Halfway River map area (NTS 094B), northeastern British Columbia: progress report; *in* Geoscience BC Summary of Activities 2009, Geoscience BC, Report 2010-1, p. 249–258, URL <http://www.geosciencebc.com/i/pdf/SummaryofActivities2009/SoA2009_Golding.pdf> [November 2011].
- Golding, M.L., Zonneveld, J-P., Orchard, M.J., Ferri, F. and Mortensen, J.K. (2011): Stratigraphic correlation and sedimentary provenance of Triassic natural gas-bearing rocks in northeastern British Columbia (NTS 094B): correlation of outcrop to the subsurface; *in* Geoscience BC Summary of Activities 2010, Geoscience BC, Report 2011-1, p. 229–238, URL <http://www.geosciencebc.com/i/pdf/SummaryofActivities2010/SoA2010_Golding_etal.pdf> [November 2011].
- Hunt, A.D. and Ratcliffe, J.D. (1959): Triassic stratigraphy, Peace River area, Alberta and British Columbia, Canada; American Association of Petroleum Geologists, Bulletin 43, p. 563–589.
- McLearn, F.H. (1946): A Middle Triassic (Anisian) fauna in Halfway, Sikanni Chief and Tetsa valleys, northeastern British Columbia; Geological Survey of Canada, Paper 46-1, 23 p.

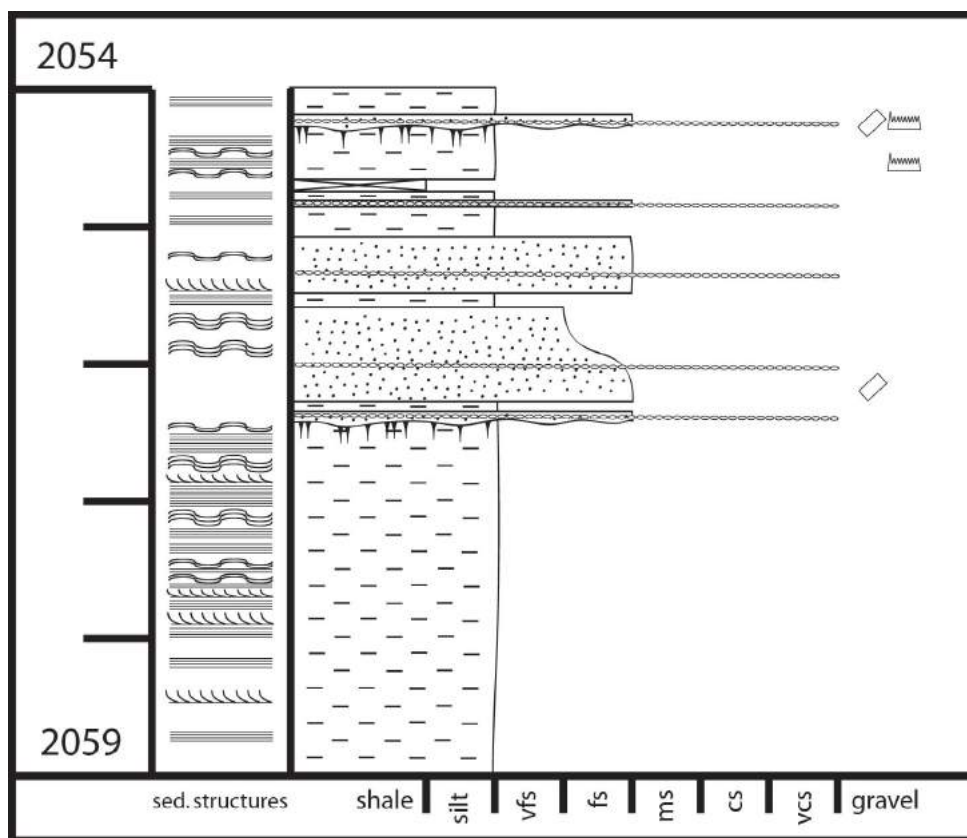


Figure 7. Sedimentary log of core from the Arc Dawson 07-13-79-15W6 well, showing location of sampled intervals. Vertical depths are shown in metres below surface. See Figure 5 for the key to symbols. Abbreviations: cs, coarse-grained sand; fs, fine-grained sand; ms, medium-grained sand; sed, sedimentary; vcs, very coarse grained sand; vfs, very fine grained sand.

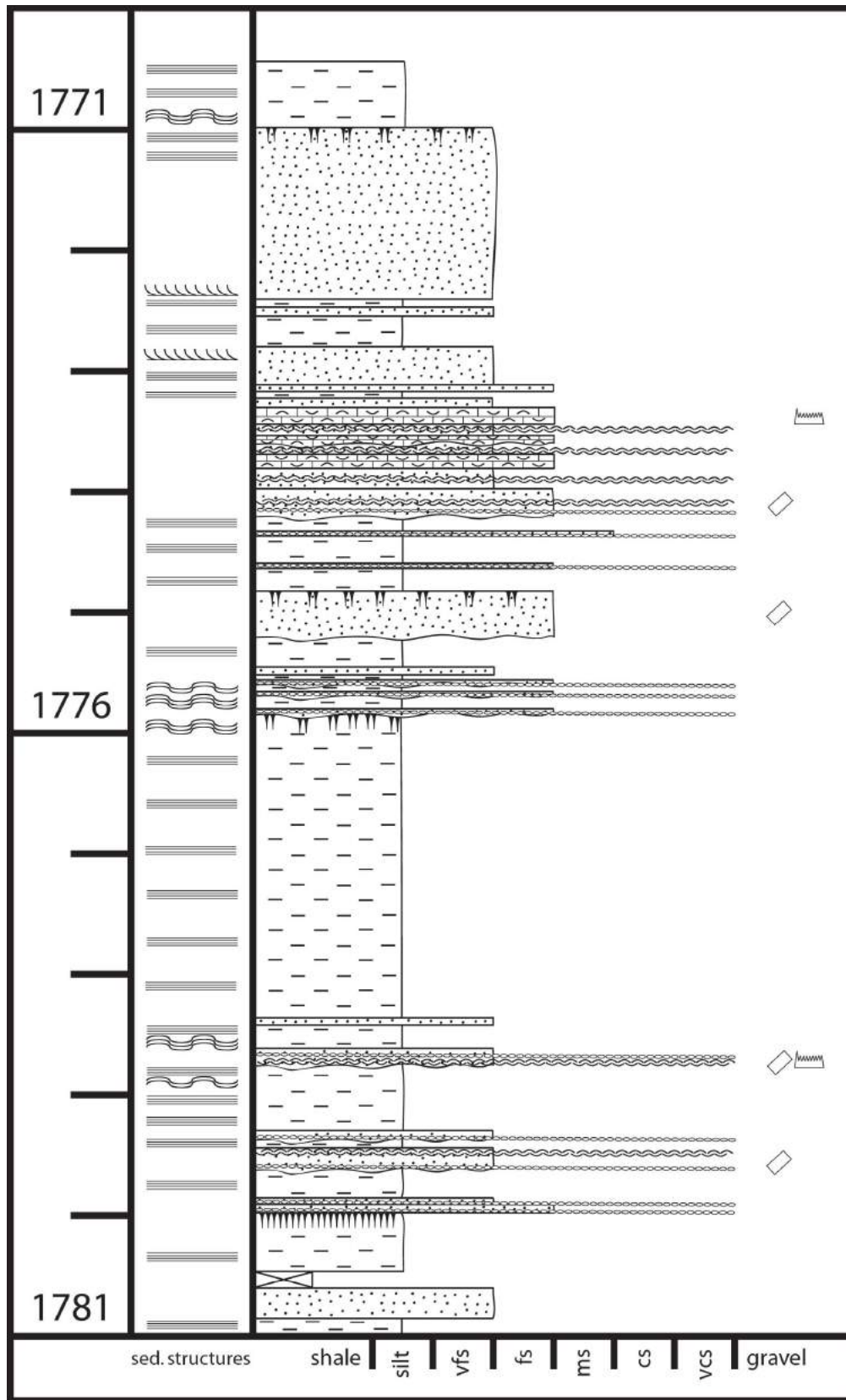


Figure 8. Sedimentary log of core from the Rocor Monias 08-22-82-20W6 well, showing location of sampled intervals. Vertical depths are shown in metres below surface. See Figure 5 for the key to symbols. Abbreviations: cs, coarse-grained sand; fs, fine-grained sand; ms, medium-grained sand; sed, sedimentary; vcs, very coarse grained sand; vfs, very fine grained sand.

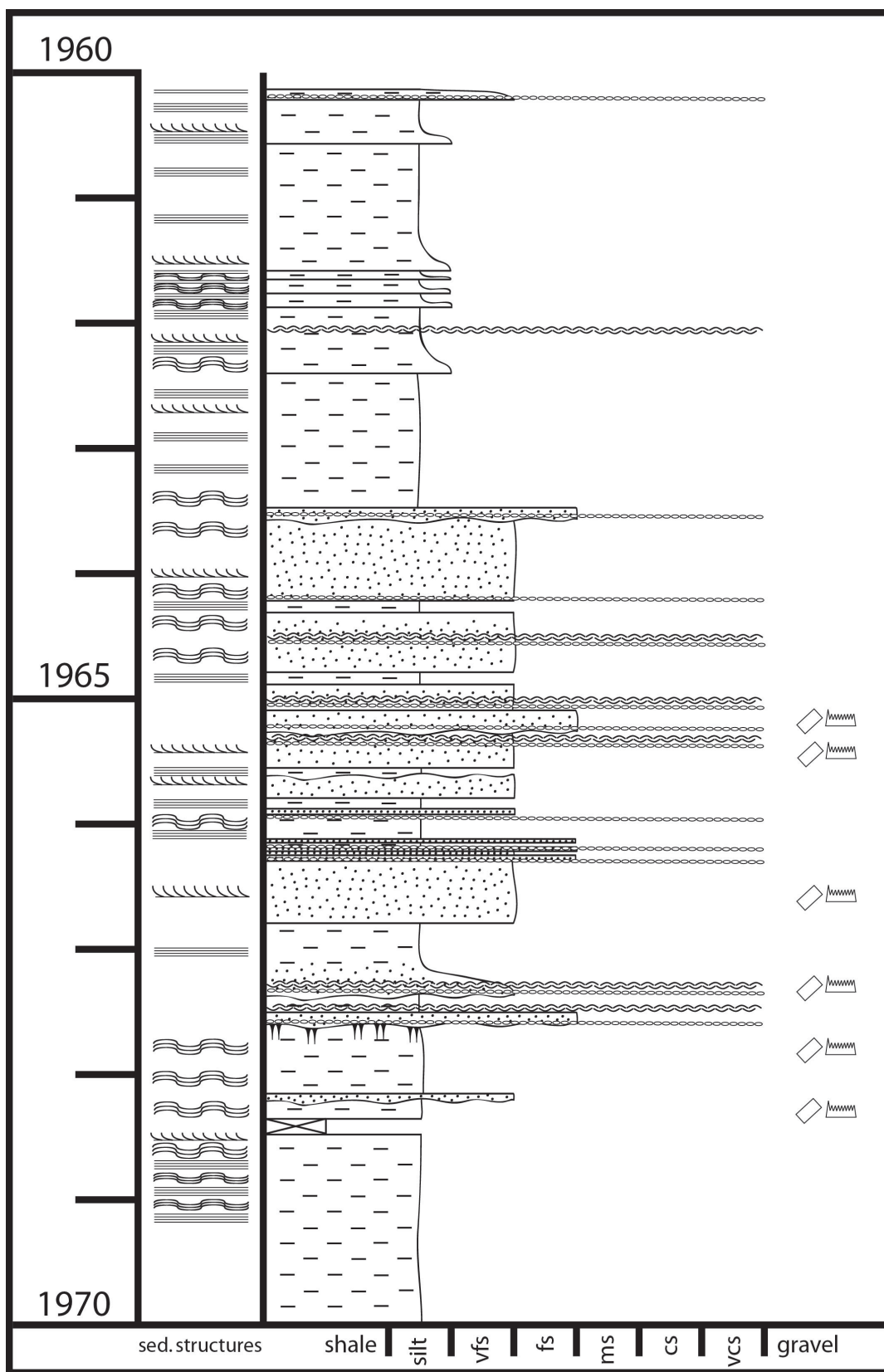


Figure 9. Sedimentary log of core from the Petro-Canada Kobes d-048-A/094-B-09 well, showing location of sampled intervals. Vertical depths are shown in metres below surface. See Figure 5 for the key to symbols. Abbreviations: cs, coarse-grained sand; fs, fine-grained sand; ms, medium-grained sand; sed, sedimentary; vcs, very coarse grained sand; vfs, very fine grained sand.

- Monger, J.W.H. and Price, R.A. (2002): The Canadian Cordillera: geology and tectonic evolution; Canadian Society of Exploration Geophysicists Recorder, February, p. 17–36, URL <[https://www.geology.ucdavis.edu/~shlemonc/html/trips/skeena_river/documents/journals/Monger\(2002\).pdf](https://www.geology.ucdavis.edu/~shlemonc/html/trips/skeena_river/documents/journals/Monger(2002).pdf)> [November 2011].
- Nelson, J.L., Colpron, M., Piercey, S.J., Dusel-Bacon, C., Murphy, D.C. and Roots, C.F. (2006): Paleozoic tectonic and metallogenic evolution of the pericratonic terranes in Yukon, northern British Columbia and eastern Alaska; *in* Paleozoic Evolution and Metallogeny of Pericratonic Terranes at the Ancient Pacific Margin of North America, Canadian and Alaskan Cordillera, M. Colpron and J.L. Nelson (ed.), Geological Association of Canada, Special Paper 45, p. 323–360.
- Orchard, M.J. and Tozer, E.T. (1997): Triassic conodont biochronology, its calibration with the ammonoid standard, and a biostratigraphic summary for the Western Canada Sedimentary Basin; *in* Triassic of the Western Canada Sedimentary Basin, T.F. Moslow and J. Wittenberg (ed.), Bulletin of Canadian Petroleum Geology, v. 45, p. 675–692.
- Pelletier, B.R. (1965): Paleocurrents in the Triassic of northeastern British Columbia; *in* Primary Sedimentary Structures and their Hydrodynamic Interpretation, G.V. Middleton (ed.), SEPM (Society for Sedimentary Geology), Special Publication 12, p. 233–245.
- Ross, G.M., Gehrels, G.E. and Patchett, P.J. (1997): Provenance of Triassic strata in the Cordilleran miogeocline, western Canada; Bulletin of Canadian Petroleum Geology, v. 45, p. 461–473.
- Thompson, R.I. (1989): Stratigraphy, tectonic evolution and structural analysis of the Halfway River map area (94B), northern Rocky Mountains, British Columbia; Geological Survey of Canada, Memoir 425, 119 p.
- Tozer, E.T. (1967): A standard for Triassic time; Geological Survey of Canada, Bulletin 156, 141 p.
- Walsh, W., Adams, C., Kerr, B. and Korol, J. (2006): Regional “shale gas” potential of the Triassic Doig and Montney formations, northeastern British Columbia; BC Ministry of Energy and Mines, Resource Development and Geoscience Branch, Petroleum Geology Open File 2006-02, 20 p., URL <<http://142.32.76.167/Mining/Geoscience/PublicationsCatalogue/OilGas/OpenFiles/Documents/PetroleumGeology/PGOF2006-2.pdf>> [November 2011].
- Zonneveld, J-P. (2010): The Triassic of northeastern British Columbia: sedimentary characteristics and stratigraphic architecture of conventional and unconventional reservoir successions; Geological Association of Canada–Mineralogical Association Joint Annual Meeting (GeoCanada 2010), Williston Lake Field Trip Guidebook, 158 p.
- Zonneveld, J-P., Gingras, M.K. and Pemberton, S.G. (2001): Trace fossil assemblages in a Middle Triassic mixed siliciclastic-carbonate marginal marine depositional system, British Columbia; Palaeogeography, Palaeoclimatology, Palaeoecology, v. 166, p. 249–276.
- Zonneveld, J-P., Moslow, T.F. and Henderson, C.M. (1997): Lithofacies associations and depositional environments in a mixed siliciclastic-carbonate depositional system, upper Liard Formation, Triassic, northeastern British Columbia; Bulletin of Canadian Petroleum Geology, v. 45, p. 553–575.

Chronostratigraphic and Tectonostratigraphic Summary of the Late Paleozoic and Early Triassic Succession in East-Central British Columbia (NTS 093I, O, P)

C.M. Henderson, University of Calgary, Calgary, AB, cmhender@ucalgary.ca

K.D. Zubin-Stathopoulos, University of Calgary, Calgary, AB

G.J. Dean, Chesapeake Energy Corporation, Oklahoma City, OK

Henderson, C.M., Zubin-Stathopoulos, K.D. and Dean, G.J. (2012): Chronostratigraphic and tectonostratigraphic summary of the Late Paleozoic and Early Triassic succession in east-central British Columbia (NTS 093I, O, P); in Geoscience BC Summary of Activities 2011, Geoscience BC, Report 2012-1, p. 115–124.

Introduction

The northwest margin of Pangea during the late Paleozoic has been historically depicted as a relatively passive margin (Barclay et al., 1990), but there is increasing evidence for active compressive tectonics. The latest Devonian Antler orogeny is recognized in the Roberts Mountain allochthon in central Nevada (Dickinson, 2006), and evidence for this event is present within the pericratonic Kootenay terrane in southern British Columbia (Richards, 1989; Dickinson, 2004). The Sonoma orogeny is recorded in the western United States by latest Permian to earliest Triassic thrusting of the Havallah Basin succession over the Antler Belt (Brueckner and Snyder, 1985; Dickinson, 2006). Several additional deformation events are recognized between the Antler and Sonoma events in the western United States during the Mississippian to Permian (Trexler et al., 2003, 2004). Critical to our understanding of the evolution of the Cordilleran margin in Canada and the United States is whether these collision and assembly events affected the North American margin or occurred in the Panthalassic Ocean, as in the SAYBIA model of Johnston (2008) and RUBIA model of Hildebrand (2009). S. Johnston (2008) argued that the best evidence for a ribbon continent forming well away from the North American margin is the fact that there was no evidence of loading causing isostatic flexure of the lithosphere within the 'Rocky Mountain Platform' (i.e., the Front Ranges of the Canadian Rockies). Root (2001), however, proposed that a Middle Devonian (upper Eifelian) event mapped in southeastern BC resulted in the development of a peripheral bulge in the Front Ranges where Frasnian strata unconformably overlie Middle Cambrian units. He suggested that this was an early manifestation of the Antler event, but admitted that one problem with his interpretation was the lack of evidence for activity on

this bulge during the Antler orogeny in latest Devonian to Early Carboniferous. However, D. Johnston et al. (2010), using a detailed isopach map based on both surface sections and subsurface wells, and supported by high-resolution conodont biostratigraphy, showed that the lack of Early Tournaisian strata of the upper Exshaw and middle Bakken formations in southwestern Alberta may indicate slight eastward migration of this same peripheral bulge. In addition, research during the past ten years on the North American craton of west-central Alberta and east-central British Columbia (BC) has shown evidence for structural inversion of block faults during the Late Paleozoic and earliest Triassic (Kendall, 1999; Panek, 2000; Fossenier, 2002; Henderson et al., 2002; Dunn, 2003; Henderson et al., 2010; Zubin-Stathopoulos et al., 2011) that significantly affects the paleogeography of the margin and the potential for hydrocarbon resources.

This paper builds on the initial stratigraphic framework of Bamber and Macqueen (1979), and represents a summary of three years of research in east-central BC that includes other evidence in support of tectonic controls on the cratonic platform succession during the Pennsylvanian and Permian. These effects, which are sometimes subtle, are now recognized because we re-examined, using high-resolution biostratigraphy, the timing of widespread unconformities that correlate all the way to Nevada. The complexity of the tectonostratigraphic framework means that this research summary is really only a beginning.

Study Area and Methods

Field sites for this study are located in the Sukunka-Kakwa area within NTS areas 093P, I and O (Figure 1), and have been described previously by Henderson et al. (2010) and Zubin-Stathopoulos et al. (2011). The outcrops are located southeast of Chetwynd, BC and are part of a southeast-trending outcrop belt that represents the westernmost extent of the Western Canada Sedimentary Basin. Outcrops were accessed by helicopter due to the remote nature of the sites. The approach was to combine high-resolution cono-

Keywords: *Pennsylvanian, Permian, Lower Triassic, conodont biostratigraphy, tectonostratigraphic framework*

This publication is also available, free of charge, as colour digital files in Adobe Acrobat® PDF format from the Geoscience BC website: <http://www.geosciencebc.com/s/DataReleases.asp>.

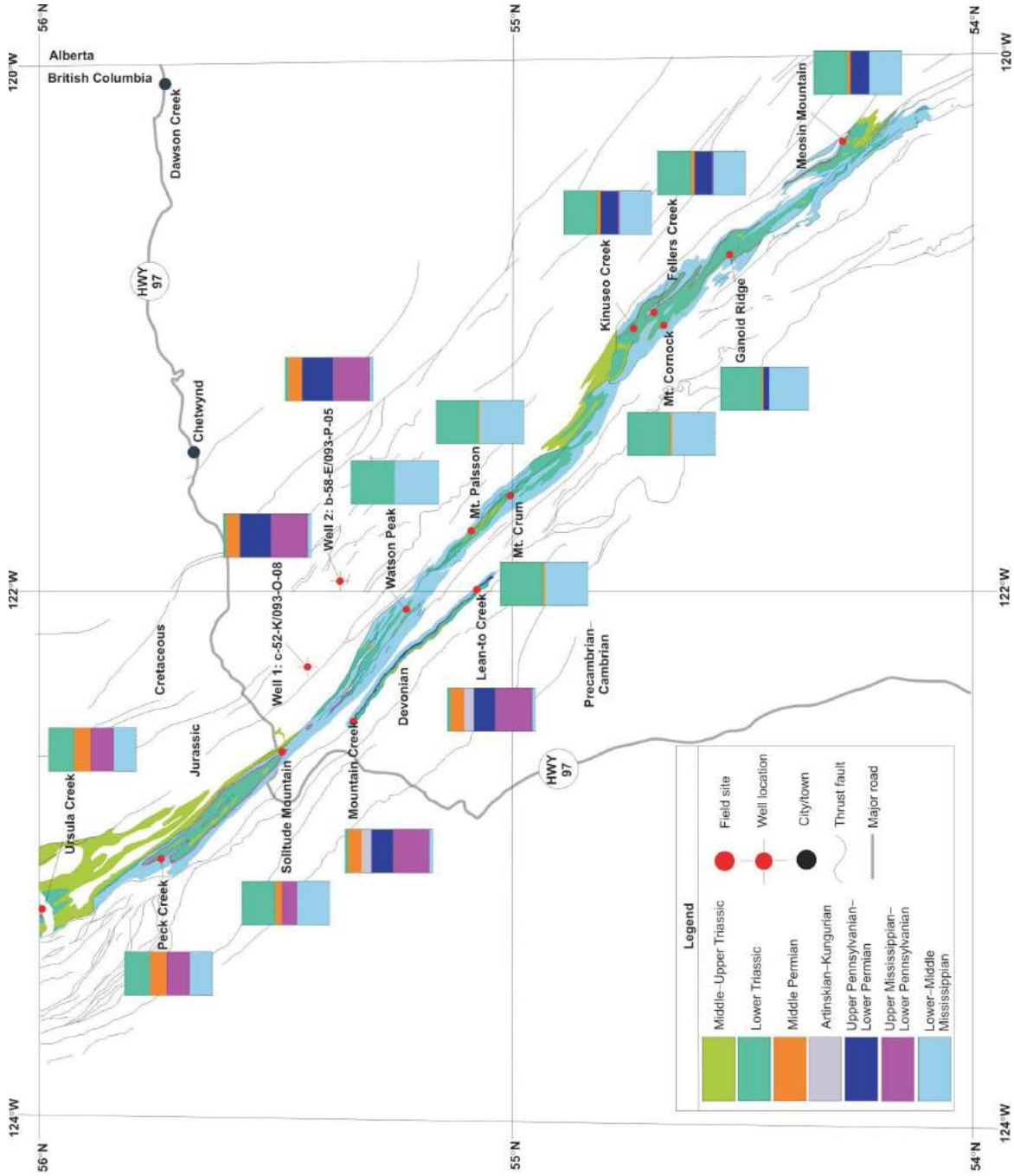


Figure 1. Study area showing studied sections and Mississippian to Triassic geology (not palinspastically restored). Schematic stratigraphic summary columns show that the overall preserved succession more or less parallels the individual thrust sheets, with the most complete succession in the westernmost sheet that includes the Mountain Creek and Lean-to Creek locations, which are the only locations in the region preserving Artinskian to Kungurian strata. Note missing Early Permian strata at Watson Peak, Mount Pailsson, Mount Crum and Mount Cornock, defining a southeast-trending western paleohigh. Modified from Zubin-Stathopoulos et al. (2011).

dent biostratigraphy with detailed section measurement and some mapping.

Evidence for Pennsylvanian–Permian Tectonics

This section summarizes the evidence for several tectonic events and highlights some of the implications each has in terms of diagenesis, fracture distribution and unit preservation. The primary line of evidence is identification and duration of unconformities within the Pennsylvanian–Permian of the study area, as determined by detailed conodont biostratigraphy (Fossenier, 2002; Dunn, 2003; Zubin-Stathopoulos, 2011). The biozonation scheme for the area was previously provided in Zubin-Stathopoulos et al. (2011). Comparisons are made to tectonostratigraphic events documented in the southwestern United States.

C4/C5 Moscovian Event

The lower Belloy Carbonate Member (Halbertsma, 1959; type section in the 12-14-78-1W6 well) was later referred to as the Ksituan Member of the Belloy Formation (Henderson et al., 1994), and a paper is in preparation to name this unit as a new formation (see Zubin-Stathopoulos, 2011). It is a distinct unit that is separated from the rest of the Belloy Formation by an entire stratigraphic sequence (Figure 2). It is contemporaneous with a post–Taylor Flat extensional event in which a peritidal to open-marine carbonate succession is widely distributed from west-central Alberta to east-central BC (Porter, 2007). The peritidal succession in Alberta is generally dolomitized and represents an important hydrocarbon-bearing unit in a relatively simple stratigraphic-fault play (see Progress Field in Dunn, 2003). In BC, the unit is variably dolomitized and represents a very important gas play in a thrust structural play, but there are many complications (see ‘Hydrocarbon Implications’). This event and overlying strata resulted in the Ely Basin in Nevada (Trexler et al., 2004).

C6 Kasimovian and P1 Asselian Events

The C6 event is one of the more prominent in Nevada that resulted in a major angular unconformity, which is especially well displayed at Carlin Canyon (Trexler et al., 2004) in the northwestern part of the Dry Mountain Trough (Figure 3). The C6 and P1 unconformities in Nevada truncate structures of two distinct events, including thrust faults and overturned folds in the C6 event and more open folds and high-angle normal faults just before the P1 unconformity (Trexler et al., 2004). We have not resolved such intense compression structures in east-central BC because the record is mostly in the subsurface and some units have been eroded. However, considerable local evidence points to this being an important tectonostratigraphic event in the region. In Alberta, the Ksituan Formation was subaerially exposed and accompanied by dolomitization and karst development

(Porter, 2007). This could be attributed simply to a lowstand of sea level, but the development of highs and basins to the west suggests that it was more complex. Zubin-Stathopoulos et al. (2011) provided evidence that a western paleohigh and eastern interior sea developed during this event (Figure 2). Local uplift removed much of the previous record of Moscovian carbonate rocks (Figure 2) and some of these clasts are found within the Asselian to lower Sakmarian Belcourt Formation. These structures were large enough to affect carbonate sedimentation that included warm-water associations in the shallow interior sea (Belcourt Formation), cool-water associations west of the paleohigh in the newly defined Mountain Creek Formation (see paper in preparation in Zubin-Stathopoulos 2011) and a thick carbonate mudstone unit in well C-52-K (Figure 2).

P2 Artinskian Event

The P2 event is a major unconformity at the regional scale in Nevada that involved the development of the Dry Mountain Trough, but the deformation geometry is less clear (Trexler et al., 2004). This event may also correlate with the Melvillian Disturbance (Beauchamp, 1995) in the Sverdrup Basin of the Canadian Arctic. In east-central BC, rocks overlying the P2 unconformity are missing except for thin units of the Kindle Formation at Mountain Creek and Lean-to Creek in westernmost exposures. At the same time, to the east in the subsurface of west-central Alberta, a new basin developed in which Belloy Formation siliciclastic rocks and minor bioclastic carbonate were deposited (Figures 2, 3). Presumably, a broad high developed that restricted these Artinskian-age deposits to the Peace River Basin (Figure 3). Sandy carbonate rocks of this age are also present in the Telford Basin (Figure 3) to the south (MacRae and McGugan, 1977). This broad high in east-central BC appears to have resulted from the amalgamation of the Sukunka Uplift and the Beatton High, which were separate structures before the Artinskian (Henderson et al., 1994); it also encompasses the western paleohigh and interior sea generated by the C6-P1 event (Figure 2). Such an extensive structure may be interpreted as a peripheral bulge (Figure 3) and the Peace River Basin as a back-bulge basin (see ‘Tectonostratigraphic Implications’). Dunn (2003) mapped Artinskian and Kungurian lithofacies that included braid deltas and what was interpreted as a barrier island with root traces paralleling the Alberta-BC border. With the interpretation of the peripheral bulge, these units can now be interpreted as a beach on the western margin of the Peace River Basin, with an adjacent braid delta indicating sediment sources from the south and west. The remainder of the marginal-marine facies in the Peace River Basin (Figure 3) includes carbonate-rich subtidal to supratidal bioclastic sandstone, with ‘early’ vadose cement locally forming beach rock.

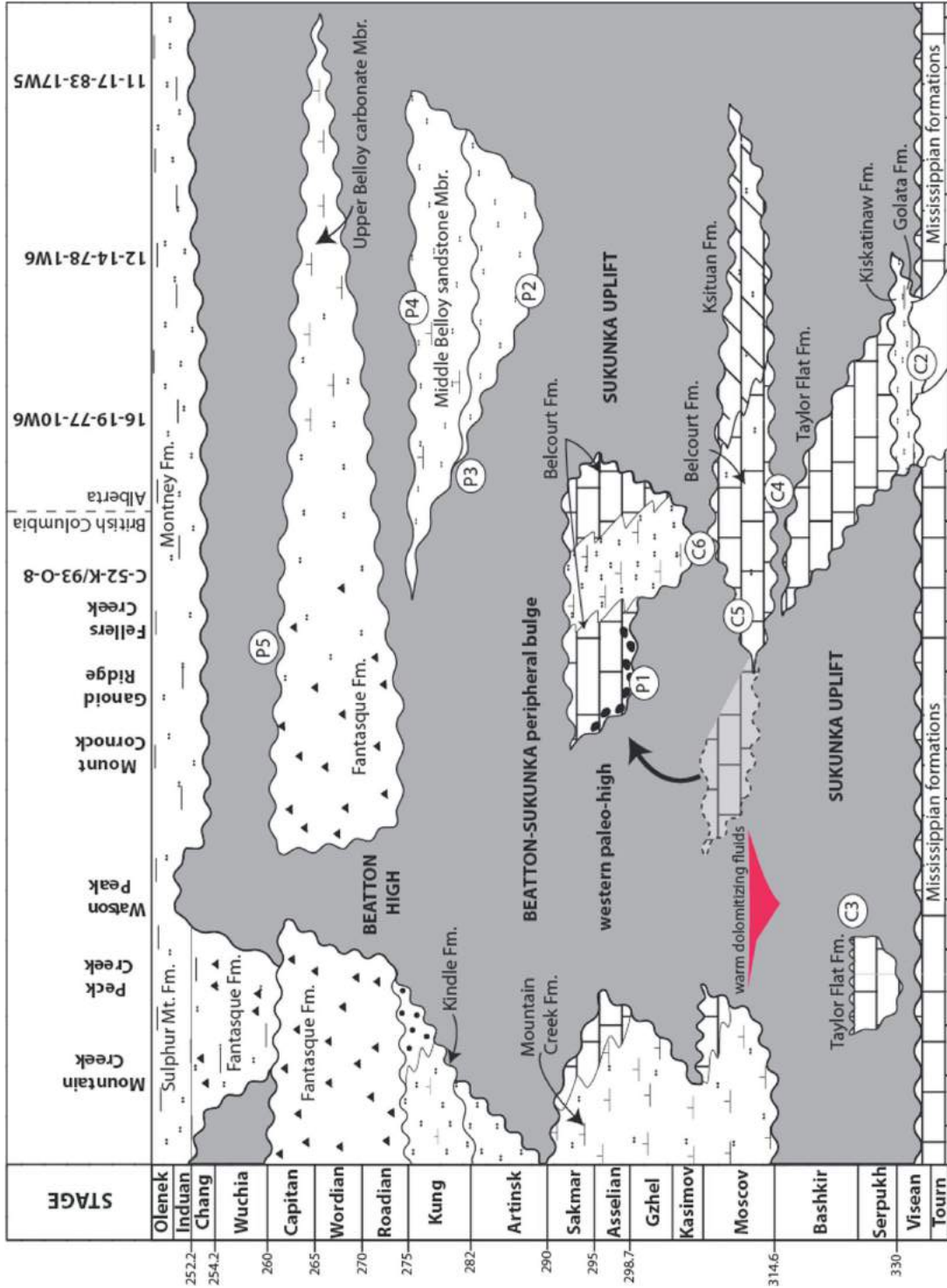


Figure 2. Chronostratigraphic diagram showing temporal and spatial distribution of major units in east-central British Columbia to west-central Alberta. The C6 event resulted in a western paleohigh that caused erosion of the underlying Moscovian succession and local deposition of Moscovian-age clasts within Early Permian sediments. The Beatton-Sukunka peripheral bulge is interpreted to have formed during P2 deformation, which also potentially drove warm dolomitizing fluids into the underlying succession. Abbreviations: Tourn, Tournaisian; Serpukh, Serpukhovian; Bashkir, Bashkirian; Moscov, Moscovian; Kasimov, Kasimovian; Gzhel, Gzhelian; Sakmar, Sakmarian; Artinsk, Artinskian; Kung, Kungurian; Capitan, Capitanian; Wuchia, Wuchiapingian; Chang, Changhsingian; Olenek, Olenekian. Modified from Zubin-Stathopoulos (2011). Locations of Alberta wells: 16-19-77-10W6 (55.6922°N, 119.5292°W; UTM Zone 11, 3414025E, 6174721N); 12-14-78-1W6 (55.7614°N, 118.0491°W; UTM Zone 11, 434168E, 6180024N); 11-17-83-17W5 (56.1974°N, 116.6534°W; UTM Zone 11, 521504E, 6228001N).

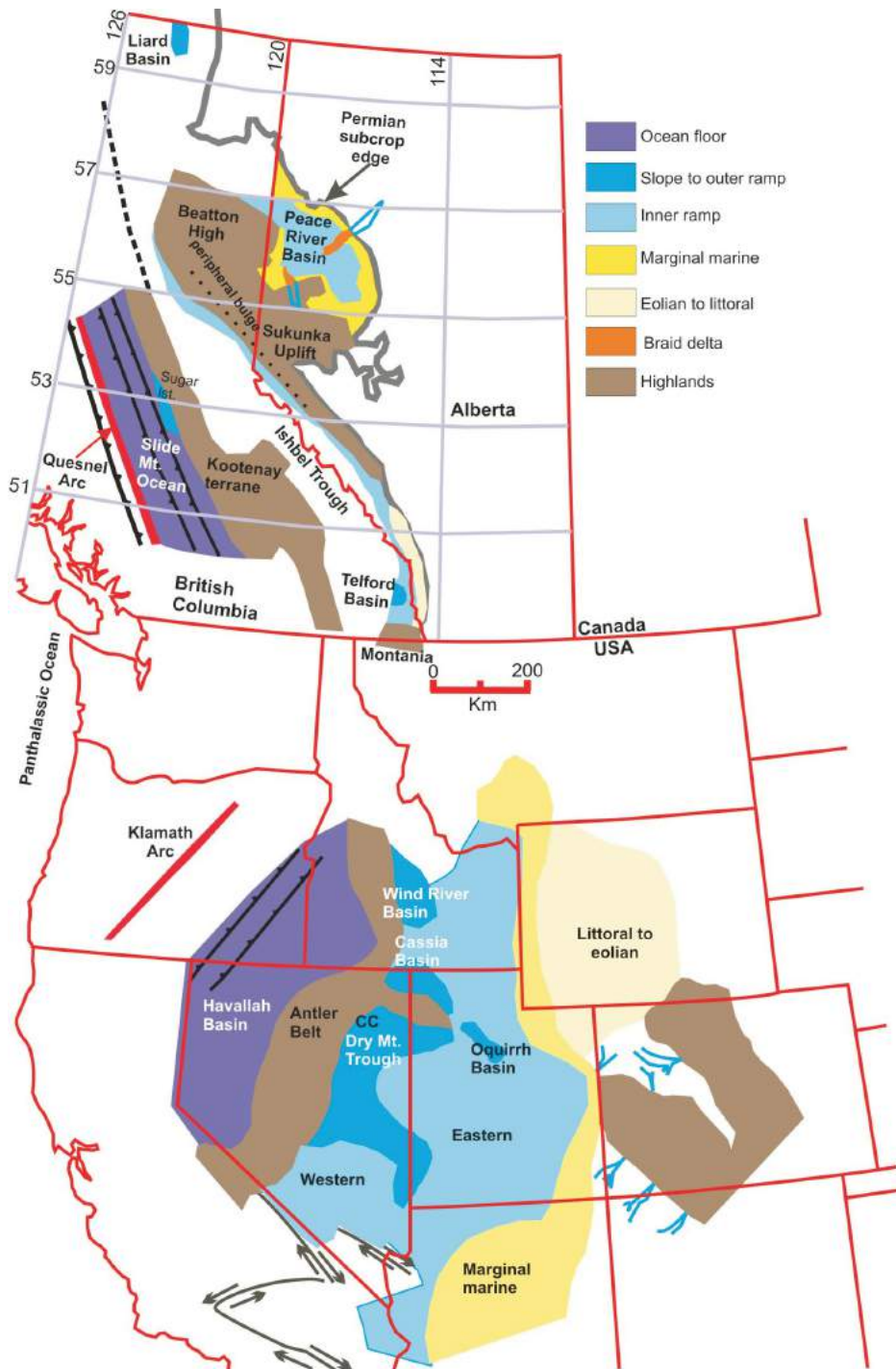


Figure 3. Schematic paleogeography of the western United States to northeastern British Columbia (BC) for the early Artinskian (modified from Zubin-Stathopoulos et al., 2011). Dotted line in Beatton High area represents former position of late Asselian interior seaway. Dashed line in northeastern BC represents southernmost position of younger dextral Tintina strike-slip fault. The geotectonic history for the succession south of this position is markedly different from that to the north. The Yukon-Tanana terrane (see several papers in Colpron and Nelson [2006], including Nelson et al. [2006]) may represent the western margin of the Slide Mountain Ocean that was later transported along strike-slip faults, including possible transfer of strike-slip motion to Permian westerly facing subduction-zone boundaries. The Lower Permian Sugar Limestone (Orchard and Struik, 1985) was deposited on the eastern margin of the Slide Mountain Ocean. The axis of the Devonian Peace River Arch and Carboniferous to Triassic Peace River Basin is perpendicular to this position as well. Position of tectonic elements is, in part, based on Gabrielse et al. (1991), Henderson et al. (1993), Wardlaw et al. (1995) and Nelson et al. (2006). Peace River Basin lithofacies from Dunn (2003). Tectonic nomenclature based on Snyder et al. (2002). Abbreviation: CC, Carlin Canyon.

P3 Kungurian Event

This is a relatively minor event in both Nevada and east-central BC, and may be attributed to a relative lowstand of sea level, as is characteristic of the Kungurian globally, or to reduced rates of subsidence and filling of the basin created by the P2 event. Artinskian and Kungurian inner-ramp facies of the Kindle Formation in east-central BC (Figure 3) and the Johnston Canyon Formation in southwestern Alberta have cool-water associations and typically are quite phosphatic.

P4 Roadian Event

This is a major event that represents the formation of the Phosphoria Basin, centred in northeastern Nevada and southern Idaho, and the development of an important intra-Permian unconformity in southeastern to east-central BC, which is overlain by a persistent thin-shelf deposit referred to as the Ranger Canyon and Fantasque formations. The Phosphoria Basin is widespread and overlaps many Early Permian tectonic basins. The Ranger Canyon Formation is also widespread (McGugan, 1965) and, in at least one locality (Crossing Creek in southeastern BC), overlies the Artinskian to Lower Kungurian Johnston Canyon Formation as an angular unconformity (McGugan and Rapson, 1962), with a phosphatic conglomerate at the base. McGugan (1965) suggested that such widespread but relatively thin deposits are more likely to be controlled by eustasy than by tectonics. The latest Kungurian to Early Roadian represents a global sea-level rise and may indicate a time of tectonic quiescence on the margin (see ‘Tectonostratigraphic Implications’).

P5 Capitanian Event

This event was a major lowstand of sea level that resulted in subaerial exposure of most of the margin. There is biostratigraphic evidence that the Fantasque Formation at Peck Creek and Ursula Creek in northeastern BC includes continuous deposition through the Late Permian (Figure 2) into the Early Triassic (Henderson, 2011). These sites were located on the down-faulted eastern margin of the Ishbel Trough.

P6 Late Changhsingian Event

This event is recognized as a combination of probable eustatic rise and tectonic-basin reorganization, including inversion of various structural elements, and requires further mapping. It coincides in timing with the Sonoman orogeny, which is better understood in the western United States, where the Havallah sequence is thrust upon coeval successions on the North American craton (Brueckner and Snyder, 1985). The Mount Crum section (Figure 1) was high during the Early Induan (Griesbachian), suggesting that collapse of the Beatton High north of this locality created a site for earliest Triassic deposition and the important

shale-gas fairway of the Montney Formation north of about 55.5°N. Zonneveld et al. (2010) also suggested an earliest Triassic sub-basin in the Ring-Border to Kahntah River fields, at about 58°N on the BC-Alberta border.

Tr1 Late Induan Event

This event is also associated with inversion of various structural elements (Kendall, 1999; Panek, 2000) and requires further mapping. The fact that turbidite successions, which may be driven by tectonically controlled slope steepening, are diachronous (Late Induan through Olenekian) across the region (Kendall, 1999; Orchard and Zonneveld, 2009; Henderson, 2011) points to the need for detailed mapping and biostratigraphic analysis.

Discussion and Conclusion

Tectonostratigraphic Implications

Nelson et al. (2006) and Colpron and Nelson (2011) summarized a model in which the Slide Mountain Ocean was the locus for back-arc seafloor spreading from mid-Carboniferous to Middle Permian, followed by a reversal in which the North American continent advanced upon the frontal arc with the back-arc basin closure attributed to the Late Permian–Early Triassic Sonoman orogeny. It is possible that such ‘accordion tectonics’ had another beat to it, as evidence continues to emerge supporting episodic thin-skinned deformation affecting the North American margin between the Antler and Sonoman orogenies. This requires an active orogenic belt to the west that affects the North American (northwestern Pangea) margin from the latitude of at least northern Nevada to east-central BC. If the broad structure affected by the P2 event is a peripheral bulge, as interpreted herein, then there must have been active uplift to the west that provided sufficient load to cause isostatic flexure of undisputed North American margin rocks in east-central BC. It is interesting that imbricate thrusts mapped within the Antler Formation of the Slide Mountain terrane near Wells in central BC involve rocks no younger than Early Permian (Struik and Orchard, 1985). This event may then have been followed by renewal of back-arc spreading, with the Slide Mountain Ocean growing to a significant extent during the early Middle Permian when the thin, widespread Fantasque Formation was deposited across east-central BC as an overlap succession, much like the coeval Phosphoria Basin to the south. Using mean global seafloor-spreading rates of 40–70 km/m.y. (Seton et al., 2009) for comparison only (Slide Mountain Ocean rates are unknown) would create an ocean at least 600–1050 km wide during the Artinskian and Kungurian, and 1200–2100 km wide if spreading also continued through the Middle Permian. A second closure of this ocean during latest Permian would then have resulted in the obduction of Slide Mountain Ocean rocks onto the Kootenay terrane, resulting in the Sonoman orogeny.

These interpretations must be reconciled with the suggestions, based on faunal similarities, by Belasky et al. (2002) that the Stikine, Quesnel and Klamath arc terranes must have been 2000–3000 km away from their latitudinal equivalents on the North American craton during the Early Permian. The driving force for these tectonic events remains equivocal, but a new dimension has been added to the discussion. This new dimension is the fact that successions on undisputed North America (the Rocky Mountain Platform of Johnston, 2008) are affected by isostatic flexure in both extensional and compressional settings at different times. This means that the Ishbel Trough was a foreland basin at various times during the Late Paleozoic and at least semi-isolated from open Panthalassic Ocean. This would seem to negatively affect one line of evidence for a single SAYBIA collision during the Late Cretaceous, but the presence of phosphate-rich facies on the eastern margin of an isolated, narrow Ishbel Trough remains a problem.

Clearly the region from central BC to west-central Alberta is critical to resolve events associated with the evolution of the North American Cordillera during the Late Paleozoic and Early Mesozoic, so we initiated a restudy of the Barkerville terrane, including the Sugar Limestone, during the summer of 2011. Furthermore, increased resolution of Cordilleran evolution will lead to a better understanding of the events that affected reservoir quality and natural gas resources in east-central BC.

Hydrocarbon Implications

The results of this study provide evidence for active tectonics creating paleogeographic highs that confine some depositional units and result in the erosion of others. Overall, the Late Paleozoic and earliest Triassic stratigraphy in east-central BC is punctuated by numerous unconformities. Two of the most important tectonic events (C6 and P2) in the region may have significant hydrocarbon implications. The most important conventional-gas reservoirs in the region are Moscovian carbonate units, but preservation is strongly affected by the C6 event (Figure 2). The P2 event is interpreted to have formed a peripheral bulge in the region, suggesting compressive tectonics to the west that may have also driven warm dolomitizing fluids into the underlying sequences (Figure 2). Wamsteeker (2007) indicated that Moscovian shelf carbonate rocks were subjected to three major diagenetic events: eogenetic processes, hydrothermal dolomitization by about 150°C fluids enriched in ¹⁸O relative to Pennsylvanian seawater, and calcite veins in Laramide fractures. Moscovian carbonate rocks may have dolomitized preferentially along pre-existing faults and fractures in the region, indicating that the best porosities in the area would be more predictable if paleostructures in the region were better known. The warm fluids may also account for the thermal-maturity anomaly (Ing and Henderson, 2009) in the region in which Pennsylvanian

rocks have higher-than-expected CAI (Colour Alteration Index from Conodonts) values compared to values in the overlying Permian (especially of Artinskian and younger). Finally, there is likely a strong inheritance between the position of Pennsylvanian and Permian faults and the breakout of Late Cretaceous thrust faults that created the anticlinal structural traps (Dunn, 2003). Therefore, successful exploitation of these resources must consider the overall complicated tectonic history of the region that affected fracture distribution (Dean, 2010), as well as deposition, diagenesis, preservation and final-stage trap location. Finally, if the Sonoman orogeny turns out to be a significant event to the west in this region, then there is a high probability that westerly derived sedimentation may also affect distribution of reservoir characteristics in the Montney Formation shale-gas play, as well as younger Triassic units.

Acknowledgments

The authors thank B. Beauchamp (University of Calgary) for reviewing the paper. Geoscience BC and Talisman Energy supplied financial support that made research in this remote area and the training of highly qualified personnel possible. This project was also financially supported by a Natural Sciences and Engineering Research Council of Canada Discovery Grant held by C.M. Henderson.

References

- Bamber, E.W. and Macqueen, R.W. (1979): Upper Carboniferous and Permian stratigraphy of the Monkman Pass and southern Pine Pass areas, northeastern British Columbia; Geological Survey of Canada, Bulletin 301, 26 p.
- Barclay, J.E., Krause, F.F., Campbell, R.I. and Utting, J. (1990): Dynamic casting and growth faulting; Dawson Creek graben complex, Carboniferous–Permian Peace River Embayment, western Canada; Bulletin of Canadian Petroleum Geology, v. 38A, p. 115–145.
- Beauchamp, B. (1995): Permian history of Arctic North America; in *The Permian of Northern Pangea, Volume 2: Sedimentary Basins and Economic Resources*, P.A. Scholle, T.M. Peryt and D.S. Ulmer-Scholle (ed.), Springer-Verlag, New York, p. 3–22.
- Belasky, P., Stevens, C.H. and Hanger, R.A. (2002): Early Permian location of western North American terranes based on brachiopod, fusulinid and coral biogeography; *Palaeogeography, Palaeoclimatology, Palaeoecology*, v. 179, p. 245–266.
- Brueckner, H.K. and Synder, W.S. (1985): Structure of the Havallah sequence, Golconda allochthon, Nevada: evidence for prolonged evolution in an accretionary prism; *Geological Society of American Bulletin*, v. 96, p. 113–1130.
- Colpron, M. and Nelson, J.L. (2006): Paleozoic evolution and metallogeny of pericratonic terranes at the ancient Pacific margin of North America; *Geological Association of Canada, Special Paper 45*, 528 p.
- Colpron, M. and Nelson, J.L. (2011): Chapter 31 – A Palaeozoic NW Passage and Timanian, Caledonian and Uralian connections of some exotic terranes in the North American Cordil-

- lera; Geological Society, London, Memoirs 2011, v. 35, p. 463–484. doi:10.1144/M35.31
- Dean, G.J. (2010): Multi-scale fracturing related to deformation and structural inheritance within the Middle Pennsylvanian to Middle Permian Belloy Formation and related units, east-central British Columbia; M.Sc. thesis, University of Calgary, Calgary, Alberta, 209 p.
- Dickinson, W.R. (2004): Evolution of the North American Cordillera; *Annual Review of Earth and Planetary Sciences*, v. 32, p. 13–45.
- Dickinson, W.R. (2006): Geotectonic evolution of the Great Basin; *Geosphere*, v. 2, no. 7, p. 353–368.
- Dunn, L. (2003): Sequence biostratigraphy and depositional environmental modeling of the Pennsylvanian–Permian Belloy Formation, northwest Alberta and northeast British Columbia; Ph.D. thesis, University of Calgary, Calgary, Alberta, 212 p.
- Fossenier, K. (2002): Stratigraphic framework of the Pennsylvanian to Permian Belloy Formation, northeastern British Columbia: a multidisciplinary approach; M.Sc. thesis, University of Calgary, Calgary, Alberta, 292 p.
- Gabrielse, H., Monger, J.W.H., Wheeler, J.O. and Yorath, C.J. (1991): Part A. Morphogeological belts, tectonic assemblages, and terranes; *in* Chapter 2 of *Geology of the Cordilleran Orogen in Canada*, H. Gabrielse and C.J. Yorath (ed.); Geological Survey of Canada, *Geology of Canada*, no. 4, p. 15–28.
- Halbertsma, H.L. (1959): Nomenclature of Upper Carboniferous and Permian strata in the subsurface of the Peace River area; *Journal of Alberta Society Petroleum Geologists*, v. 7, p. 109–118.
- Henderson, C.M. (2011): Biostratigraphic correlation and shale fabric of Lower Triassic strata, east-central British Columbia (NTS 093I, O, P); *in* *Geoscience BC Summary of Activities 2010*, Geoscience BC, Report 2011-1, p. 223–228, URL <http://www.geosciencebc.com/i/pdf/SummaryofActivities2010/SoA2010_Henderson.pdf> [November 2011].
- Henderson, C.M., Bamber, E.W., Richards, B.C., Higgins, A.C. and McGugan, A. (1993): Permian; *in* *Sedimentary Cover of the North American Craton*, D.F. Stott and J.D. Aitken (ed.), Geological Survey of Canada, *Geology of Canada*, no. 6, p. 271–293 (also Geological Society of America, *Geology of North America*, v. D-1).
- Henderson, C.M., Dunn, L., Fossenier, K. and Moore, D. (2002): Sequence biostratigraphy and paleogeography of the Pennsylvanian–Permian Belloy Formation and outcrop equivalents in western Canada; *Canadian Society of Petroleum Geologists, Memoir 19*, p. 934–947.
- Henderson, C.M., Richards, B.C. and Barclay, J.E. (1994): Permian strata of the Western Canada Sedimentary Basin; *in* *Geological Atlas of the Western Canada Sedimentary Basin*, G.D. Mossop and I. Shetsen (comp.), Canadian Society of Petroleum Geologists and Alberta Research Council, p. 251–258.
- Henderson, C.M., Zubin-Stathopoulos, K., Dean, G., Spratt, D. and Chau, Y.P. (2010): Tectonic history, biostratigraphy and fracture analysis of upper Paleozoic and lowest Triassic strata of east-central British Columbia; *in* *Geoscience BC Summary of Activities 2009*, Geoscience BC, Report 2010-1, p. 259–270, URL <http://www.geosciencebc.com/i/pdf/SummaryofActivities2009/SoA2009_Henderson.pdf> [November 2011].
- Hildebrand, R.S. (2009): Did west subduction cause Cretaceous–Tertiary orogeny in the North American Cordillera?; Geological Society of America, *Special Paper 457*, 71 p.
- Ing, J. and Henderson, C.M. (2009): Thermal maturity within the Western Canada Sedimentary Basin, west-central Alberta to northeastern British Columbia and its tectonic implications for Pennsylvanian and Permian strata; *in* *International Commission on Stratigraphy (ICOS) 2009 Abstracts*, C.M. Henderson and C. MacLean (ed.), *Permophiles* (Newsletter of the Subcommission on Permian Stratigraphy), no. 53, supplement 1 (ISSN 1684-5927), p. 21–22.
- Johnston, D.I., Henderson, C.M. and Schmidt, M.J. (2010): Upper Devonian to Lower Mississippian conodont biostratigraphy of uppermost Wabamun Group and Palliser Formation to lowermost Banff and Lodgepole formations, southern Alberta and southeastern British Columbia, Canada: implications for correlations and sequence stratigraphy; *Bulletin of Canadian Petroleum Geology*, v. 58, no. 4, p. 295–341.
- Johnston, S.T. (2008): The Cordilleran ribbon continent of North America; *Annual Review of Earth and Planetary Science*, v. 36, p. 495–530.
- Kendall, D.R. (1999): Sedimentology and stratigraphy of the Lower Triassic Montney Formation, Peace River Basin, subsurface of north-western Alberta; M.Sc. thesis, Department of Geoscience, University of Calgary, Calgary, Alberta, 386 p.
- MacRae, J. and McGugan, A. (1977): Permian stratigraphy and sedimentology, southwestern Alberta and southeastern British Columbia; *Bulletin of Canadian Petroleum Geology*, v. 25, p. 752–766.
- McGugan, A. (1965): Occurrence and persistence of thin shelf deposits of uniform lithology; *Geological Society of America Bulletin*, v. 76, p. 125–130.
- McGugan, A. and Rapson, J.E. (1962): Permo–Carboniferous stratigraphy, Crowsnest area, Alberta and British Columbia; *Journal of Alberta Society of Petroleum Geologists*, v. 10, p. 352–368.
- Nelson, J.L., Colpron, M., Piercey, S.J., Dusel-Bacon, C., Murphy, D.C. and Roots, C.F. (2006): Paleozoic tectonic and metallogenic evolution of the pericratonic terranes in Yukon, northern British Columbia and eastern Alaska; *in* *Paleozoic Evolution and Metallogeny of Pericratonic Terranes at the Ancient Pacific Margin of North America*, Geological Association of Canada, *Special Paper 45*, p. 323–360.
- Orchard, M.J. and Struik, L.C. (1985): Conodonts and stratigraphy of upper Paleozoic limestones in Cariboo gold belt, east-central British Columbia; *Canadian Journal of Earth Sciences*, v. 22, p. 538–552.
- Orchard, M.J. and Zonneveld, J.P. (2009): The Lower Triassic Sulphur Mountain Formation in the Wapiti Lake area: lithostratigraphy, conodont biostratigraphy, and a new biozonation for the lower Olenekian (Smithian); *Canadian Journal of Earth Sciences*, v. 46, p. 757–790.
- Panek, R. (2000): The sedimentology and stratigraphy of the Lower Triassic Montney Formation in the subsurface of the Peace River area, northwestern Alberta; M.Sc. thesis, University of Calgary, Calgary, Alberta, 275 p.
- Porter, I. (2007): Sequence biostratigraphy: Ksituan Member of the Belloy Formation in the Alberta Peace River Basin; B.Sc. thesis, University of Calgary, Calgary, Alberta, 106 p.
- Richards, B.C. (1989): Upper Kaskaskia Sequence: Uppermost Devonian and Lower Carboniferous; *in* *Western Canada*

- Sedimentary Basin—A Case History, B.D. Ricketts (ed.), Canadian Society of Petroleum Geologists, Special Publication 30, p. 165–201.
- Root, K.G. (2001): Devonian Antler fold and thrust belt and foreland basin development in the southern Canadian Cordillera: implications for the Western Canada Sedimentary Basin; *Bulletin of Canadian Petroleum Geology*, v. 49, p. 7–36.
- Seton, M., Gaina, C., Muller, R.D. and Heine, C. (2009): Mid-Cretaceous seafloor spreading pulse: fact or fiction?; *Geology*, v. 37, p. 687–690.
- Snyder, W.S., Trexler, J.H., Jr., Davydov, V.I., Cashman, P., Schiappa, T.A. and Sweet, D. (2002): Upper Paleozoic tectonostratigraphic framework for the western margin of North America; *in* Proceedings of ‘Late Paleozoic Tectonics and Hydrocarbon Systems of Western North America—The Greater Ancestral Rocky Mountains’, American Association of Petroleum Geologists, Hedberg Conference, Vail, Colorado, AAPG Search and Discovery Article 90012, 4 p.
- Struik, L.C. and Orchard, M.J. (1985): Late Paleozoic conodonts from ribbon chert delineate imbricate thrusts within the Antler Formation of the Slide Mountain terrane, central British Columbia; *Geology*, v. 13, p. 794–798.
- Trexler, J.H., Cashman, P.H., Cole, J.C., Snyder, W.S., Tosdal, R.M. and Davydov, V.I. (2003): Widespread effects of middle Mississippian deformation in the Great Basin of western North America; *Geological Society of America Bulletin*, v. 115, p. 1278–1288.
- Trexler, J.H., Cashman, P.H., Snyder, W.S. and Davydov, V.I. (2004): Late Paleozoic tectonism in Nevada: timing, kinematics, and tectonic significance; *Geological Society of America Bulletin*, v. 116, p. 525–538.
- Wamsteeker, M.L. (2007): Diagenetic and geochemical characterization of the Ksituan Member of the Belloy Formation, east-central British Columbia foothills; B.Sc. thesis, University of Calgary, Calgary, Alberta, 78 p.
- Wardlaw, B.R., Snyder, W.S., Spinosa, C. and Gallegos, D.M. (1995): Permian of the western United States; *in* The Permian of Northern Pangea, Volume 2: Sedimentary Basins and Economic Resources, P.A. Scholle, T.M. Peryt and D.S. Ulmer-Scholle (ed.), Springer-Verlag, New York, p. 23–40.
- Zonneveld, J.P., MacNaughton, R.B., Utting, J., Beatty, T.W., Pemberton, S.G. and Henderson, C.M. (2010): Sedimentology and ichnology of the Lower Triassic Montney Formation in the Pedigree–Ring/Border–Kahntah River area, northwestern Alberta and northeastern British Columbia; *Bulletin of Canadian Petroleum Geology*, v. 58, no. 2, p. 115–140.
- Zubin-Stathopoulos, K.D. (2011): Tectonic evolution, paleogeography and paleoclimate of Pennsylvanian–Permian strata in east-central British Columbia: implications from conodont biostratigraphy and carbonate sedimentology; M.Sc. thesis, Department of Geoscience, University of Calgary, Calgary, Alberta, 164 p.
- Zubin-Stathopoulos, K.D., Dean, G.J., Beauchamp, B., Spratt, D.A. and Henderson, C.M. (2011): Tectonic evolution and paleogeography of Pennsylvanian–Permian strata in east-central British Columbia (NTS 093I, O, P): implications from stratigraphy, fracture analysis and sedimentology; Geoscience BC Summary of Activities 2010, Geoscience BC Report 2011-1, p. 209–222.

Rock Physical-Property Measurements for the Nechako Basin Oil and Gas Region, Central British Columbia (Parts of NTS 093B, C, E, F, G, K, L)

A. Kushnir, Centre for Experimental Studies of the Lithosphere, Department of Earth and Ocean Sciences, University of British Columbia, Vancouver, BC V6T 1Z4

G. Andrews, Earth Research Institute, University of California Santa Barbara, Santa Barbara, CA 93106

J.K. Russell, Volcanology and Petrology Laboratory, Department of Earth and Ocean Sciences, University of British Columbia, Vancouver, BC V6T 1Z4

R.J. Enkin, Natural Resources Canada, Geological Survey of Canada–Pacific, 9860 West Saanich Road, Sidney, BC V8L 4B2

L.A. Kennedy, Centre for Experimental Studies of the Lithosphere, Department of Earth and Ocean Sciences, University of British Columbia, Vancouver, BC V6T 1Z4

M.J. Heap, Laboratoire de géophysique expérimentale, Institut de physique du globe de Strasbourg (UMR 7516 CNRS, Université de Strasbourg/EOST), 5 rue René Descartes, 67084 Strasbourg CEDEX, France

S. Quane, Quest University Canada, 3200 University Boulevard, Squamish, BC V8B 08N

Kushnir, A., Andrews, G., Russell, J.K., Enkin, R.J., Kennedy, L.A., Heap, M.J. and Quane, S. (2012): Rock physical-property measurements for the Nechako Basin oil and gas region, central British Columbia (parts of NTS 093B, C, E, F, G, K, L); in Geoscience BC Summary of Activities 2011, Geoscience BC, Report 2012-1, p. 125–150.

Abstract

The Mesozoic hydrocarbon-prospective Nechako (sedimentary) Basin in central British Columbia is buried by a variably thick and variably extensive, lithologically diverse assemblage of Cenozoic volcanic and sedimentary rocks. To assist in the interpretation of geophysical surveys, physical and geophysical properties (density, porosity, magnetic susceptibility and remanence, electrical resistivity and chargeability, and seismic velocity) have been measured on a sample suite covering the eleven stratigraphic units within, and stratigraphically above, the Nechako Basin. The eleven basic stratigraphic units are grouped into six major lithostratigraphic packages (combined on the basis of age, geography and lithology) for the purposes of comparing physical and geophysical properties. Each lithostratigraphic package is distinguishable on the basis of one or more physical or geophysical properties; for example, potential Cretaceous reservoir rocks (e.g., Jackass Mountain Group) have relatively high porosities (=17%), low resistivities and low seismic velocities. Generally, volcanic rocks are easily distinguished from sedimentary rocks, and the crystalline basement is distinguished from both. This dataset is available for incor-

poration into ongoing and future geophysical surveys of the Nechako Basin, and can be used retrospectively to assess previous interpretations. Such integrated datasets are necessary to provide a comprehensive geological and geophysical interpretation.

Introduction

The Mesozoic Nechako Basin in south-central British Columbia (BC; Figure 1) has underexplored potential for oil and gas deposits hosted in Cretaceous strata (Hannigan et al., 1994; Hayes, 2002). First-order geological interpretations of the subsurface are hampered by the basin's structural complexity, which results from extensive polyphase deformation and partial burial beneath significant extents and variable thicknesses of Cenozoic volcanic, volcanoclastic and sedimentary rocks (Riddell, 2006, 2011).

The lack of continuity in outcrop and stratigraphy has hindered reconstructions of the basin and efforts to identify potential hydrocarbon traps. In an effort to address this, geophysical surveys were conducted in the mid-2000s across portions of the Interior Plateau (e.g., Kim, 2010; Hayward and Calvert, 2011; Idowu et al., 2011; Spratt and Craven, 2011). Interpretation of these new data, coupled with a re-assessment of existing geophysical datasets (e.g., Hayward and Calvert, 2009), is made difficult by a lack of rock physical-property data for the corresponding rocks within the Nechako Basin and a fragmentary understanding of even the near-surface geology (e.g., Dohaney et al., 2010; Andrews et al., 2011). Establishing the extent of buried Cenozoic

Keywords: *Nechako Basin, rock properties, physical properties, geophysical properties*

This publication is also available, free of charge, as colour digital files in Adobe Acrobat® PDF format from the Geoscience BC website: <http://www.geosciencebc.com/s/DataReleases.asp>.

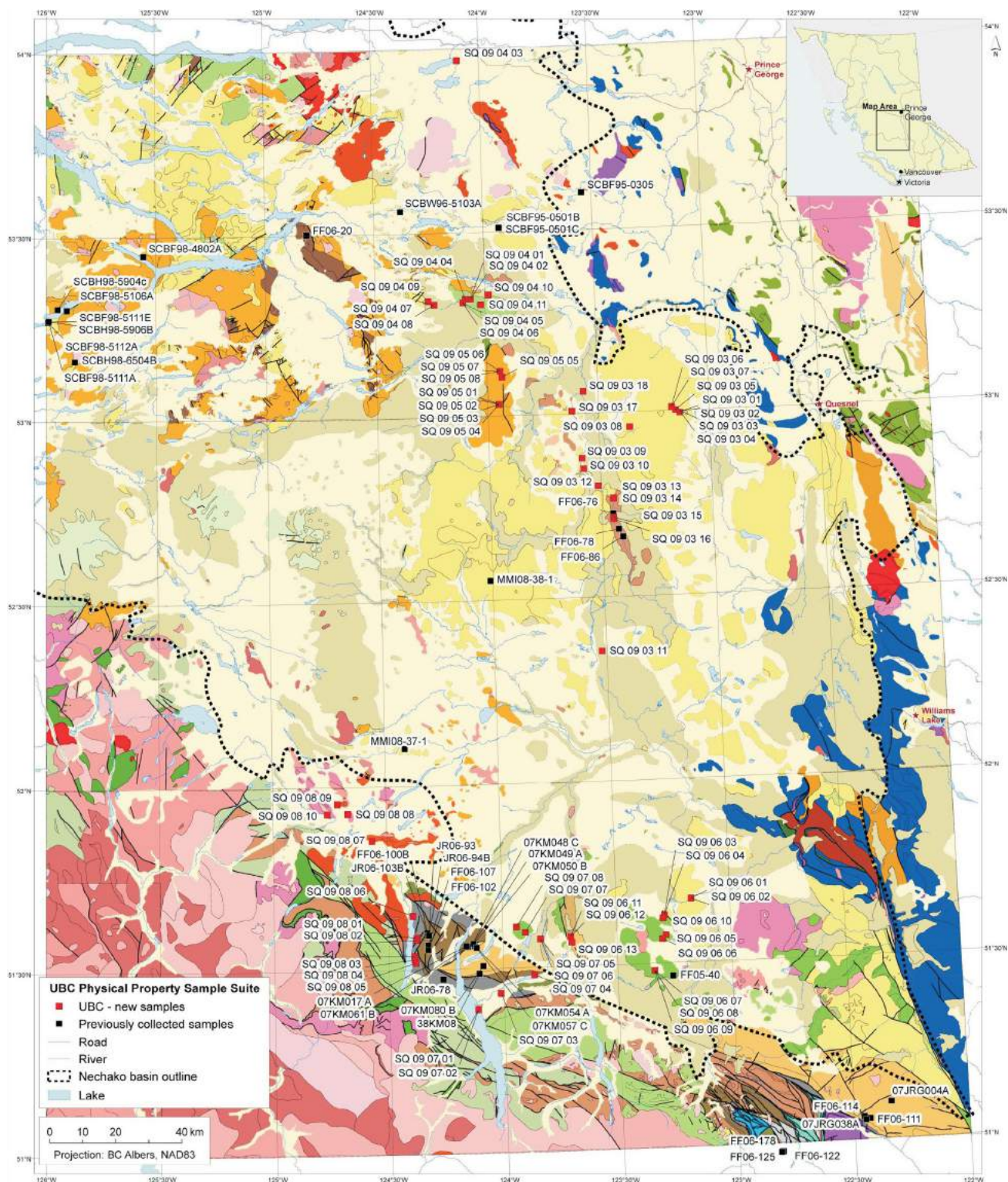


Figure 1. Geology of the Nechako Basin, showing the 81 sample sites and the 167 samples collected. Geology adapted from Riddell (2006) and prepared by F. Ma of Geoscience BC.

volcanic rocks and distinguishing them from buried and deformed Mesozoic successions are particularly challenging.

Geoscience BC funded an investigation of the rock physical properties of the Nechako Basin and overlying units. We assembled a representative suite of 167 samples from existing collections and from a focused field campaign to extend the sample diversity. Samples were prepared at the University of British Columbia and subjected to a comprehensive suite of experiments to measure bulk density, connected porosity, magnetic susceptibility, magnetic remanence, Koenigsberger ratio, electrical resistivity, chargeability and ultrasonic velocity. All measurements were performed at 1) the Centre for Experimental Study of the Lithosphere (CESL) at the University of British Columbia (UBC); 2) the Paleomagnetism and Petrophysics Laboratory at Geological Survey of Canada–Pacific, Sidney

(GSC-P); and 3) the Laboratoire de Géophysique Expérimentale at l'Université de Strasbourg, France (EOST). Experimental results are presented as a comprehensive series of tables and crossplots that emphasize parameters that can be used to distinguish between the various units.

This report summarizes the results of the first comprehensive, multiparameter rock-property study of the Nechako Basin and overlying units. The dataset discussed herein is available in Andrews et al. (2011). It is also expected that the associated electronic database will, in turn, be integrated into other provincial and national rock-property databases (e.g., Salisbury and Iulicucci, 2001; Mira Geoscience, 2008; Parsons et al., 2009). These data are intended for use in ongoing and future geophysical experiments, and will enable better differentiation between units;



this will, in turn, allow better understanding of the structure, tectonic evolution and hydrocarbon potential of the Nechako Basin.

Geology of the Nechako Basin

The Nechako Basin is an area of approximately 75 000 km² bounded to the south and west by the Coast Mountains, to the north by the Skeena Arch, and to the east by the Bonaparte Plateau and Cariboo Mountains (Figure 1; Hayes, 2002; Riddell, 2006). It underlies much of the present-day Fraser River Basin, including important tributaries such as the Chilcotin, Chilko and Taseko rivers. The Nechako Basin is interpreted to have developed as a foreland basin during the Late Jurassic to mid-Cretaceous on basement comprising integral parts of the Intermontane Superterrane, namely the Cache Creek and Stikine terranes. Stikine terrane basement is present at the surface in the west and north of the basin (Riddell, 2006), where it is represented by the Early–Middle Jurassic Hazelton volcanic arc (Hazelton Group). Oceanic rocks of the Cache Creek terrane rocks outcrop in the east and northeast. There is no inferred hydrocarbon resource in the basement.

The Nechako Basin was filled with clastic sedimentary rocks from the Middle Jurassic (Ladner Group) to the Early Cretaceous (Relay Mountain Group). Clastic marine sedimentation continued through the Cretaceous (Hauterivian–Cenomanian Jackass Mountain Group, Albian Taylor Creek and Skeena groups, and Albian–Cenomanian Silverquick Formation) and was interspersed with deposition of volcanic and volcanoclastic rocks of the Albian–Santonian Spences Bridge and Kasalka groups, and the Turonian–Campanian Powell Creek Formation and informally named Taseko River strata. Numerous Mesozoic and Cenozoic plutons intruded the basin. All appreciable hydrocarbon potential is within the Cretaceous succession. Figure 2 provides a generalized and schematic stratigraphic summary of the basin.

The Nechako Basin is buried beneath 0–4000 m of Eocene, Miocene and Pliocene volcanic, volcanoclastic and sedimentary rocks belonging mainly to the Endako, Ootsa Lake and Chilcotin groups (Riddell, 2006; Andrews and Russell, 2007, 2008; Andrews et al., 2011; Bordet and Hart, 2011). A diverse range of mafic and felsic volcanic and volcanoclastic rocks occur, including ash-flow tuff that is indicative of caldera-forming eruptions. The Pliocene–Holocene Anahim volcanic belt trends east across the centre of the ba-

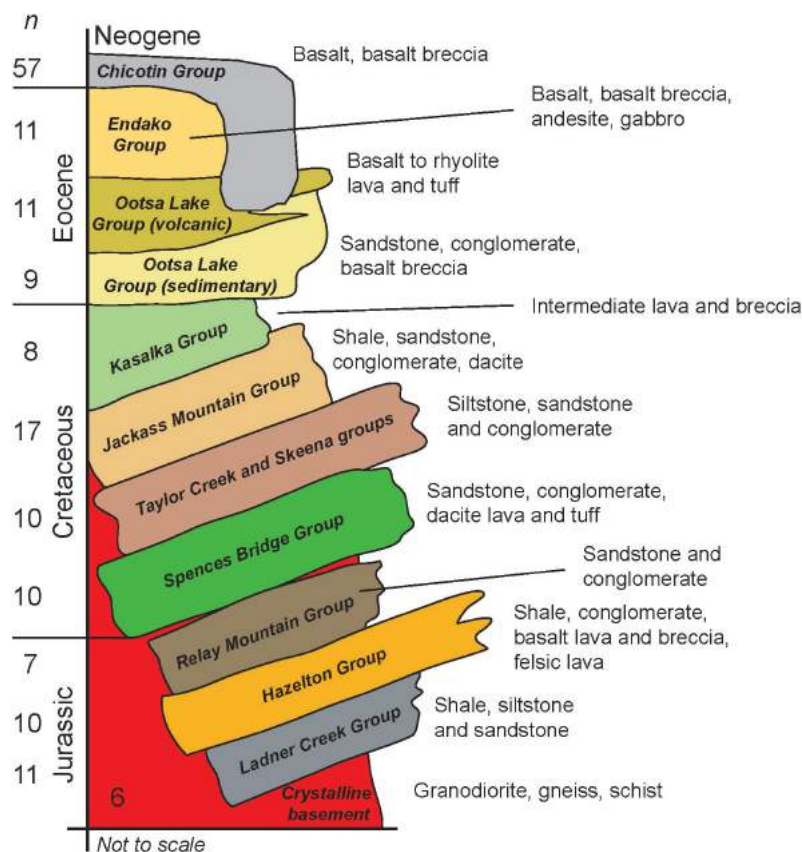


Figure 2. Schematic representation of stratigraphic relationships between map units sampled within the Nechako Basin. Number of samples collected from each stratigraphic unit is given on left.

sin. The basin and overlying Cenozoic rocks are buried beneath a 1–100 m thick veneer of glacial sediments, including till and glaciolacustrine and glaciofluvial successions (e.g., Andrews et al., 2011). There is no inferred hydrocarbon resource in the Cenozoic succession.

The structural geology of the Nechako Basin is poorly understood, so the architecture of potential hydrocarbon traps has not been established. Preliminary geological and geophysical surveys have identified sub-basins (e.g., Hayward and Calvert, 2009), high- and low-angle faults, folds and unconformities (e.g., Mihalynuk et al., 2009); however, a lack of stratigraphic control due to the paucity of boreholes in the basin makes lateral correlation and section-balancing impossible. A dedicated rock-property suite from the known Nechako Basin stratigraphy will allow for improved geophysical imaging of the subsurface geology.

Sample Suite

During the 1980s, seismic-reflection and gravity surveys were completed in the Nechako Basin and additional exploration wells were drilled; new vibroseis seismic-reflection and magnetotelluric datasets were collected in 2008 (Calvert et al., 2009; Craven and Spratt, 2011). There is a pressing need for better constraints on a range of physical and geophysical rock properties from the diverse suite of volcanic and sedimentary rocks in the basin. For example, magnetotelluric studies have highlighted the need for good resolution in electrical-resistivity data to differentiate the widespread Cretaceous and Eocene sequences (e.g., Craven and Spratt, 2011). Similarly, seismic inversions (e.g., Hayward and Calvert, 2009) suggest nonintuitive variations in compressional-wave velocities for individual for-

mations, specifically overlap in inferred seismic velocities between the Eocene and Jurassic–Cretaceous successions. Quantitative, experimental physical-properties data from this sample suite will aid the interpretations of these surveys and help to distinguish the prospective, non-hydrocarbon Eocene basinal sequence from the Jurassic–Cretaceous basinal sequence.

The UBC experimental program identified and sampled stratigraphic groups that are most important to the interpretation of seismic datasets and the delineation of exploration targets within the Nechako Basin (Figure 2, Table 1).

The **Chilcotin Group** (CB, Table 1) comprises Miocene-age basaltic lavas. The Chilcotin is areally extensive and comprises thin (<50 m) basaltic lavas and breccias. The porosity (vesicularity) of these deposits is highly variable laterally and with depth. Infilled paleovalley sections may be up to 200 m thick and filled mainly with porous, poorly consolidated breccias (Andrews and Russell, 2007).

The package of **Eocene volcanic and sedimentary rocks** (EVS, Table 1) features deposits that are highly variable in thickness (absent to >1000 m) and, in part, cover the Jurassic and Cretaceous rocks that form the Nechako Basin. These stratigraphic units blanket, obscure and complicate the interpretation of structure and stratigraphy of the Jurassic source rocks and Cretaceous reservoir rocks. Specific lithostratigraphic packages studied include the Endako and Ootsa Lake groups (e.g., Bordet and Hart, 2011). The Endako Group comprises coherent, mafic lavas, which need to be distinguished from Chilcotin Group rocks. The Ootsa Lake Group includes both volcanoclastic and coherent facies. The volcanoclastic succession comprises a series

Table 1. Description of sample suite in terms of stratigraphic group and lithological type.

Group name	No. of samples (N)	Lithological types	Stratigraphic package
Chilcotin	57	Vesicular basaltic lava; basaltic breccia	CB
Endako	11	Vesicular basaltic lava; amygdaloidal basalt lava; basalt breccia; andesite; gabbro	EVS
Ootsa Lake (coherent)	11	Intermediate and felsic lava; rhyolitic welded tuff; basaltic lava; microgranite	EVS
Ootsa Lake (noncoherent)	9	Sandstone; conglomerate; volcanic breccia	EVS
Kasalka / Powell Creek / Taseko River	8	Andesite; lapilli tuff; breccia; conglomerate	KVS
Jackass Mountain	17	Arkose conglomerate; black shale; dacite intrusions; sandstone	KVS
Taylor Creek and Skeena	10	Sandstone; chert-pebble conglomerate; siltstone	KVS
Spences Bridge	10	Dacite lava; conglomerate; sandstone; andesitic tuff	KVS
Relay Mountain	7	Sandstone; conglomerate	JS
Ladner	11	Calcareous shale; shale; sandstone	JS
Hazelton	10	Felsic lava; volcanic breccia; mudstone; sandstone; granite; conglomerate; shale	JVS
Mesozoic Plutonic	6	Granodiorite, diorite, orthogneiss	MB _p

of felsic volcanoclastic rocks and associated bedded sedimentary rocks, and are difficult to discriminate geophysically from older Cretaceous volcanoclastic and sedimentary successions. Coherent facies are defined by intermediate to felsic lavas and lava domes, which need to be discriminated from Endako Group lavas.

The **Cretaceous volcanoclastic and sedimentary rocks** (KVS, Table 1) are the potential hydrocarbon reservoir rocks within the Nechako Basin. They are strongly bedded, weakly deformed and of exceptionally variable thickness. The lateral continuity of stratigraphy has not yet been fully resolved (Ferri and Riddell, 2006), so it was necessary to sample several units in multiple locations. Despite this procedure, we acknowledge that there may be facies variations of these units that remain unsampled. We have characterized the geophysical properties of the following lithostratigraphic packages within this broad time grouping:

- Jackass Mountain Group: coarse-grained clastic sedimentary rocks inferred to be the most likely surface correlative of the subsurface Skeena assemblage, which has been identified as the most significant potential reservoir in the Nechako Basin (MacLaurin et al., 2011); best exposed and studied along the southern margin of the Nechako Basin near Taseko Lake
- Taylor Creek Group and Skeena Group: clastic sedimentary rocks and minor volcanic rocks exposed along, and encountered in the subsurface of, the Nazko River area
- Spences Bridge Group: intermediate lavas and tuffs, and minor sedimentary rocks exposed in the southern Nechako Basin
- Kasalka Group, Powell Creek Group and ‘Taseko River strata’: intermediate lavas and tuffs, and associated clastic sedimentary rocks (including conglomerate and sandstone in the ‘Taseko River strata’) found in many areas throughout the basin; likely a very extensive sequence

The **Middle–Late Jurassic sedimentary rocks** (JS, Table 1) are the most probable source rocks for hydrocarbon reserves hosted by the Nechako Basin. This lithostratigraphic package is expected to form the lowermost parts of the basinal sequence. Our sampling includes 1) the Ladner Group, comprising fine- to coarse-grained calcareous clastic rocks and carbonates exposed around Chilko Lake in the southern part of the basin; and 2) the Relay Mountain Group, best exposed in the Nemaiah Valley and Chilko Lake areas in the southern part of the basin and comprising fine- to coarse-grained clastic and carbonaceous rocks that underlie the Jackass Mountain Group.

The **Lower–Middle Jurassic volcanic and sedimentary rocks** (JVS, Table 1) are a package of intermediate to felsic lavas and tuffs, and minor clastic and carbonate sedimentary rocks (e.g., Puntzi Lake and west of Nechako).

The last package of samples is the **Mesozoic basement rocks** (MB_p, Table 1). The Nechako Basin is underlain by Permian, Triassic and Jurassic rocks of the Cache Creek and Stikine terranes, and intrusions of Jurassic–Eocene age. These rocks tend to be more homogeneous in character and more easily differentiated from the overlying Cretaceous and Eocene stratigraphy. The more abundant of these stratigraphic units include 1) Jurassic–Cretaceous intrusive rocks (e.g., Taseko River); and 2) the mid-Triassic Cache Creek Group, comprising limestone, chert, clastic sediments, metamorphic rocks and basalt (e.g., Blackwater River, Hanceville).

Methodology

A large suite of rock samples was collected from formations representing the key Mesozoic and Tertiary rock types/stratigraphic units within the Nechako Basin. From this collection, 167 samples were chosen for experimental work to be performed at CESL (UBC), GSC-P and EOST. The Nechako sample suite comprises rocks of various types, sampled from 12 distinct stratigraphic units distributed across the Nechako Basin. Each of the 167 samples was drilled to obtain a cylindrical rock core measuring 25 mm in diameter by ~50 mm in length. The ends of each core were ground and polished at right angles to the cylinder side to create a smooth (~0.02 mm precision) end surface. The polished ends are critical for the experimental measurement of seismic velocity because they provide perfect sample geometry and ensure that there is good contact between the end caps of the seismic-velocity transducer and the sample. All sample preparation (e.g., cleaning, trimming, coring, drying) was carried out at CESL, with some modification at EOST. Different sets of geophysical properties were measured on the same sample cores by JKR’s team at CESL and EOST, and by RJE’s team at GSC-P. The following properties were measured for each sample core: bulk density (EOST), porosity (EOST), magnetic susceptibility (CESL and GSC-P), remanent magnetization (GSC-P), electrical resistivity (GSC-P), induced-polarization chargeability (GSC-P), and seismic-wave velocities (EOST and CESL). These data are given in Tables 2 and 3.

Density and Porosity

Dry bulk density (ρ_d), wet bulk density (ρ_w) and framework density (ρ_f) were measured for all samples. Bulk density is the density of the entire sample (i.e., rock plus pore space). The pore space includes connected and isolated pores. Bulk densities are calculated from the geometry and mass (dry or wet) of the sample core. The framework density is the den-

sity of the rock itself (i.e., excluding pore space) and is measured using the hydrostatic weighing method, as derived from Archimedes' Buoyancy Law. Using this method, the framework density actually measures the density of the rock and its isolated porosity, if there is any present. In the Nechako Basin sample suite, isolated porosity is assumed to be negligible.

All sample cores were dried at 40°C under a vacuum for 24 hours. After the dry mass (m_d) of each core was measured, all samples were vacuum saturated with agitated, deionized, distilled water for a minimum of 15 hours to allow the water to fill all connected pore space within the sample. The mass of the water-saturated sample was then weighed in air (m_w) and while it was fully submerged in water (m_b). Wet bulk density (ρ_w) was calculated for each water-saturated sample to estimate the density of the rock plus its water-saturated pore space and any residual isolated pore space. These values are required for determination of wet seismic velocity.

The density of the rock framework (plus any remaining isolated pores) was then computed using the relationship

$$\rho_f = \rho_{H_2O} \frac{m_d}{m_d + m_b}, \quad (1)$$

where (ρ_{H_2O}) is the density of the water under ambient lab conditions. Values of ρ_d and ρ_f are sufficient to estimate porosity (%) using

$$\phi = 100 \times \frac{m_w - m_d}{m_w - m_b}. \quad (2)$$

Magnetic Susceptibility

Magnetic susceptibility (k) is primarily a result of the presence of magnetic minerals in rocks, magnetite being the most ubiquitous of these minerals (Telford et al., 1976). There is substantial variability in k within and between rock types (Telford et al., 1976). For instance, igneous rocks have the highest average k values ($0-200 \times 10^3$ SI), whereas metamorphic rocks range between 0 and 70×10^3 SI, and sedimentary rocks between 0 and 20×10^3 SI (Telford et al., 1976).

Magnetic susceptibility was measured on hand samples in the lab using a GF Instruments model SM-20 pocket magnetic-susceptibility meter, with a sensitivity of 10^{-6} SI volume units. The measurement coil has a 5 cm diameter, and ~90% of the measured response comes from the top 2 cm of the sample. We investigated the effect of small sample size on the measurements and found that samples more than 3 cm thick allow accurate magnetic-susceptibility determinations. Generally, three measurements were taken on different surfaces of the sample and the average is reported. The standard deviation of the three measurements is typically 10% due to spatial variations in magnetite concentration. Susceptibility measurements on cores were measured

with a Sapphire Instruments model SI2B susceptibility meter, accurate to 10^{-7} SI. These measurements were used in preference to the SM-20 measurements.

Magnetic Remanence and Koenigsberger Ratio

Natural remanent magnetization (NRM), if present, is a significant contributor to the overall magnetization of rocks (Telford et al., 1976). Magnetization is strongly dependent on the existing magnetic field and the mineralogical content of rocks, as well as the impact of emplacement conditions (Telford et al., 1976). Most relevant to the Nechako Basin is thermoremanent NRM due to the emplacement of hot volcanic rocks.

Magnetic remanence was measured using an Agico Inc. model JR5-A spinner magnetometer (sensitivity 10^{-5} A/m). The full vector was measured, but only the total vector magnitude of the remanence is reported in the database. The Koenigsberger ratio (K_N) compares the relative strength of the natural remanent magnetization (NRM) to the induced magnetism in the geomagnetic field and is calculated as

$$K_N = \text{NRM} / (H_0 \chi_0), \quad (3)$$

where χ_0 is the magnetic susceptibility and the geomagnetic field strength (H_0) is approximated as a constant 40 A/m (or $\mu_0 H_0 = 50 \mu\text{T} = 50000 \gamma$). For $K_N > 1$, magnetic-anomaly interpretation will be incorrect if magnetic remanence is not taken into consideration.

Electrical Resistivity and Chargeability

Complex electrical-impedance frequency spectra were measured using a Solartron Analytical model 1260 impedance spectrum analyzer, based on the method of Katsube (2001). Sample cylinders were vacuum impregnated in distilled water and allowed to soak for at least 24 hours, to allow original groundwater solutes precipitated in the sample porosity to dissolve and approximate original groundwater conductivity. The impedance was measured with five frequencies per decade from 1 MHz to 0.03 Hz. The scalar resistance was picked as the real impedance at the frequency that displays minimum imaginary impedance, typically around 1000 Hz. Resistivity (in ohm·m, or $\Omega\cdot\text{m}$) is the scalar resistance multiplied by the sample geometric factor (i.e., the cross-sectional area divided by the length). Conductivity (Mho/m) is the reciprocal of the resistivity.

Induced-polarization chargeability was calculated after converting the frequency-domain impedance spectrum to the time-domain response to a step function, $V(t)$. Using the Newmont Standard (Sumner, 1976), the chargeability (m_T) is

$$m_T = \int_{400ms}^{1100ms} \frac{V(t)}{V(0)} dt. \quad (4)$$

Table 2. Physical and geophysical properties of Nechako Basin sample suite, organized by stratigraphic groups (Table 1) and summarized as maximum, minimum and average values.

Group name:	Chilcotin ^{1,2}	Endako	Ootsa Lake (coherent)	Ootsa Lake (noncoherent)	Kasalka / Powell Creek / Taseko River	Jackass Mountain	
Dry average V_p (km/s) ³	Max.	5.99	5.82	5.72	5.19	5.66	6.17
	Min.	4.24	3.31	3.25	2.25	4.23	3.25
	Avg.	5.25	4.93	4.40	3.44	4.73	5.24
Wet average V_p (km/s) ³	Max.	n/a	6.63	5.81	5.52	5.91	6.49
	Min.	n/a	3.88	4.16	3.62	4.78	4.82
	Avg.	n/a	5.53	4.98	4.40	5.36	5.82
Dry average V_s (km/s) ³	Max.	n/a	3.44	3.25	2.43	2.96	3.33
	Min.	n/a	1.59	2.08	1.04	1.97	1.99
	Avg.	n/a	2.64	2.60	1.49	2.56	2.79
Wet average V_s (km/s) ³	Max.	n/a	4.10	3.40	2.67	3.07	3.65
	Min.	n/a	1.77	1.77	1.50	2.15	1.67
	Avg.	n/a	2.81	2.54	1.98	2.67	2.83
Dry bulk density (g/cc) ³	Max.	2.99	2.89	2.68	2.65	2.87	2.80
	Min.	2.49	1.98	2.23	1.87	2.41	2.54
	Avg.	2.72	2.53	2.43	2.13	2.64	2.70
Wet bulk density (g/cc) ³	Max.	n/a	2.90	2.69	2.67	2.89	2.80
	Min.	n/a	2.25	2.35	2.16	2.49	2.60
	Avg.	n/a	2.61	2.49	2.31	2.69	2.72
Wet framework density (g/cc) ³	Max.	3.02	3.02	2.75	2.75	2.91	2.82
	Min.	2.56	2.47	2.45	2.47	2.64	2.67
	Avg.	2.87	2.78	2.59	2.66	2.78	2.75
Dry Poisson's ratio	Max.	n/a	0.36	0.29	0.41	0.40	0.38
	Min.	n/a	0.22	0.08	0.36	0.12	0.20
	Avg.	n/a	0.30	0.22	0.38	0.27	0.29
Wet Poisson's ratio	Max.	n/a	0.45	0.39	0.45	0.38	0.45
	Min.	n/a	0.04	0.23	0.18	0.26	0.23
	Avg.	n/a	0.30	0.32	0.35	0.33	0.33
Dry Young's modulus (GPa)	Max.	n/a	84.36	64.82	42.45	52.01	78.45
	Min.	n/a	13.44	22.67	5.49	28.62	24.18
	Avg.	n/a	48.54	41.53	15.29	43.94	56.62
Wet Young's modulus (GPa)	Max.	n/a	94.08	69.94	51.17	71.57	93.62
	Min.	n/a	19.31	20.83	13.87	31.63	21.23
	Avg.	n/a	55.45	43.68	25.82	52.12	59.94
Dry V_p/V_s	Max.	n/a	2.13	1.83	2.53	2.43	2.24
	Min.	n/a	1.67	1.48	2.14	1.52	1.63
	Avg.	n/a	1.89	1.69	2.32	1.88	1.89
Wet V_p/V_s	Max.	n/a	3.20	2.40	3.30	2.27	3.28
	Min.	n/a	1.44	1.68	1.60	1.75	1.68
	Avg.	n/a	2.07	2.00	2.31	2.03	2.15
Porosity (%) ³	Max.	16.55	26.74	14.06	29.44	8.42	6.06
	Min.	0.15	0.75	0.32	1.60	1.18	0.27
	Avg.	5.57	8.25	5.68	18.76	4.63	1.72
Magnetic susceptibility (SI) ^{1,2}	Max.	0.11	0.05	0.04	0.03	0.04	0.01
	Min.	b.d.	b.d.	0.01	b.d.	b.d.	b.d.
	Avg.	0.01	0.01	0.01	0.01	0.01	b.d.
Resistivity (ohm-m) ¹	Max.	95646	17560	23035	9941	20796	29011
	Min.	127	49	82	37	139	116
	Avg.	4541	6135	5098	1518	4886	5101
Koenigsberger ratio (K_N) ¹	Max.	80.90	34.90	6.95	23.35	25.28	30.38
	Min.	0.09	0.01	0.09	0.04	0.06	0.08
	Avg.	13.03	10.24	2.28	8.23	5.37	3.77
Natural remanent magnetization (NRM; A/m) ¹	Max.	48.00	24.80	2.66	27.70	11.70	15.10
	Min.	b.d.	b.d.	0.04	b.d.	b.d.	b.d.
	Avg.	3.17	3.47	0.78	5.37	3.06	1.04
Chargeability (ms) ³	Max.	n/a	18.70	15.10	11.90	45.20	19.10
	Min.	n/a	0.01	0.03	0.02	0.36	0.28
	Avg.	n/a	5.76	3.36	3.85	7.89	4.48

¹Measurements conducted at Centre for Experimental Study of the Lithosphere at University of British Columbia (CESL-UBC) under supervision of J.K. Russell.

²Measurements conducted at Geological Survey of Canada Pacific, Sidney (GSC-P) under supervision of R.J. Enkin.

³Measurements conducted at Laboratoire de Géophysique Expérimentale à l'Université de Strasbourg, France (EOST) under supervision of M.J. Heap. All seismic velocity measurements (except Chilcotin basalt samples) made under atmospheric pressure with nominal stress of 1 MPa applied to ends of sample. Compressional wave (P-wave) measurements made on samples using a frequency of 700 kHz; shear wave (S-wave) measurements made using a frequency of 300 kHz.

Abbreviations: b.d., below detection; n/a, not measured; VP, P-wave velocity; VS, S-wave velocity.

Table 2 (continued)

	Group name:	Taylor Creek and Skeena	Spences Bridge	Relay Mountain	Ladner	Hazelton	Mesozoic plutonic
Dry average V_P (km/s) ³	Max.	4.79	5.81	5.61	5.85	5.96	5.46
	Min.	1.65	3.42	4.20	5.22	2.57	3.44
	Avg.	3.40	5.12	5.17	5.65	4.33	4.31
Wet average V_P (km/s) ³	Max.	5.27	6.15	5.78	6.21	6.50	6.07
	Min.	3.02	4.39	5.16	5.47	3.40	4.33
	Avg.	4.16	5.57	5.60	5.86	5.21	5.45
Dry average V_S (km/s) ³	Max.	3.22	3.47	3.11	3.39	4.04	3.15
	Min.	1.04	1.89	2.45	3.20	1.51	2.00
	Avg.	2.16	2.84	2.88	3.32	2.39	2.61
Wet average V_S (km/s) ³	Max.	3.11	3.56	3.52	3.39	3.66	3.33
	Min.	1.47	1.99	2.07	3.03	1.66	2.18
	Avg.	2.28	2.80	2.83	3.24	2.59	2.73
Dry bulk density (g/cc) ³	Max.	2.63	2.87	2.80	2.77	2.75	2.78
	Min.	2.05	2.30	2.51	2.19	1.91	2.33
	Avg.	2.34	2.63	2.68	2.60	2.45	2.65
Wet bulk density (g/cc) ³	Max.	2.65	2.87	2.81	2.77	2.76	2.79
	Min.	2.21	2.45	2.54	2.20	2.21	2.45
	Avg.	2.45	2.68	2.70	2.61	2.54	2.68
Wet framework density (g/cc) ³	Max.	2.73	2.99	2.82	2.80	2.78	2.82
	Min.	2.65	2.66	2.72	2.74	2.62	2.65
	Avg.	2.68	2.81	2.77	2.76	2.71	2.74
Dry Poisson's ratio	Max.	0.29	0.35	0.35	0.27	0.37	0.25
	Min.	0.09	0.20	0.20	0.14	0.07	0.14
	Avg.	0.15	0.27	0.26	0.23	0.24	0.21
Wet Poisson's ratio	Max.	0.42	0.44	0.42	0.30	0.42	0.37
	Min.	0.03	0.17	0.18	0.25	0.06	0.28
	Avg.	0.23	0.31	0.31	0.28	0.32	0.33
Dry Young's modulus (GPa)	Max.	54.42	78.59	66.15	76.53	96.54	69.20
	Min.	5.21	23.85	37.49	62.64	11.52	26.32
	Avg.	28.66	55.50	56.99	70.23	38.38	45.42
Wet Young's modulus (GPa)	Max.	57.48	85.20	78.46	81.94	78.79	79.58
	Min.	15.24	30.47	33.12	51.70	17.62	31.00
	Avg.	32.90	55.93	57.82	70.50	47.53	54.60
Dry V_P/V_S	Max.	1.85	2.08	2.06	1.78	2.21	1.73
	Min.	1.49	1.63	1.63	1.54	1.33	1.55
	Avg.	1.58	1.81	1.80	1.71	1.84	1.66
Wet V_P/V_S	Max.	2.76	3.02	2.76	1.86	2.64	2.20
	Min.	1.43	1.59	1.60	1.74	1.46	1.82
	Avg.	1.90	2.05	2.05	1.81	2.07	2.01
Porosity (%) ³	Max.	17.07	16.21	3.49	1.60	30.06	11.97
	Min.	2.54	0.60	0.35	0.19	0.43	1.00
	Avg.	11.37	5.11	1.87	0.81	8.48	3.41
Magnetic susceptibility (SI) ^{1,2}	Max.	b.d.	0.01	b.d.	b.d.	0.04	0.01
	Min.	b.d.	b.d.	b.d.	b.d.	b.d.	b.d.
	Avg.	b.d.	b.d.	b.d.	b.d.	0.01	0.01
Resistivity (ohm-m) ¹	Max.	3650	3433	19199	49883	12338	10771
	Min.	208	428	460	1586	46	152
	Avg.	1190	1635	5348	8617	3864	4402
Koenigsberger ratio (K_N) ¹	Max.	1.37	23.43	0.16	24.90	45.35	5.90
	Min.	0.13	0.68	0.04	0.02	0.05	0.69
	Avg.	0.66	9.19	0.09	2.56	7.78	3.64
Natural remanent magnetization (NRM; A/m) ¹	Max.	0.02	4.77	0.02	1.03	4.56	2.52
	Min.	b.d.	0.14	b.d.	b.d.	b.d.	0.03
	Avg.	b.d.	1.21	b.d.	0.10	1.38	0.98
Chargeability (ms) ³	Max.	19.60	11.80	5.46	55.60	16.80	23.40
	Min.	0.07	1.15	0.30	0.47	0.89	3.30
	Avg.	4.62	5.59	1.73	7.22	4.85	14.73

Table 3. Physical and geophysical properties of Nechako Basin sample suite, organized by packages on the basis of lithostratigraphy and summarized as maximum, minimum and average values.

Package name:	Miocene Chilcotin (CB)	Eocene Volcanic and Sedimentary (EVS)	Cretaceous Volcanic and Sedimentary (KVS)	
Group name:		Endako, Ootsa Lake	Kasalka / Powell Creek / Taseko River, Jackass Mountain, Taylor Creek and Skeena, Spences Bridge	
No of samples:	57	31	45	
Dry average V_p (km/s)	Max.	5.99	5.82	6.17
	Min.	4.24	2.25	1.65
	Avg.	5.25	4.40	4.67
Wet average V_p (km/s)	Max.	n/a	6.63	6.49
	Min.	n/a	3.62	3.02
	Avg.	n/a	5.08	5.27
Dry average V_s (km/s)	Max.	n/a	3.44	3.47
	Min.	n/a	1.04	1.04
	Avg.	n/a	2.37	2.61
Wet average V_s (km/s)	Max.	n/a	4.10	3.65
	Min.	n/a	1.50	1.47
	Avg.	n/a	2.52	2.66
Dry bulk density (g/cc)	Max.	2.99	2.89	2.87
	Min.	2.49	1.87	2.05
	Avg.	2.72	2.41	2.59
Wet bulk density (g/cc)	Max.	n/a	2.90	2.89
	Min.	n/a	2.16	2.21
	Avg.	n/a	2.50	2.64
Wet framework density (g/cc)	Max.	3.02	3.02	2.99
	Min.	2.56	2.45	2.64
	Avg.	2.87	2.69	2.76
Dry Poisson's ratio	Max.	n/a	0.41	0.40
	Min.	n/a	0.08	0.09
	Avg.	n/a	0.29	0.25
Wet Poisson's ratio	Max.	n/a	0.45	0.45
	Min.	n/a	0.04	0.03
	Avg.	n/a	0.32	0.30
Dry Young's modulus (GPa)	Max.	n/a	84.36	78.59
	Min.	n/a	5.49	5.21
	Avg.	n/a	38.56	47.22
Wet Young's modulus (GPa)	Max.	n/a	94.08	93.62
	Min.	n/a	13.87	15.24
	Avg.	n/a	44.51	50.86
Dry V_p/V_s	Max.	n/a	2.53	2.43
	Min.	n/a	1.48	1.49
	Avg.	n/a	1.91	1.79
Wet V_p/V_s	Max.	n/a	3.30	3.28
	Min.	n/a	1.44	1.43
	Avg.	n/a	2.10	2.04
Porosity (%)	Max.	16.55	29.44	17.07
	Min.	0.15	0.32	0.27
	Avg.	5.57	9.64	5.57
Magnetic susceptibility (SI)	Max.	0.11	0.05	0.04
	Min.	b.d.	b.d.	b.d.
	Avg.	0.01	0.01	b.d.
Resistivity (ohm-m)	Max.	95646	23035	29011
	Min.	127	37	116
	Avg.	4541	4445	3521
Koenigsberger ratio (K_N)	Max.	80.9	34.9	30.4
	Min.	0.1	b.d.	0.1
	Avg.	13.0	6.8	4.1
Natural remanent magnetization (NRM; A/m)	Max.	48.0	27.7	15.1
	Min.	b.d.	b.d.	b.d.
	Avg.	3.17	3.05	1.22
Chargeability (ms)	Max.	n/a	18.7	45.2
	Min.	n/a	0.0	0.1
	Avg.	n/a	4.4	5.4

Abbreviations: b.d., below detection; n/a, not measured

Table 3 (continued)

Package name:	Middle Late Jurassic Sedimentary (JS)	Lower Middle Jurassic Volcanic and Sedimentary (JVS)	Mesozoic Basement (MB _p)	
Group name:	Relay Mountain, Ladner	Hazleton		
No of samples:	18	10	6	
Dry average V_P (km/s)	Max.	5.85	5.96	5.46
	Min.	4.20	2.57	3.44
	Avg.	5.38	4.33	4.31
Wet average V_P (km/s)	Max.	6.21	6.50	6.07
	Min.	5.16	3.40	4.33
	Avg.	5.72	5.21	5.45
Dry average V_S (km/s)	Max.	3.39	4.04	3.15
	Min.	2.45	1.51	2.00
	Avg.	3.08	2.39	2.61
Wet average V_S (km/s)	Max.	3.52	3.66	3.33
	Min.	2.07	1.66	2.18
	Avg.	3.01	2.59	2.73
Dry bulk density (g/cc)	Max.	2.80	2.75	2.78
	Min.	2.19	1.91	2.33
	Avg.	2.65	2.45	2.65
Wet bulk density (g/cc)	Max.	2.81	2.76	2.79
	Min.	2.20	2.21	2.45
	Avg.	2.66	2.54	2.68
Wet framework density (g/cc)	Max.	2.82	2.78	2.82
	Min.	2.72	2.62	2.65
	Avg.	2.76	2.71	2.74
Dry Poisson's ratio	Max.	0.35	0.37	0.25
	Min.	0.14	0.07	0.14
	Avg.	0.25	0.24	0.21
Wet Poisson's ratio	Max.	0.42	0.42	0.37
	Min.	0.18	0.06	0.28
	Avg.	0.30	0.32	0.33
Dry Young's modulus (GPa)	Max.	76.53	96.54	69.20
	Min.	37.49	11.52	26.32
	Avg.	62.88	38.38	45.42
Wet Young's modulus (GPa)	Max.	81.94	78.79	79.58
	Min.	33.12	17.62	31.00
	Avg.	63.46	47.53	54.60
Dry V_P/V_S	Max.	2.06	2.21	1.73
	Min.	1.54	1.33	1.55
	Avg.	1.76	1.84	1.66
Wet V_P/V_S	Max.	2.76	2.64	2.20
	Min.	1.60	1.46	1.82
	Avg.	1.94	2.07	2.01
Porosity (%)	Max.	3.49	30.06	11.97
	Min.	0.19	0.43	1.00
	Avg.	1.40	8.48	3.41
Magnetic susceptibility (SI)	Max.	b.d.	0.04	0.01
	Min.	b.d.	b.d.	b.d.
	Avg.	b.d.	0.01	0.01
Resistivity (ohm-m)	Max.	49883	12338	10771
	Min.	460	46	152
	Avg.	7271	3864	4402
Koenigsberger ratio (K_N)	Max.	24.9	45.4	5.9
	Min.	b.d.	0.1	0.7
	Avg.	1.5	7.8	3.6
Natural remanent magnetization (NRM; A/m)	Max.	1.0	4.6	2.5
	Min.	b.d.	b.d.	b.d.
	Avg.	0.06	1.38	0.98
Chargeability (ms)	Max.	55.6	16.8	23.4
	Min.	0.3	0.9	3.3
	Avg.	5.0	4.9	14.7

The main parameters affecting chargeability in laboratory experiments are mineralogy, grain size and the presence of pore-filling ionic fluids (Telford et al., 1976). Chargeability is increased by large surface-to-volume ratios between grains (Telford et al., 1976). Values of chargeability for common rock types vary over 3–4 orders of magnitude: 10–20 ms for carbonate rocks versus 2000–3000 ms for sulphide minerals (Telford et al., 1976). Of particular interest to the Nechako Basin dataset are the average ranges of chargeability cited for volcanic tuff (300–800 ms), dense volcanic rocks (100–500 ms), sedimentary rocks (100–500 ms) and igneous rocks (10–50 ms; Telford et al., 1976).

Seismic Wave Velocities

Two fundamental body-wave types travel through material: compressional (P) waves and shear (S) waves. For P waves, material moves parallel to the direction of propagation; for S waves, material moves in a plane perpendicular to the direction of wave propagation. For energy to travel through a given elastic material, there must be a resulting restoring force that resists deformation (Telford et al., 1976). For instance, when a material experiences strain, that strain must be accommodated by a change in shape of the material. Because fluids cannot sustain a shear force, S waves do not propagate through fluids. The P-wave arrivals are always precursory to S-wave arrivals and are therefore easiest to identify. Knowledge of the velocities of P and S waves (i.e., V_P and V_S , respectively) passing through geological materials can be used to identify subsurface rock types. Thus, our measurements of values of V_P and V_S for this diverse suite of samples, under dry and wet conditions, will facilitate interpretation of seismic sections for which subsurface velocity structures have been derived via inversion.

The values of ultrasonic P-wave velocities (V_P) are most important to the ongoing seismic surveys, since inversions of the seismic-survey data are based mainly on V_P . Values of S-wave velocities (V_S) are more difficult to carry out inversions for, but they are useful for refining interpretations of seismic profiles. The distribution of pore fluids and pore-fluid pressures in the subsurface of the Nechako Basin are unknown but are unlikely to be negligible. Furthermore, pore-fluid pressure exerts a significant influence on seismic reflection. On this basis, we elected to make both ‘Dry’ and ‘Wet’ (i.e., water-saturated) ultrasonic measurements of V_P and V_S for each sample core.

The P- and S-wave arrival times for sample cores were measured using a bench-top apparatus at EOST. Measurements were made using an Agilent Technologies model DSO5012A digital-storage oscilloscope, an Agilent Technologies model 33210A 10 MHz function/waveform generator, and two broadband PZT piezoelectric transducer crystals (100 kHz to 1 MHz frequency), one located at each end of the sample. Measurements were made under a stress

of approximately 1 MPa to ensure good contact between the instrument’s end caps and the polished ends of the sample core. The P-wave measurements were based on a transmitted frequency of 700 kHz; S-wave measurements used a frequency of 300 kHz. The P-wave arrivals were chosen as the first clearly identified signal following the triggering pulse from the function generator. The S-arrival is characterized by a distinct change in the ultrasonic response of the sample with time. The onsets of the S-wave arrivals were determined by identifying the first significant change in signal amplitude or the first distinct inflection point in the slope of the signal following the P-wave arrival.

Derivative (Computed) Properties

The measured values of V_P and V_S for cores of rock samples allow the calculation of derivative properties, namely several elastic (dynamic) properties (Table 2). In this section, we review the calculation of Poisson’s ratio and Young’s modulus (Tables 2 and 3).

Elastic compression and extension are described by Hooke’s Law,

$$\sigma = E \cdot \varepsilon, \quad (5)$$

where σ is the normal stress and ε is the elongation or normal strain. Young’s modulus (E) is the measure of stiffness and is traditionally taken as the ratio between the tensile stress and tensile strain. Here, we define E as the ratio of uniaxial stress to uniaxial strain. Young’s modulus calculated from ultrasonic velocities is an indirect and nondestructive way of determining the stiffness of rock samples. For most rocks, E has values between 10 and 200 GPa (Telford et al., 1976).

Poisson’s ratio is the ratio between the shortening and expansion of a material under uniaxial compression. Most rocks have Poisson’s ratios between 0.05 (for very hard, rigid rock) to 0.45 (for soft, poorly consolidated material; Telford et al., 1976).

Using ultrasonic measurements of P- and S-wave velocities, the dynamic elastic moduli can be computed for Poisson’s ratio (ν_d) as

$$\nu_d = \frac{V_P^2 - 2V_S^2}{2(V_P^2 - V_S^2)} \quad (6)$$

and for Young modulus (E_d) as

$$E_d = \rho \times \left[\frac{V_S^2(3V_P^2 - 4V_S^2)}{V_P^2 - V_S^2} \right], \quad (7)$$

where ρ is the bulk density of the sample (g/cc).

Results

We describe in this section the experimental results obtained for each of the six lithostratigraphic packages (Ta-

bles 1 and 3). The range of values measured for the various properties across all lithostratigraphic packages is extreme (Table 3):

- porosity: 0.15–30.06%
- density: 2.45–3.02 g/cc
- chargeability: 0.0–55.6 ms
- NRM: 1.0–48.0
- resistivity: 46–95646 $\Omega \cdot m$
- magnetic susceptibility: 0.01–0.11 SI
- dry V_p : 1.65–6.17 km/s
- dry V_s : 1.04–4.04 km/s
- wet V_p : 3.02–6.63 km/s
- wet V_s : 1.47–4.10 km/s

Variation within lithostratigraphic packages is substantially less and reflects the physical and lithological variations within each package. Some packages comprise a narrow range of rock types (e.g., Miocene Chilcotin basalts [CB]) and can show a correspondingly narrow range of physical and geophysical properties (Table 3). Other lithostratigraphic packages comprise a diverse range of rock types (e.g., Eocene volcanic and sedimentary rocks [EVS]) and show a correspondingly wide range of properties. Ultimately, this extensive and high-quality dataset is intended for Geoscience BC’s digital database and promises to facilitate geophysical interpretations of the geology in the Nechako Basin region of central BC. Data from each of the six lithostratigraphic packages have been plotted on

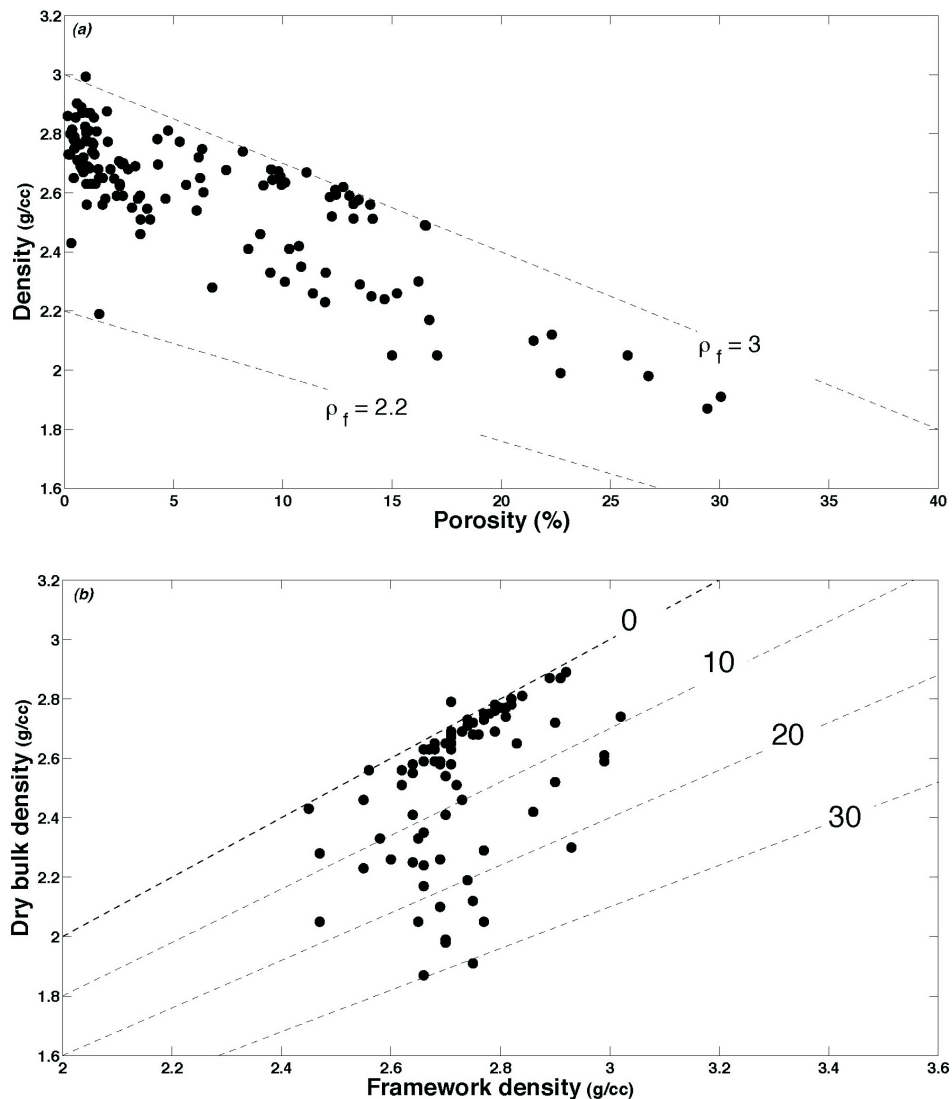


Figure 3. Density and porosity ranges for the entire suite of samples collected within the Nechako Basin: **a)** measured values of dry bulk density plotted versus porosity, ranging from 0% to 30%, confirming the expected negative correlation; the broad trend described by the dataset lies between model density–porosity lines for samples having framework density (ρ_f) values of 2.2 and 3 g/cc; **b)** measured values of bulk density and framework density, which varies from ~2.4 to 3.1 g/cc and represents the skeletal density plus any isolated pore space (<1% in these samples); contours map the decrease in bulk density due to increasing porosity (%).

multiparameter diagrams (Table 3) to characterize the within-package variations in physical properties.

As part of our physical-property characterization of the samples, we measured bulk and framework densities and porosity. Many geophysical properties are, themselves, dependent on or sensitive to these physical properties. The suite of 167 samples has a porosity range of 0–30 vol. % (Figure 3a); the porosity is assumed to be fully connected. On the basis of the different methods used to measure density, we saw no evidence for a substantial fraction of isolated porosity. Bulk density (rock plus pore space) ranges from ~1.8 to 3.0 g/cc, whereas the corresponding framework density varies between ~2.4 and 3.0 g/cc. The relationship between bulk and framework density and porosity is illustrated in Figure 3b. At zero porosity, bulk and framework density are equivalent. The contours in Figure 3b illustrate the effect of porosity in reducing the bulk density of samples relative to their framework density.

The magnetic properties of the six lithostratigraphic packages are shown in Figure 4 (Table 3; Figure 4a–f). The K_N values for the entire suite vary over four orders of magnitude, from 10^{-2} to 10^2 . Magnetic susceptibility varies over three orders of magnitude, from 10^{-4} to 10^{-1} ms. High val-

ues of K_N indicate rocks that have preserved the magnitude and direction of the global magnetic field at the time of emplacement. For samples having high values of K_N (>1), the measured values of magnetic susceptibility need to be corrected in order to use the data to identify and interpret magnetic anomalies. Within the Nechako Basin, K_N is a relatively good indicator of volcanic rocks emplaced at elevated temperature (exhibiting thermoremanent NRM), whereas sedimentary rocks have low K_N values. In most rocks, variations in k mainly reflect modal variations in magnetic minerals (particularly magnetite; Telford et al., 1976). However, given the large variability of k within rock types and the significant overlap in k values across rock types, k is, by itself, a poor discriminator of lithostratigraphic packages. The Chilcotin basalts are characterized by high K_N values (~1–100), and their k values vary over three orders of magnitude. The EVS package has very similar ranges of K_N and k , although fewer samples were measured. The KVS rocks show a greater range in K_N and have a lower mean value, while showing an identical variation in k . The wide range of K_N values for the KVS package indicates a broad range of rock types incorporated into this package. The JS samples are distinguished by low values of K_N and restricted and low values of k . This reflects the fact that they are dominantly sedimentary in provenance. Con-

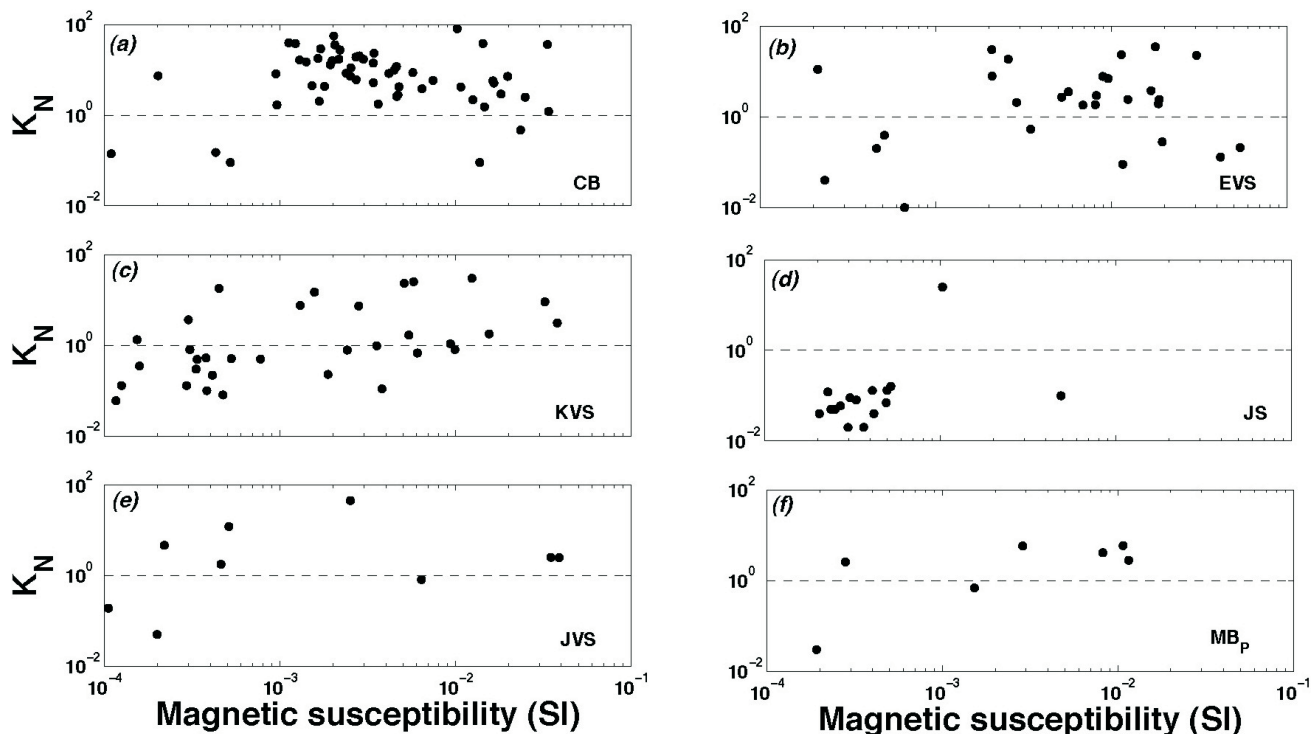


Figure 4. Relationship between K_N (Koenigsberger ratio) and magnetic susceptibility for the lithostratigraphic packages listed in Table 1: **a)** Chilcotin Group basaltic lavas (CB), **b)** Eocene volcanic and sedimentary rocks (EVS), **c)** Cretaceous volcanoclastic and sedimentary rocks (KVS), **d)** Middle–Late Jurassic sedimentary rocks (JS), **e)** Lower–Middle Jurassic volcanic and sedimentary rocks (JVS), and **f)** Mesozoic basement rocks (MB_p). The dashed lines at $K_N = 1$ indicate the threshold above which the magnetic-anomaly interpretation needs to be corrected for remanent magnetization (NRM; see text); the data presented are not corrected for NRM. For example, nearly all CB basalts have K_N values >1 and require corrections to the experimentally measured values of magnetic susceptibility. Conversely, JS samples are largely unaffected by NRM.

versely the small numbers of samples within the JVS package suggest wide-ranging K_N and k properties similar to those observed in the EVS and KVS packages. The basement rocks (MB_p) have intermediate to low K_N and a range of k values. These properties are largely a reflection of the variable modal mineralogy of the plutonic rocks collected to represent the basement to the Nechako Basin.

The resistivity values for each lithological package are plotted as a function of sample porosity (Figure 5). Figure 5a demonstrates clearly that the range of resistivities in CB ($127\text{--}95\,646\ \Omega\cdot\text{m}$) is controlled by mineralogical composition and has very little dependence, if any, on sample porosity. The CB rocks are relatively lithologically homogeneous but vary widely in porosity ($\sim 0\text{--}17\%$) due to their varying vesicularity. This wide range of porosity has no apparent effect on the resistivity of the CB sample package. Conversely, the variation in sample resistivity of two orders of magnitude seen in these basalts is likely a reflection of variations in crystallinity, grain size and bulk mineralogy. The EVS sample package (Figure 5b) clearly shows a decrease in resistivity by three orders of magnitude (from approximately 10^4 to $10^1\ \Omega\cdot\text{m}$) as a function of porosity. This sample package is more lithologically varied and, although there is some variation in resistivity at constant porosity, the

emergent trend demonstrates that mineralogy and bulk composition are likely secondary contributors to resistivity. The resistivity of the KVS sample package decreases more than two orders of magnitude (from 10^4 to $10^2\ \Omega\cdot\text{m}$) with porosity (Figure 5c), a variation that is less pronounced than in the EVS package. This may suggest that both composition and porosity control resistivity in this lithostratigraphic package. The JS package shows a resistivity range of two orders of magnitude (from $10^4\text{--}10^2\ \Omega\cdot\text{m}$) over a change of less than 5% in porosity (Figure 5d). The tight clustering of data suggests that JS rocks can be discriminated from other packages on the basis of measured porosity and resistivity. Resistivity of the JVS sample package decreases with increasing porosity (Figure 5e). As this package is lithologically uniform, it is expected that most variation in resistivity ($10^4\text{--}10^2\ \Omega\cdot\text{m}$) is porosity controlled. Lastly, the relatively homogeneous lithology and generally low porosity of the basement rocks (MB_p) results in a tight clustering of data (Figure 5f) similar to that observed for the JS rocks. In every case where porosity variation is large, save for the CB package, resistivity decreases with increasing porosity.

The ranges of values for resistivity and chargeability are organized by lithostratigraphic package (with the exception

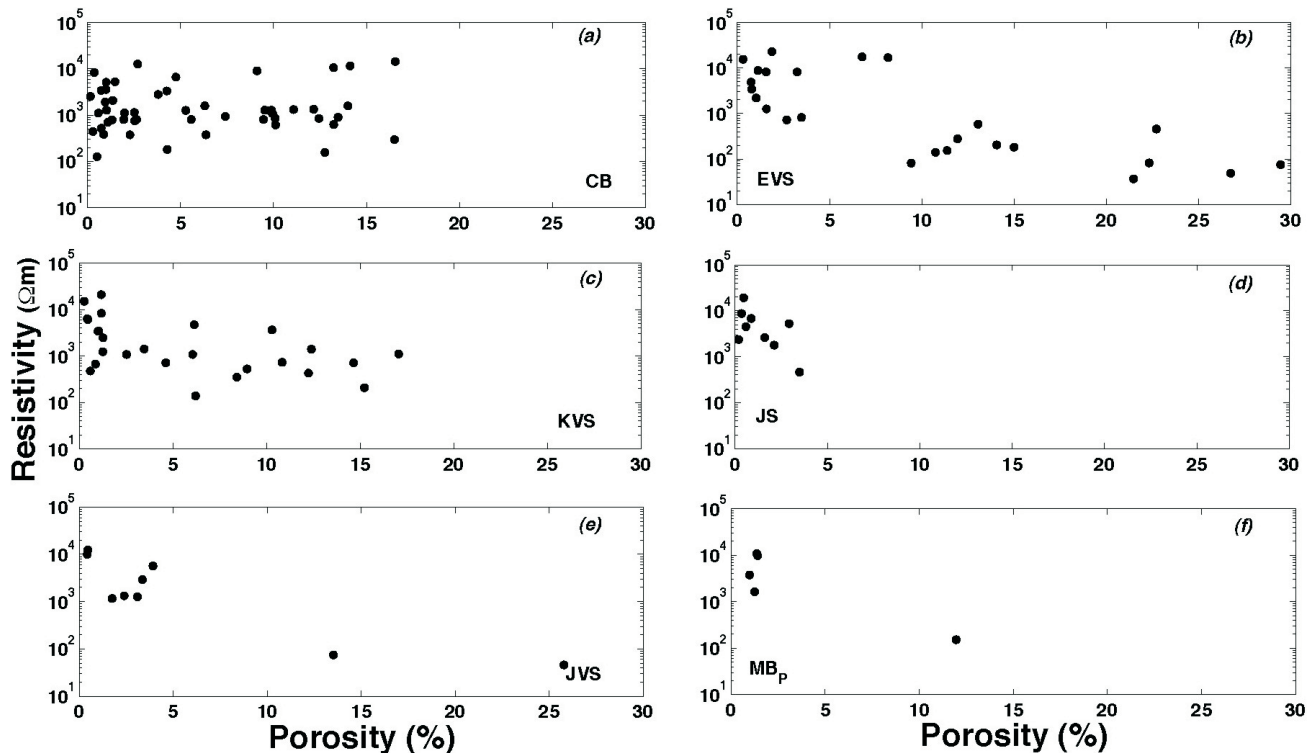


Figure 5. Experimentally measured values of resistivity (Table 2) plotted against total porosity of each sample for the lithostratigraphic packages listed in Table 1: **a)** Chilcotin Group basaltic lavas (CB), **b)** Eocene volcanic and sedimentary rocks (EVS), **c)** Cretaceous volcanoclastic and sedimentary rocks (KVS), **d)** Middle–Late Jurassic sedimentary rocks (JS), **e)** Lower–Middle Jurassic volcanic and sedimentary rocks (JVS), and **f)** Mesozoic basement rocks (MB_p). Resistivity commonly decreases with porosity (cf. parts b–f). Samples of CB show two orders of magnitude variation in resistivity that does not correlate with porosity, the implication being that resistivity in these basalts is controlled by variations in crystallinity, grain size or bulk mineralogy.

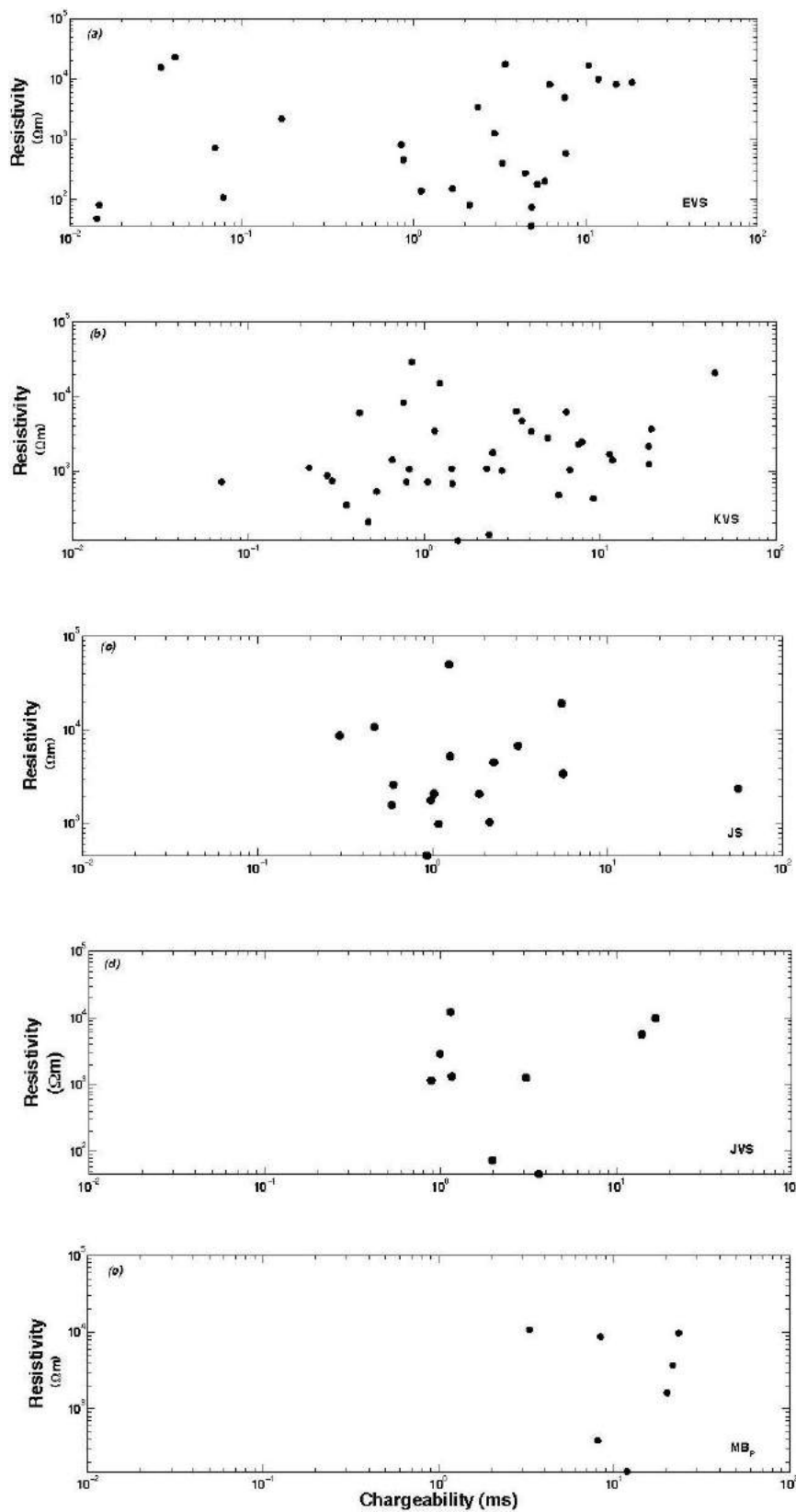


Figure 6. Experimentally measured values of resistivity and chargeability (Table 2) plotted for all lithostratigraphic packages listed in Table 1: **a)** Eocene volcanic and sedimentary rocks (EVS), **b)** Cretaceous volcanoclastic and sedimentary rocks (KVS), **c)** Middle–Late Jurassic sedimentary rocks (JS), **d)** Lower–Middle Jurassic volcanic and sedimentary rocks (JVS), and **e)** Mesozoic basement rocks (MB_p).

of CB) in Figure 6a–e. The resistivity range of EVS (Figure 6a) is less than three orders of magnitude, and chargeability varies by as much as four orders of magnitude. This broad range of values is largely controlled by lithology, although enhanced by the wide range of porosity in the EVS sample package. Resistivity measurements were conducted under distilled water-saturated conditions. Such conditions are expected to dissolve any late-stage groundwater-derived mineral precipitates lining the pore spaces, thereby creating ionic pore fluids and a more conductive sample. However, as shown in Figure 5, resistivity decreases with increasing preserved porosity, suggesting a paucity of such mineral precipitates in these pore spaces. Likewise, KVS (Figure 6b) also demonstrates a broad range of resistivities and chargeabilities, testament to the broad range in lithology and variation in porosity of the sample package. The JS sample package (Figure 6c) ranges in resistivity and chargeability across two and a half orders of magnitude. The resistivity range of JVS (Figure 6d) is approximately 2.5 orders of magnitude, whereas the chargeability range of this package is slightly greater than one order of magnitude. The tighter range of chargeability values for both JS and JVS is controlled predominantly by lithology. Lithological variation within each package is limited, suggesting that any scatter in resistivity is due to porosity. The porosity of the JS package rocks is negligible compared to that of the JVS package, suggesting that the narrower range of resistivities within the JS package is lithologically controlled. Figure 6e shows the ranges in resistivity (approximately two orders of magnitude) and chargeability (ap-

proximately one order of magnitude) for the MB_p rocks. This package contains lithologically similar rocks (plutonic rocks) of relatively low porosity, ensuring that the range in measured electrical properties is small.

The seismic properties of the Nechako Basin sample suite are possibly the most useful for package discrimination. Figure 7 displays the P-wave velocity (V_p) of the Chilcotin basalts (CB) as a function of sample density under various confining pressures. Dashed lines indicate the corresponding porosities for all samples. It is clear that V_p increases with decreasing porosity and increasing confining pressure; V_p is therefore highest for stronger, low-porosity rocks. With increasing confining pressure, V_p increases as pore space is closed and the rock becomes more coherent.

Figure 8a–e shows the dry and wet V_p and V_s values for the EVS, KVS, JS, JVS, and MB_p lithological packages. Dry samples have lower V_p/V_s values (1.5–2) than water saturated samples (1.75–3). Dashed lines indicate V_p/V_s ratios of 1, 1.5, 2 and 3. Wet V_p/V_s ratios for all packages (1.75–3) are consistently higher than the same ratios calculated for dry samples (1.5–2; O’Connell and Budiansky, 1974). Figure 8a (EVS), 8b (KVS) and 8d (JVS) shows the most variation in V_p/V_s ratios (1.5–3 for EVS and KVS), testament to the variable lithology in each package (which includes both volcanic and sedimentary rocks of varying porosity). Ratios for the JS (Figure 8c) and MB_p (Figure 8e) packages are relatively well constrained between 1.5 and 2. Ratios of V_p/V_s have been demonstrated to be strong indicators of variations in fluid-saturation conditions within rocks

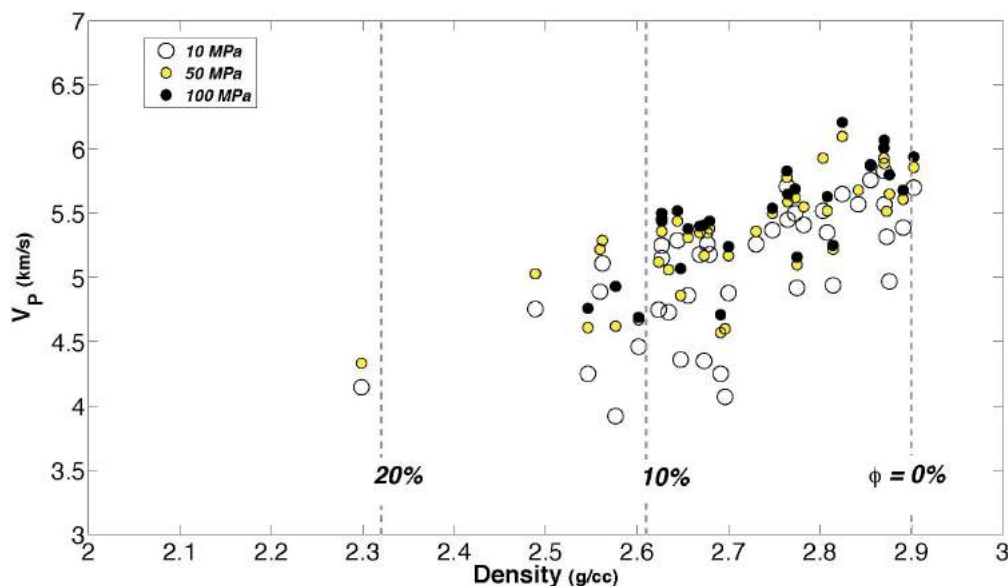


Figure 7. Plot of compressional-wave (P-wave) velocity (V_p) versus bulk density for core samples of Chilcotin basalts. Both V_p and density are measured on dry, as opposed to water-saturated, sample cores. Values of V_p are measured under load pressures of 10, 50 and 100 MPa. Dashed lines denote model values of density for samples having total porosities (ϕ) of 0%, 10% and 20%, and assuming a skeletal density of 2.9 g/cc. Values of V_p increase with increasing confining pressure (i.e., load) and decrease with decreasing porosity (increasing density).

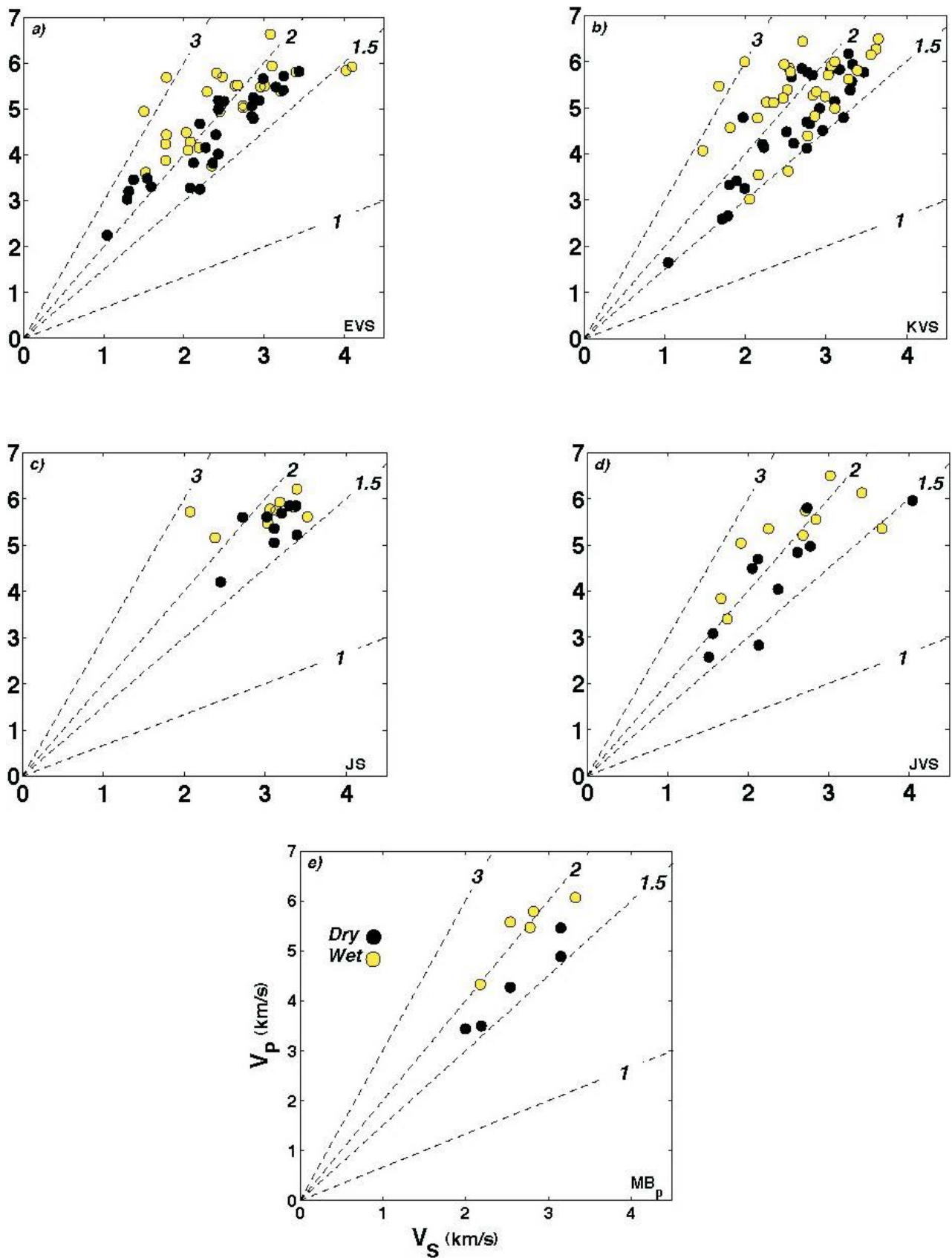


Figure 8. Plots of compressional-wave velocity (V_P) versus shear-wave velocity (V_S) measured on dried (black symbols) and water-saturated (yellow symbols) cores taken from all samples (Table 2) except the CB package. Diagram is contoured for ratios of V_P/V_S of 1, 1.5, 2 and 3.

(O'Connell and Budiansky, 1974). On this basis, further investigation of seismic velocities within the Nechako Basin could elucidate both density of crack distributions within the underlying stratigraphy and, more importantly, the degree of fluid saturation of these cracks. The latter (e.g., fluid distribution) relates directly to our capacity to assess the hydrocarbon potential of the basin.

Figures 9–13 show the dependence of both dry and wet ultrasonic velocities on bulk density and porosity, and the dependence of dry and wet elastic moduli on porosity. For all figures, (a) plots wet and dry P-wave velocities as a function of density; (b) plots wet and dry S-wave velocities as a function of density; (c) plots wet and dry P-wave velocities as a function of porosity; (d) plots wet and dry P-wave velocities as a function of porosity; (e) plots wet and dry Young's modulus as a function of porosity; and (f) plots wet and dry Poisson's ratio as a function of porosity. All dry ultrasonic velocities are plotted against dry bulk densities; likewise, all wet ultrasonic velocities are plotted as functions of their wet bulk densities. Each figure deals with a different package of rocks.

The same relationships are observed in all plots (Figures 9–13), although those packages with both larger sample suites and greater heterogeneity in bulk density and porosity display these relationships more clearly. Figures 9a–13a and 9b–13b exhibit increasing ultrasonic velocity with increasing sample bulk density. Conversely, although perhaps intuitively, these same ultrasonic velocities decrease with increasing porosity (Figures 9c–13c and 9d–13d). The presence of dry void space or water-saturated void space affects both P- and S-wave velocities considerably for all rocks (O'Connell and Budiansky, 1976). Most samples exhibit higher ultrasonic velocities when saturated in water, and this becomes more pronounced with increasing porosity. Elastic moduli are frequency dependent (Walsh, 1965; O'Connell and Budiansky, 1976) and sensitive to sample saturation, which increases seismic velocity. Figures 9e–13e show that the Young's modulus of all rocks decreases with porosity, reflecting decreasing stiffness (Walsh, 1965). Poisson's ratio is the ratio between transverse strain to longitudinal strain and can be estimated from the velocities of compressional (longitudinal) and shear (transverse)

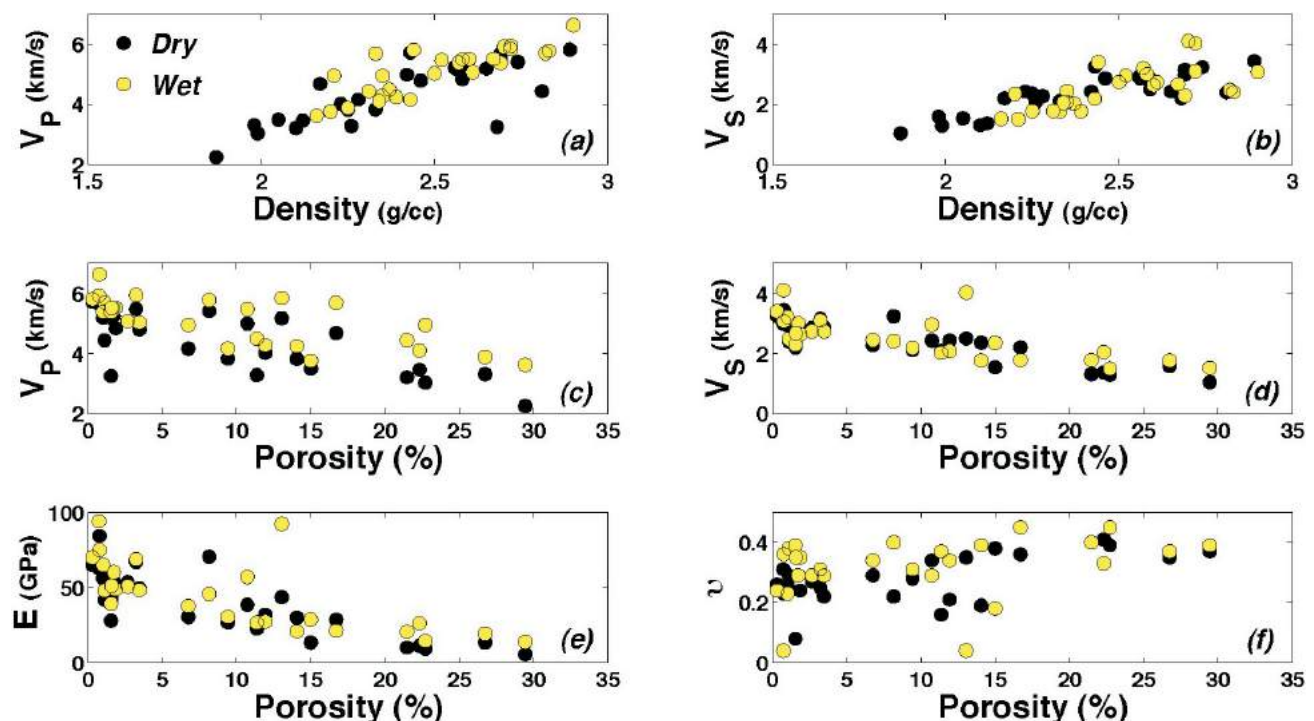


Figure 9. Dependence of dry and wet ultrasonic velocities on bulk density and porosity, and dependence of dry and wet elastic moduli on porosity for Eocene volcanic and sedimentary rocks (EVS; Table 3): **a)** V_P as a function of bulk density; **b)** V_S as a function of bulk density; **c)** V_P as a function of connected porosity; **d)** V_S as a function of connected porosity; **e)** dynamic Young's modulus (E_d) as a function of connected porosity; **f)** Poisson's ratio (ν), calculated from measured values of V_P and V_S , as a function of connected porosity. In parts (a) and (b), dry ultrasonic velocities are plotted against dry bulk densities, and wet ultrasonic velocities against wet bulk densities. Values of V_P and V_S increase with bulk density and decrease with porosity. Young's Modulus decreases with increasing porosity due to the inherent weakness of porous rock. V_P and V_S and moduli are consistently larger for water-saturated samples than for dry samples.

waves. Figures 9f–13f show that there appears to be little relationship between the calculated Poisson's ratios and porosities of the six Nechako Basin packages.

Geophysical Discrimination within the Nechako Basin

In this section, we develop a decision table (Table 4) to facilitate geophysical discrimination of lithostratigraphic units in the subsurface to the Nechako Basin. We highlight the most reliable indices for discrimination between the six major lithostratigraphic packages described in Table 1. Each cell in Table 4 contains physical properties appropriate for distinguishing between the units of the intersecting column and row. This is not an exhaustive set of discriminators. In part, the decision table reflects, and is limited by, the fact that we have packaged the rocks on the basis of age, geography and lithology.

The Miocene Chilcotin basalts (CB) are one of the most distinctive lithostratigraphic packages underlying the Nechako Basin. These rocks have higher dry V_p values (4.2–6.0 km/s) than the range of values observed for the Eocene volcanic and sedimentary (EVS) package (2.2–5.8 km/s). The V_p values for CB rocks (4.2–6.0 km/s) overlap those measured for Cretaceous volcanoclastic and sedimentary

(KVS) rocks (1.6–6.2 km/s) but are generally higher; the overlap is a reflection of the diverse range of V_p values within the KVS package. The CB package is easily distinguished from rock types within the Middle–Late Jurassic sedimentary (JS) package on the basis of NRM. The CB package shows a large range of values from below detection (b.d.) to 48 A/m; in contrast, the JS rocks have a limited range (b.d. to 1.0 A/m), and most samples have NRM values of <0.1 A/m. Distinguishing CB rocks from rocks of the Lower–Middle Jurassic volcanic and sedimentary (JVS) package is more uncertain. The dry V_p offers partial discrimination of CB (4.2–6.0 km/s) from JVS (2.5–5.9 km/s), in that CB rocks have V_p values restricted to the upper range of JVS values. The difficulty in discriminating between these two lithostratigraphic packages reflects the lithological diversity of the JVS package and the fact that it contains many similar volcanic rocks. Similarly, CB rocks are poorly distinguished from the Mesozoic basement rocks (MB_p), although they have a higher mean V_p (4.2–6.0 km/s) than the MB_p package (3.4–5.5 km/s).

The EVS package is indistinguishable from the KVS package in terms of all the measured geophysical properties: this is not surprising, given that the lithological make-up of both packages is very similar. The sole distinguishing prop-

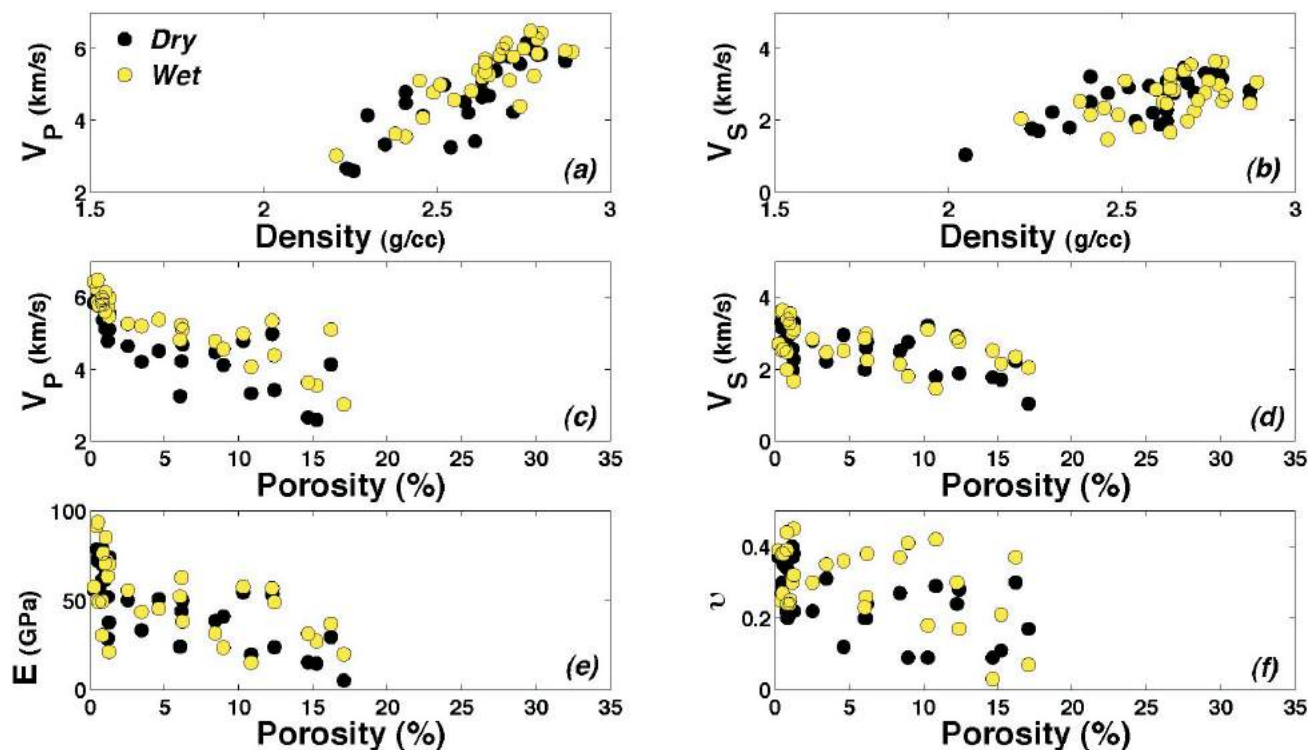


Figure 10. Dependence of dry and wet ultrasonic velocities on bulk density and porosity, and dependence of dry and wet elastic moduli on porosity for Cretaceous volcanoclastic and sedimentary rocks (KVS; Table 3): **a)** V_p as a function of bulk density; **b)** V_s as a function of bulk density; **c)** V_p as a function of connected porosity; **d)** V_s as a function of connected porosity; **e)** dynamic Young's modulus (E_d) as a function of connected porosity; **f)** Poisson's ratio (ν), calculated from measured values of V_p and V_s , as a function of connected porosity. In parts (a) and (b), dry ultrasonic velocities are plotted against dry bulk densities, and wet ultrasonic velocities against wet bulk densities. Values of V_p and V_s increase with bulk density and decrease with porosity.

erty is porosity: the EVS package has higher porosity (~30%) than the KVS package, which is consistently less than 17%. Although not ideal, this is the only viable way of distinguishing between the EVS and KVS packages. Rocks of the EVS package are easily distinguished from those of the JS package in the following ways: 1) NRM values for EVS rocks (b.d. to 28 A/m) are substantially higher than those of JS rocks (most are <0.004 A/m); 2) values of chargeability (m_T) can also help distinguish EVS (b.d. to 19 ms) from JS (0.3–56 ms); 3) values of dry and water-saturated V_p values overlap, but EVS rocks (2.35–5.8 and 3.6–6.6 km/s) show a greater range than JS rocks (4.2–5.8 and 5.2–6.2 km/s); 4) on average, EVS rocks are less resistive (37–23 035 $\Omega\cdot\text{m}$) than JS rocks (460–49 883 $\Omega\cdot\text{m}$), but there is complete overlap between the ranges. As with KVS rocks, JVS rocks cannot be reliably distinguished from EVS rocks by any geophysical property reported; this is due to the similar lithological components in each package. The EVS rocks are also poorly distinguished from MB_p rocks, although all MB_p geophysical-property ranges are narrower and lie completely within EVS ranges. This is due to the variety of rock types within the EVS package, which also includes some igneous samples.

As with the EVS package, it is difficult to distinguish the various lithological packages from the Cretaceous volcanic and sedimentary (KVS) package. Discrimination is hindered by the variety of rock types grouped under the KVS label, which has resulted in a large scatter of geophysical-property data. There is poor distinction between KVS and JVS, since both packages encompass similar rock types, although resistivity has potential as a geophysical discriminator. The resistivity ranges of both packages overlap considerably, although KVS resistivities (116–29 011 $\Omega\cdot\text{m}$) are consistently higher than those characterizing the JVS package (46–12 338 $\Omega\cdot\text{m}$). There is significant overlap between KVS and JVS ultrasonic velocities, rendering these two packages seismically indistinguishable. As with the EVS package, NRM values for KVS (b.d. to 15.1 A/m) are substantially higher than those of JS rock units (most are <0.004 A/m). Ultrasonic velocities of KVS rocks vary greatly due to lithological diversity in this package. However, JS rocks are both lithologically and physically similar (porosities are <3.5%), resulting in narrow ranges for their seismic velocities (V_{pDry}^{JS} of 4.2–5.8 km/s; V_{sDry}^{JS} of 2.4–3.4 km/s), which are consistently much higher than those of

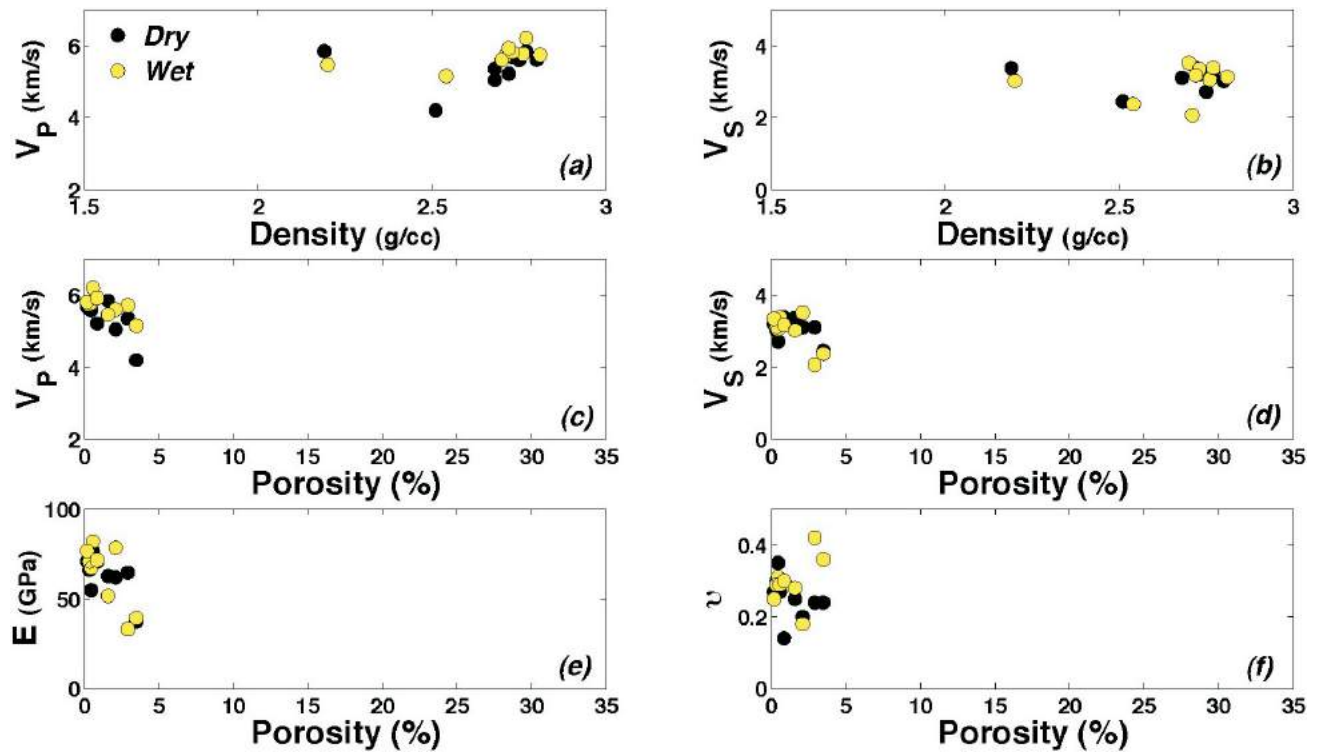


Figure 11. Dependence of dry and wet ultrasonic velocities on bulk density and porosity, and dependence of dry and wet elastic moduli on porosity for Middle–Late Jurassic sedimentary rocks (JS; Table 3): **a)** V_p as a function of bulk density; **b)** V_s as a function of bulk density; **c)** V_p as a function of connected porosity; **d)** V_s as a function of connected porosity; **e)** dynamic Young’s modulus (E_d) as a function of connected porosity; **f)** Poisson’s ratio (ν), calculated from measured values of V_p and V_s , as a function of connected porosity. In parts (a) and (b), dry ultrasonic velocities are plotted against dry bulk densities, and wet ultrasonic velocities against wet bulk densities.

KVS ($V_{P_{Dry}}^{KVS}$ of 1.6–6.2 km/s; $V_{S_{Dry}}^{KVS}$ of 1.0–3.5 km/s). The ranges of all physical properties for MB_p rocks are consistently narrower than for KVS rocks, due to the compositional and physical similarity of all the basement rocks. However, the ranges of values for every measured geophysical property of MB_p rocks lie within the broader ranges of properties of the KVS package. Geophysical identification of MB_p rocks in the subsurface thus requires the use of all properties.

Jurassic sedimentary (JS) rocks are poorly distinguished from the Jurassic volcanic and sedimentary (JVS) package, but resistivity values may offer some potential. Although there is overlap in resistivity values between JS and JVS, resistivities of JS rocks (460–49 883 Ω·m) are consistently higher than those of JVS rocks (46–12 338 Ω·m). The ranges of all physical properties for MB_p are consistently narrower than those for JVS rocks but are fully enclosed by the large ranges of the JVS package. It is recommended that all the available properties be used when identifying MB_p rocks in the subsurface.

Both the JS and MB_p packages represent lithologically well-defined rock packages that populate distinct geophysical-property ranges, which makes their distinction relatively easy compared to other packages. Their ranges in-

resistivity and seismic velocity have relatively little overlap and are the most useful properties for discrimination. The resistivity range for JS rocks is 460–49 883 Ω·m, which is considerably higher than that for MB_p (152–10 771 Ω·m). Ultrasonic velocities also offer adequate discrimination because JS velocities ($V_{P_{Dry}}^{JS}$ of 4.20–5.85 km/s; $V_{S_{Dry}}^{JS}$ of 2.45–3.39 km/s) are higher than those of MB_p rocks ($V_{P_{Dry}}^{MBp}$ of 3.44–5.46 km/s; $V_{S_{Dry}}^{MBp}$ of 2.00–3.15 km/s).

Summary

The Nechako Basin represents one of the most challenging areas for mineral and oil exploration in British Columbia. The challenge is that the basin is likely to be underlain by stratigraphically and structurally complex geology. This complexity is exacerbated by the fact that the quality and distribution of bedrock exposure is highly variable; overall, the exposure is poor throughout the region. In addition, only a limited amount of knowledge of the subsurface geology has been derived from previous oil-exploration efforts. These early oil-exploration efforts provided few drillholes and geophysical surveys. However, the last decade has seen a tremendous increase in new knowledge derived from mapping (e.g., Riddell, 2006, 2011; Dohaney et al., 2010; Andrews et al., 2011; Bordet and Hart, 2011) and multi-

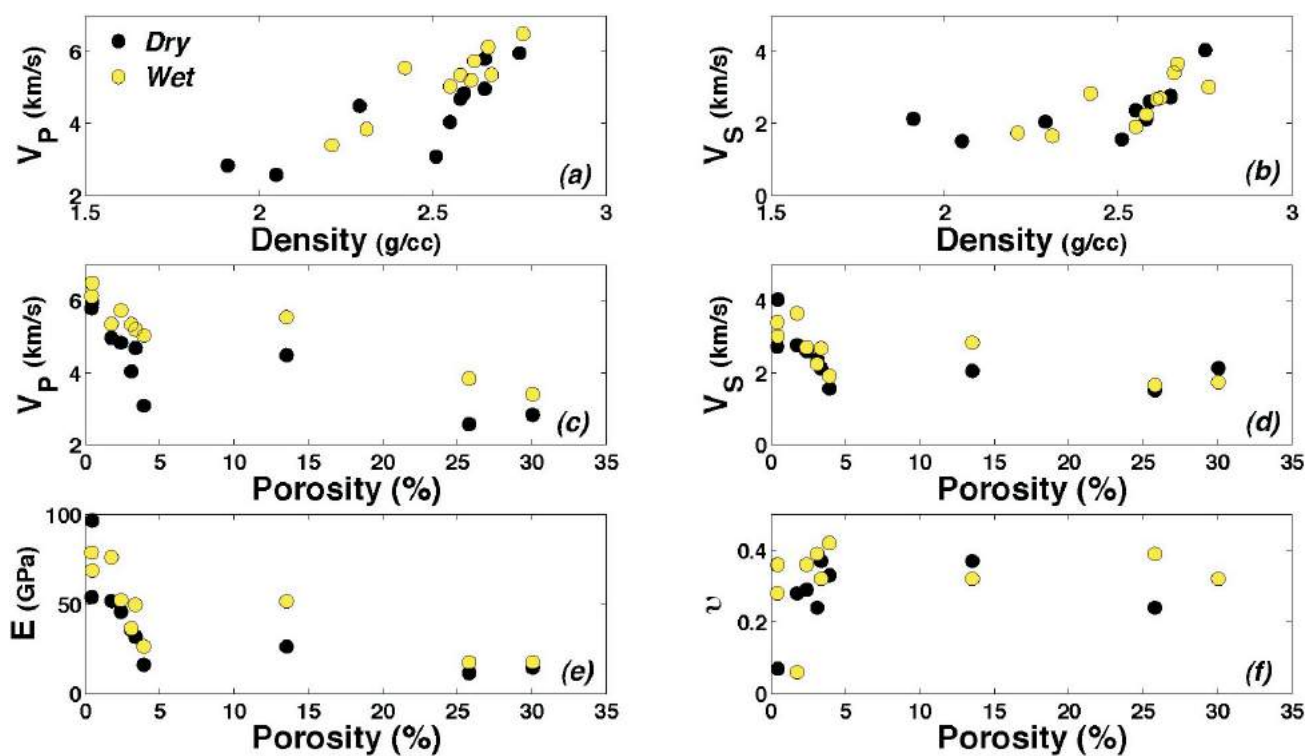


Figure 12. Dependence of dry and wet ultrasonic velocities on bulk density and porosity, and dependence of dry and wet elastic moduli on porosity for Lower–Middle Jurassic volcanic and sedimentary rocks (JVS; Table 3): **a)** V_P as a function of bulk density; **b)** V_S as a function of bulk density; **c)** V_P as a function of connected porosity; **d)** V_S as a function of connected porosity; **e)** dynamic Young’s modulus (E_d) as a function of connected porosity; **f)** Poisson’s ratio (ν), calculated from measured values of V_P and V_S , as a function of connected porosity. In parts (a) and (b), dry ultrasonic velocities are plotted against dry bulk densities, and wet ultrasonic velocities against wet bulk densities.

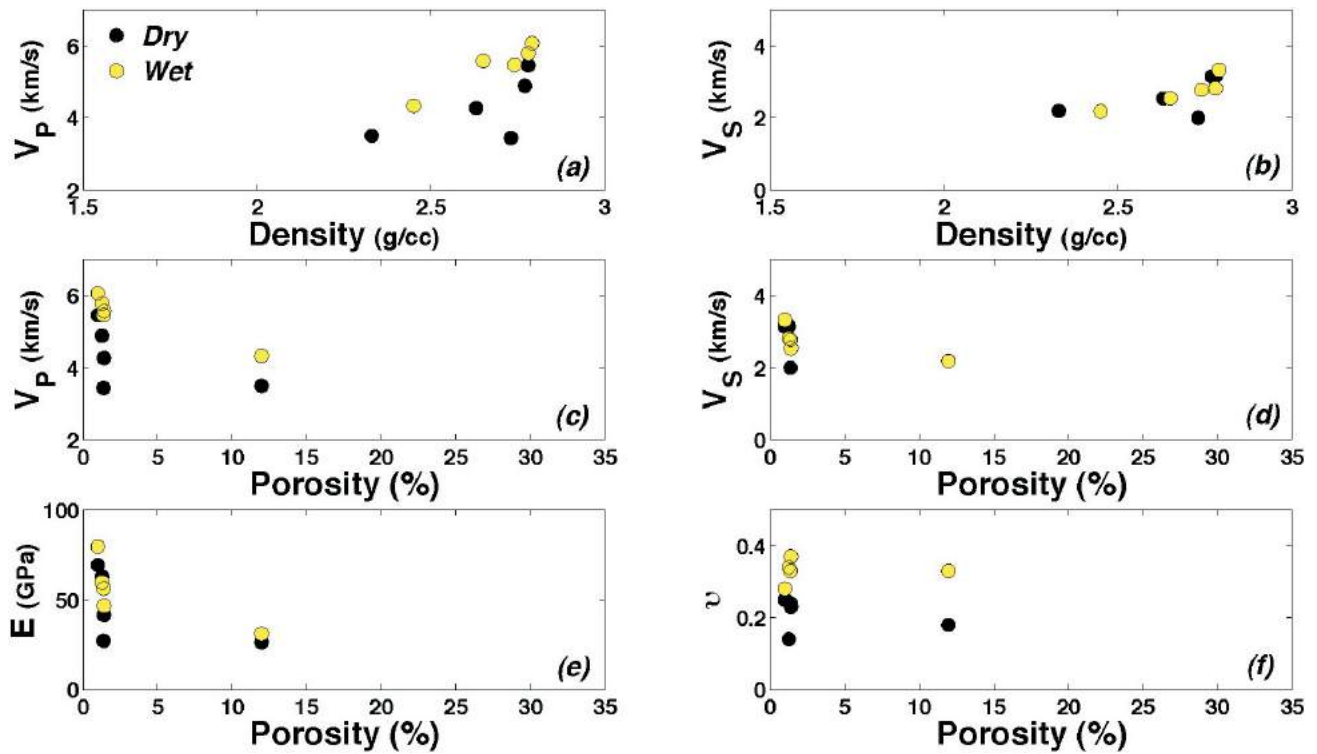


Figure 13. Dependence of dry and wet ultrasonic velocities on bulk density and porosity, and dependence of dry and wet elastic moduli on porosity for Mesozoic basement rocks (MB_p; Table 3): **a)** V_P as a function of bulk density; **b)** V_S as a function of bulk density; **c)** V_P as a function of connected porosity; **d)** V_S as a function of connected porosity; **e)** dynamic Young’s modulus (E_d) as a function of connected porosity; **f)** Poisson’s ratio (ν), calculated from measured values of V_P and V_S , as a function of connected porosity. In parts (a) and (b), dry ultrasonic velocities are plotted against dry bulk densities, and wet ultrasonic velocities against wet bulk densities.

parameter geophysical surveys (e.g., Hayward and Calvert, 2011; Idowu et al., 2011; Spratt and Craven, 2011).

The range of possible geophysical responses from subsurface stratigraphic packages must be known in order to extract the maximum information from these large-scale field-based geophysical campaigns. The project reported here was a field-supported experimental program designed to measure a broad range of physical and geophysical properties of rock samples representing the lithostratigraphic diversity of the subsurface to the Nechako Basin. We sampled more than 11 major formations or mappable strati-

graphic units (Table 1; Figure 2) across an area of >50 000 km² (Figure 2).

Measurements were taken of the physical (e.g., density, porosity) and geophysical (e.g., chargeability, seismic velocity) properties of the sample suite, with the aim of providing data that would facilitate interpretation of geophysical surveys probing the Nechako Basin subsurface. The full range of measurements included bulk density, porosity, magnetic susceptibility, remanent magnetization, electrical resistivity, induced-polarization chargeability and seismic-wave velocities. Ranges of values were then determined for each

Table 4. Decision table for discrimination of stratigraphic packages within the Nechako Basin on the basis of physical and geophysical properties.

EVS	KVS	JS	JVS	MB _p	Stratigraphic package
V_p	V_p	NRM	V_p	V_p	CB
	ϕ	$V_p; V_s; m_T; \text{NRM}$	$m_T; V_s$	$V_p; V_s; m_T; \text{Res}$	EVS
		$V_p; V_s; \text{NRM}; \text{Res}$	Res	$V_p; V_s; m_T; \text{Res}; \text{NRM}$	KVS
			$V_p; V_s; \text{Res}$	$V_p; V_s; m_T; \text{Res}; \text{NRM}; k$	JS
				$V_p; V_s; \text{NRM}; \text{Res}; m_T$	JVS

Stratigraphic package abbreviations: EVS, Eocene volcanic and sedimentary rocks; KVS, Cretaceous volcaniclastic and sedimentary rocks; JS, Middle–Late Jurassic sedimentary rocks; JVS, Lower–Middle Jurassic volcanic and sedimentary rocks; MB_p, Mesozoic basement rocks

Rock property abbreviations: k, magnetic susceptibility; Res, resistivity; V_p , compressional wave (P-wave) velocity; V_s , shear wave (S-wave) velocity; m_T , chargeability; NRM, natural remanent magnetization; ϕ , porosity

of six lithostratigraphic packages created by combining stratigraphic units on the basis of age, lithology and geography. Our compilation culminated in a decision table that summarizes the best opportunities for discriminating stratigraphic packages within the subsurface. Some units are not easily distinguished (e.g., Eocene and Cretaceous sedimentary and volcanic rocks), but there is good potential for discriminating between several important stratigraphic packages (Chilcotin basalts and Cretaceous sedimentary and volcanic rocks). Henceforth, these data should be used in the interpretation and reinterpretation of Nechako Basin geophysical surveys, and correlated with new and existing boreholes.

Acknowledgments

This study was supported by Geoscience BC project grant 2008-028 and Geological Survey of Canada contract 23254-096844-001-VAN, awarded to JKR. We thank J. Riddell, B. Struik, M. Mihalynuk, K. MacLaurin and P. Mustard for providing their archived samples. Sample preparation at UBC was conducted by P. Van de Reep and H. Dhillon. H. Linton and A. Tkachyk performed the lab work at the Geological Survey of Canada. Figure 1 was created by F. Ma of Geoscience BC. The authors thank L. Porritt and S. Kolzenburg for peer review comments that helped clarify the paper.

References

- Andrews, G., Quane, S., Enkin, R.J., Russell, K., Kushnir, A., Kennedy, L., Hayward, N., and Heap, M. (2011): Rock physical property measurements to aid geophysical surveys in the Nechako Basin oil and gas region, central British Columbia; Geoscience BC, Report 2011-6, 40 p. and Excel® database, URL <<http://www.geosciencebc.com/s/2011-06.asp>> [November 2011].
- Andrews, G.D.M., Plouffe, A., Ferbey, T., Russell, J.K., Brown, S.R. and Anderson, R.G. (2011): The thickness of Neogene and Quaternary cover across the central Interior Plateau, British Columbia: analysis of water-well drill records and implications for mineral exploration potential; Canadian Journal of Earth Sciences, v. 48, p. 973–986.
- Andrews, G.D.M. and Russell, J.K. (2007): Mineral exploration potential beneath the Chilcotin Group (NTS 0920, P, 093A, B, C, F, G, I, J, K), south-central British Columbia: preliminary insights from volcanic facies analysis; in Geological Fieldwork 2006, BC Ministry of Energy and Mines, Paper 2007-1 and Geoscience BC, Report 2007-1, p. 229–238, URL <<http://www.empr.gov.bc.ca/Mining/Geoscience/PublicationsCatalogue/Fieldwork/Documents/22-Andrews.pdf>> [November 2011].
- Andrews, G.D.M. and Russell, J.K. (2008): Cover thickness across the southern Interior Plateau, British Columbia (NTS 0920, P; 093A, B, C, F): constraints from water-well records; in Geoscience BC Summary of Activities 2007, Geoscience BC, Report 2008-1, p. 11–20, URL <http://www.geosciencebc.com/i/pdf/SummaryofActivities2007/SoA2007-Andrews_original.pdf> [November 2011].
- Bordet, E. and Hart, C.J.R. (2011): Characterization and structural framework of Eocene volcanic sequences in the Nechako region, central British Columbia (NTS 092N, O, 093B, C, G); in Geoscience BC Summary of Activities 2010, Geoscience BC, Report 2011-1, p. 239–254, URL <<http://www.geosciencebc.com/i/pdf/SummaryofActivities2010/SoA2010-Bordet&Hart.pdf>> [November 2011].
- Calvert, A.J., Hayward, N., Smithyman, B.R. and Takham Takougang E.M. (2009): Vibroseis survey acquisition in the central Nechako Basin, south-central British Columbia; in Geoscience BC Summary of Activities 2008, Geoscience BC, Report 2009-1, p. 145–150, URL <http://www.geosciencebc.com/i/pdf/SummaryofActivities2008/SoA2008-Calvert_original.pdf> [November 2011].
- Dohaney, J., Andrews, G.D.M., Russell, J.K. and Anderson, R.G. (2010): Distribution of the Chilcotin Group, Taseko Lakes and Bonaparte Lake map areas, British Columbia; Geological Survey of Canada, Open File 6344, URL <http://geopub.nrcan.gc.ca/moreinfo_e.php?id=261655> [November 2011].
- Ferri, F. and Riddell, J. (2006): The Nechako Basin project: new insights from the southern Nechako Basin; in Summary of Activities 2006, BC Ministry of Energy and Mines, pages 89–124, URL <<http://www.em.gov.bc.ca/subwebs/oilandgas/pub/reports.htm>> [November 2011].
- Hannigan, P., Lee, P.J., Osadetz, K.G., Dietrich, J.R. and Olsen-Heise, K. (1994): Oil and gas resource potential of the Nechako-Chilcotin area of British Columbia; BC Ministry of Energy and Mines, Geofile 2001-6, 38 p. plus appendices and maps, URL <http://www.empr.gov.bc.ca/Mining/Geoscience/PublicationsCatalogue/GeoFiles/Pages/2001-6.aspx> [November 2011].
- Hayes, B.J. (2002): Petroleum exploration potential of the Nechako Basin, British Columbia; BC Ministry of Energy and Mines, Petroleum Geology Special Paper 2002-3.
- Hayward, N. and Calvert, A.J. (2009): Eocene and Neogene volcanic rocks in the southeastern Nechako Basin, British Columbia: interpretation of the Canadian Hunter seismic reflection surveys using first-arrival tomography; Canadian Journal of Earth Sciences, v. 46, p. 707–720.
- Hayward, N. and Calvert, A.J. (2011): Interpretation of structures in the southeastern Nechako Basin, British Columbia, from seismic reflection, well log, and potential field data; Canadian Journal of Earth Sciences, v. 48, p. 1000–1020.
- Idowu, O.A., Frederiksen, A.W. and Cassidy, J.F. (2011): Imaging the Nechako Basin, British Columbia, using ambient seismic noise; Canadian Journal of Earth Sciences, v. 48, p. 1038–1049.
- Katsube, T.J. (2001): An analytical procedure for determining spectral induced polarization characteristics of anisotropic rocks, Yellowknife mining district, Northwest Territories; Geological Survey of Canada, Current Research 2001-E3, 29 p., URL <http://geopub.nrcan.gc.ca/moreinfo_e.php?id=212683> [November 2011].
- Kim, H-S. (2010): Mapping crustal structure of the Nechako Basin using teleseismic receiver functions; M.Sc. thesis, University of Victoria, Victoria, BC, 112 p.
- MacLaurin, C.I., Mahoney, J.B., James W. Haggart, J.W., Goodin, J.R. and Mustard, P.S. (2011): The Jackass Mountain Group of south-central British Columbia: depositional setting and evolution of an Early Cretaceous deltaic complex; Canadian Journal of Earth Sciences, v. 48, p. 930–951, doi:10.1139/e11-035

- Mihalynuk, M.G., Orovan, E.A., Larocque, J.P., Friedman, R.M. and Bachiu, T. (2009): Geology, geochronology and mineralization of the Chilanko Forks to southern Clusko River area, west-central British Columbia (NTS 093C/01, 08, 09S); *in* Geological Fieldwork 2008, BC Ministry of Energy and Mines, Paper 2009-1, p. 81–100, URL <http://www.empr.gov.bc.ca/Mining/Geoscience/PublicationsCatalogue/Fieldwork/Documents/08_Mihalynuk_2008.pdf> [November 2011].
- Mira Geoscience (2008): Development and application of a rock property database for British Columbia; Geoscience BC, Report 2008-9, 66 p., URL <<http://www.geosciencebc.com/s/2008-09.asp>> [November 2011].
- O’Connell, R.J. and Budiansky, B. (1974): Seismic velocities in dry and saturated cracked solids; *Journal of Geophysical Research*, v. 79, p. 5412–5426.
- Parsons, S., McGaughey, J., Mitchinson, D., Phillips, N. and Lane, T.E. (2009): Development and application of a rock property database for British Columbia; *in* Geoscience BC Summary of Activities 2008, Geoscience BC, Report 2009-1, p. 137–144, URL <http://www.geosciencebc.com/i/pdf/SummaryofActivities2008/SoA2008-Parsons_original.pdf> [November 2011].
- Riddell, J.M. (2006): Geology of the southern Nechako Basin; BC Ministry of Energy and Mines, Oil and Gas Division, Petroleum Geology Map 2006-1, scale 1:400 000.
- Riddell, J.M. (2011): Lithostratigraphic and tectonic framework of Jurassic and Cretaceous Intermontane sedimentary basins of south-central British Columbia; *Canadian Journal of Earth Sciences*, v. 48, no. 6, p. 870–896, doi:10.1139/e11-034
- Salisbury, M. and Iuliucci, R. (2011): Physical rock properties database; Geological Survey of Canada–Atlantic, URL <http://gdr.nrcan.gc.ca/rockprop/rock_e.php> [November 2011].
- Spratt, J. and Craven, J. (2011): Near-surface and crustal-scale images of the Nechako basin, British Columbia, Canada, from magnetotelluric investigations; *Canadian Journal of Earth Sciences*, v. 48, p. 987–999.
- Sumner, J.S. (1976): Principles of Induced Polarization for Geophysical Exploration; Elsevier Scientific Publishing Company, Amsterdam., The Netherlands, 277 p.
- Telford, W.M., Geldart, L.P., Sheriff, R.E. and Keys, D.A. (1976): Applied Geophysics; Cambridge University Press, London, United Kingdom, 860 p.
- Walsh, J.B. (1965): The effect of cracks on the compressibility of rock; *Journal of Geophysical Research*, v. 70, p. 381–389.

Analysis of Magnetotelluric Transfer Functions to Determine the Usefulness of ZTEM Data in the Nechako Basin, South-Central British Columbia (Parts of NTS 092O, N, 093B, C, F, G)

J.E. Spratt, Geophysical Consultant, Wakefield, QC, jessicaspratt@sympatico.ca

C.G. Farquharson, Memorial University of Newfoundland, St. John's, NL

J.A. Craven, Natural Resources Canada, Geological Survey of Canada–Central Canada, Ottawa, ON

Spratt, J.E., Farquharson, C.G. and Craven, J.A. (2012): Analysis of magnetotelluric transfer functions to determine the usefulness of ZTEM data in the Nechako Basin, south-central British Columbia (parts of NTS 092O, N, 093B, C, F, G); in Geoscience BC Summary of Activities 2011, Geoscience BC, Report 2012-1, p. 151–162.

Introduction

As part of Geoscience BC's initiative to develop the potential for hydrocarbon resources in central British Columbia (BC), several geological and geophysical projects have been undertaken within the Nechako Basin, including a high-density broadband and audio-magnetotelluric survey. The Nechako Basin is an Upper Cretaceous to Oligocene sedimentary basin located in the interior plateau of BC between the Coastal Mountains and the Rocky Mountains (Figure 1). The potential for reservoir sands has been noted in the Cretaceous sedimentary packages of the basin (Hannigan et al., 1994; Riddell, 2006); however, these packages are extensively overlain by variable thicknesses of Eocene and Neogene volcanics, as well as Quaternary and glacial deposits, thus limiting the surficial exposure of the sediments and interfering with interpretations of the subsurface structure. Magnetotelluric (MT) data collected within the Nechako Basin in 2007 were used successfully to image the conductivity structure beneath two-dimensional (2-D) profiles and show that the method can differentiate between varying rock types and identify structural features in the subsurface (Spratt and Craven, 2011).

It has been suggested that acquiring airborne z-axis tipper electromagnetic (ZTEM) data over the Nechako Basin could be useful for mapping the thickness of overlying volcanic layers and identifying areas of reservoir potential, particularly in the regions between the MT profiles where the conductivity structure is unknown. The ZTEM method measures airborne electromagnetic data that provide information on the 3-D conductivity structure of the shallow subsurface. It is a cost-effective way to record tipper data, calculated from the vertical component of the magnetic field, over a broad region with a high-density sampling distribu-

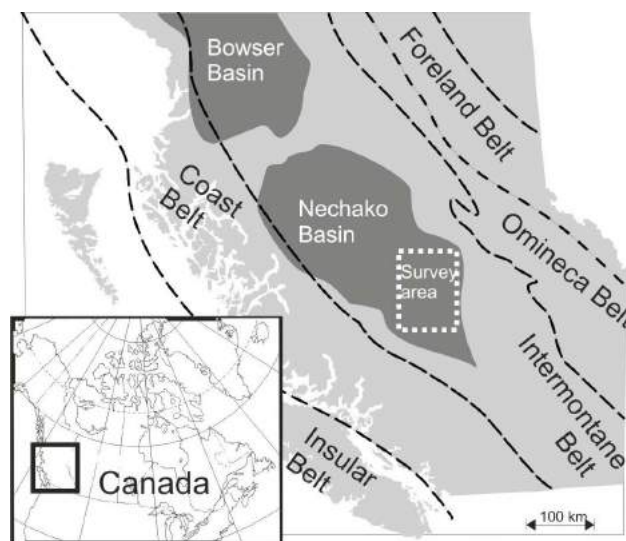


Figure 1. Location of the Nechako Basin and the magnetotelluric survey area.

tion; however, the data are not sensitive to 1-D layers (Holtham and Oldenburg, 2010), and limitations on the frequencies measured may result in low resolution of the models and shallow penetration depths. As MT data record the horizontal and vertical components of magnetic field, along with the electric fields, the tipper data are available at each recorded site. Transfer functions from measured MT data, as well as synthetic data calculated from the existing 2-D conductivity models, have been analyzed to determine which features could be resolved with additional airborne ZTEM data.

Geological and Geophysical Background

Geological Setting

A series of Mesozoic and Cenozoic clastic basins formed within the Intermontane Belt of the Canadian Cordillera in response to oceanic and island-arc terrane amalgamation along the western edge of ancestral North America (Mon-

Keywords: Nechako Basin, magnetotellurics, ZTEM, hydrocarbon exploration, electromagnetics

This publication is also available, free of charge, as colour digital files in Adobe Acrobat® PDF format from the Geoscience BC website: <http://www.geosciencebc.com/s/DataReleases.asp>.

ger et al., 1972, 1982; Gabrielse and Yorath, 1991). Postaccretionary sedimentary and volcanic sequences are preserved in the study area within the Nechako Basin. These are underlain by the Carboniferous to Early Cretaceous Stikine island-arc terrane and the Permian to Middle Triassic oceanic Cache Creek terrane. Extension during the Eocene resulted in magmatism, regional transcurrent faulting and volcanism (Price, 1994; Struik and MacIntyre, 2001). Volcanism during the Miocene and Pliocene produced the mafic volcanic rocks that blanket much of the region (Mathews, 1989; Andrews and Russell, 2007).

The Nechako Basin is up to 5 km thick and consists of three primary geological elements: Early Cretaceous clastic marine and fluvial rocks of the Taylor Creek and Skeena groups, Eocene volcanoclastic rocks that include the Endako and Ootsa Lake groups, and Neogene Chilcotin Group basalts (Figure 2). The Taylor Creek and Skeena groups in the study area are composed of interbedded chert, pebble conglomerate, sandstone, siltstone and shale (Riddell, 2006). The Endako Group comprises andesitic to basaltic volcanic flows, tuff, breccia and minor amounts of sedi-

mentary rocks (Riddell, 2006), whereas the Ootsa Lake Group has intermediate to felsic flows and a higher amount of sedimentary material (Riddell, 2006, 2011). The near-horizontal basaltic flows of the Chilcotin Group blanket portions of the region with an average thickness of <20 m, reaching up to 200 m in localized paleochannels (Andrews and Russell, 2008; Andrews et al., 2011).

Geophysical Investigations

Several geological and geophysical surveys have been undertaken to ascertain the distribution of Cretaceous rocks, which are the most prospective for oil and gas. Since the 1960s, several exploration wells drilled through the Nechako Basin by Canadian Hunter Exploration Limited, Esso, Honolulu Oil Corporation Limited and Hudson's Bay Oil and Gas Company Limited (shown on Figure 2) have provided stratigraphic information and borehole logs of petrophysical properties (Hannigan et al., 1994; Riddell et al., 2007; Smith, 2007). Analysis of this information indicated that reservoir-quality rock was only present in Cretaceous sedimentary packages, primarily the Taylor Creek and

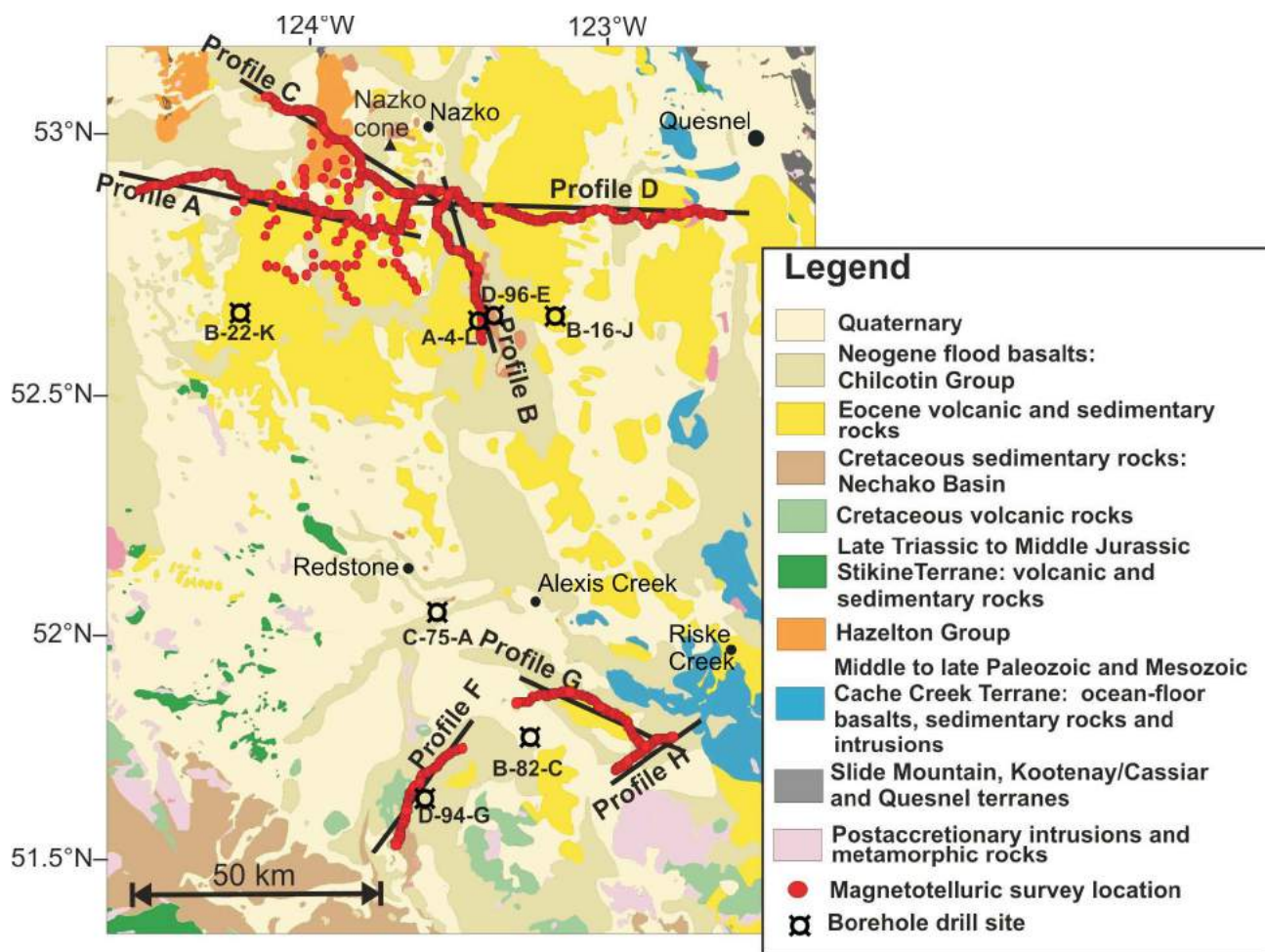


Figure 2. Detailed geology of the study area, showing the location of the magnetotelluric survey sites and the two-dimensional profile traces (modified from Riddell, 2006).

Skeena groups (Riddell et al., 2007). Interpretations of early 1980s Canadian Hunter gravity and seismic data, as well as new seismic data collected by Geoscience BC in 2008, suggest that the sedimentary packages are located in separate sub-basins rather than one larger basin (Hayward and Calvert, 2008; Calvert et al., 2011). This implies that the units with hydrocarbon potential may not regionally underlie the extensive volcanic cover. Locating the regional extent of Cretaceous sedimentary rocks is therefore crucial in developing an understanding of this potential. The presence of near-surface volcanic rocks significantly complicates the interpretation of some geophysical methods.

Overview of Magnetotelluric Results

The magnetotelluric (MT) method provides information on the present-day, in situ electrical conductivity of the subsurface by measuring natural time-varying electromagnetic fields at the Earth's surface (e.g., Jones, 1992). The MT method involves comparison of the horizontal components of the electric and magnetic fields of the Earth, measured at the surface. These are related to each other by a 2 by 2 complex impedance tensor that varies as a function of frequency and position of observation (Wait, 1962). The vertical magnetic field is also recorded and is related to the horizontal magnetic components by the geomagnetic-transfer function (TF). The depth of penetration of the fields is dependent on frequency (i.e., the lower the frequency the greater the depth) and the resistivity of the material (i.e., the greater the resistivity, the greater the depth; Cagniard, 1953). The transverse electric (TE) and transverse magnetic (TM) modes of electromagnetic (EM)-field propagation refer to the directions parallel and perpendicular to geoelectric strike, respectively. Modelling the vertical field-transfer functions, typically displayed as induction vectors that point towards current concentrations in the Earth, can identify conductors in the subsurface.

In the fall of 2007, combined high-frequency audio-magnetotelluric (AMT) and broadband magnetotelluric (BBMT) data were collected at a total of 734 sites through the southern part of the Nechako Basin at a site spacing of <500 m (Figure 2; Spratt and Craven, 2009). The data were processed by Geosystem Canada using robust remote-reference techniques that generally resulted, in excellent data quality covering a range of nearly seven period decades (orders of magnitude) from 0.0001 to 1000 s (Spratt and Craven, 2009). The dataset was divided into seven separate profiles for analysis and subsequent inversions. Each site was analyzed for distortion, dimensionality and directionality, and a 2-D model was generated along each profile by inverting data from the TM-, TE- and TF-mode data (Spratt and Craven, 2010, 2011).

Results of 2-D modelling of the TE-mode, TM-mode and vertical-field transfer-function (HZ) components of the

MT data indicate that the method can differentiate between varying rock types and reveal structure in the subsurface (Figure 3; Spratt and Craven, 2011). The 2-D MT models generated along the profiles, in general, reveal three distinct horizontal units that characterize the conductivity structure of the Nechako Basin; these units are best resolved in the models along profiles A, B, C and F (Figure 3). A near-surface resistive layer (>500 Ω -m) is interpreted as the Chilcotin basalts, which blanket portions of the region to depths of <50 m but can locally thicken up to 200 m in paleochannels. A low-resistivity unit underlying the near-surface resistor varies in thickness between 0 and 4000 m, and appears to have two end members with varying resistivity signatures. The Cretaceous sedimentary units are characterized by moderate resistivities (10–100 Ω -m) that are laterally highly variable, whereas lower, more uniform conductivity values (<4 Ω -m) appear to be associated with the Eocene volcanoclastic groups. The base of the Nechako Basin is marked by an increase in resistivity (>200 Ω -m) associated with the deeper underlying Cretaceous volcanic units or island-arc terranes. In addition to the layered resistivity structure, the data also image folding and faulting of the Nechako sediments, structural features that may provide an environment for trapping hydrocarbons.

Transfer-Function Data

ZTEM Method

Similar to the MT method, ZTEM uses natural fields as the source of transmitted energy to resolve a conductivity-depth profile of the Earth. The method involves interpretation of transfer functions that relate the local airborne vertical field to mutually perpendicular horizontal magnetic fields recorded at a reference station on the ground. Common line spacings used in airborne ZTEM surveys are 100–400 m (e.g., Geotech Limited, 2009; Lo et al., 2009; Sattel et al., 2010), data are recorded at an output sampling rate of 2.5 samples/second and the recording equipment is typically flown at a speed of 80 km/h for a nominal sample spacing of 8 m along each line flown (e.g., Holtham and Oldenburg, 2010). In theory, current ZTEM instrumentation can measure data in the frequency range 22–2800 Hz; however, typical surveys process data at 30, 45, 90, 180, 360 and occasionally 720 Hz (e.g., Geotech Limited, 2009; Lo et al. 2009).

The MT skin depth of the magnetic fields can be a useful guide in estimating the penetration depths of the fields at specific periods. In a uniform half space, it is given by

$$d = 503(\rho T)^{1/2},$$

where d is the depth in metres, ρ is the resistivity value and T is the period (Cagniard, 1953). At the longest ZTEM period (0.033 s), we would expect penetration depths (and model resolution) of approximately 2 km in the Chilcotin

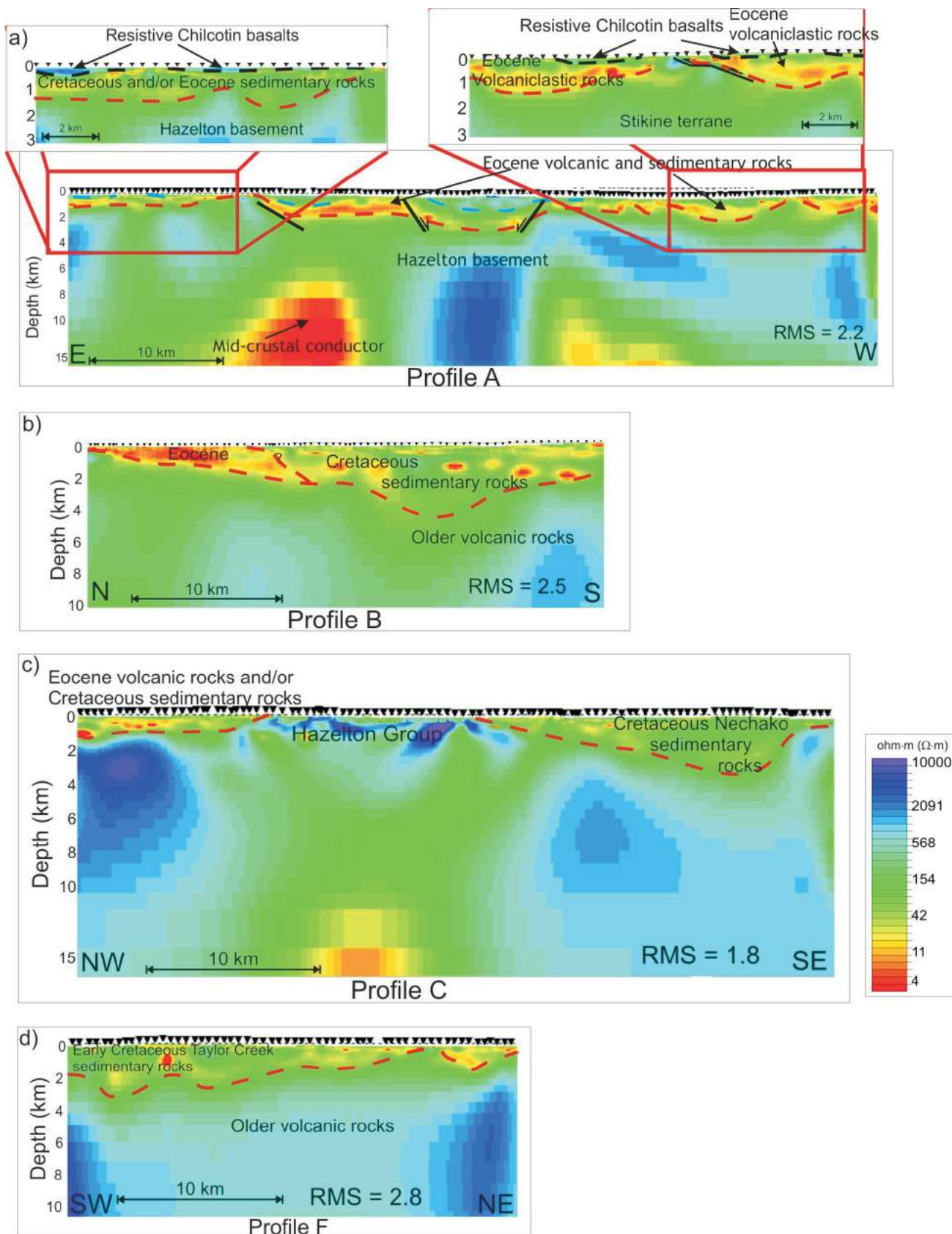


Figure 3. Two-dimensional conductivity models and interpretations for a) profile A, b) profile B, c) profile C, and d) profile F. The red dashed line illustrates the interpreted base of the Nechako Basin and the black lines represent faults.

Group ($>500 \Omega\cdot\text{m}$), 900 m in the Cretaceous groups (10–100 $\Omega\cdot\text{m}$) and 200 m in the Eocene group ($<4 \Omega\cdot\text{m}$), where the units are sufficiently thick. This suggests that the method may be capable of differentiating between different

rock types at shallow depths but will not be able to image the base of the basin.

For every three successive sites during acquisition the Nechako Basin MT data in 2007 (Figure 4), the vertical-

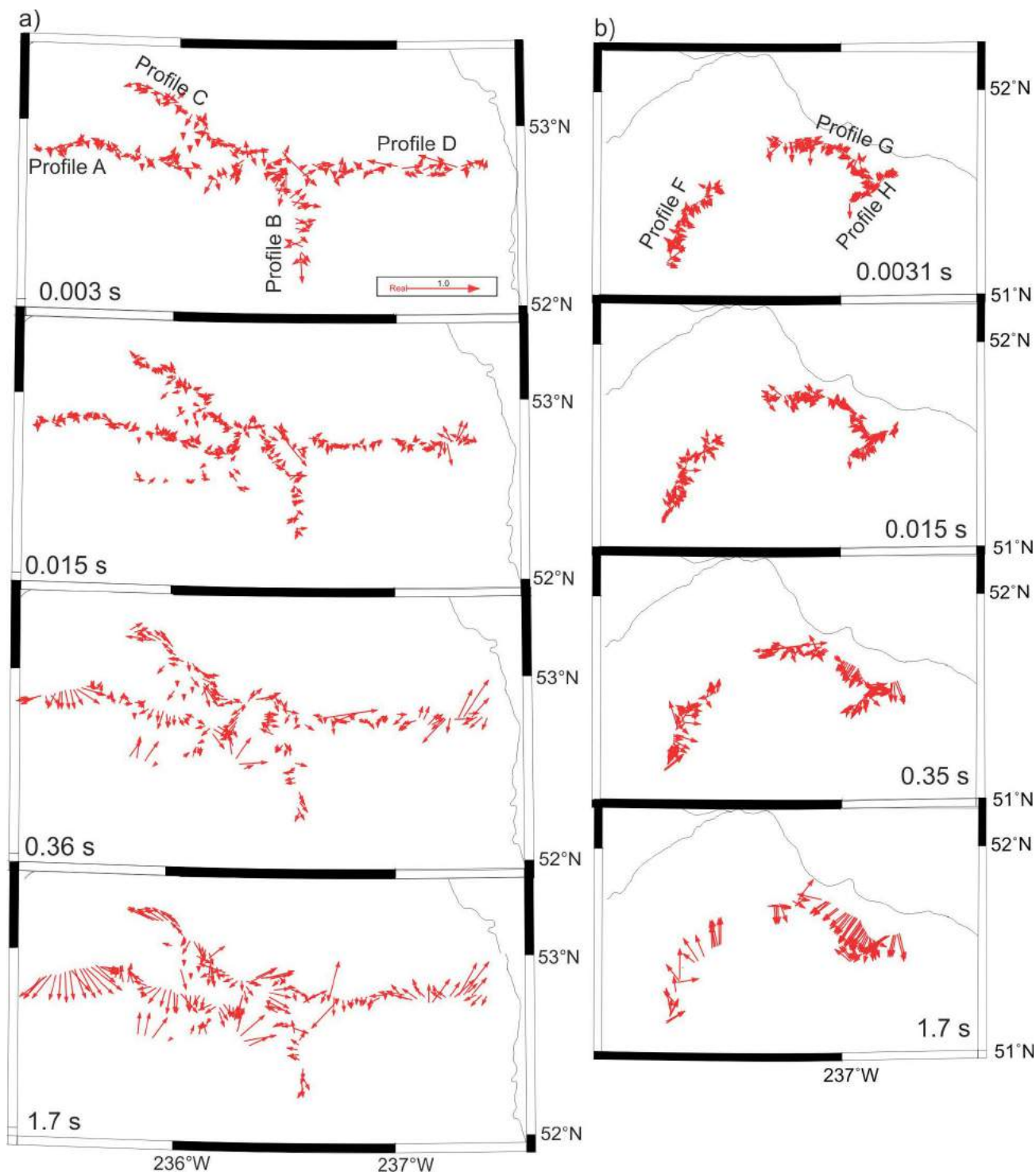
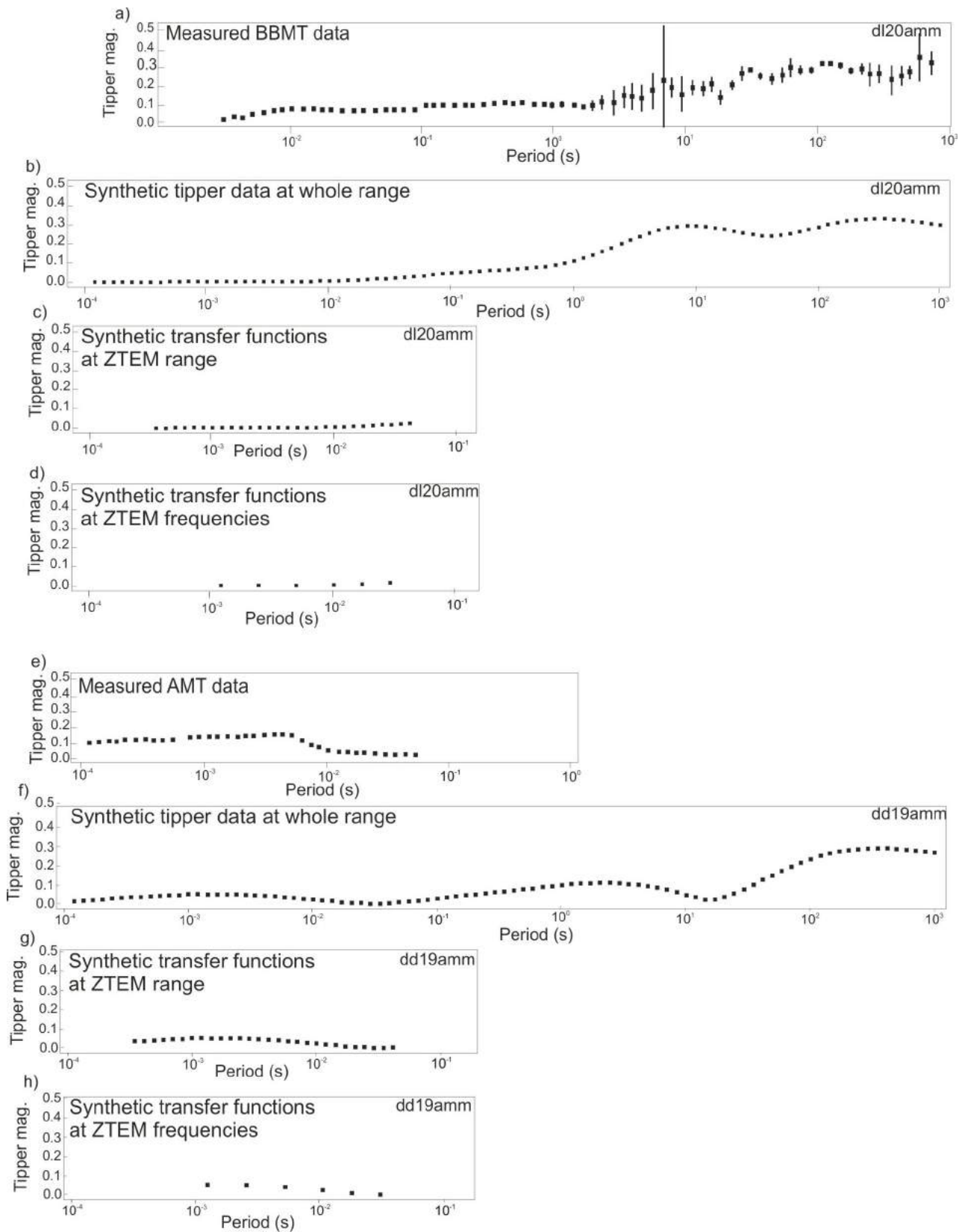


Figure 4. Induction vectors from transfer functions of measured vertical-field magnetotelluric data at periods of 0.003, 0.015, 0.36 and 1.7 s, showing data from the northern (a) and southern (b) portions of the survey area. The arrows point towards conductors with a magnitude of less than 1.

field data were recorded in the BBMT range (200–0.0001 Hz) at the first site (Figure 5a) and the AMT range (10 000–1 Hz) at the second site (Figure 5e), and no verti-

cal-field data were recorded at the third site (Figure 4). In general, the data quality is excellent to periods below 1 s (Figure 5a, e). Figure 5 shows examples of different fre-



quency ranges used in various 2-D model inversions for two sites: one located above conductive Eocene volcanoclastic rocks (Figure 5a–d) and the other located above exposed Cretaceous sedimentary units (Figure 5e–h).

Deriving Synthetic Data

Synthetic transfer-function data have been computed from the 2-D conductivity models produced by the inversion of all components of the MT data using the GEOSYSTEM SRL WinGlink[®] MT interpretation software package (Figures 5b, f). The data have been computed at a site spacing of 100 m along each of the MT profiles, a site spacing that reaches the limit of the modelling program. These synthetic data have been generated by creating additional sites along the profiles, importing the final 2-D models, running a forward inversion and then saving the calculated responses as station data. Note that no noise was added to the synthetic data. New models were then generated along the profiles using these synthetic data and various frequency ranges: the entire frequency range (0.001–10 000 Hz, Figure 5b, f), the frequency range of the ZTEM data (22–2800 Hz, Figure 5c, 5h), and the specific frequencies used in the ZTEM surveys (Figure 5d, 5h).

Two-Dimensional Modelling

Several 2-D conductivity models have been generated, using the WinGlink[®] interpretation software package, along the main MT profiles. More than 200 iterations have been employed in the inversion for each model, using either the measured or the synthetic transfer-function data at various frequencies. Examples of the data used in the various models are shown in Figure 5. Each inversion was initiated with a uniform half space of 500 Ω ·m as a starting model. The inversions of measured data used a smoothing value (τ) of 3, a Tyz absolute data-error floor of 0.01 and existing data errors. Each inversion of synthetic data used a τ of 3, a Tyz absolute data-error floor of 0.001 and a standard deviation error of 1%.

Two-dimensional inversions were carried out on the measured 2007 MT magnetic-transfer functions (e.g., Figure 5a, e). The results of these inversions serve as a bench mark

←
Figure 5. Plots of the tipper magnitude for two sites at the various frequency distributions included in inversions: **a)** measured data from broadband-magnetotelluric (BBMT) site dd22amm, located above the conductive Eocene volcanoclastic rocks; **b)** synthetic data derived from the 2-D magnetotelluric (MT) model at site dd22amm; **c)** synthetic data at site dd22amm, over the z-axis tipper electromagnetic (ZTEM) period range; **d)** synthetic data at site dd22amm, at the periods typically analyzed using the ZTEM method; **e)** measured data from high-frequency audio-magnetotelluric (AMT) site dl19aam, located above exposed Cretaceous sedimentary rocks; **f)** synthetic data derived from the 2-D MT model at site dl19aam; **g)** synthetic data at site dl19aam, over the ZTEM period range; and **h)** synthetic data at site dl19aam, at the periods typically analyzed using the ZTEM method.

against which the results obtained from the synthetic ZTEM data can be measured. The subset of the measured vertical-field MT data that corresponds to the frequency range appropriate for ZTEM surveys has been modelled to show what can be obtained from ZTEM data were they to be collected along the MT profiles, and under the best possible conditions. The synthetic transfer-function data have been inverted using data in the MT measurable frequency range (0.001–10000 Hz; Figure 5b, f), in the ZTEM measurable range (22–2800 Hz; Figure 5c, g) and at the six frequencies specific to typical ZTEM analysis (30, 45, 90, 180, 360, 720 Hz; Figure 5d, h).

Results and Conclusion

Results of the 2-D modelling of profiles A, B, C, and F are presented in Figures 6–9. For each profile, the original 2-D model derived from all three components of the data measured and at each MT site location over the entire measured frequency range are shown (Figures 6a, 7a, 8a, 9a). Also shown are models derived using only the HZ component of the measured data over the entire frequency range (Figures 6c, 7b, 8b, 9b); models derived from the HZ component of the measured data at the recordable ZTEM frequency range (Figures 6d, 7c, 8c, 9c); and models generated using only the HZ component of the synthetic data over the entire frequency range (Figures 6e, 7d, 8d, 9d), at the recordable ZTEM frequency range (Figures 6f, 7e, 8e, 9e) and at the specific frequency used in ZTEM surveys (Figure 6g, 7f, 8f, 9f).

In order to test the modelling parameters applied, an additional model was generated along profile A by inverting all three components of the synthetic MT data (TM-mode, TE-mode and transfer-function HZ data; Figure 6b). When compared to the original 2-D model, the synthetic data show good resolution of the subsurface-conductivity structure, indicating that the modelling program and selected parameters are capable of generating an accurate image of the subsurface-conductivity structure. Modelling of the transfer functions from measured MT data alone does not appear to resolve the subsurface-conductivity structure along any of the profiles, regardless of the frequency range that was inverted (Figures 6c, 6d, 7b, 7c, 8b, 8c, 9b, 9c). This may be due to inherent errors associated with real data and, if so, it should be noted that we expect the airborne data to have higher errors. It could also be a result of the large station spacing compared to airborne ZTEM surveys. Along profile A, synthetic data were modelled at the measured station spacing for comparison with those modelled at a spacing of 100 m. Additionally, a model was generated for a small section at the easternmost end of profile A using synthetic data at a site spacing of 25 m. Although the resulting model was much smoother, the structural resolution was not improved with a higher station density.

Along profile A (Figure 6), the conductivity structure is not well resolved using the synthetic HZ data over the entire frequency range (Figure 6e) when compared to the original 2-D model. Models of the synthetic HZ data using frequencies limited to the ZTEM range, however, reveal features that are similar to the original 2-D model, resulting in reasonable conductivity values to appropriate depths and significant structural detail (Figure 6f). This resolution is lost when further limiting the frequencies to the six ZTEM frequencies (Figure 6g).

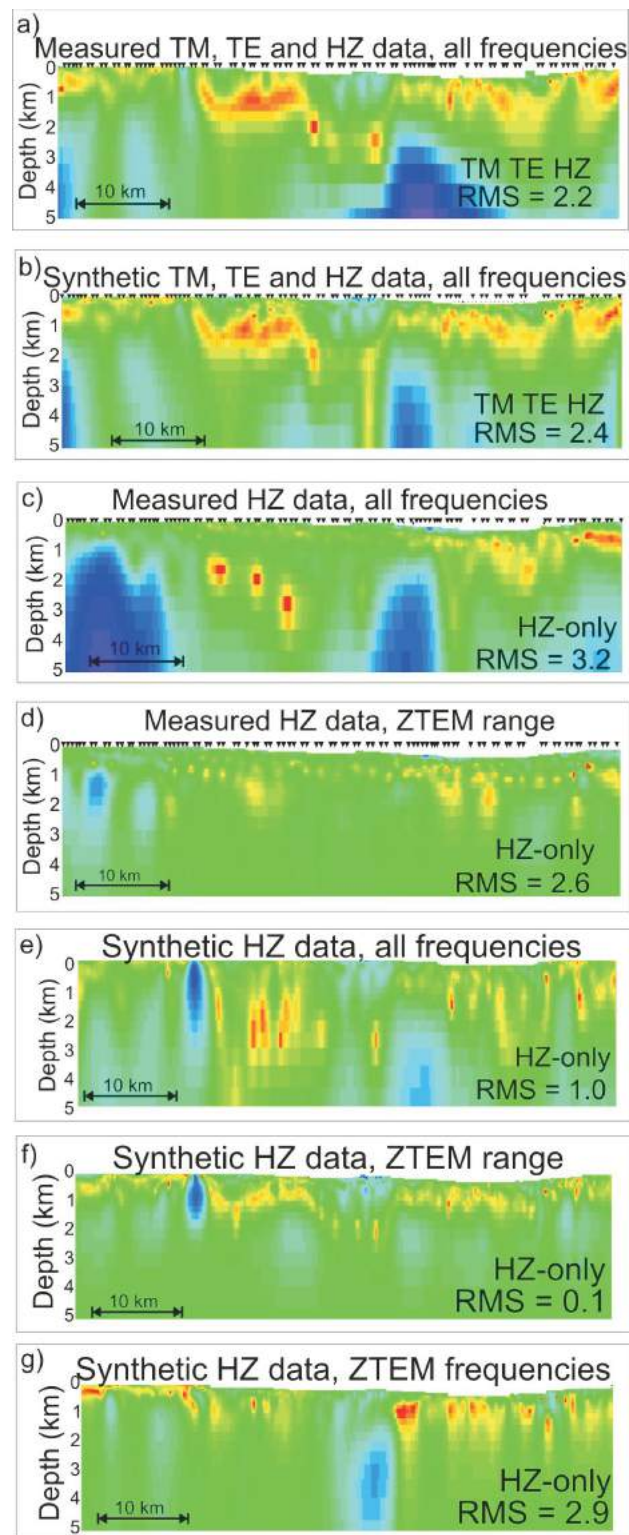
In comparison to the original 2-D model along profile B (Figure 7a), inversion of the synthetic data over the entire frequency range reveals the general subsurface-conductivity structure, including the highly conductive Eocene volcanoclastic rocks at the north end of the profile and the laterally variable and moderate conductivities of the Cretaceous sediments over the southern half of the profile, and it shows an appropriate basin depth beneath the entire profile (Figure 7d). Results using both the ZTEM range and the six specific ZTEM frequencies show the highly conductive Eocene units, but these are only observed to depths of <200 m (Figure 7e, f). The Cretaceous sedimentary rocks are imaged as laterally variable and moderately conductive in the ZTEM-based model (Figure 7f), consistent with the key signature observed in the original MT data-based models (Figure 7a); however, the overall structure and specific conductivity variations within this unit are significantly different from the original 2-D model.

Results along profile C are illustrated in Figure 8. These show that the synthetic data resolve well the resistive Hazelton Group units to reasonable depths of 2–3 km, regardless of the frequency distribution that is inverted (Figure 8d–f). The lateral continuity of the moderate conductivities at the southeastern end of the profile, interpreted as Cretaceous sedimentary rocks, is broken but the conductivity values are significantly lower ($<4 \Omega \cdot \text{m}$), closer to those of the Eocene groups. In addition, the overall structure or distribution of conductivity variations is different from that of the original 2-D model, particularly when using the six ZTEM frequencies (Figure 8f). The moderate conductivities at the northwestern end of the profile were interpreted as Eocene and/or Cretaceous groups in the original 2-D model because the conductivity signature was difficult to classify (Figure 8a). Although the synthetic data inverted

Figure 6. Results of two-dimensional (2-D) modelling of measured and synthetic MT data along profile A: **a)** original 2-D model derived from all components of the measured MT data (equivalent to upper 5 km of Figure 3); **b)** model of all components of the synthetic data over the seven-decade frequency range; **c)** model of the measured HZ data over the seven-decade frequency range; **d)** model of the measured HZ data over the ZTEM frequency range; **e)** model of the synthetic HZ data over the seven-decade frequency range; **f)** model of the synthetic HZ data over the ZTEM frequency range; and **g)** model of the synthetic data at the six specific ZTEM frequencies.

over the ZTEM range image this feature reasonably well, the model including just the six ZTEM frequencies shows a laterally uniform, highly conductive unit that would be interpreted as Eocene volcanoclastic rocks (Figure 8f).

Figure 9 shows the results for profile F. Here, consistent with borehole lithology, the original 2-D model revealed



Cretaceous Taylor Creek sedimentary rocks to depths of 2–3 km (Figure 9a). Inversion of the synthetic HZ data shows laterally variable conductivities, the values being slightly lower but comparable to those associated with Cretaceous sedimentary rocks. The general structure, distribution of the conductivity variations and depth of the units, however, are not well resolved, particularly when using just the six ZTEM frequencies (Figure 9f).

Inversions of synthetic data indicate that modelling the transfer-function data alone can give a reasonable image of the conductivity structure of the subsurface; however, revealing specific features at depth is highly dependent on the frequencies included in the inversion. In ideal geological terranes, where the depth to target, conductivity value and structure are suitable (e.g., imaging moderate conductivities at depths of <1 km), the ZTEM method may be very useful in determining the conductivity structure. Within the Nechako Basin, where the thickness of units, conductivity values and lateral structure are highly variable, the method may be capable of identifying the conductive Eocene volcanoclastic rocks to shallow depths but incapable of differentiating between the Eocene groups and the Cretaceous sedimentary rocks. It is hoped that this work will serve as a guide to the circumstances under which ZTEM surveys will be most useful in identifying the stratigraphic units and structures of interest to mineral or hydrocarbon exploration. Future work includes synthesizing the results of the remaining three profiles.

Acknowledgments

This work was supported by Geoscience BC. The authors thank M. Pilkington for his rapid review of this manuscript.

Natural Resources Canada, Earth Science Sector contribution 20110267.

References

- Andrews, G.D.M. and Russell, J.K. (2007): Mineral exploration potential beneath the Chilcotin Group, south-central BC: preliminary insights from volcanic facies analysis; *in* Geological Fieldwork 2006, Geoscience BC, Report 2007-1, p. 229–238, URL <<http://www.empr.gov.bc.ca/Mining/Geoscience/PublicationsCatalogue/Fieldwork/Documents/22-Andrews.pdf>> [November 2011].
- Andrews, G.D.M. and Russell, J.K. (2008): Cover thickness across the southern Interior Plateau, British Columbia (NTS 0920,

P, 093A, B, C, F): constraints from water-well records; *in* Geoscience BC Summary of Activities 2007, Geoscience BC, Report 2008-1, p. 11–20, URL <http://www.geosciencebc.com/i/pdf/SummaryofActivities2007/SOA2007-Andrews_original.pdf> [November 2011].

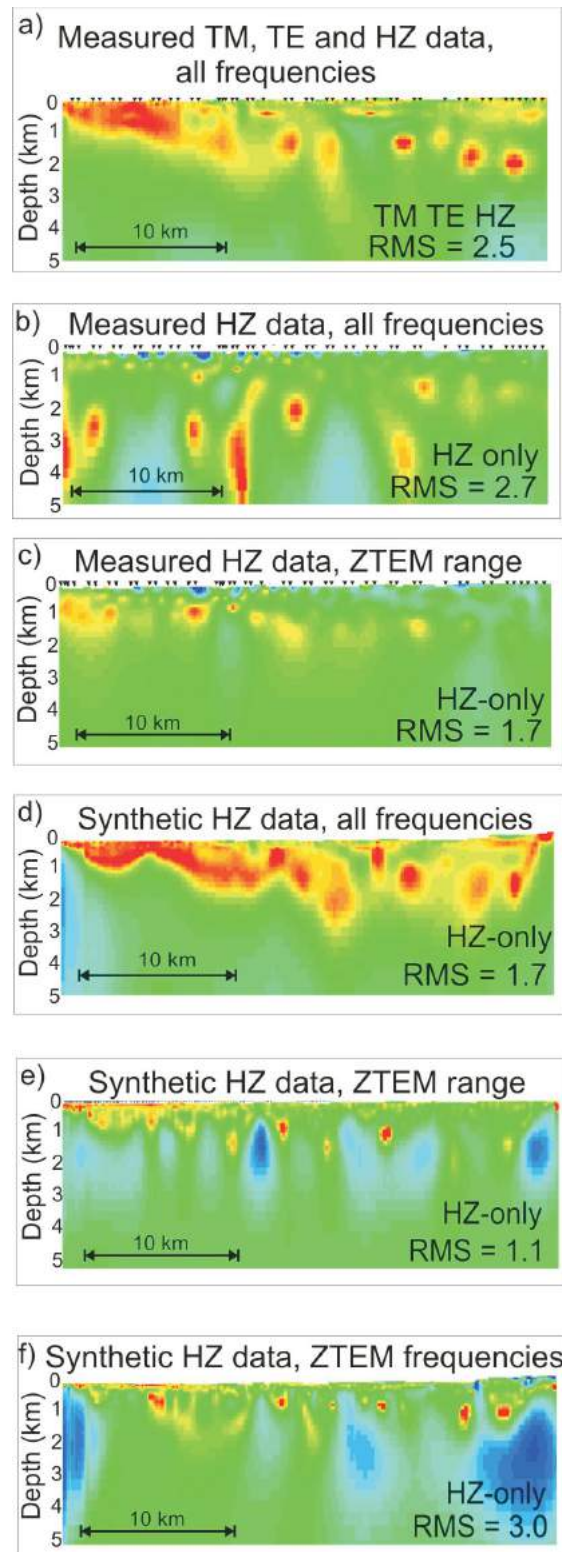


Figure 7. Results of two-dimensional (2-D) modelling of measured and synthetic MT data along profile B: **a)** original 2-D model derived from all components of the measured MT data; **b)** model of the measured HZ data over the seven-decade frequency range; **c)** model of the measured HZ data over the ZTEM frequency range; **d)** model of the synthetic HZ data over the seven-decade frequency range; **e)** model of the synthetic HZ data over the ZTEM frequency range; and **f)** model of the synthetic HZ data at the six specific ZTEM frequencies.

Andrews, G.D.M., Plouffe, A., Ferbey, T., Russell, J.K., Brown, S.R. and Anderson, R.G. (2011): The thickness of Neogene and Quaternary cover across the central Interior Plateau, British Columbia: analysis of water-well drill records and implications for mineral exploration potential; *Canadian Journal of Earth Sciences*, v. 48, no. 6, p. 973–986.

Cagniard, L. (1953): Basic theory of the magnetotelluric method of geophysical prospecting; *Geophysics*, v. 18, p. 605–635.

Calvert, A.J., Hayward, N.E., Spratt, J.E. and Craven, J.A. (2011): Seismic reflection constraints on upper crustal structures in the volcanic-covered central Nechako basin, British Columbia; *Canadian Journal of Earth Sciences*, v. 48, no. 6, p. 1021–1037.

Gabrielse, H. and Yorath, C.J. (1991): Tectonic synthesis; *in* *Geology of the Cordilleran Orogen in Canada*, H. Gabrielse and C.J. Yorath (ed.), Geological Survey of Canada, Geology of Canada, no. 4, p. 677–705 (also Geological Society of America, *Geology of North America*, v. G-2).

Geotech Limited (2009): Helicopter-borne z-axis tipper electromagnetic (ZTEM) and aeromagnetic survey, Mt. Milligan test block; Geoscience BC, Report 2009-7, 51 p., URL <<http://www.geosciencebc.com/s/2009-07.asp>> [November 2011]

Hannigan, P., Lee, P.J., Osadetz, K.J., Dietrich, J.R. and Olsen-Heise, K. (1994): Oil and gas resource potential of the Nechako-Chilcotin area of British Columbia; BC Ministry of Energy and Mines, GeoFile 2001-6, 5 maps at 1:1 000 000 scale, URL <<http://www.empr.gov.bc.ca/Mining/Geoscience/PublicationsCatalogue/GeoFiles/Pages/2001-6.aspx>> [November 2011].

Hayward, N. and Calvert, A.J. (2008): Structure of the southeastern Nechako Basin, south-central British Columbia (NTS 092N, O; 093 B, C): preliminary results of seismic interpretation and first-arrival tomographic modelling; *in* *Geoscience BC Summary of Activities 2007*, Geoscience BC, Report 2008-1, p. 129–134, URL <http://www.geosciencebc.com/i/pdf/SummaryofActivities2007/SoA2007-Hayward_original.pdf> [November 2011].

Holtham, E. and Oldenburg, W. (2010): Three-dimensional inversion of ZTEM data; *Geophysical Journal International*, v. 182, p. 168–192, doi:10.1111/j.1365-246X.2010.0463.x

Jones, A.G. (1992): Electrical conductivity of the continental lower crust; *in* *Continental Lower Crust*, D.M. Fountain, R.J. Arculus and R.W. Kay (ed.), Elsevier, Amsterdam, The Netherlands, p. 81–143.

Lo, B., Legault, J., Kuzmin, P. and Fisk, K. (2009): Advances in airborne EM: introducing ZTEM; *South African Geophysical Association (SAGA), 11th Biennial Technical Meeting and Exhibition*, extended abstracts, p. 101–104.

Mathews, W.H. (1989): Neogene Chilcotin basalts in south-central British Columbia: geology, ages, and geomorphic history; *Canadian Journal of Earth Sciences*, v. 26, p. 969–982.

Monger, J.W.H., Price, R.A. and Templeman-Kluit, D. (1982): Tectonic accretion of two major metamorphic and plutonic belts in the Canadian Cordillera; *Geology*, v. 10, p. 70–75.

Monger, J.W.H., Souther, J.G. and Gabrielse, H. (1972): Evolution of the Canadian Cordillera—a plate tectonic model; *American Journal of Science*, v. 272, p. 577–602.

Price, R.A. (1994): Cordilleran tectonics in the evolution of the Western Canada Sedimentary Basin; *in* *Geological Atlas of the Western Canada Sedimentary Basin*, G.D. Mossop and I.

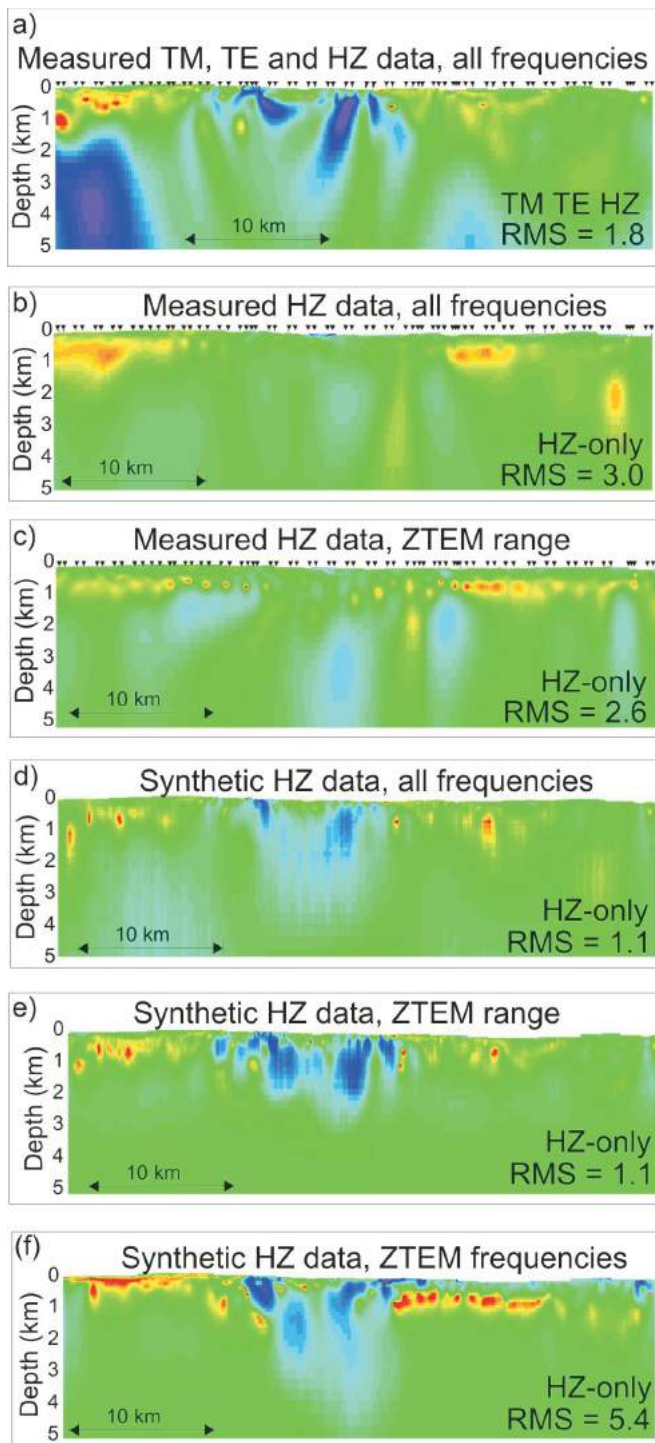
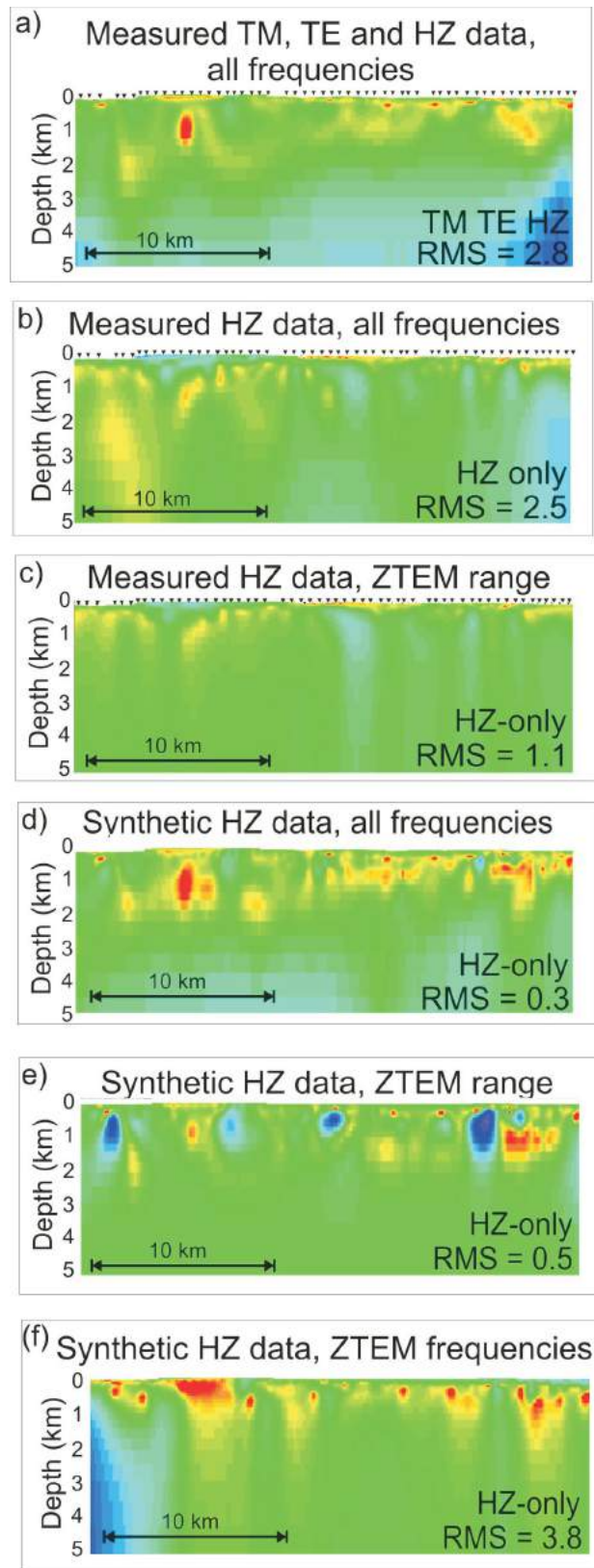


Figure 8. Results of two-dimensional (2-D) modelling of measured and synthetic MT data along profile C: **a)** original 2-D model derived from all components of the measured MT data; **b)** model of the measured HZ data over the seven-decade frequency range; **c)** model of the measured HZ data over the ZTEM frequency range; **d)** model of the synthetic HZ data over the seven-decade frequency range; **e)** model of the synthetic HZ data over the ZTEM frequency range; and **f)** model of the synthetic HZ data at the six specific ZTEM frequencies.

- Shetsen (comp.), Canadian Society of Petroleum Geologists and Alberta Research Council, 510 p., URL <http://www.ags.gov.ab.ca/publications/wcsb_atlas/atlas.html> [November 2011].
- Riddell, J.M., comp. (2006): Geology of the southern Nechako Basin, NTS 92N, 92O, 93B, 93C, 93F, 93G; BC Ministry of Energy and Mines, Petroleum Geology Map 2006-1, 3 sheets at 1:400 000 scale.
- Riddell, J. (2011): Lithostratigraphic and tectonic framework of Jurassic and Cretaceous intermontane sedimentary basins of south-central British Columbia; Canadian Journal of Earth Sciences, v. 48, no. 6, p. 870–896.
- Riddell, J., Ferri, F., Sweet, A. and O’Sullivan, P. (2007): New geoscience data from the Nechako Basin project; in Nechako Initiative Geoscience Update 2007, BC Ministry of Energy and Mines, Petroleum Geology Open File 2007-1, URL <<http://www.empr.gov.bc.ca/Mining/Geoscience/PublicationsCatalogue/OilGas/OpenFiles/Pages/PGOF2007-1.aspx>> [November 2011].
- Sattel, D., Witherly, K. and Becken, M. (2010): A brief analysis of ZTEM data from the Forrestarian test site, WA; Australian Society of Exploration Geophysicists (ASEG), Extended Abstracts, v. 2010, no. 1, p. 1–4.
- Smith, I.F. (2007): Petrophysical analysis—Nechako Basin; in Nechako Initiative Geoscience Update 2007, BC Ministry of Energy and Mines, Petroleum Geology Open File 2007-1, URL <<http://www.empr.gov.bc.ca/Mining/Geoscience/PublicationsCatalogue/OilGas/OpenFiles/Pages/PGOF2007-1.aspx>> [November 2011].
- Spratt, J.E. and Craven, J.A. (2009): Preliminary images of the conductivity structure of the Nechako Basin, south-central British Columbia (NTS 092N, O, 093B, C, F, G) from magnetotelluric methods; in Geoscience BC Summary of Activities 2008, Geoscience BC, Report 2009-1, URL <http://www.geosciencebc.com/i/pdf/SummaryofActivities2008/SoA2008-Spratt_original.pdf> [November 2011].
- Spratt, J.E. and Craven, J. (2010): Magnetotelluric imaging of the Nechako Basin, British Columbia, Canada; Geological Survey of Canada, Current Research, 2010-3, 12 p., URL <http://geopub.nrcan.gc.ca/moreinfo_e.php?id=261488> [November 2011].
- Spratt, J. and Craven, J. (2011): Near-surface and crustal-scale images of the Nechako basin, British Columbia, Canada, from magnetotelluric investigations; Canadian Journal of Earth Sciences, v. 48, p. 987–999.
- Struik, L.C. and MacIntyre, D.G. (2001): Introduction to the special issue of Canadian Journal of Earth Sciences: The Nechako NATMAP Project of the central Canadian Cordillera; Canadian Journal of Earth Sciences, v. 38, p. 485–494.
- Wait, J.R. (1962): Theory of magnetotelluric fields; Journal of Research of the National Bureau of Standards, Part D: Radio Properties, v. 66d, p. 509–541.

Figure 9. Results of two-dimensional (2-D) modelling of measured and synthetic MT data along profile F: **a)** original 2-D model derived from all components of the measured MT data; **b)** model of the measured HZ data over the seven-decade frequency range; **c)** model of the measured HZ data over the ZTEM frequency range; **d)** model of the synthetic HZ data over the seven-decade frequency range; **e)** model of the synthetic HZ data over the ZTEM frequency range; and **f)** model of the synthetic HZ data at the six specific ZTEM frequencies.





Geoscience BC is an industry-led, industry-focused not for profit society that works to attract mineral and oil and gas investment to British Columbia through collection and marketing of geoscience data.

Suite 440 – 890 West Pender Street
Vancouver BC V6C 1J9

info@geosciencebc.com
www.geosciencebc.com

Geoscience BC is funded through grants from the Provincial Government of British Columbia